Evaluation of Technical Feasibility of Homogeneous Charge Compression Ignition (HCCI) Engine Fueled with Hydrogen, Natural Gas, and DME

Final Report

10/1/2004 to 3/31/2007

Prepared by
John M. Pratapas, Gas Technology Institute
&
Dr. Daniel Mather and Anton Kozlovsky, Digital Engines

M 2008

DE-FC26-04NT42236

Gas Technology Institute
1700 South Mount Prospect Road
Des Plaines, IL 60018

Digital Engines, LLC
4337 Mineral Point Road
Madison, WI 53705-5042

Disclaimer

Abstract

The objective of the proposed project was to confirm the feasibility of using blends of hydrogen and natural gas to improve the performance, efficiency, controllability and emissions of a homogeneous charge compression ignition (HCCI) engine. The project team utilized both engine simulation and laboratory testing to evaluate and optimize how blends of hydrogen and natural gas fuel might improve control of HCCI combustion.

GTI utilized a state-of-the art single-cylinder engine test platform for the experimental work in the project. The testing was designed to evaluate the feasibility of extending the limits of HCCI engine performance (i.e., stable combustion, high efficiency and low emissions) on natural gas by using blends of natural gas and hydrogen. Early in the project Ricardo provided technical support to GTI as we applied their engine performance simulation program, WAVE, to our HCCI research engine. Modeling support was later provided by Digital Engines, LLC to use their proprietary model to predict peak pressures and temperatures for varying operating parameters included in the Design of Experiments test plan. Digital Engines also provided testing support for the hydrogen and natural gas blends. Prof. David Foster of University of Wisconsin-Madison participated early in the project by providing technical guidance on HCCI engine test plans and modeling requirements.

The main purpose of the testing was to quantify the effects of hydrogen addition to natural gas HCCI. Directly comparing straight natural gas with the hydrogen enhanced test points is difficult due to the complexity of HCCI combustion. With the same air flow rate and lambda, the hydrogen enriched fuel mass flow rate is lower than the straight natural gas mass flow rate. However, the energy flow rate is higher for the hydrogen enriched fuel due to hydrogen's significantly greater lower heating value, 120 mJ/kg for hydrogen compared to 45 mJ/kg for natural gas.

With these caveats in mind, an analysis of test results indicates that hydrogen enhanced natural gas HCCI (versus neat natural gas HCCI at comparable stoichiometry) had the following characteristics:

- Substantially lower intake temperature needed for stable HCCI combustion
- Inconclusive impact on engine BMEP and power produced,
- Small reduction in the thermal efficiency of the engine,
- Moderate reduction in the unburned hydrocarbons in the exhaust,
- Slight increase in NOx emissions in the exhaust,
- Slight reduction in CO2 in the exhaust.
- Increased knocking at rich stoichiometry

The major accomplishments and findings from the project can be summarized as follows:

1. A model was calibrated for accurately predicting heat release rate and peak pressures for HCCI combustion when operating on hydrogen and natural gas blends.
2. A single cylinder research engine was thoroughly mapped to compare performance and emissions for micro-pilot natural gas compression ignition, and HCCI combustion for neat natural gas versus blends of natural gas and hydrogen.

3. The benefits of using hydrogen to extend, up to a limit, the stable operating window for HCCI combustion of natural gas at higher intake pressures, leaner air to fuel ratios or lower inlet temperatures was documented.

Table of Contents

EXECUTIVE SUMMARY

HCCI combustion is a process in which a homogeneous mixture of fuel and oxidant is compression ignited. HCCI offers the potential to increase engine thermal efficiency and reduce NOx emissions significantly. Another advantage of HCCI is that it enables broader fuel capability. While HCCI provides good operating characteristics at part-load conditions, there are some challenges that currently limit its commercial potential. These issues include:

1. Accurate control of HCCI combustion
2. Extension of the operating range while maintaining the full benefits of the HCCI engine
3. Lower power density
4. Difficult to operate at higher loads
5. Difficulty with cold start
6. High HC and CO at light loads
7. Increased NOx at high loads

Properties of Hydrogen (high flame speed, broad flammability limits) make it an ideal candidate fuel for blending with natural gas to extend the operating range of the HCCI engine and give better control of auto-ignition timing. The high cetane number of DME (55-60) suggested that, if needed, it would be an ideal fuel for aiding in the control of HCCI combustion. To address start-up issues, the plan was to evaluate micro-pilot injection of a Fischer-Tropsch synthetic diesel fuel. The F-T fuel was proposed because of its very high cetane number (>75), no sulfur and very low aromatics.

The control strategy chosen for the HCCI testing was to set a limit for the maximum rate of pressure rise within the cylinder while primary control parameters were varied. These parameters include:

- Fueling rate of natural gas, H2, and DME
- Intake charge temperature
- Intake boost pressure
- Coolant temperature

The major accomplishments and findings from the project can be summarized as follows:

The GTI single cylinder engine was configured for HCCI operation. Baseline HCCI mapping with natural gas was successfully completed for both NA and intake charge-boosted conditions. The engine map is shown in Figure 1. For all cases, the use of the Peak Pressure Location (PPL) was a good indicator for controlling the HCCI engine fueled with natural gas. The PPL was controlled by using the intake charge temperature, which is only valid when the oil and coolant temperatures are kept constant. With this strategy, consistent data were taken.

It is clear that intake boosting is very important for a HCCI engine for high power density. In addition, the required intake temperature decreases linearly with increasing intake boost pressure. For example, the required temperature decreased about 66°C when the intake pressure increased from 1 bar to 1.6 bar at the engine speed of 1000 rpm. This result implies that a HCCI engine with a high pressure-ratio turbocharger or supercharger with a small-size intercooler may not need additional thermal energy in order to achieve HCCI combustion for stationary applications. The small-size intercooler is to control the intake charge temperature. In addition,

as shown in the figure, engine power density is proportional to intake boost pressure. Therefore, higher intake boost pressure will lead to higher power density, which is equivalent to those of conventional natural gas engines or at least close to their maximum power density. In the current study, the NMEP up to about 8 bar was attained when the intake boost pressure was about 2.2 bar.

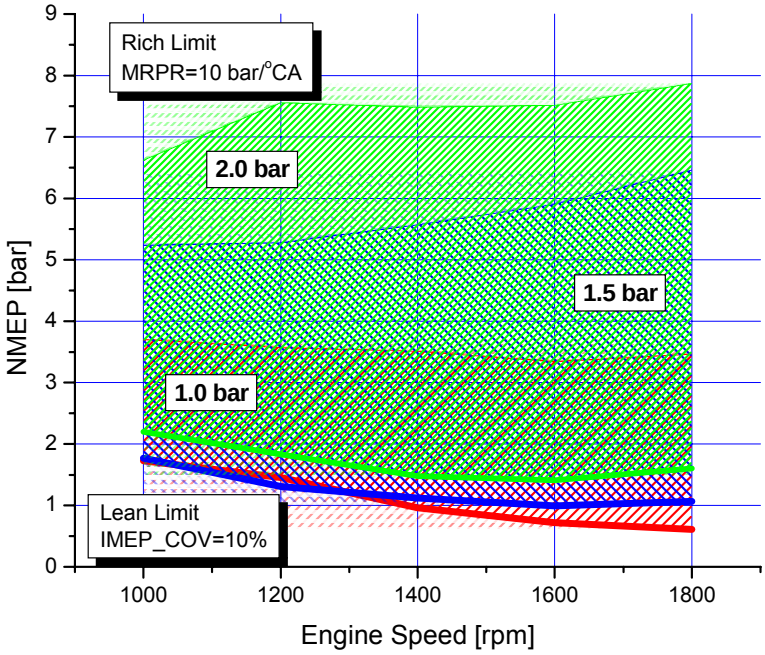

Figure 1 HCCI engine map-Neat Natural Gas

Figure 2 shows the IMEP versus excess air ratios for diesel, micro-pilot natural gas, natural gas HCCI and natural gas + H2 HCCI modes from the same single-cylinder engine. All data is reported at an engine speed of 1800 rpm. The HCCI mode overlaps the diesel mode from almost medium to light loads when the intake pressure is 2.2 bar. If one increases the intake pressure close to 3 bar or higher, the IMEP can be higher than 10 bar. For even high loads, the micro-pilot natural gas mode can be applied. This suggests that a hybrid of HCCI and micro-pilot natural gas modes could be used for stationary applications. The H2 enhanced HCCI test points are focused on air fuel ratio between λ=2.5 to 3.5 which produce higher IMEP. The higher IMEP values would allow HCCI to compete with diesel, micro-pilot and spark ignited natural gas combustion as a viable commercial engine design.

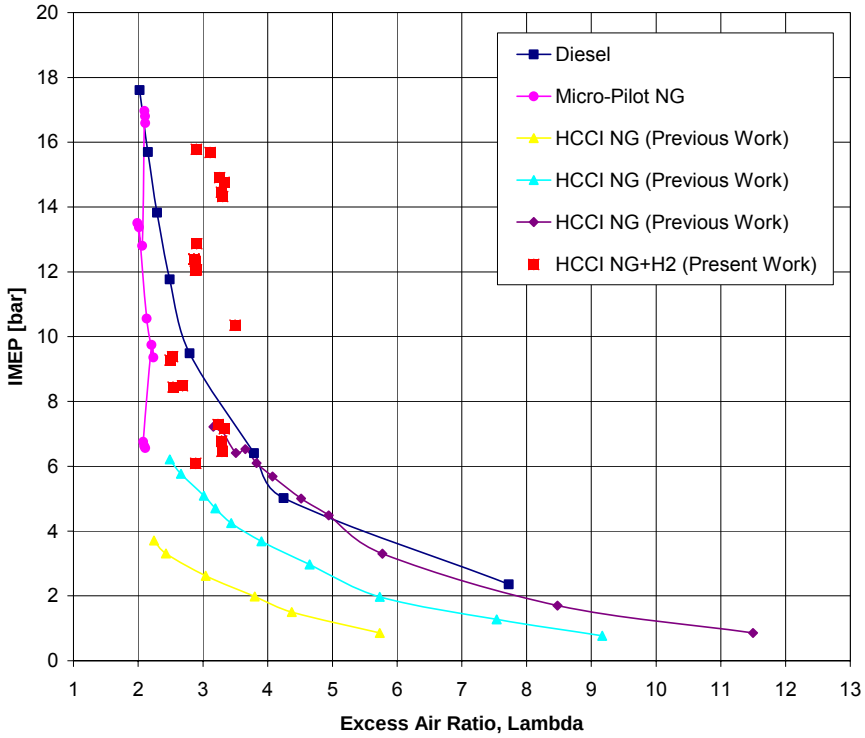

Figure 2 Comparison of IMEP for conventional diesel, micro-pilot natural gas, and natural gas HCCI combustion (with and without H2)

Digital Engines developed and used a model in this project to predict heat release rates and peak pressures for proposed H2+natural gas test conditions. This was done to predict whether any conditions might result in over-temperature or over-pressure of the engine. Test data obtained in the project was used to calibrate the model.

The testing confirmed that, for the boosted conditions tested, hydrogen enhanced natural gas HCCI combustion resulted in:

- Substantially lower intake temperature needed for stable HCCI combustion
- Inconclusive impact on the engine BMEP and power produced
- Small reduction in the thermal efficiency of the engine
- Moderate reduction in the unburned hydrocarbons in the exhaust
- Slight increase in NOx emissions in the exhaust
- Slight reduction in CO2 in the exhaust
- Increased knocking at rich stoichiometry

HCCI combustion resulted in hydrocarbon (HC) and carbon monoxide (CO) emissions were equivalent to or lower than conventional natural gas engines. Furthermore, HC and CO emissions were significantly lower than other reported HCCI data particularly at very light loads. Hydrogen enhanced HCCI reduced hydrocarbon emissions further.

REPORT DETAILS

Overview

The report is organized to provide an accounting of the research results relative to the contract scope of work. This scope of work is comprised of Tasks that were established under the contract.

The initial tasks were directed toward preparing the test bench for the experimental work. This test bench was the GTI research engine modified for HCCI combustion on natural gas and hydrogen/natural gas blends. To help guide the experimental work, numerical modeling was proposed to predict the stable HCCI configuration and safely guide the transition to blends of hydrogen and natural gas without over-pressuring the engine or unstable combustion leading to damaging knocking.

For each task, a brief statement of objectives will be provided followed by a reporting of work performed including any potential issues or adjustments to the technical approach.

Task 1 Preparation of HCCI Engine Facility

The objective of Task 1 was to prepare the existing engine bench (AVL Model LEF/VOLVO 5312 research engine) for the HCCI engine testing. To meet the project objectives, GTI proposed to add hydrogen and dimethyl ether (DME) fuel trains to the engine intake system.

To support attainment of the project objectives, GTI modified its AVL Model LEF/VOLVO 5312 research engine test bench for HCCI operation. The primary equipment modifications included installing an intake air (electric) heater system and gas mixing system for delivering and metering bottled hydrogen and dimethyl ether (DME) to the engine intake system. Pictures of these systems are provided in Appendix A.

HCCI engine testing requires an electric heater because intake manifold temperature is used as one of the major parameters for controlling the start of combustion. A 20 kW in-line electric heater (Chromalox) was designed, procured, and installed on the engine test bench. The in-line electric heater was located between the intake air flow control valve and the intake surge tank. A control box was specified and installed. The electric heater is controlled with 4-20 ma signal from the engine data acquisition and control (DAC) system. (See Figure 1A-Appendix)

At the outset of the project, the GTI research engine was configured for natural gas as primary fuel and pilot injection of diesel fuel as its ignition source. Natural gas was premixed with air downstream of the intake surge tank and upstream of the intake manifold. The premixed natural gas and air was compressed and auto-ignited by the pilot injection of diesel fuel.

Table 1 shows the operating conditions of the natural gas engine with diesel micro-pilot injection as its ignition source. For the current testing, 100% engine brake torque was set at 235.6 Nm. The start of injection (SOI) and injection duration were varied to minimize the coefficient of variance of IMEP (IMEP_COV). Maximum injection pressure was determined by monitoring any changes in the engine combustion at rated speed and load. The maximum injection pressure was turned out to be 130 MPa. Also, we tried to maintain the location of peak in-cylinder pressure between 8 and 9°CA. Intake air temperature and exhaust back-pressure were not controlled in this case. However, intake air pressure was controlled to supply the required

amount of air. Therefore, this test condition is similar to a supercharged engine. For all cases, the excess air ratio was maintained at approximately 2.0. Coolant and oil temperatures were maintained at 80.3°C and 95.7°C, respectively. The diesel fuel temperature was also maintained at 35.6°C.

Table 1 Operating conditions of the GTI natural gas engine with diesel micro-pilot injection

Engine Load [%]	100	75.54	52.19	27.90
Engine speed [rpm]	1799.5	1799.5	1799.5	1799.5
Power [kW]	44.44	33.55	23.25	12.38
Torque [Nm]	235.60	177.97	122.97	65.72
Excess air ratio, λ	2.10	2.02	2.19	2.09
Start of injection [° ATDC]	-28	-28	-26	-22
Duration of injection [°CA]	3.0	3.0	3.0	3.0
Injection pressure [MPa]	130	130	130	130
Peak in-cylinder pressure [bar]	164.25	128.39	96.73	59.12
Peak in-cylinder pressure location [°ATDC]	8.12	8.72	8.81	8.12
IMEP [bar]	16.95	13.25	9.88	6.72
IMEP_COV [bar]	4.53	3.12	6.45	5.89
PMEP [bar]	0.48	0.22	0.15	-0.18
FMEP [bar]	1.82	1.97	2.06	2.46
Intake manifold temperature [°C]	26.85	28.38	29.56	29.14
Intake manifold pressure [bar]	2.36	1.81	1.66	1.14
Exhaust manifold temperature [°C]	380.49	403.98	347.70	399.38
Exhaust manifold pressure [bar]	1.13	1.08	1.08	1.04

Natural gas composition was obtained from Nicor (composition in March 2005). Other natural gas properties were calculated based on the obtained gas composition. The methane number of the natural gas tested was 90.9. Table 2 shows the properties of the natural gas tested.

Table 2 Properties of natural gas tested

Natural Gas		
Density @ 0C, 1 atm	0.75645 kg/m3	
Lower heating value	47521.5 kJ/kg	
Stoichiometric air/fuel ratio	16.1949 kg_air/kg_gas	
Methane number	90.9	
Composition	**Volume %**	**Mass %**
CO_2	0.88	2.3
N_2	1.57	2.60
CH_4	94.88	89.91
C_2H_6	2.31	4.14
C_3H_8	0.27	0.72
C_4H_{10}	0.07	0.25
C_5H_{12}	0.02	0.09

Figure 3 compares the BMEP (left) and brake efficiency (right) of natural gas and diesel engine testing. The BMEP of the natural gas engine was maintained equivalent to that of the diesel engine. The natural gas engine showed higher brake efficiency above 50% load, while the diesel engine showed higher efficiency below 50% load for the current conditions. The brake efficiency of the natural gas engine with micro-pilot injection was above 40%.

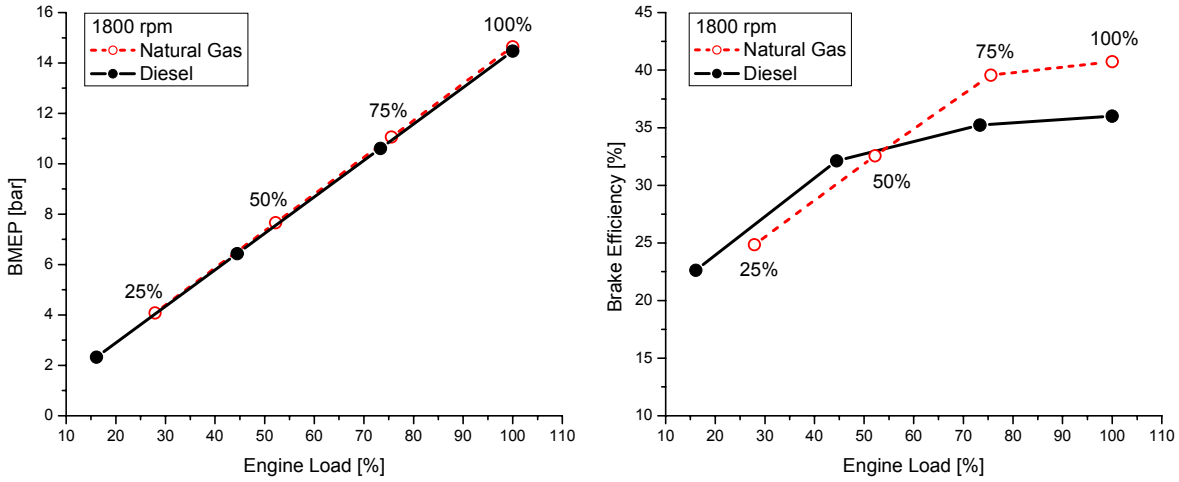

Figure 3 BMEP (left) and brake efficiency (right) as a function of engine load for natural gas and diesel

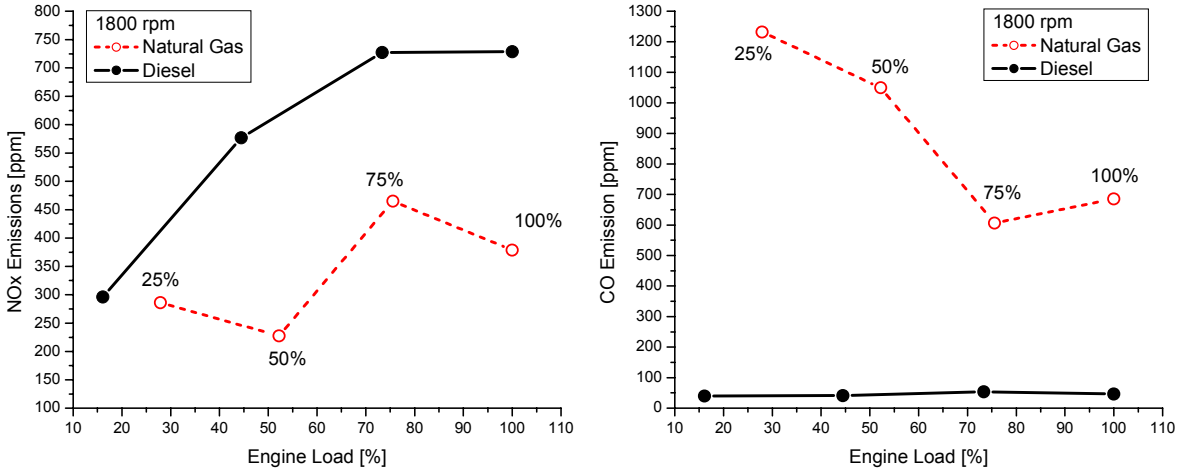

Figure 4 NOx (left) and CO emissions as a function of engine load for natural gas and diesel

Figure 4 shows the comparison of NOx and CO emissions between natural gas and diesel testing. The natural gas engine with micro-pilot injection showed much lower NOx emissions compared

to the diesel engine. Unlike the diesel engine, which shows dramatic increase in NOx emissions as the engine load increases, the natural gas engine showed slow increase in NOx emissions with increasing engine load. The diesel engine showed extremely low CO emissions and the CO emissions increased slowly as the engine load increased. However, the natural gas engine showed much higher CO emission than the diesel engine. CO emissions from the natural gas engine decreased as the engine load increased. This is the same phenomena that can be observed in a typical HCCI engine.

Figure 5 shows the comparison of THC and CH_4 (left) and CO_2 and O_2 (right) between the natural gas engine and diesel engine. The natural gas engine emitted extremely high THC and CH_4 emissions. At lighter loads, the concentrations of the THC and CH_4 were out of the measurement ranges of the current analyzers. As an example, THC emissions from a SI lean-burn natural gas engine (λ=1.7) are about 1700 ppm on average. The GTI single-cylinder natural gas engine, which operated at λ=2, emitted THC emissions of about 5000 ppm. The difference in the excess air ratio might explain this. As the air-fuel ratio gets leaner, THC emissions increase. Surprisingly, CH_4 emission is about 88% of the THC emissions for natural gas engines. This result is similar to that of a typical HCCI engine. If we utilize hydrogen-enhanced combustion, there are opportunities to reduce THC, CH_4, and CO emissions. In Figure 5 (right), the diesel engine showed increasing CO_2 and decreasing O_2 as the engine load increased. However, the natural gas engine showed consistent CO_2 and O_2 throughout the engine load. O_2 concentration in the exhaust was about 11% and CO_2 was about 4% for the natural gas engine.

Figure 6 shows the in-cylinder pressure of the natural gas engine. Looking at the pressure profiles, they are almost the same as those of a SI lean-burn natural gas engine.

Figure 7 shows the rate of heat release for 4 different engine loads for the natural gas engine. Although it was not clear in the pressure profiles, the effect of the micro-pilot injection of diesel fuel is shown in the heat release rate profile. This is more obvious at the lighter loads. At higher loads, the effect of the micro-pilot injection became less evident. Figure 8 shows the accumulative heat release measured with the natural gas engine for the ISO 8178 test cycle. It was determined that the heat release rate is more rapid at higher loads.

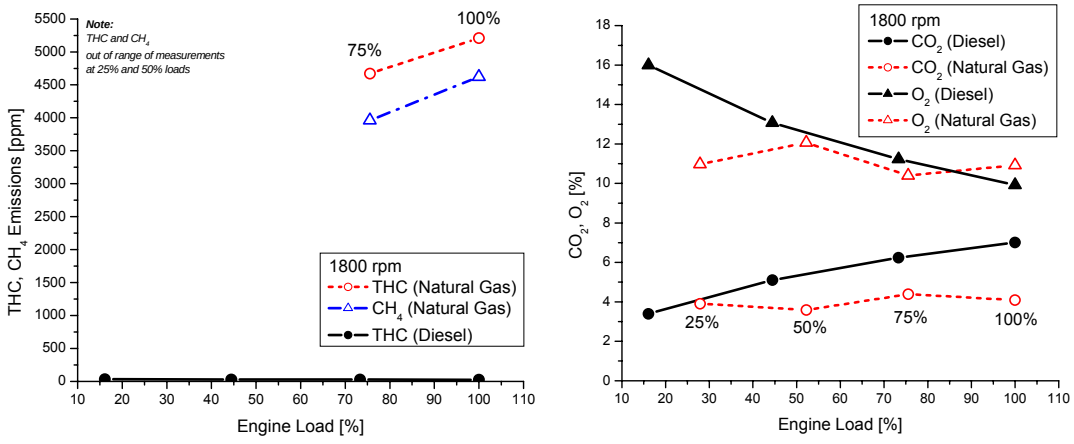

Figure 5 THC, CH_4 (left) and CO_2, O_2 (right) as a function of engine load for natural gas and diesel

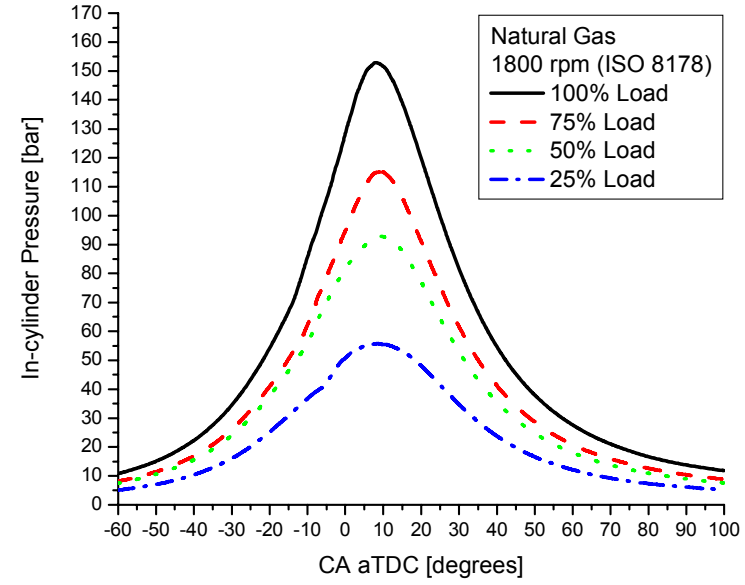

Figure 6 In-cylinder pressures of the natural gas engine tested under ISO 8178 cycle

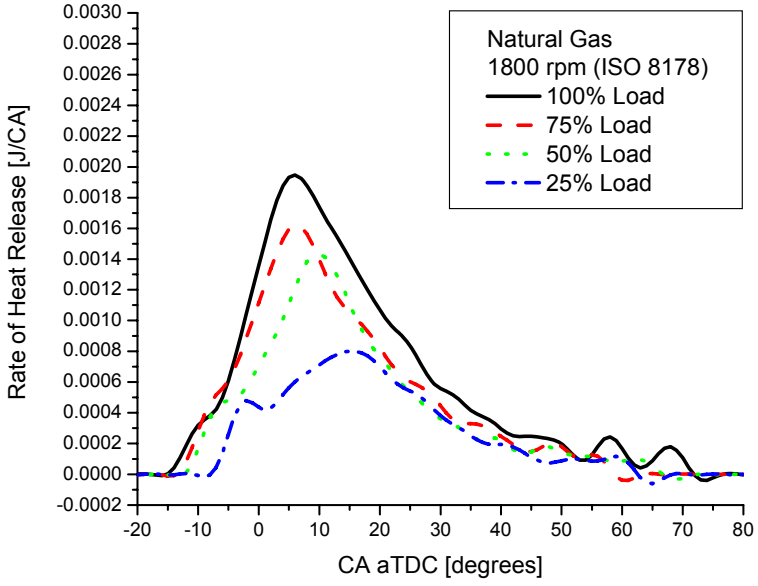

Figure 7 Rate of heat release (10^{-5}) of the natural gas engine tested under ISO 8178 cycle

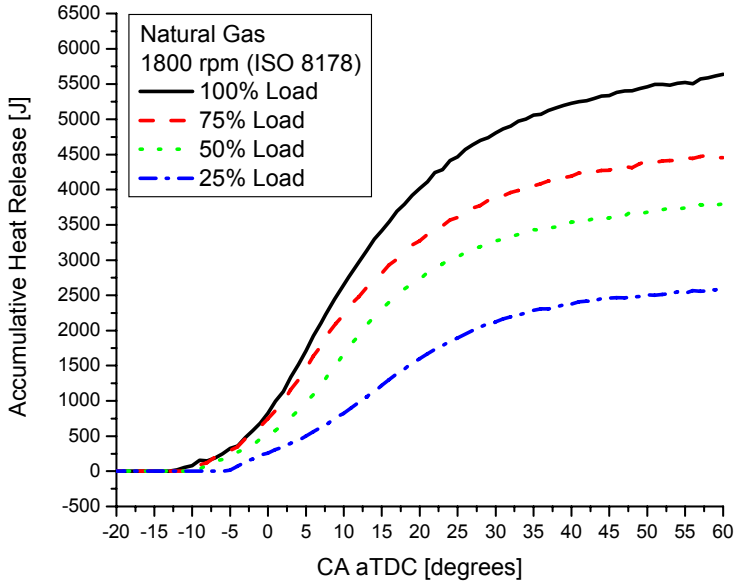

Figure 8 Accumulative heat release of the natural gas engine tested under ISO 8178 cycle

For conversion of the engine to HCCI, a mixing chamber was designed, fabricated, and installed. The mixing chamber was cylindrical in shape and had 8 ports (1/4" OD) in 2 rows. To improve mixing, a baffle was located downstream of the fuel inlet ports. Natural gas was introduced into the 4 ports in the first row and hydrogen and DME were introduced into the mixing chamber through the 4 ports (2 each) in the second row. (See Figure 2A-Appendix) In the event of potential flashback, a thermocouple was installed just downstream of the mixing chamber. If this thermocouple detected any sudden temperature rise in the intake manifold, all the fuel control valves (natural gas, hydrogen, DME, and pilot injection fuel) were immediately closed.

A fuel train for hydrogen and DME was designed, fabricated, and installed (See Figure 3A-Appendix). For this work, flow sensors and transmitters for each gas were specified, procured, and installed. The flow sensors and flow transmitters were purchased from Micro Motion. Flow control valves (Badger Valves) were also specified, procured, and installed. The flow meters and flow control valves were interfaced with the DAC system and tuned. Pressure transducers and thermocouples were installed and wired into the DAC system. Initially, three hydrogen-cylinder bottles and two DME-cylinder bottles were purchased. Other items installed included check valves and safety valves for each train.

Data Acquisition Systems and Methods

The GTI combustion laboratory uses three separate data acquisition tools. They are the MTS Adapt, MTS CAS, and Horiba MEXA 7100. The Horiba MEXA 7100 measures and reports all emissions data. The emissions data is recorded by the MTS Adapt. Cylinder pressure traces and heat release data are measured and recorded by the MTS CAS. The peak cylinder pressure, timing of peak cylinder pressure, and various heat release data are exported to the MTS Adapt. The MTS Adapt serves as both laboratory control and as primary data acquisition. Laboratory temperatures and pressures are recorded. Air and fuel flow rates are recorded, and for the

straight natural gas test cases, the air/fuel ratio and lambda are calculated. Dynamometer speed and torque are recorded, and power and BMEP are calculated. All emissions data is brought in from the Horiba system.

In addition to the data recorded by the laboratory equipment, Digital Engines (DE) uses the data to calculate a few key parameters. The temperature difference between the intake the exhaust is calculated. The brake specific fuel consumption for the natural gas cases is calculated. Also calculated are the natural gas and hydrogen energy flow rates, and the actual percentage of energy from hydrogen. Knowing the energy flow rates and the power produced, the thermal efficiency is produced. In addition, the actual lambda is calculated.

Task 2 HCCI Engine Configuration

The established HCCI engine was to be configured to operate with natural gas only within a range of values for the parameters of air/fuel ratio, engine speed, and brake mean effective pressure (BMEP). The boundaries of the operating range of the HCCI engine would be ignition and knocking limits. The obtained baseline data will also be used in Subtask 3.1 for the calibration of the engine simulation program. GTI will perform this task.

Naturally Aspirated HCCI Engine Mapping

The HCCI engine mapping was successfully completed for NA conditions and the results are presented in this section of the report. Before starting testing, a thorough review of related literature and consulting with Dr. Dave Foster was conducted. Reaction Design's Chemkin v4.0 and the Ideal Gas Law were used to predict the required temperatures for the HCCI combustion. These temperatures were used as the starting points in the actual engine testing. At the same time, a test plan and strategy was used to guide the engine testing.

Data taken included engine performance (power output, fuel consumption rate, IMEP, BMEP, PMEP, FMEP, etc.), efficiency (indicated thermal efficiency (ITE), brake thermal efficiency (BTE), combustion efficiency, etc.), combustion (cylinder pressure, rate of heat release rate, heat release, locations of heat release 10%, 50%, and 90%, max rate of pressure rise (MRPR), location of peak pressure, start of combustion (SOC), etc.), and emissions (i.e. NOx, CO, THC, CH_4, and CO_2). Only the most informative data are included in this report.

Diesel micro-pilot injection was used to warm up the engine and to initiate HCCI combustion. Later, the engine was warmed up without the diesel micro-pilot and HCCI combustion was attained. Therefore, it was concluded that the micro-pilot would not be required for start up for future testing. Table 3 shows the test plan and strategy for the HCCI engine fueled with natural gas.

Table 3 Natural gas HCCI engine test plan and strategy

Speed points	1000, 1200, 1400, 1600, 1800 rpm • Start at the lowest engine speed (1000 rpm)
Load points	Lean limit to rich limit @ each speed
Intake temperature	Need to be found • Start at ball-park high temperature determined with Chemkin and thermodynamics • Higher engine speed may require higher charge temperature • Leaner fuel/air mixture may require higher charge temperature

Intake pressure	Start with 1 bar (naturally-aspirated conditions)
Exhaust pressure	1 bar
Engine compression ratio	13.8:1 (fixed)
EGR	No EGR • Un-cooled EGR can be considered in the HCCI engine, which is not included in the current project. If the project continues, un-cooled EGR can be one of the thermal energy sources for HCCI combustion. GTI can perform HCCI with un-cooled EGR with a small addition to the current system such as an EGR valve. GTI's emissions benches have the EGR capability.
Fuel introduction	Natural gas fumigation (premixed with air @ intake manifold) • Start at very lean and add more fuel progressively
Coolant and oil temperatures	Maintain constant at 100°C • Coolant temperature was controlled to see the sensitivity of the HCCI combustion. Data were taken but not included in this report.
Combustion phasing	Maintain peak pressure location between 6 to 10°ATDC • Increase the intake charge temperature with engine speed • Increase the intake charge temperature with leaner fuel/air mixture
Lean limit indication	IMEP_COV≥10%
Knock limit indication	MRPR (dP/dCA)≥10 bar/°CA as well as knock intensity

Figure 9 shows the theoretical relationship of the intake charge temperature and the in-cylinder mean temperature for motored operating conditions. The reference natural gas auto-ignition temperature is about 540°C (or 1004°F). The corresponding intake charge temperature is about 190°C. This theoretical calculation is independent of engine speed; however, intake charge temperature is dependent on engine speed and air/fuel ratio (AFR). Furthermore, coolant and oil temperatures affect the HCCI combustion. However, this theoretical temperature can be used as a ball-park temperature (or starting point) for HCCI combustion testing.

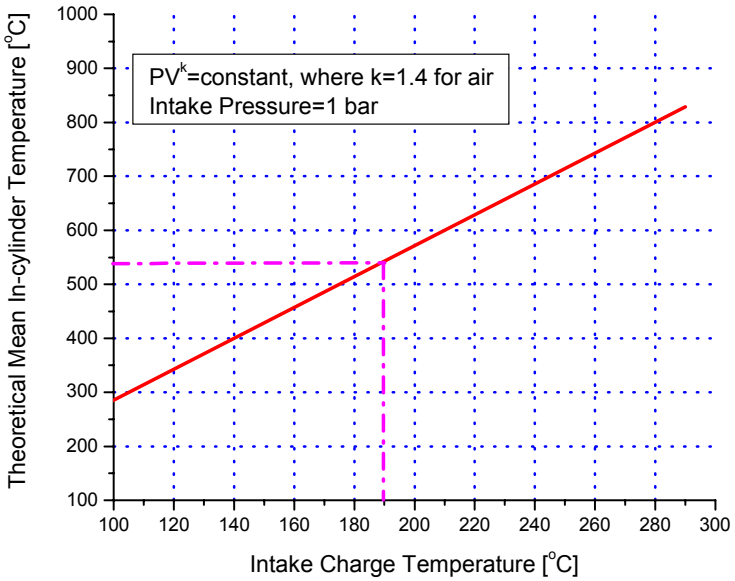

Figure 9 Theoretical mean in-cylinder temperature versus intake charge temperature

HCCI combustion was attained with natural gas only on the GTI single-cylinder research engine. Testing was performed based on the test plan and strategy shown in Table 1. Table 4 shows the properties of the natural gas tested in June 2005.

Table 4 Properties of natural gas tested (June 2005)

Natural Gas		
Density @ 0C, 1 atm	0.75791 kg/m3	
Lower heating value	47447.5 kJ/kg	
Stoichiometric air/fuel ratio	16.1693 kg_air/kg_gas	
Methane number	90.8	
Composition	**Volume %**	**Mass %**
CO_2	0.95	2.48
N_2	1.55	2.56
CH_4	94.75	89.61
C_2H_6	2.39	4.28
C_3H_8	0.26	0.69
C_4H_{10}	0.07	0.25
C_5H_{12}	0.02	0.08
C_6H_{14}	0.01	0.05

HCCI Engine Operating Regime

Figure 10 shows the required intake manifold temperature for HCCI combustion fueled with natural gas for various engine speeds and AFR. The highest intake temperature required for the HCCI combustion was about 285°C at close to the lean limit at 1400 rpm. In the lean and rich sides, it seems that they have a linear relationship; however, the intake temperature does not have a linear relationship with excess air ratio (λ) for the entire operating regime. The required intake temperature rapidly increased at lower engine speed and less and less rapidly increased as the engine speed increased. The required intake temperature remained almost constant above certain λ for a respective engine speed. At lower engine speed, this temperature was reached at a lower excess air ratio. Boosted conditions require lower intake charge temperature for HCCI combustion.

Figure 11 shows λ versus the engine speed for the naturally-aspirated (NA) conditions. The operating regime of the HCCI engine extended as the engine speed increased. Rich limit was reduced slightly with the engine speed; however, the lean limit exponentially increased with the engine speed. At the lean limit or leaner AFR, the engine speed had more impact on the engine operating regime. However, at richer AFR, the engine speed had a slight impact on the operating regime of the HCCI engine fueled with natural gas. The lowest λ tested was approximately 1.8 and the highest λ was 6.2 for the HCCI engine.

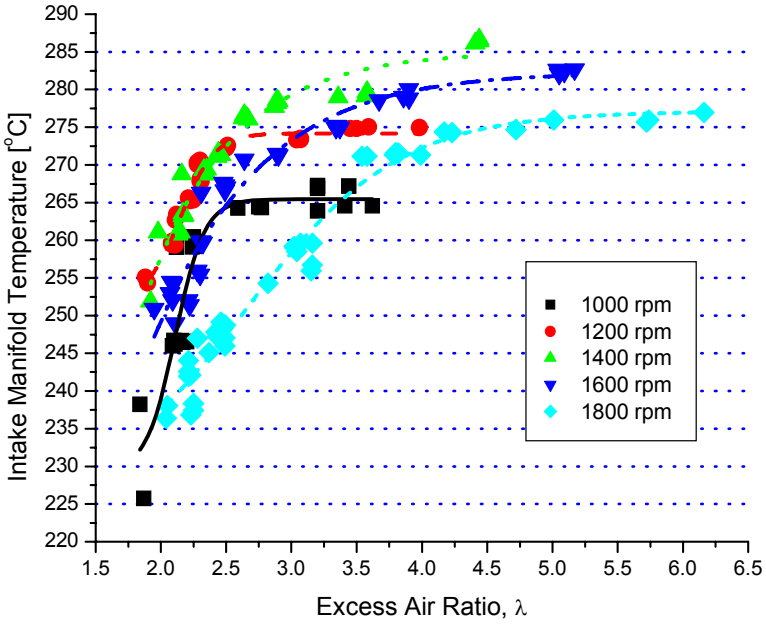

Figure 10 Intake manifold temperature versus excess air ratio (λ) for various engine speeds

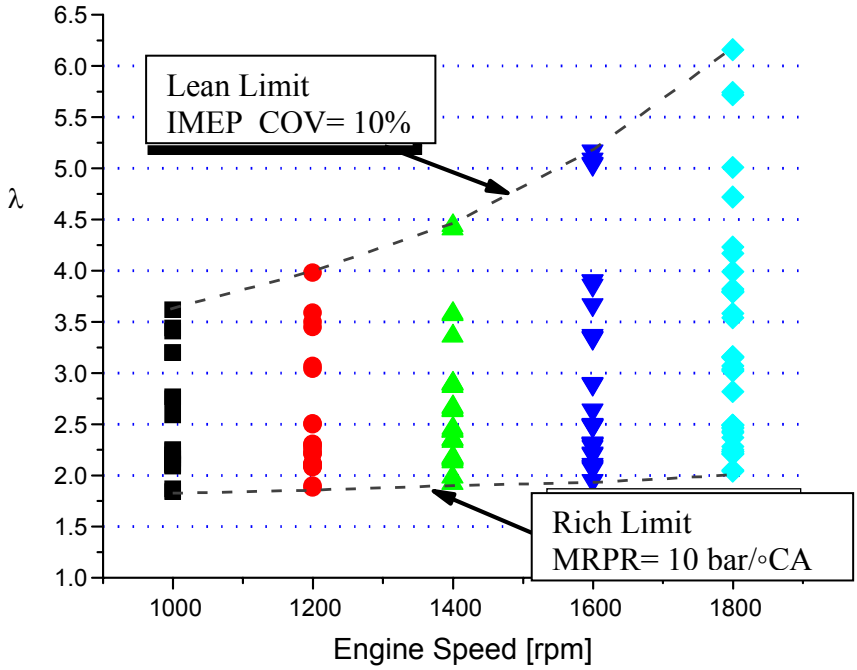

Figure 11 Excess air ratio (λ) versus engine speed (rpm)

Figure 12 shows the indicated mean effective pressure (IMEP) versus the engine speed for the NA conditions. The highest IMEP achievable was approximately 4 bar and the lowest IMEP was about 0.7 bar for the conditions tested. The highest IMEP was not affected much with the

engine speed; however, the lowest IMEP decreased with the engine speed, particularly between the engine speeds of 1200 and 1600 rpm. In contrast, the brake mean effective pressure (BMEP) decreased almost linearly with the engine speed as shown in Figure 13, which led to a narrow operating regime of positive power output at higher engine speeds. Higher BMEP was attained at the lowest engine speed which was because the magnitude of the PMEP increased linearly with the engine speed (see Figure 14) and the friction mean effective pressure (FMEP) also increased almost linearly with the engine speed (see Figure 15). FMEP also increased linearly with the AFR (see Figure 15 – right). Therefore, the lowest BMEP was observed at the highest engine speed and the leanest AFR at that speed. It should be noted here that this observation agrees only with NA operating conditions. Boosted intake charge will change all these observations because PMEP and FMEP become almost negligible or a small portion of the energy balance at boosted conditions.

Figure 16 shows the coefficients of variance (COV) of IMEP versus λ for various engine speeds. IMEP_COV exponentially increased with λ at 1000 rpm and it less rapidly increased with λ as the engine speed increased. This resulted in narrow operating regime at lower engine speed.

Figure 17 shows the maximum rate of pressure rise (MRPR) versus λ for various engine speeds. The MRPR exponentially decreased with λ and remained constant after it reached approximately 1. Although there are slight deviations at 1800 rpm, the MRPR seems to be independent of the engine speed and λ at which the MRPR is constant seems almost the same for all engine speeds. Some knocking sound started when the MRPR reached above 8 or 9.

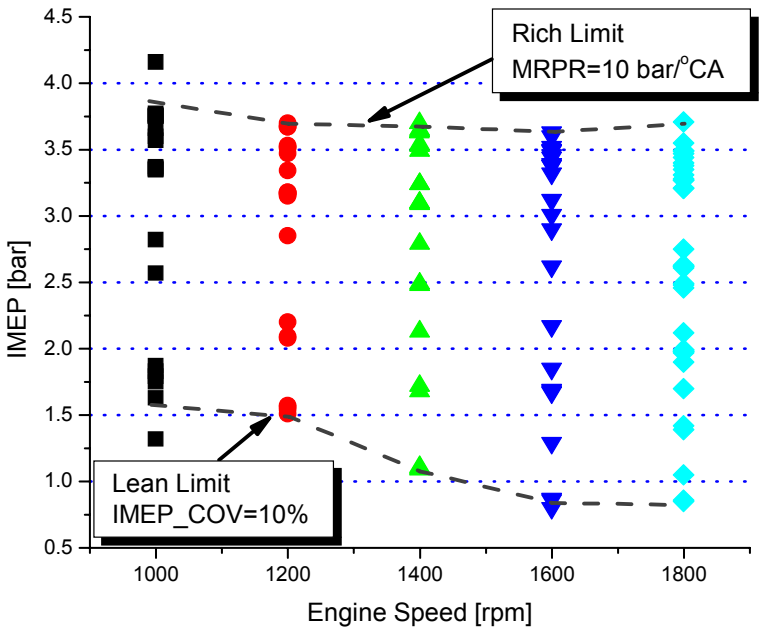

Figure 12 Indicated mean effective pressure (IMEP) versus engine speed (rpm)

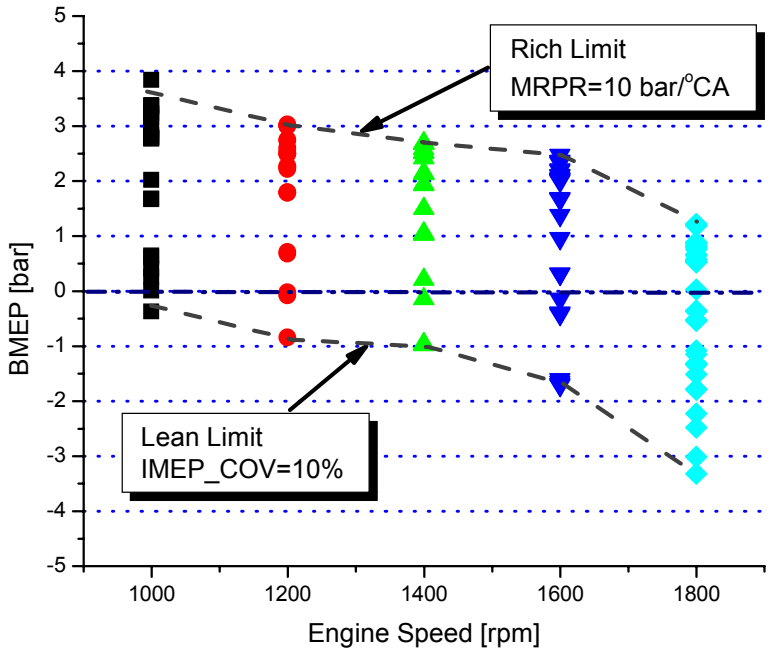

Figure 13 Brake mean effective pressure (BMEP) versus engine speed (rpm)

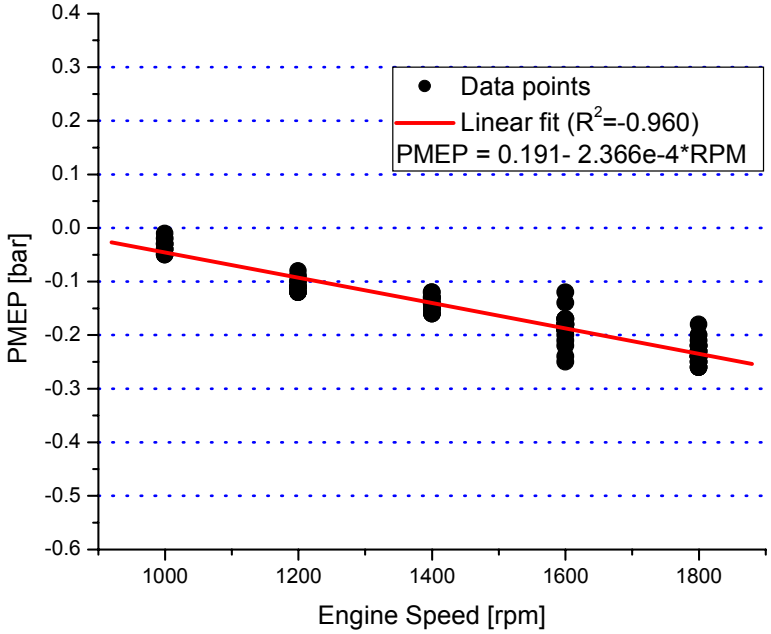

Figure 14 Pumping mean effective pressure (PMEP) versus engine speed (rpm)

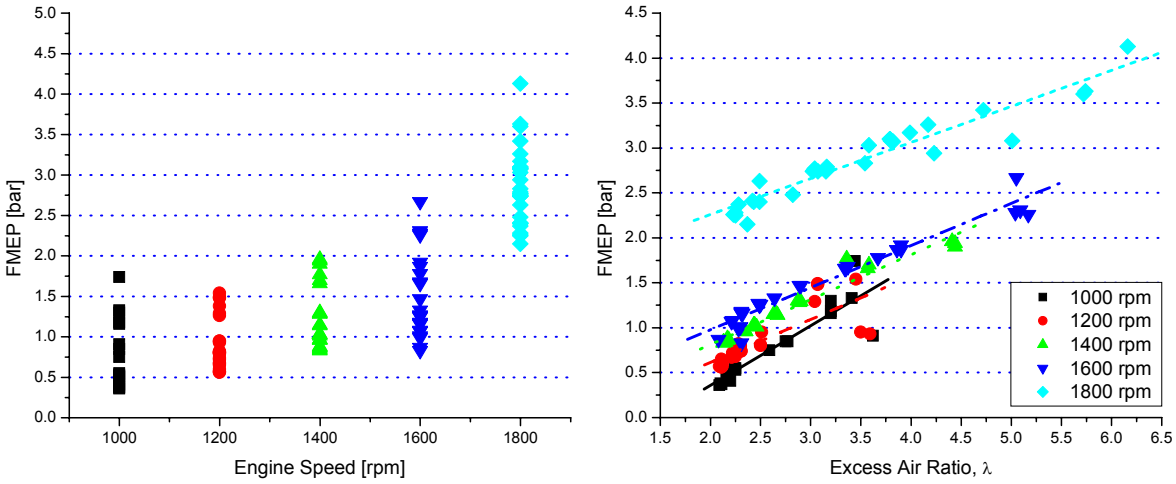

Figure 15 Friction mean effective pressure (FMEP) versus engine speed (rpm) (left) and excess air ratio (λ) (right)

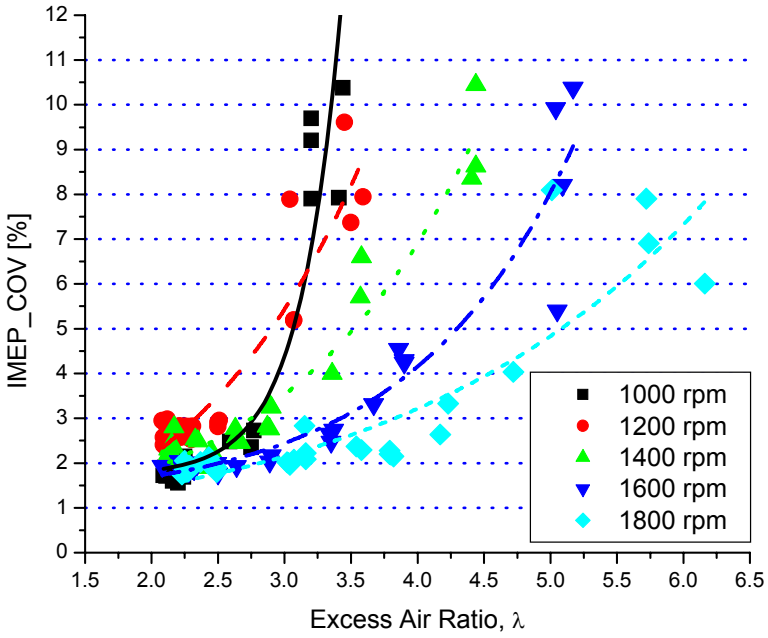

Figure 16 Coefficients of variance (COV) of IMEP versus excess air ratio (λ) for various engine speeds

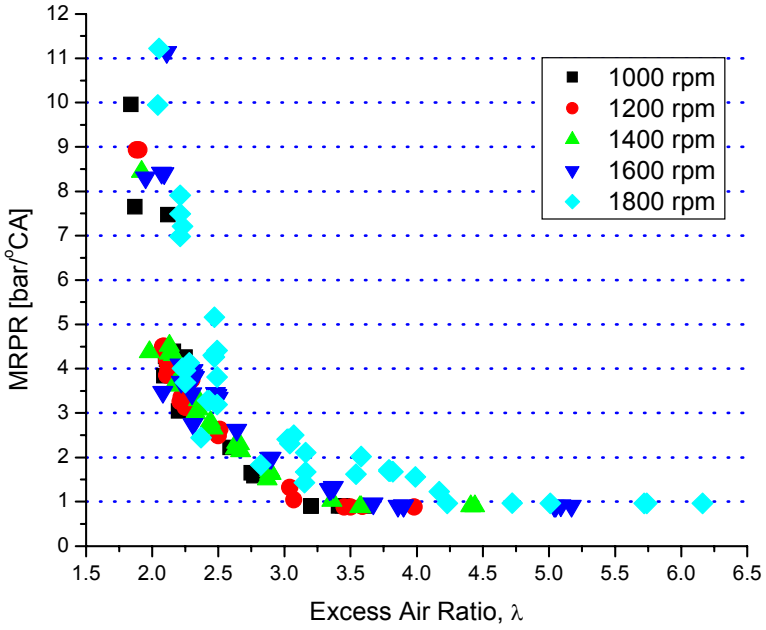

Figure 17 Maximum rate of pressure rise (MRPR) versus excess air ratio (λ) for various engine speeds

In contrast, the knock intensity was dependent on the engine speed as shown in Figure 18. The knock intensity decreased more rapidly as the engine speed increased. Engine knock was observed when the knock intensity was above 15. Data at knocking were not plotted in this figure in order to obtain exponential relationship between the knock intensity andλ.

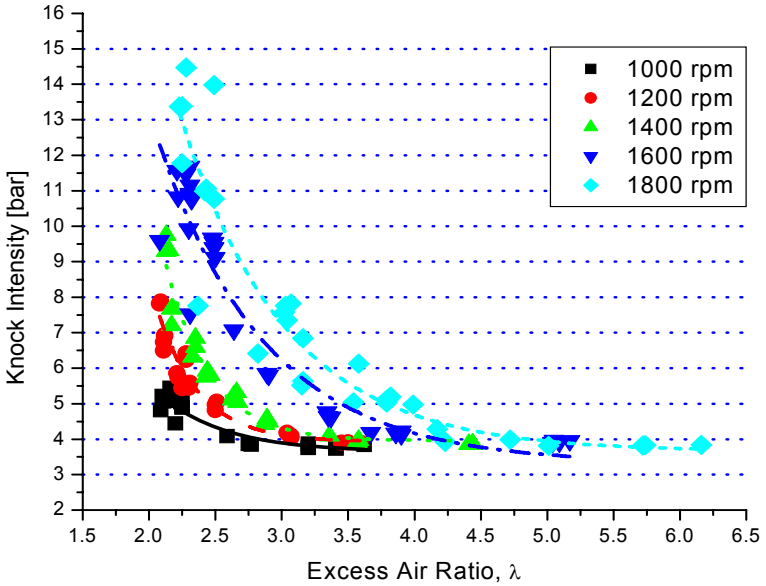

Figure 18 Knock intensity versus excess air ratio (λ) for various engine speeds

The location of peak in-cylinder pressure (PPL) was kept within 6 to 10°ATDC as shown in Figure 19, which resulted in the start of combustion (SOC) within -4 to 0°ATDC (see Figure 20). However, it was difficult to keep the PPL within the specified range at the operating conditions

of lean and rich limits. Figures 19 and 20 confirm that the PPL advanced at the lean limit. This is because the fired peak pressure was almost the same or slightly lower than the motored peak pressure.

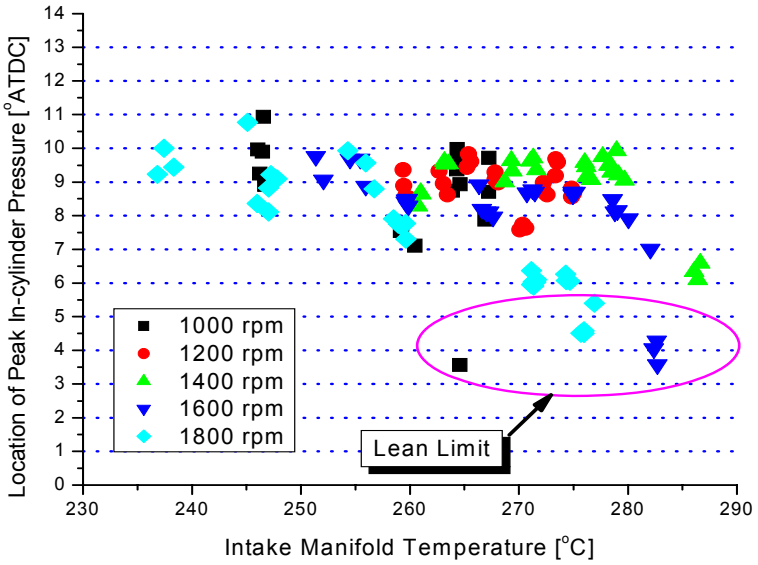

Figure 19 Location of peak in-cylinder pressure (PPL) versus intake manifold temperature for various engine speeds

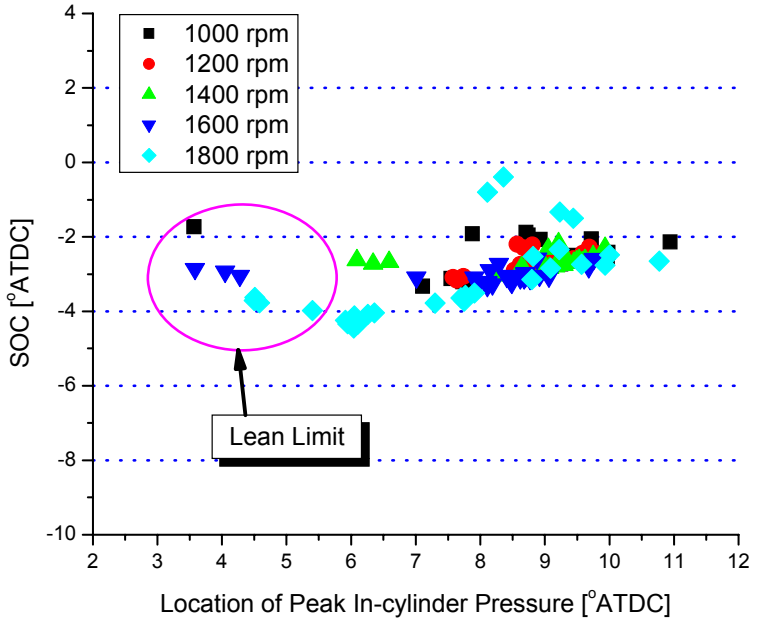

Figure 20 Start of combustion (SOC) versus location of peak in-cylinder pressure (PPL) for various engine speeds

HCCI Engine Performance

Figure 21 shows the combustion efficiency (%) versus λ of the HCCI engine for various engine speeds. The combustion efficiency was not greatly different at knock limit of the HCCI engine.

Higher engine speed showed higher combustion efficiency and the location of the peak combustion efficiency for each engine speed moved to the leaner side with the engine speed. The combustion efficiency of the HCCI engine was about 74% at knock limit for all engine speeds and about 84% at λ≈6 for the engine speed of 1800 rpm. The highest combustion efficiency (i.e. ~92.5%) was attained at λ≈4.2 for the engine speed of 1800 rpm.

Figure 22 shows the indicated thermal efficiency (ITE) versus λ for various engine speeds. The ITE decreased in a parabolic manner and the highest ITE was observed at close to the knock limit, which was about 42%. The ITE decreased rapidly with λ at 1000 rpm and it decreased slowly as the engine speed increased. The highest ITE was approximately 37% at 1000 rpm. The ITE at the lean limit was between 21% and 26% for all engine speeds. In contrast, the brake thermal efficiency (BTE) decreased linearly with λ and it was independent of the engine speed except for 1800 rpm (see Figure 23), in which the friction loss increased rapidly (see Figure 15). Again, it should be noted that this trend will be different for turbocharged or supercharged engines. This observation is only valid for NA engines. Boosted intake charge will increase the efficiency of the HCCI engine, especially in the lean side.

In Figure 24, the indicated specific fuel consumption (ISFC) increased exponentially withλ. Again, the ISFC increased more rapidly at lower engine speeds and it slowed down as the engine speed increased. The lowest ISFC was observed at close to the knock limit at 1000 rpm; however, it slowly moved to the leaner side as the engine speed increased.

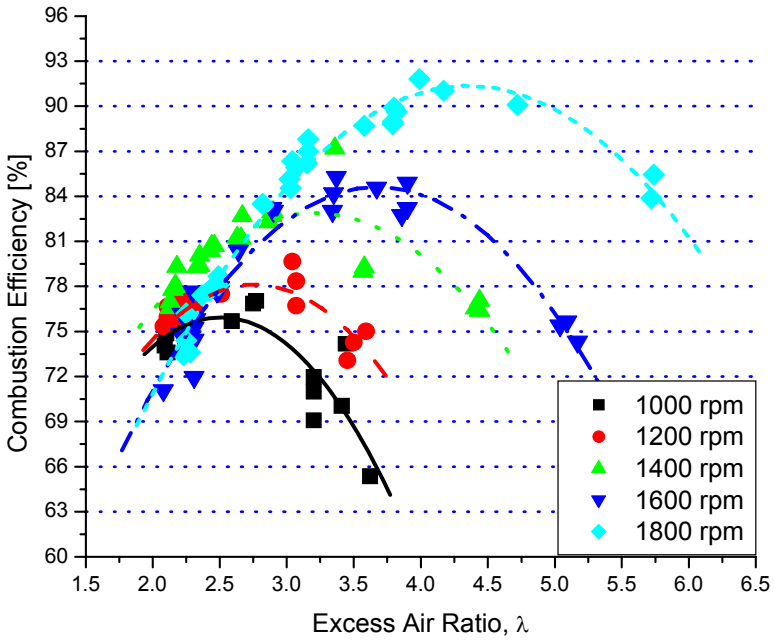

Figure 21 Combustion efficiency (%) versus excess air ratio (λ) for various engine speeds

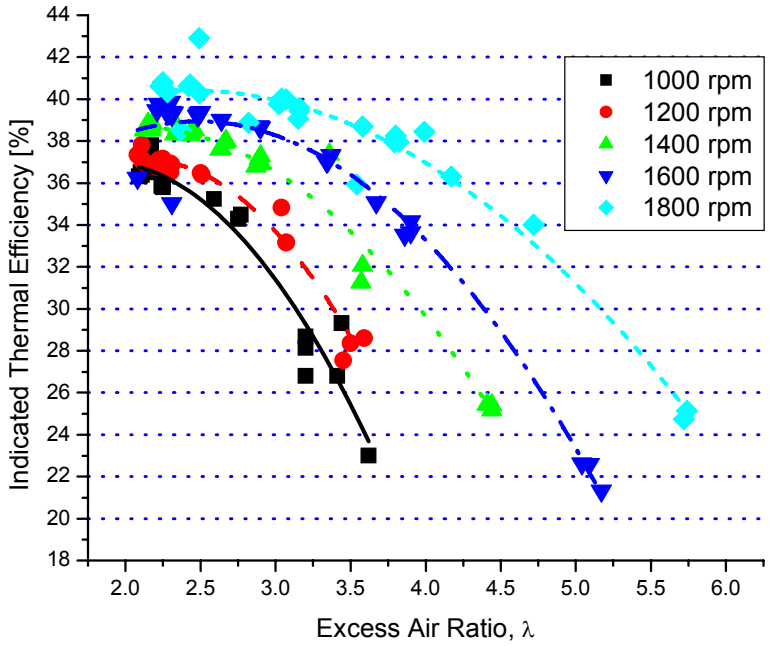

Figure 22 Indicated thermal efficiency (ITE) versus excess air ratio (λ) for various engine speeds

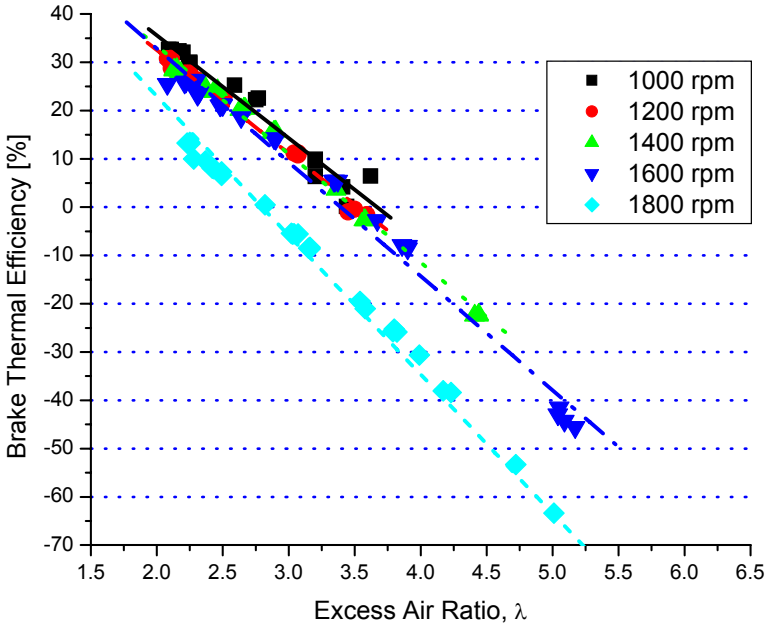

Figure 23 Brake thermal efficiency (BTE) versus excess air ratio (λ) for various engine speeds

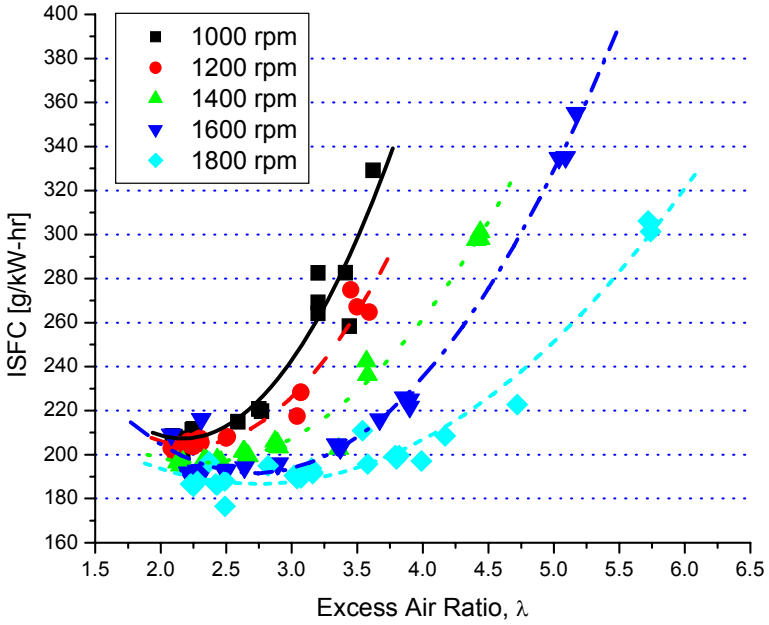

Figure 24 Indicated specific fuel consumption (ISFC) versus excess air ratio (λ) for various engine speeds

HCCI Engine Emissions

Figure 25 shows oxides of nitrogen (NOx) emissions versus λ for various engine speeds. NOx emissions were independent of the engine speed. It exponentially decreased and stayed constant close to 0 as λ increased above 3.5. The inset zoomed in Figure 25 to highlight the NOx emissions below 10 ppm. NOx emissions became below 5 ppm when λ was above approximately 2.7. This result indicates that NOx emissions are more a function of AFR rather than engine speed in a HCCI engine fueled with natural gas when it is controlled to maintain the peak location of in-cylinder pressure within 6~10°ATDC. Figure 26 shows NOx emissions and its curve fitting; and the curve fitted equation is shown in Equation 1 as well. This equation will work for a HCCI engine fueled with natural gas and followed the operating procedure described earlier. Its accuracy will get lower when λ≤2.5 because NOx emissions exponentially increase withλ.

$$\mathrm{NOx[ppm]} = -0.03 + 5\times10^{6}\, e^{(-\lambda/0.198)} \qquad \text{(Equation 1)}$$

Figure 27 shows carbon monoxide (CO) emission versus λ for various engine speeds. CO emission was less dependent on the engine speed at close to the knock limit; however, it became significantly dependent on the engine speed as λ increased. Again, CO emission increased exponentially with λ and it was more rapid at lower engine speed.

In Figure 28, total hydrocarbon (THC) emissions increased in a 2nd order polynomial manner with λ with lower engine speed increasing more rapidly. As the engine speed increased, the minimum point moved to the leaner side. In the case of 1800 rpm, the minimum CO emission was observed at λ≈3.8. Since methane (CH_4) emission consists of about 80~85% of the THC emissions, CH_4 emission showed the same trend as the THC emissions as shown in Figure 29.

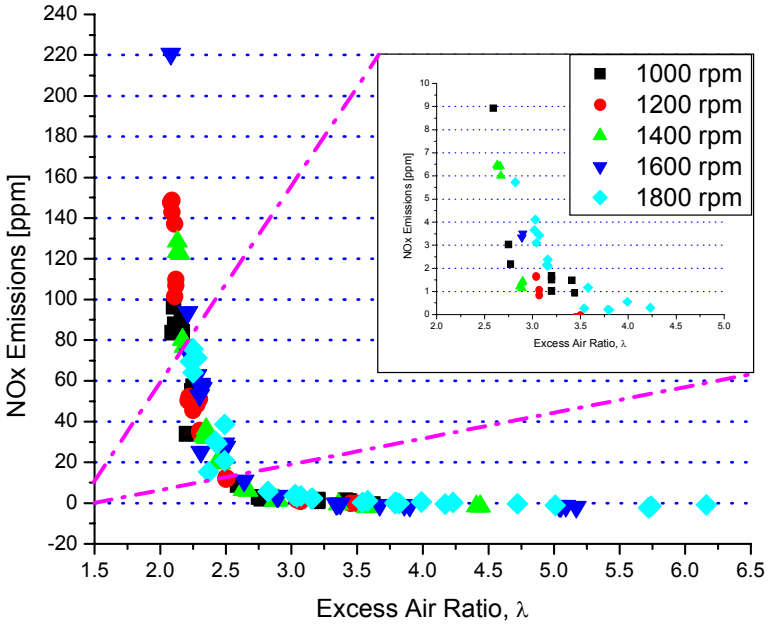

Figure 25 Oxides of nitrogen (NOx) emissions versus excess air ratio (λ) for various engine speeds

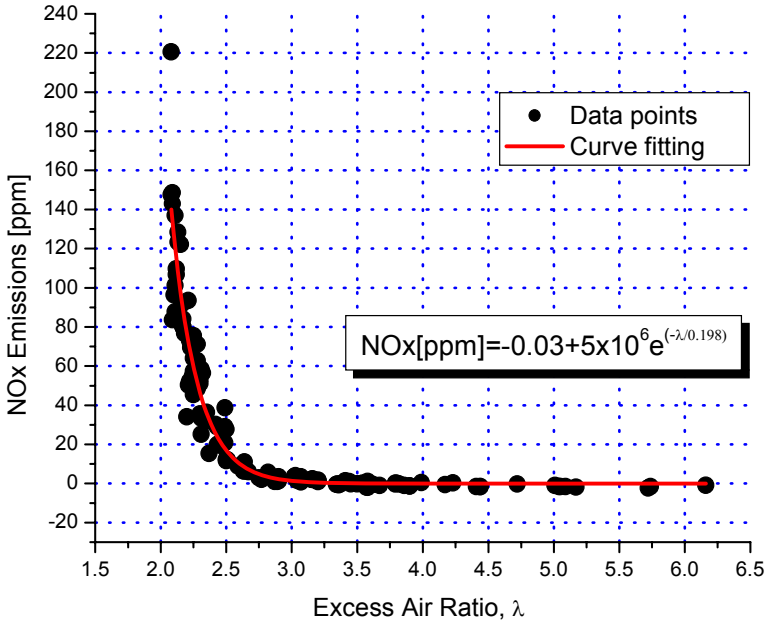

Figure 26 Oxides of nitrogen (NOx) emissions versus excess air ratio (λ) for various engine speeds: data points and curve fit

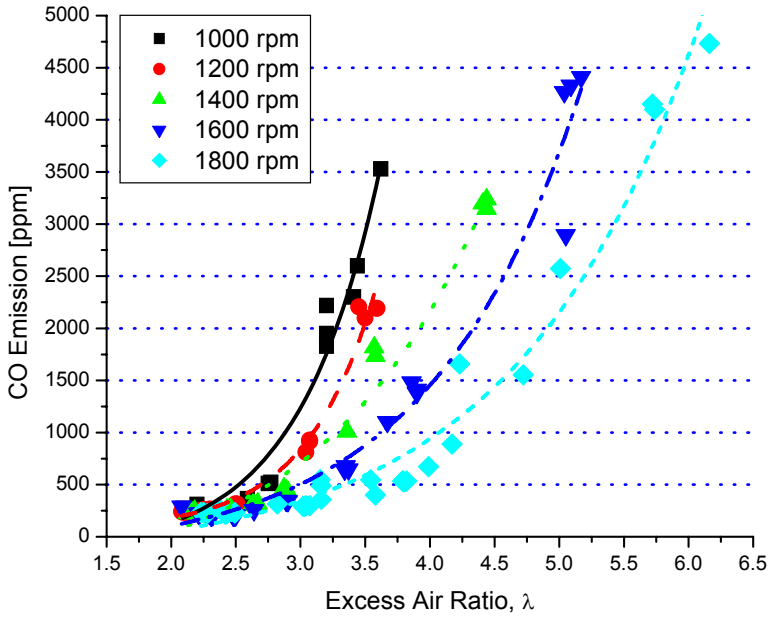

Figure 27 Carbon monoxide (CO) emission versus excess air ratio (λ) for various engine speeds

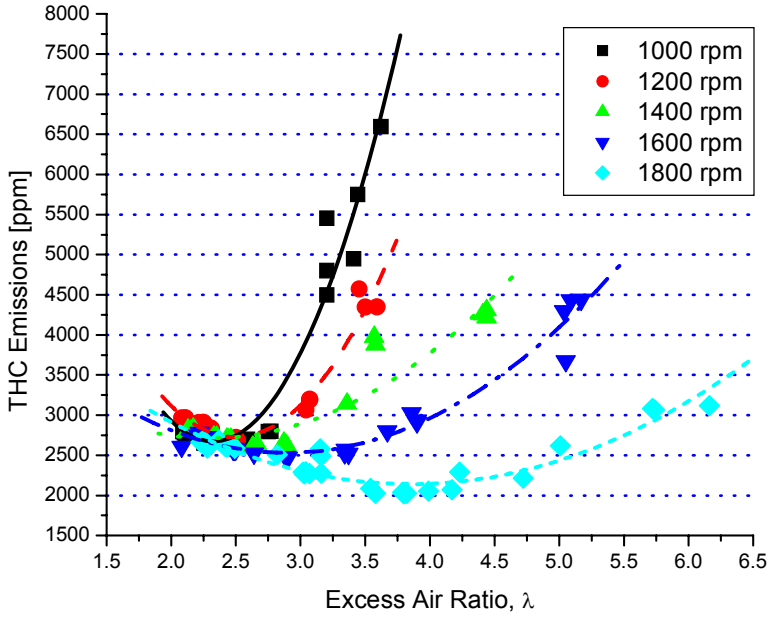

Figure 28 Total hydrocarbon (THC) emissions versus excess air ratio (λ) for various engine speeds

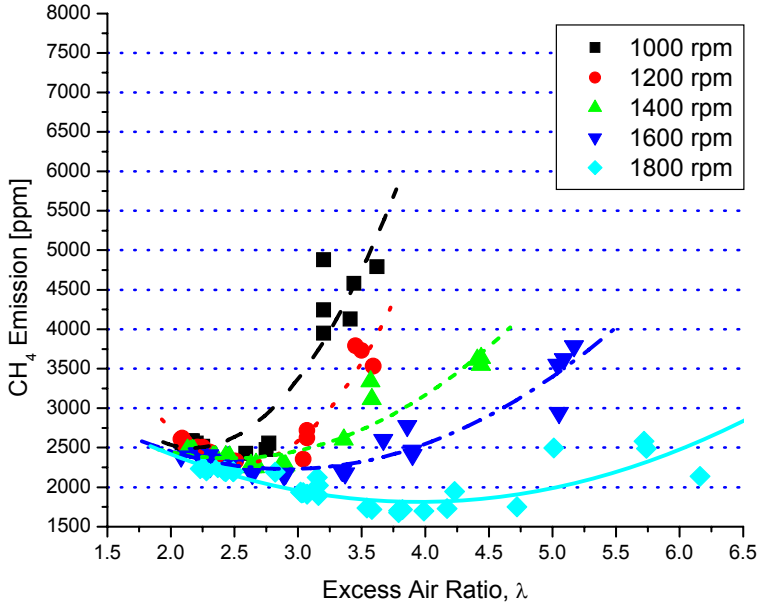

Figure 29 Methane (CH_4) emission versus excess air ratio (λ) for various engine speeds

Figure 30 shows carbon dioxide (CO_2) emission versus λ for various engine speeds. CO_2 was about 4% at close to the knock limit and it decreased in a 2nd order polynomial manner as λ increased. Although higher engine speeds showed slower decrease in CO_2 with increasingλ, CO_2 was slightly dependent on the engine speed. CO_2 was about 0.7% at close to the lean limit. Oxygen (O_2) increased in a Boltzmann function manner with increasing λ as shown in Figure 31. Again, although O_2 increased more rapidly at lower engine speeds, it was slightly dependent on the engine speed.

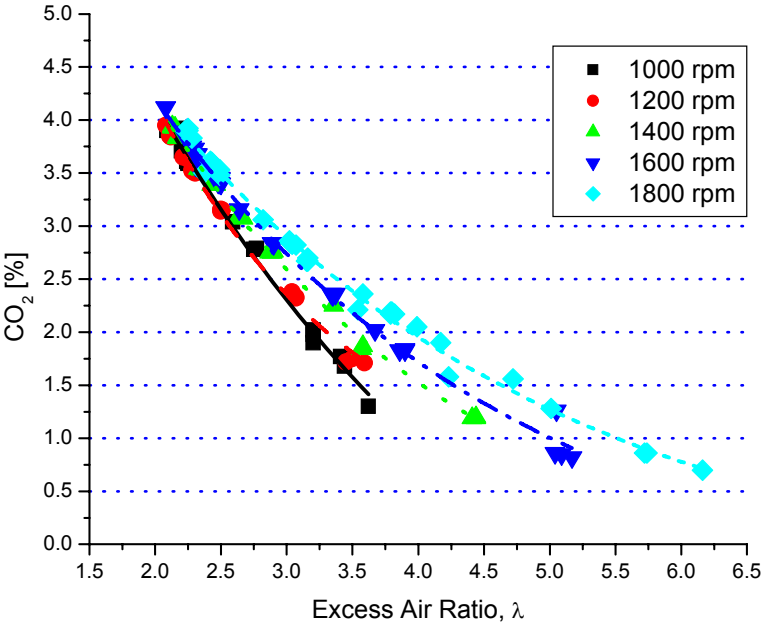

Figure 30 Carbon dioxide (CO_2) emission versus excess air ratio (λ) for various engine speeds

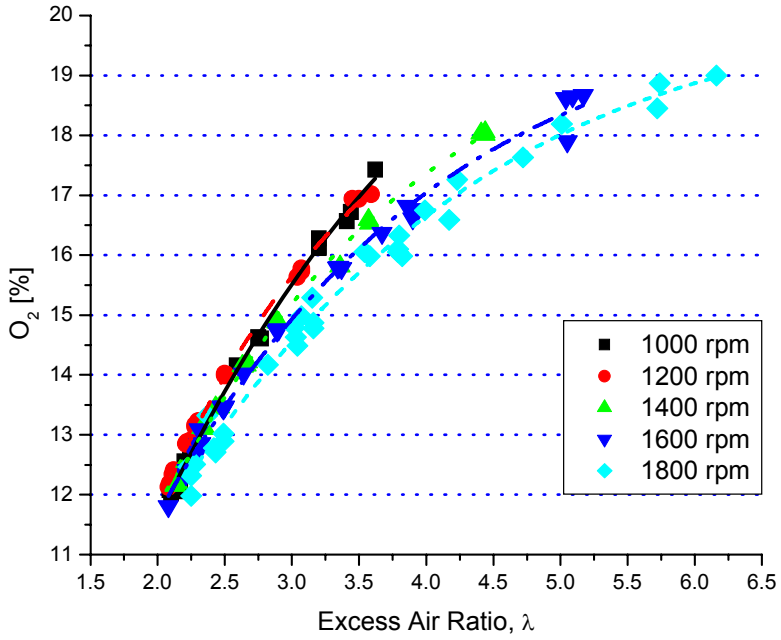

Figure 31 Oxygen (O_2) versus excess air ratio (λ) for various engine speeds

HCCI Engine Combustion-1200 rpm-Naturally Aspirated

In this section, although the same data were taken for all the speeds tested in the project, data will be presented only at 1200 rpm. Data and plots for 1800 rpm are presented later for both naturally aspirated and boosted conditions. Figure 32 shows the in-cylinder pressure versus crank angle for various λ at 1200 rpm. The location of the peak in-cylinder pressure was maintained within 6 to 8°ATDC. It is obvious that the combustion occurred more rapidly as λ decreased (or equivalence ratio (ϕ) increased). Figure 33 shows the rate of heat release (ROHR) versus crank angle for various λ at 1200 rpm. Although combustion started at almost the same crank angle or at least within a couple of crank angle degrees, heat released more rapidly with decreasingλ. Combustion duration was about 40 degrees and it was almost the same for all the excess air ratios; however, the main combustion duration became shorter and the peak heat release increased sharply as λ decreased. Figure 34 shows the heat release (HR) versus crank angle for various λ at 1200 rpm, which is another way of looking heat release phenomena. It was observed that although the starting and ending points were similar to all the excess air ratios tested, the main combustion regions showed much faster combustion with decreasingλ. After the rapid combustion, the tails of the combustion were again similar to all the excess air ratios tested. Figure 35 obviously shows this trend, which represents 10%, 50%, 90% heat release (HRCA10, HRCA50, and HRCA90) versusλ. HRCA10 slightly advanced as λ decreased; however, HRCA50 rapidly advanced with decreasingλ. HRCA90 was not noticeably varied with varyingλ.

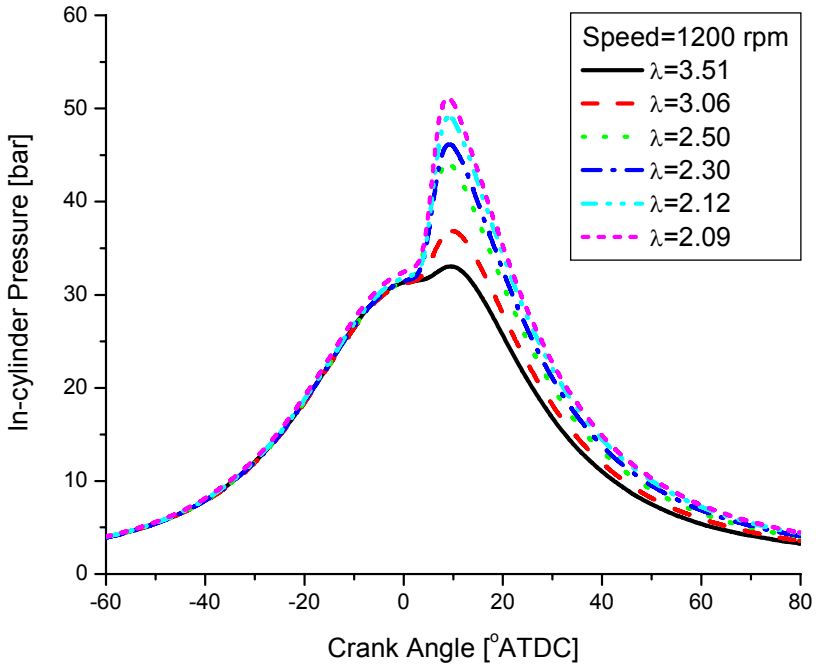

Figure 32 In-cylinder pressure versus crank angle for various excess air ratios at 1200 rpm

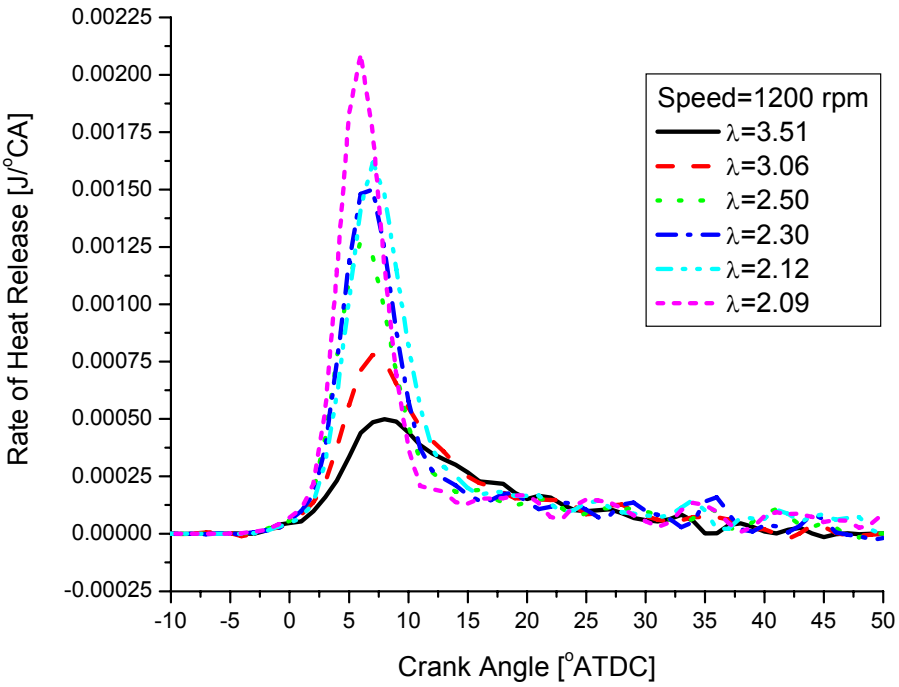

Figure 33 Rate of heat release (ROHR) (10^{-5}) versus crank angle for various excess air ratios at 1200 rpm

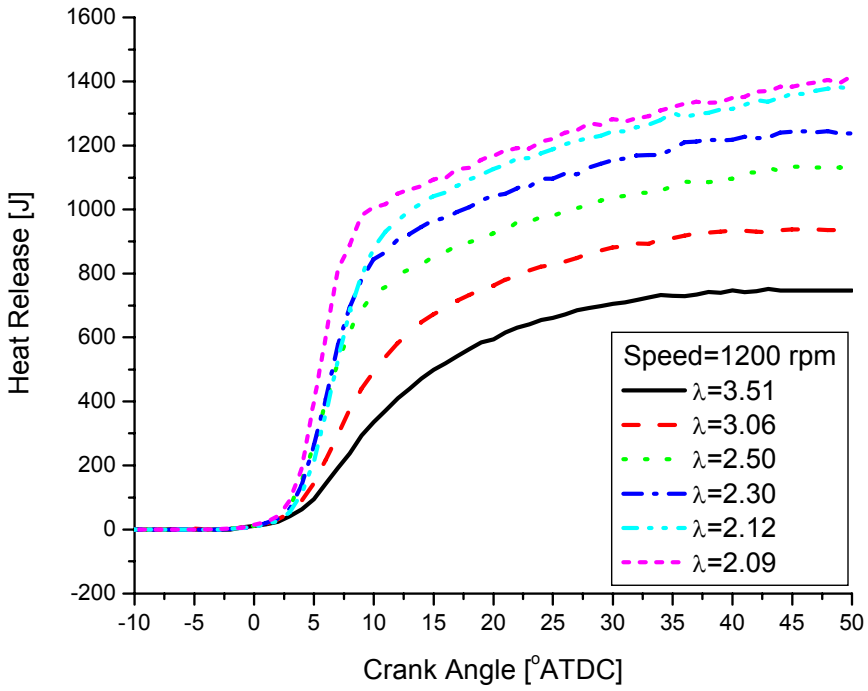

Figure 34 Heat release (HR) versus crank angle for various excess air ratios at 1200 rpm

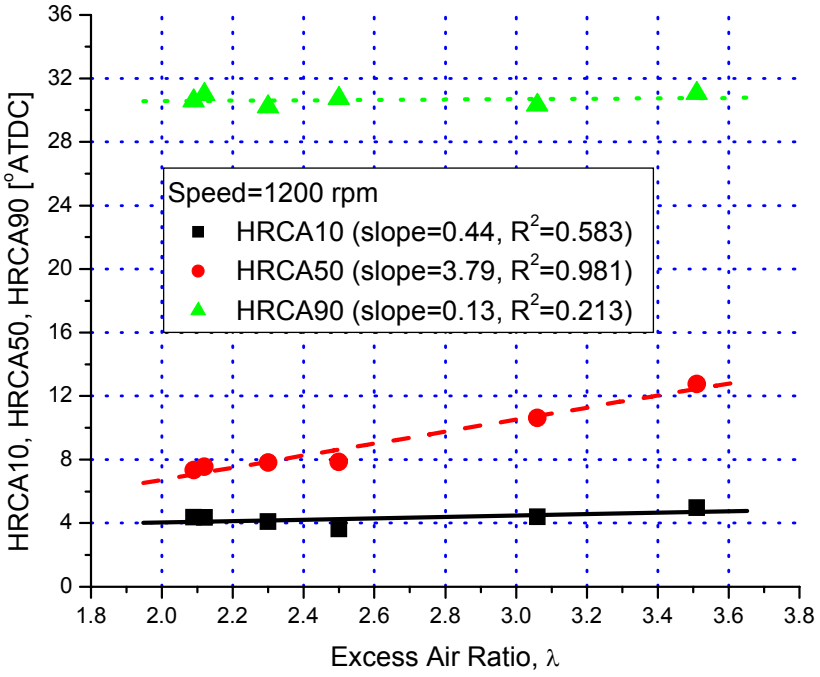

Figure 35 HRCA10, HRCA50, and HRCA90 versus excess air ratios at 1200 rpm

Summary-Naturally Aspirated (NA) Conditions

HCCI engine configuration was successfully completed for NA conditions. Use of the PPL was a good indicator for controlling the HCCI engine fueled with natural gas. The PPL was controlled by using the intake charge temperature, which is only valid when the oil and coolant temperatures are kept constant. With this strategy, consistent data were taken. Although excellent data sets were taken with NA conditions in this task, a HCCI engine should be used with a turbocharger or supercharger in order to produce reasonable power output.

HCCI engine testing with boosted intake charge

Approach

Homogeneous charge compression ignition (HCCI) combustion phasing was controlled with intake temperature. Peak pressure location (PPL) was maintained within 6 to 10°ATDC in order to produce the highest thermal efficiency at each operating condition. We found the linear relationship between indicated mean effective pressure (IMEP) and fuel flow rate as shown in Figure 37. Fuel flow rate could be increased with increasing intake pressure. This enabled us to extend the acceptable HCCI operating regime to higher loads.

The required intake air temperature increased logarithmically with increasing excess air ratio as shown in Figure 38. For the highest efficiency operating conditions, intake temperature showed a non-linear relationship with excess air ratio. Data presented in Figure 39 indicates that IMEP has a linear relationship with intake pressure. We believe that this is because more fuel could be burnt when the excess air ratio was kept constant. Therefore, it is better to increase the intake pressure as high as practicable in order to attain higher engine loads in HCCI engines.

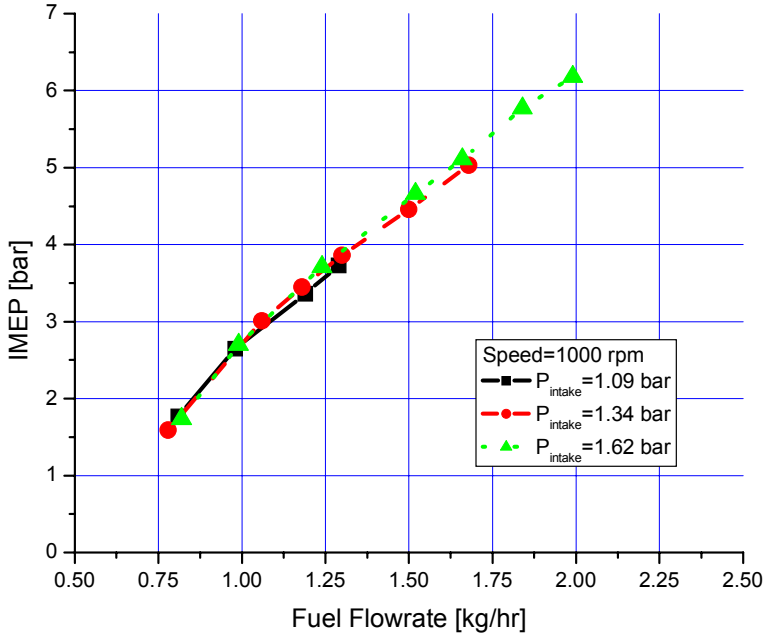

Figure 37 Indicated mean effective pressure versus fuel flow rate

The required intake air temperature increased with the engine speed up to 1300 rpm and then it decreased with increasing engine speed for the same excess air ratio as shown in Figure 40. As the engine speed increases, more air is inducted into the combustion chamber. Therefore, higher intake temperature is required. However, as the engine speed increased, there was less time for heat transfer through the cylinder walls. Thus, there was a trade-off between required intake temperature and heat transfer when the combustion phasing was controlled for the highest thermal efficiency.

Data reported in Figure 41 indicates that the required intake temperature decreases as the intake pressure increases. This implies that the required thermal energy for HCCI combustion is the same regardless of intake pressure. This result shows that using a turbocharger or supercharger will be an advantage for HCCI engines. Higher intake pressure will lead to higher attainable engine loads and require lower intake temperature.

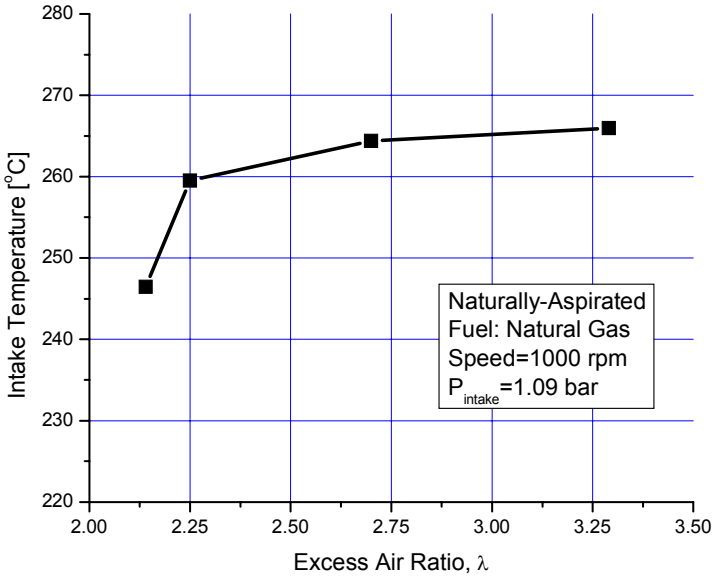

Figure 38 Intake temperature versus excess air ratio

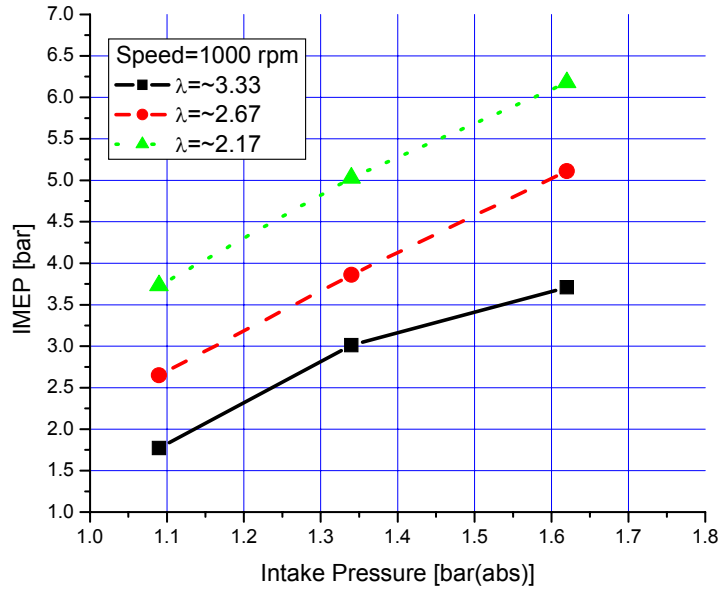

Figure 39 Indicated mean effective pressure versus intake pressure

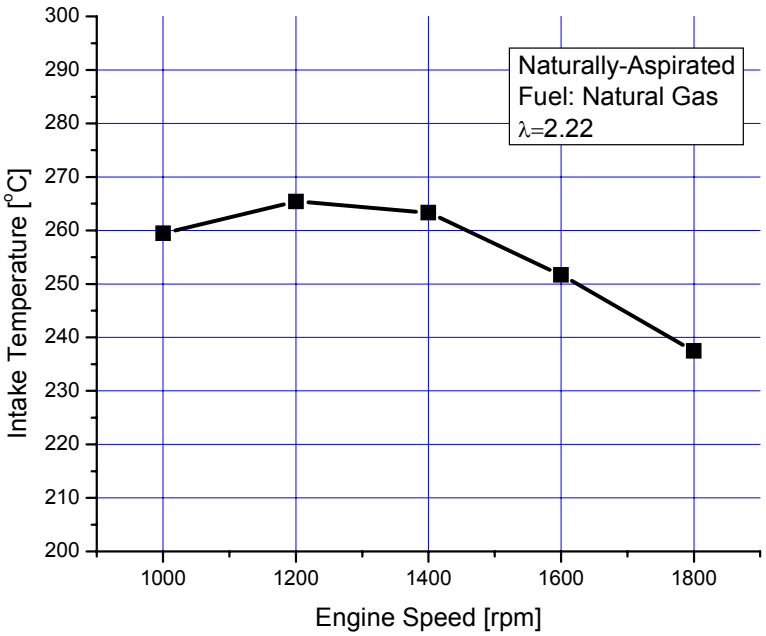

Figure 40 Intake temperature versus engine speed

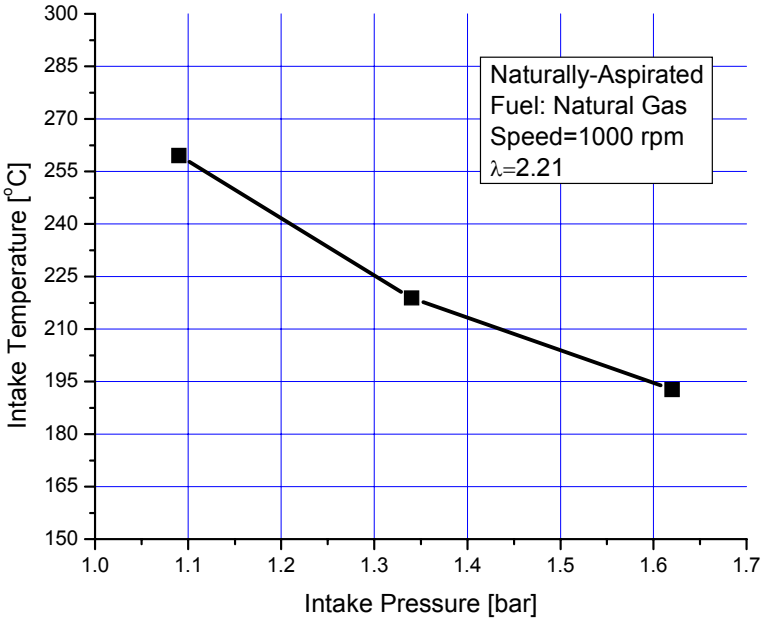

Figure 41 Intake temperature versus intake pressure

Effect of Intake Boost on HCCI Engine Performance-1800 rpm

The HCCI engine was operated under various excess air ratios ranging from lean limit (i.e. misfiring) to rich limit (i.e. knocking) and at the engine speeds of 1000, 1200, 1400, 1600, and 1800 rpm. Data taken at 1800 rpm, the normal rated speed of commercial gas engines used in power generation, are presented in the body of this report. Results at 1000 rpm are included in the Appendix.

The engine was operated under several different loads at a rated speed of 1800 rpm. The intake temperature of the air/fuel mixture was used to control the SOC of the HCCI engine. Oil and coolant temperatures were set at 100°C. Intake boost pressure was increased to 2.5 bar absolute to increase engine power output.

Location of peak in-cylinder pressure (PPL) was maintained within 6~9° ATDC to obtain maximum thermal efficiency by initiating the SOC close to top dead center (TDC). This resulted in the linear relationship between NMEP and fuel flow rate as shown in Figure 42. This result indicates that higher fuel supply will lead to higher power density. However, this is limited by engine knocking. Excess air ratio should be kept above a minimum to prevent engine knocking. NMEP is proportional to intake boost pressure as shown in Figure 43. This result clearly shows that intake boosting is highly beneficial in HCCI engines to increase power density. Another advantage of higher boost pressure is a lower intake temperature required for HCCI combustion, as shown in Figure 44. As the intake boost pressure increased, the required intake temperature decreased linearly. The required intake temperature decreased about 90°C when the intake pressure increased from about 1 bar to 2.5 bar.

Data reported in Figure 45 shows that higher excess air ratio requires higher intake temperature. For example, increasing excess air ratio from 2.5 to 5.4 increased the required intake temperature approximately 40°C when the intake pressure was 1.6 bar. The required intake temperature increased logarithmically with increasing excess air ratios when the PPL was maintained within 6-9° ATDC. The required temperature reached an asymptote when a certain excess air ratio was reached at constant intake pressure.

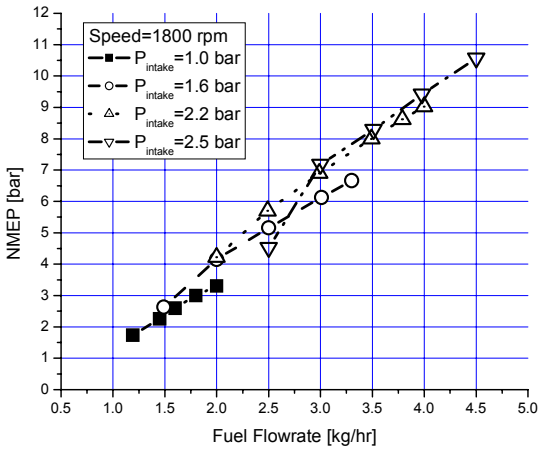

Figure 42 NMEP versus fuel flow rates

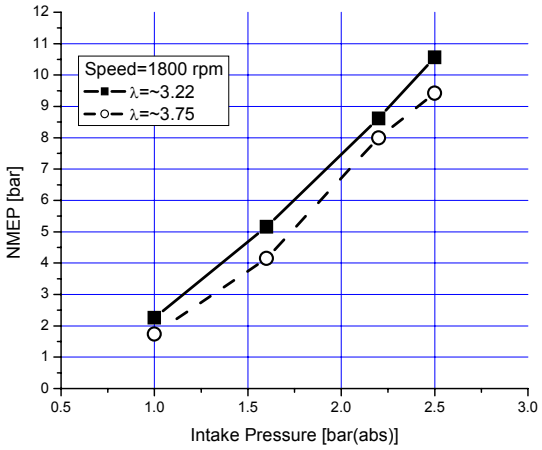

Figure 43 NMEP versus intake pressures

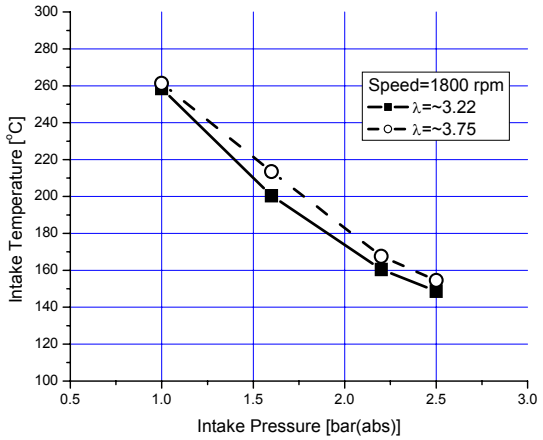

Figure 44 Intake temperatures versus intake pressures

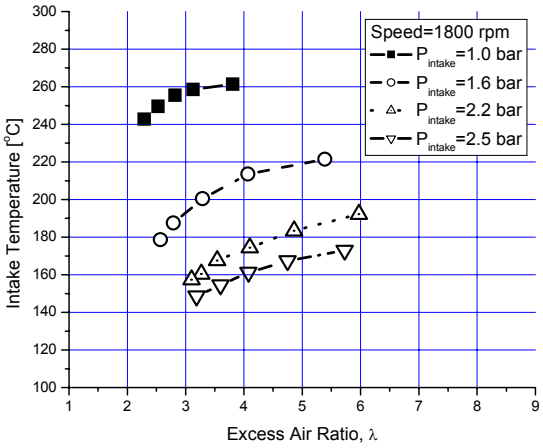

Figure 45 Intake temperatures versus excess air ratios

Figure 46 shows the intake temperature versus fuel flow rate. The required intake temperature decreased linearly with increasing fuel flow rates. However, this was dependent on intake pressure. As mentioned earlier, a higher intake pressure required a lower intake temperature.

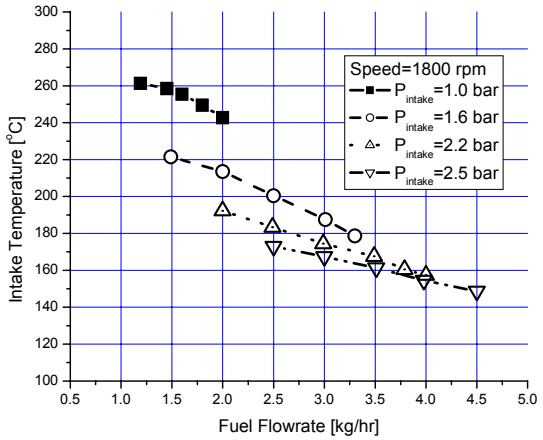

Figure 46 Intake temperatures versus fuel flow rates

The coefficients of variations of IMEP (IMEP_COV) and maximum rate of pressure rise (MRPR) were used as criteria for determining the operating regime of the HCCI engine. The IMEP_COV of 10% was used to define the lean limit or misfiring; and, the MRPR equal to 10 bar/°CA was used to determine the knocking limit (in addition to auditory indicators). The IMEP_COV of 9 to 10% was a good indicator of misfiring for the engine and operating conditions tested in this research as shown in Figure 47. The MRPR equal to 10 bar/°CA was consistent with the auditory evidence of knocking except for the intake pressure of 1 bar which is shown in Figure 48. The error bars in both figures are standard deviations.

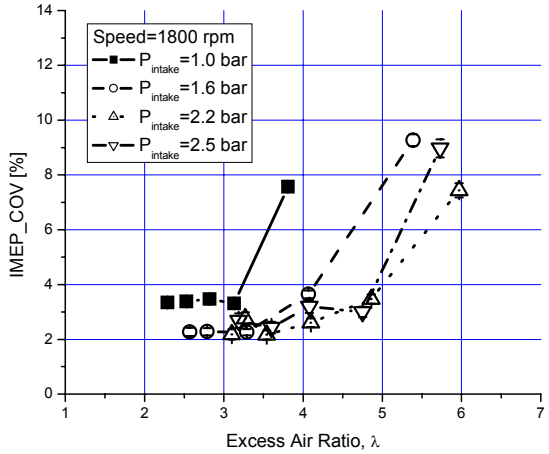

Figure 47 IMEP_COV versus excess air ratios for various intake pressures

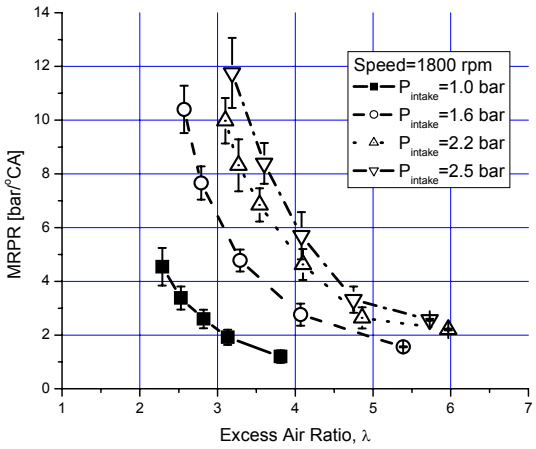

Figure 48 MRPR versus excess air ratios for various intake pressures

Combustion Analysis-1800 rpm

Figure 49 shows the cylinder pressure and rate of heat release (RoHR) with crank angle degrees (CAD) at the excess air ratio of approximately 3.22 for various intake pressures. The PPL was well maintained between 8 and 9° ATDC for the conditions shown in the figure. The overall combustion duration was virtually independent of the intake pressure; however, the rapid combustion duration was significantly dependent on the intake pressure.

Figure 50 shows the 10-90% burn duration as a function of the excess air ratios. The 10-90% burn duration was independent of the intake pressure except for the intake pressure of 1 bar and had a negligible dependence on the intake pressure when the excess air ratio was above 3 even for the intake pressure of 1 bar.

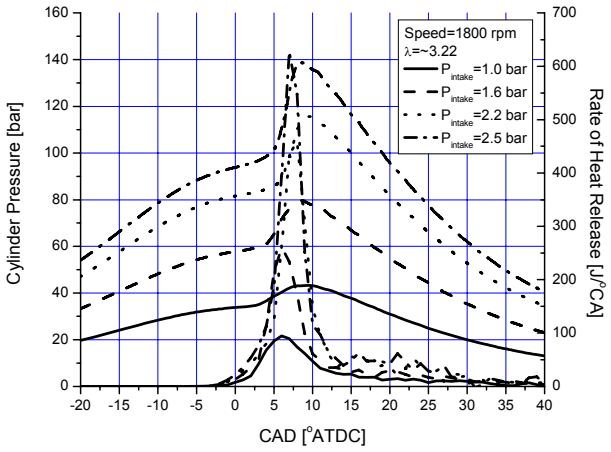

Figure 49 Cylinder pressure and rate of heat release versus crank angle for various intake pressures

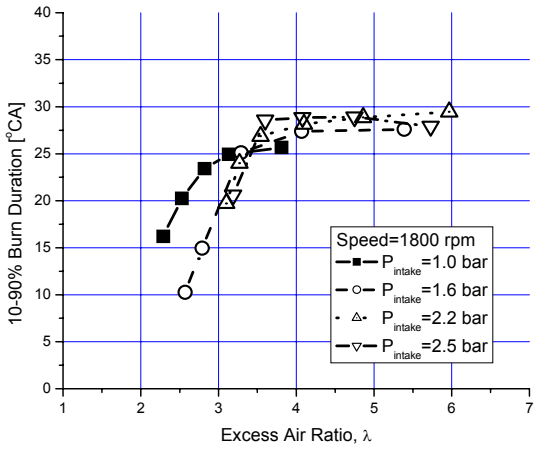

Figure 50 Plot of 10-90% burn duration versus excess air ratios for various intake pressures

Engine Performance-1800 rpm

In Figure 51, NMEP decreased linearly with increasing excess air ratios and increased proportionally with intake boost pressures. The highest NMEP was 10.6 bar at the intake pressure of 2.5 bar. The increasing intake pressure extended the lean operating regime of the HCCI engine. The higher intake pressure moved the audible knocking and misfiring (detected by pressure trace) limits to higher excess air ratios; but, the misfiring limit was extended further than the knocking limit.

Figure 52 shows the indicated specific fuel consumption (ISFC) versus excess air ratio at constant intake pressures. It should be noted that the power required to boost the intake pressure was not considered in the ISFC. It is clear that the intake boosting maintained low ISFC to higher excess air ratios than the naturally-aspirated (NA) conditions. The ISFC was similar for the intake pressures of 2.2 and 2.5 bar, for λ values less than 5.

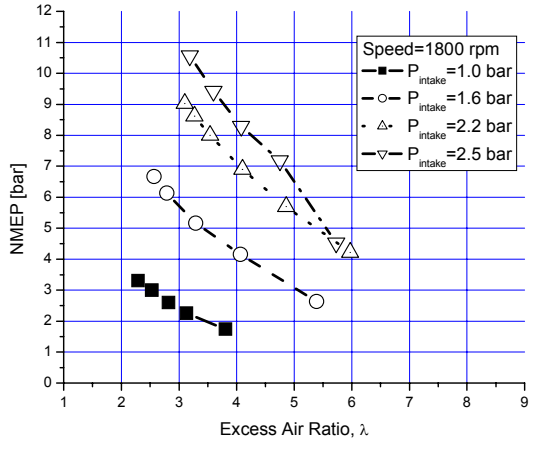

Figure 51 NMEP versus excess air ratios for various intake pressures

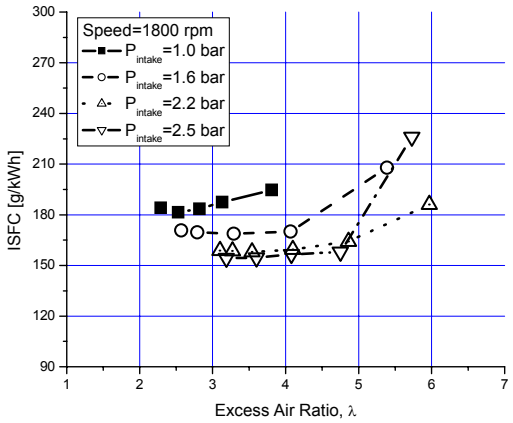

Figure 52 ISFC versus excess air ratios for various intake pressures

Figure 53 shows the combustion efficiencies for various intake pressures as a function of the excess air ratios. The combustion efficiency was calculated based on the engine exhaust gas composition (i.e. CO, non-methane hydrocarbons (NMHC), CH4, CO2, O2, and NO). The highest combustion efficiency achievable with the HCCI engine was approximately 94% regardless of intake pressure. The combustion efficiency decreased rapidly when the excess air ratio reached a certain point for a respective intake pressure due to incomplete bulk gas reactions. Intake pressure boosting could maintain the high combustion efficiency at higher excess air ratios.

The indicated thermal efficiency (ITE) is shown as a function of the excess air ratio in Figure 54. The highest ITE achievable with the HCCI engine was about 49%. The ITE increased proportionally with the increasing intake pressure. As with the combustion efficiency, the ITE was extended to higher excess air ratios with the increasing intake pressure. It should be noted again that the power required for the intake boosting was not considered in the ITE. Therefore, the actual improvements in the ITE with the increasing intake pressure would be a little lower than what are shown here. However, the ITE may be equivalent to that of a diesel engine.

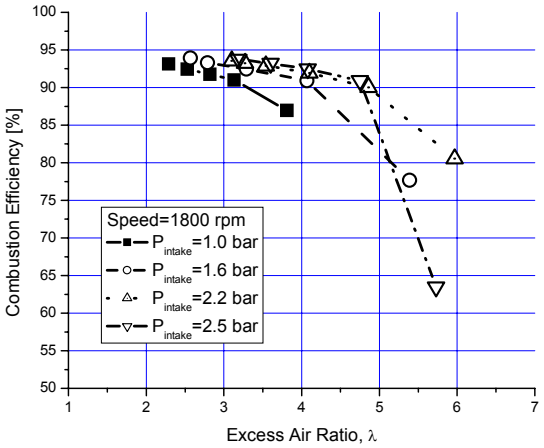

Figure 53 Combustion efficiency versus excess air ratios for various intake pressures

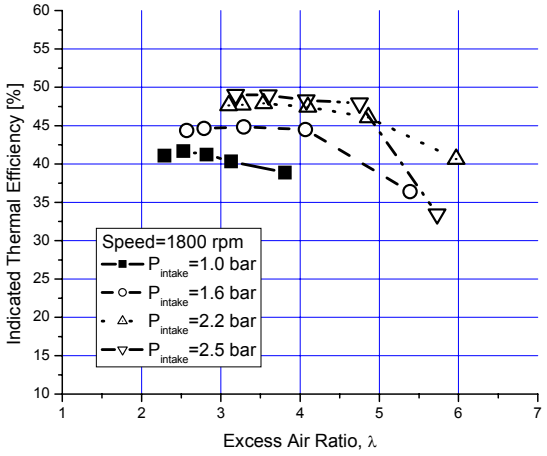

Figure 54 Indicated thermal efficiency versus excess air ratios for various intake pressures

Emissions-1800 rpm

All gaseous emissions were corrected to a 15% oxygen level to make it easy to compare emissions from different sources or facilities with substantially different oxygen concentrations in the gas stream. All the gaseous emissions are also based on dry concentrations.

Figure 55 shows the NOx emissions as a function of the excess air ratios for various intake pressures. The NOx emissions were below 75 ppm for all intake pressures tested. For all the intake pressures, the NOx emissions were below 10 ppm at excess air ratios greater than 3. The NOx emissions were below 5 ppm when the excess air ratio was greater than 3.5. The NOx emissions at the knocking limit decreased rapidly with increasing intake pressures as shown in Figure 56. The NOx emissions were independent of the intake pressure when the intake pressure was above 2.1 bar.

The CO emissions increased exponentially with the increasing excess air ratios as shown in Figure 57. Again, the intake boosting maintained low CO emissions at higher excess air ratios due to improved combustion efficiency. The CO emissions stayed below 2000 ppm until a specific excess air ratio was reached for a respective intake pressure. Then it suddenly increased to extremely high CO levels due to incomplete bulk gas reactions.

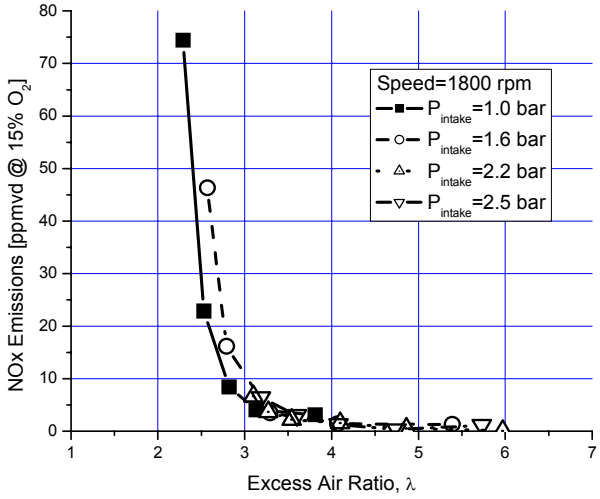

Figure 55 NOx emissions versus excess air ratios for various intake pressures

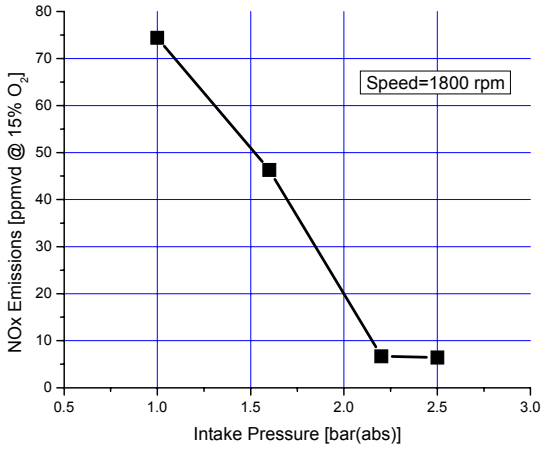

Figure 56 NOx emissions versus intake pressures at the knocking limit

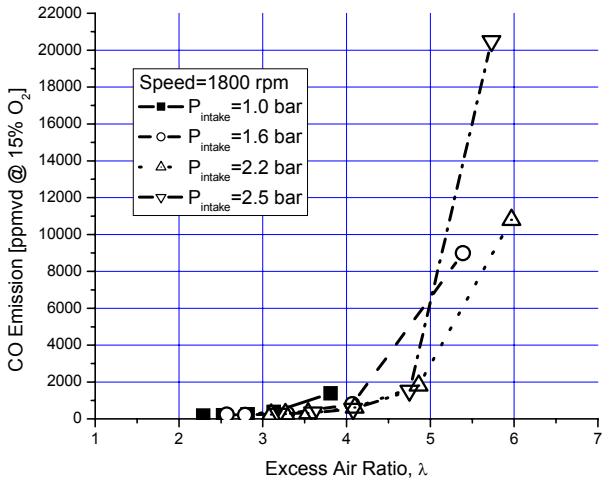

Figure 57 CO emission versus excess air ratios for various intake pressures

Figure 58 shows the THC emissions as a function of the excess air ratios for various intake pressures. Similar to the CO emissions, the THC emissions increased exponentially with increasing excess air ratio. The intake boosting maintained the THC emissions below 2000 ppm at higher excess air ratios, again due to higher combustion efficiencies at the higher excess air ratios for the boosted conditions. The CH_4 emissions from the natural gas HCCI engine consisted of approximately 83~88% of the THC emissions. Therefore, it followed exactly the same trend as the THC emissions as shown in Figure 59.

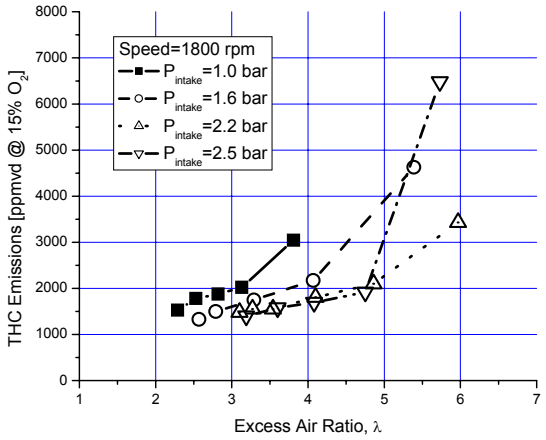

Figure 58 THC emissions versus excess air ratios for various intake pressures

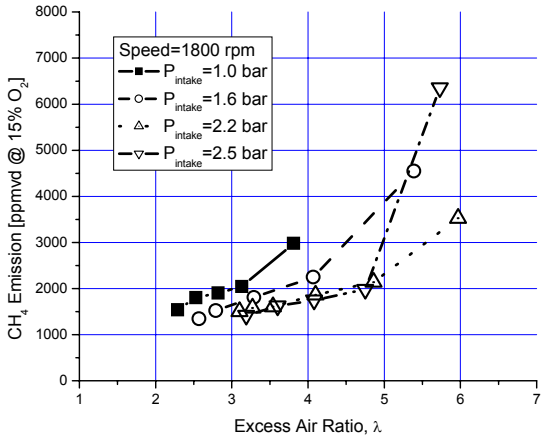

Figure 59 CH_4 emissions versus excess air ratios for various intake pressures

Comparison with Other Combustion Modes

Diesel and diesel micro-pilot natural gas combustion modes were tested using the same engine. The only difference in the engine configuration was the compression ratio of the diesel mode testing, which was 17.28:1. The diesel testing was performed using a simulated turbo-charging which followed that of a Volvo D-12A 6-cylinder engine. The diesel micro-pilot natural gas mode was matched to the highest output of the diesel mode and its excess air ratio was maintained close to 2. Details of these results are discussed earlier in this report.

As shown in Figure 60, the HCCI configuration (at comparable boost pressure) attained almost 62% of the full load of diesel or micro-pilot mode. The indicated thermal efficiencies of the three combustion modes are compared in Figure 61. The diesel-like thermal efficiencies were attained for the HCCI combustion mode when the intake pressure was above 2.1 bar. The micro-pilot combustion mode also showed the diesel-like thermal efficiencies for high loads, for λ values less than 5.0.

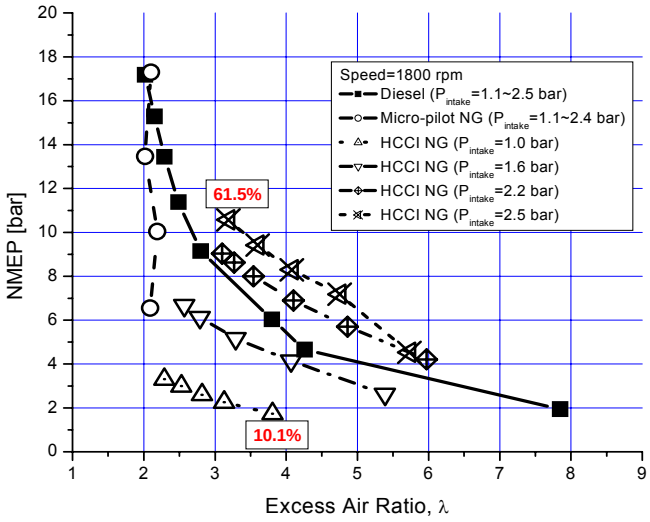

Figure 60 NMEP versus excess air ratios for diesel, micro-pilot natural gas, and HCCI natural gas combustion

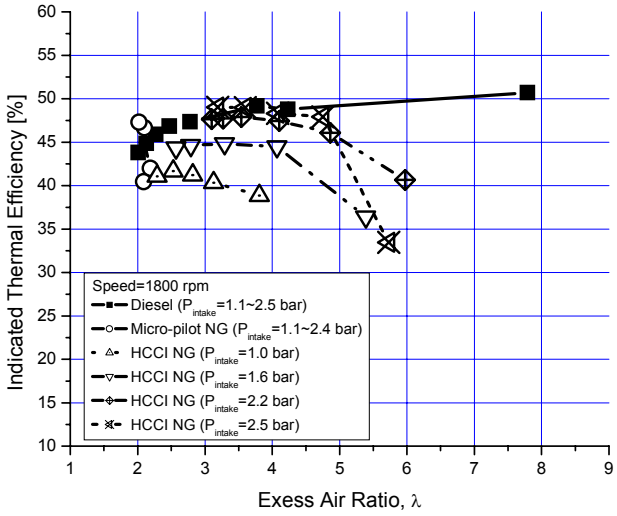

Figure 61 Indicated thermal efficiency versus excess air ratios for diesel, micro-pilot natural gas, and HCCI natural gas combustion

The HCCI combustion mode showed diesel-like thermal efficiencies and its NOx emissions were below 10 ppm for lambda in the range of 2.7 to 5.0. The CO and THC emissions were equivalent to those of other advanced natural gas engines in the good HCCI operating regimes. The combustion of the HCCI engine was reliably controlled under steady state operating conditions. The challenge for implementation is then how to deliver the thermal energy for the air/fuel mixture heating and how to boost the intake pressure.

Summary of HCCI Intake Boost Configuration Results

Our baseline results indicate that intake boosting was very important for achieving high power density with an HCCI engine. It was determined that the required intake temperature (to maintain PPL within 6-10°ATDC) decreased significantly as the intake boost pressure increased. In the results reported herein, net mean effective pressure (NMEP) of up to 8 bar was attained at an intake pressure of about 2.2 bar and engine speed of 1800 rpm. Increasing the intake pressure to 2.5 bar resulted in NMEP of 11 bar. Further increases in the intake pressure would lead to higher NMEP. The combustion efficiency approached 94% at 1800 rpm. Oxides of nitrogen (NOx) emissions were below 10 ppm when the excess air ratio was above 2.7. Intake boosting had little effect on NOx emissions when the PPL was maintained within 6-10°ATDC with increasing intake pressure. This result conflicts with other published research on HCCI testing (SAE 2005-01-2136). In those tests, NOx emissions increased with higher intake boost pressures.

Task 3. WAVE v5.1/Chemkin Calibration and Simulation

Chemical kinetics plays a significant role in the HCCI combustion, which typically has both low-temperature and high-temperature energy release with a short delay period in between. GTI had previously contracted with the Engine Research Center (ERC) of the University of Wisconsin-Madison (UW-Madison) to develop an interface that enables the WAVE engine performance simulation to use Chemkin as its combustion model. GTI's plan was to utilize this interface to optimize the HCCI engine combustion and support the laboratory testing.

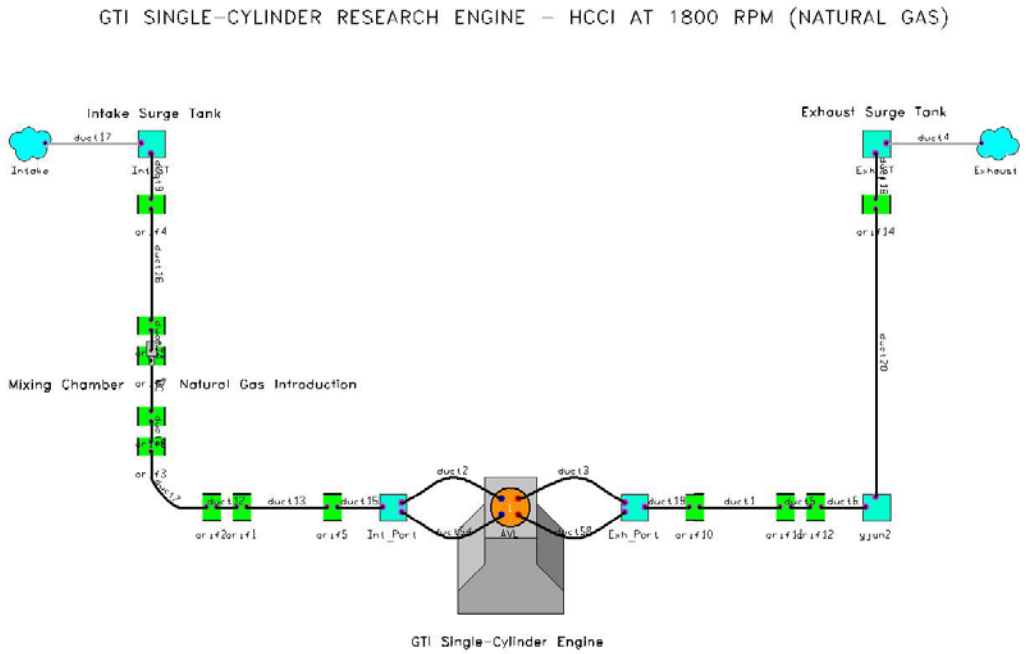

Figure 62 WAVE model of the GTI single-cylinder HCCI engine

Using the intake and exhaust system geometries, a WAVE model of the HCCI engine was built of the engine bench, the intake and exhaust valve lift profiles and port flow coefficients of the

engine, and the swirl ratio of the intake port as shown in Figure 62. The plan was to use this model to optimize the HCCI engine fueled with natural gas, hydrogen, and possibly DME.

GTI received a WAVE/Chemkin Interface from UW-Madison and GTI learned how to use the interface. With funding from the Gas Research Institute, UW-Madison wrote a computer program that allows information exchange between the commercial computer software programs WAVE and Chemkin so that engine performance, engine heat rejection and composition of exhaust gases could be estimated.

UW-Madison demonstrated that the interface had the ability to transfer all necessary information between the two commercial programs. The interface was given to GTI along with instructions on its use. When GTI tried to use the interface for the HCCI project and compared it to experimental data, it found that there was not good agreement between the modeled and experimental results.

After learning that Ricardo had an evaluation license to Reaction Design's Kinetics (Chemkin) code, GTI decided to have its subcontractor Ricardo work on an interface between its WAVE model and the Chemkin code. Ricardo reported that it established a WAVE/Chemkin link using an external cylinder and ran simulations using the methane only cases provided by GTI. (GTI had some test data from the single cylinder engine for some to these cases). Ricardo reported that it ran some cases and performed a brief review of the results. It appeared that the interface was providing reasonable results but further analysis would be required and Ricardo did not have a license to Chemkin. If GTI wanted further analysis the project would have provide a license to Ricardo.

This option, along with alternatives for carrying out model simulations in support of the project, was reviewed with DOE.

Subtask 3.1 WAVE v5.1/Chemkin Calibration

The WAVE/Chemkin engine simulation program was to be calibrated for the GTI single-cylinder HCCI engine. This calibration is the required first step when utilizing any kind of engine simulation program for a specific application. This calibration would require some baseline data from the HCCI engine testing. A precise calibration of the WAVE/Chemkin to the HCCI engine is critical for reliable optimization simulation in a subsequent task.

The WAVE/Chemkin simulation was intended to be used to guide the experiments and to interpret the experimental data. Selected results are presented in this report.

For example, Figure 63 compares the predicted NMEP with the experimental data at the engine speed of 1000 rpm for naturally-aspirated conditions. As shown in the figure, the predicted NMEP showed a good agreement with the experimental data. The predicted NMEP was over-predicted at the excess air ratios close to lean limit. This is because the experimental data have large deviations at close-to lean limit as the combustion became unstable. ISFC is compared between the simulation and experiment in Figure 64. The predicted ISFC agreed well with the experimental data, again except for the case of lean limit. Figure 65 shows the predicted ITE with the experimental ITE. The predicted ITE agreed well with the experimental data, except for the excess air ratios close to lean limit. In general, the engine cycle simulation could predict the experimental data well except for extreme cases such as lean or rich limit.

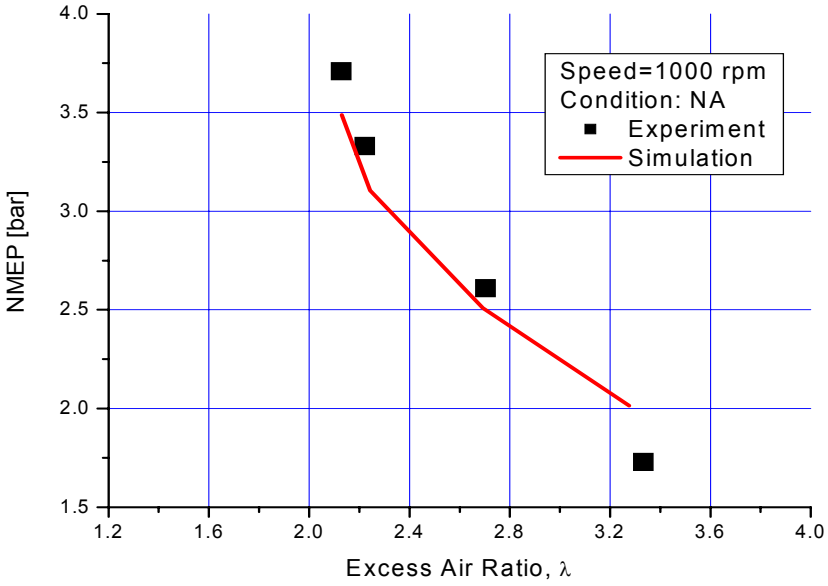

Figure 63 Comparison of predicted and experimental net mean effective pressure (NMEP)

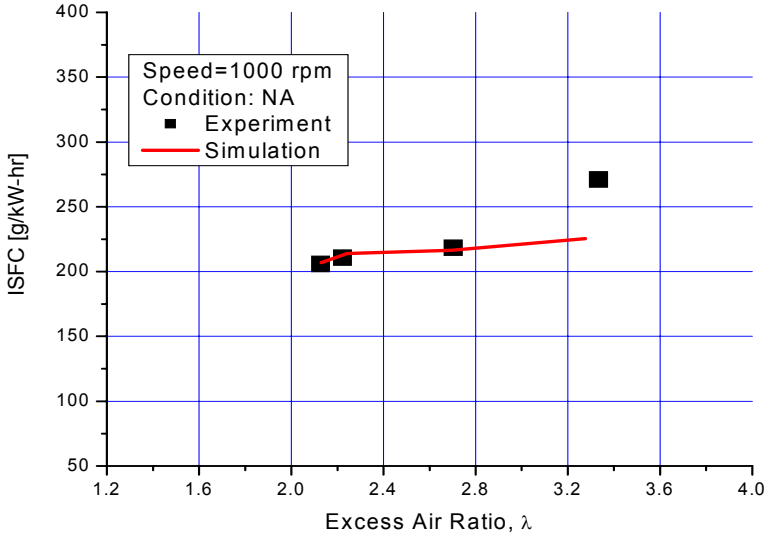

Figure 64 Comparison of predicted and experimental indicated specific fuel consumption (ISFC)

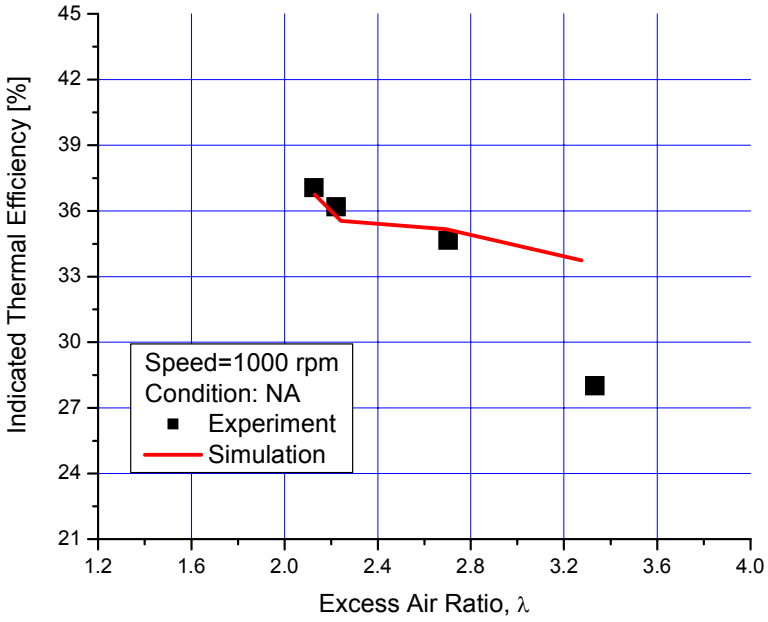

Figure 65 Comparison of predicted and experimental indicated thermal efficiency (ITE)

Subtask 3.2 WAVE v5.1/Chemkin Simulation

The calibrated WAVE/Chemkin engine simulation program was to be used to simulate the performance, efficiency, and emissions of the HCCI engine that we are testing. In this task, the main goal was to find out the optimum operating conditions of the HCCI engine with the minimum number of the laboratory engine tests.

The central problem with HCCI combustion is the control of ignition. With conventional spark ignited and diesel combustion systems, the ignition is timed to the engine through mechanical means. The ignition in an HCCI combustion system is the result of spontaneous chemical reactions occurring throughout the combustion chamber. By adding hydrogen and possibly DME, better control of the combustion and an increase in the operating envelope of natural gas HCCI combustion was considered possible.

By having the ignition and combustion occur simultaneously throughout the combustion chamber with HCCI, it is possible to realize significant gains in both engine efficiency and reduced engine pollutant emissions. However, the lack of direct control of the ignition timing means that poor ignition is possible, which could potentially be damaging to the engine. One scenario is that the ignition "runs away" and occurs earlier than intended, which causes the peak cylinder pressure to exceed the design cylinder pressure, risking catastrophic damage to the engine. The other scenario is that the ignition occurs later than intended and the exhaust temperatures rise to the point where they cause damage to the exhaust system, and, perhaps, hot spots in the combustion chamber that would lead to pre-ignition.

The strategy selected for reducing the chance of runaway HCCI ignition destroying the test engine was to gain experience with operating the engine through computer simulation before

performing the same experiments in the laboratory. The approach taken was to exercise a computer simulation for each of the HCCI engine operating conditions in the test matrix developed from the design of experiments step of this project. The main objectives of the simulations were to estimate the initial temperature required to achieve HCCI ignition at the desired time in the engine cycle and to estimate the resulting peak cylinder pressure.

The computer simulations code used models the engine from the time of intake valve closing (IVC) to the time of exhaust valve opening (EVO). It is assumed that the combustion chamber is entirely homogeneous in terms of thermodynamic state (e.g., chemical composition, temperature, pressure.) The simulation then models a representative parcel of the combustion chamber as a single closed homogeneous thermodynamic system, shown in Figure 66.

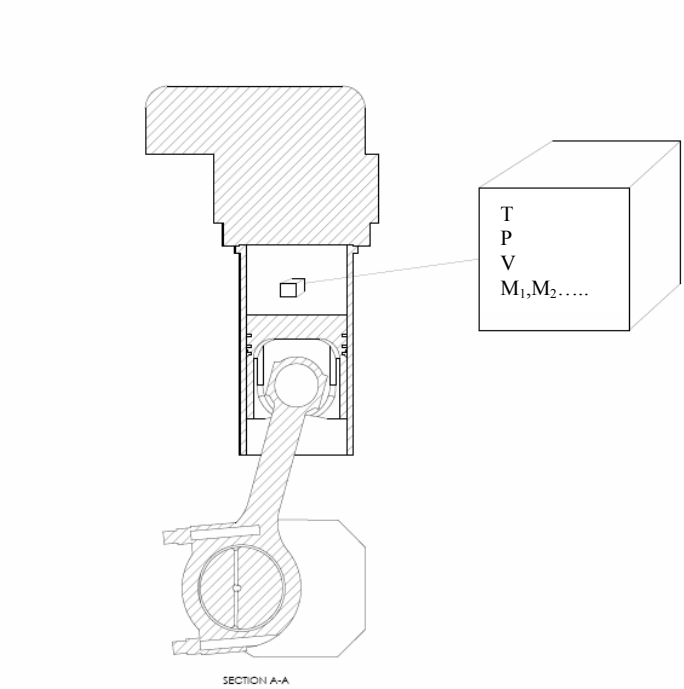

Figure 66 System Boundaries for Detailed Kinetics Simulation of GTI HCCI Engine (Source-Digital Engines)

The complexity of this model lies in the detailed treatment of the ignition and combustion chemistry occurring in the engine. The project employed Digital-Engines' proprietary detailed chemical kinetics solver and engine simulator to solve a reaction mechanism for natural gas ignition and combustion. The reaction mechanism is based on the Lawrence Livermore Natural Gas Mechanism with 79 species and 351 reactions.

The intent with the present simulations is not that they exactly match the experimental results, but rather that they function as a guide for conducting the experiments. The assumptions of entirely homogeneous combustion, perfect gas exchange, and adiabatic compression and expansion make it unlikely that the simulations would match the values observed in the engine experiments. However, the trends predicted are expected to be the same as what would be observed in the planned experiments.

Table 5 summarizes the key design and operating parameters for GTI single-cylinder research engine that was simulated.

Table 5 GTI Single-Cylinder Research Engine Specifications

Make/Model	Model AVL LEF / VOLVO 5312
Compression Ratio	13.8:1
Connecting Rod Length	260mm
Bore/Stroke	131mm/150mm
Piston Pin Offset	None
Boost Pressure	1.6 to 3.9 bar, absolute
Intake Valve Close	122 CA° BTDC
Exhaust Valve Open	122 CA° ATDC
Peak Cylinder Pressure	180 bar, absolute
Peak Intake Temperature	477 K

One of the concerns of conducting HCCI research is that fuel effects can be very important. Table 6 provides compares various gas compositions with methane. The first column is pure methane, which is expected to have very different combustion behavior than natural gas. The second column is the baseline gas composition that was used in the subject simulation study. The third column is an average natural gas composition measured at GTI during some of the engine testing.

Table 6 Baseline Gas Composition used in Simulations

Species	Methane	Baseline	GTI
CO2		0.009	0.0093
N2		0.021	0.0136
CH4	1.0	0.944	0.9437
C2H6		0.026	0.0255
C3H8			0.0042
C4H10			0.0014
C5H12			0.0005
C6H14			0.0005

The simulations were setup for an excess air ratio, percent hydrogen content, and inlet pressure, as given in the proposed test matrix from the design of experiments (See Task 4.1 below). The ratio of hydrogen to natural gas was computed on a percent energy content basis using the lower

heating values of CH4, C2H6, and H2. The simulations were then run for a sweep of inlet temperatures until the temperature that yielded the desired timing of peak cylinder pressure was found. To assess the sensitivity of the combustion to slight changes in the operating condition the inlet temperature was varied by +/- 5°K and the hydrogen composition was varied by +/-10%.

The detailed results from the modeling are included in the Appendix to this report. The simulations identified that proposed test points 1, 7, 14, 23, and 24 could result in peak pressures that exceeded the 180 bar absolute limit prescribed by the engine manufacturer AVL. From an intake temperature perspective, only Run 22 was identified as potentially requiring a GTI test cell intake temperature that might exceed the limits of the heater.

Task 4 HCCI Engine Testing

In this task, GTI proposed to test the HCCI engine in the GTI engine laboratory. Based on the engine simulation and baseline data, GTI planned to design an optimized experimental matrix, perform engine testing according to the matrix, and collect data. Experiments were to be coordinated with the engine simulation task.

Test Plan for H_2-Enriched HCCI Combustion

Table 7 shows the experimental matrix as a function of fuels, and control parameters as of mid 2005. Engine testing and data analyses with natural gas only had been completed without the need for micro-pilot for start-up or DME. The HCCI engine testing with hydrogen-enriched natural gas was planned be completed by the end of November 2005.

Table 7 Experimental matrix

Fuels	Major Control Parameter	Engine Control Parameters	Status
HCCI with natural gas	Excess air ratio (λ) – lean limit to rich limit	Speed – 1000, 1200, 1400, 1600, 1800 rpm Intake pressure (1 bar) Coolant temperature (100 C) Oil temperature (100 C) Intake temperature to maintain the PPL within 6-10 ATDC	**Completed**
HCCI with natural gas	Intake pressure (MAP) – 1 ~ 2.2 bar (abs)	Excess air ratio- lean limit to rich limit Speed (1000, 1200, 1400, 1600, 1800 rpm) Coolant temperature (100 C) Oil temperature (100 C) Intake temperature to maintain the PPL within 6-10 ATDC	**Completed**
HCCI with hydrogen and natural gas (DME based on engine controllability)	Excess air ratio (λ) – lean limit to rich limit	Speed – 1200 and 1800 rpm Intake pressure (1 bar) Coolant temperature (100 C) Oil temperature (100 C) Intake temperature to maintain the PPL within 6-10 ATDC	**In progress**
HCCI with hydrogen and natural gas (DME based on engine controllability)	Intake pressure (MAP) – 1 ~ 2.2 bar (abs)	Excess air ratio – lean limit to rich limit Speed – 1200 and 1800 rpm Coolant temperature (100 C) Oil temperature (100 C) Intake temperature to maintain the PPL within 6-10 ATDC	**Future (Nov 2005)**

Subtask 4.1 HCCI Experimental Design

The design of experiments is becoming more important these days to increase efficiency and optimize project expenses. Since the potential number of fuel blends will be large, it is important

to screen out fuel blends, with guidance from the simulations, and test only fuel blends of significant interest at optimum engine operating conditions.

Having adequately mapped the HCCI engine for neat natural gas fueled-operation, the objective with the Design of Experiments was to quickly and efficiently find the optimum conditions for hydrogen-enhanced operation that would enable increased thermal efficiency and higher BMEP. As mentioned above, GTI did not have a calibrated WAVE/Chemkin model to help guide this effort. As stated in the proposal, because "the potential number of fuel blends will be large, it is important to screen out fuel blends, with guidance from simulations, and test only blends of significant interest at optimum engine operating conditions."

From meetings and discussion with our subcontractor at the time (Ricardo), the variables selected for the test plan were boost pressure, peak pressure location, %H2 energy content, and lambda. The number of tests proposed in the test plan. became a function of the number of variables selected, the available schedule and estimated time required per test point. Based upon four variables and budgetary limitations, 27 tests were proposed in the test plan. and are listed below in Table 8:

Table 8 Design of Experiments Test Matrix for Task 4.1

RunOrder	Engine Speed	PeakPrPos	Lambda	H_2 Content	Pinlet	NG A/F_stoi	H_2 A/F_stoi	AirFlow	NGFlow	H_2Flow
-	rev/min	degCA ATDC	-	%H_2 Energy Content	bar abs			kg/hr	kg/hr	kg/hr
1		5.0	2.5	0.0	3.5	16.195	34.060		0.00	
2		10.0	2.9	0.0	2.8	16.195	34.060		0.00	
3		15.0	3.3	0.0	2.0	16.195	34.060	180.0	3.37	
4		10.0	2.9	25.0	2.8	16.195	34.060		0.00	
5		10.0	2.9	10.0	1.6	16.195	34.060		0.00	
6		5.0	2.5	0.0	2.0	16.195	34.060		0.00	
7		5.0	3.3	0.0	3.5	16.195	34.060		0.00	
8		15.0	2.5	0.0	3.5	16.195	34.060		0.00	
9		15.0	2.5	20.0	3.5	16.195	34.060		0.00	
10		5.0	3.3	20.0	2.0	16.195	34.060		0.00	
11		15.0	3.3	0.0	3.5	16.195	34.060		0.00	
12		10.0	3.5	10.0	2.8	16.195	34.060		0.00	
13		17.5	2.9	10.0	2.8	16.195	34.060		0.00	
14	1800	10.0	2.9	10.0	3.9	16.195	34.060		0.00	
15		10.0	2.3	10.0	2.8	16.195	34.060		0.00	
16		15.0	3.3	20.0	2.0	16.195	34.060		0.00	
17		10.0	2.9	10.0	2.8	16.195	34.060		0.00	
18		5.0	2.5	20.0	2.0	16.195	34.060		0.00	
19		10.0	2.9	10.0	2.8	16.195	34.060		0.00	
20		15.0	2.5	0.0	2.0	16.195	34.060		0.00	
21		10.0	2.9	10.0	2.8	16.195	34.060		0.00	
22		5.0	3.3	0.0	2.0	16.195	34.060		0.00	
23		5.0	2.5	20.0	3.5	16.195	34.060		0.00	
24		5.0	3.3	20.0	3.5	16.195	34.060		0.00	
25		2.5	2.9	10.0	2.8	16.195	34.060		0.00	
26		15.0	3.3	20.0	3.5	16.195	34.060		0.00	
27		15.0	2.5	20.0	2.0	16.195	34.060		0.00	

Testpoint setting procedure:
Set speed and inlet manifold pressure
Use the amount of fuel to set the target Lambda
Use the inlet manifold temperature to control the position of maximum cylinder pressure

Input

LHV_H2	120	MJ/kg
LHV_NG	47.59	MJ/kg
AFR_H2_ST	34.06	
AFR_NG_ST	16.1949	
AFR_DME_ST	8.891	

Subtask 4.2 HCCI Engine Testing with Hydrogen-Enriched Fuel

Based on the experiment design, GTI proposed to test the HCCI engine to investigate the technical feasibility of burning blends of natural gas, hydrogen, and DME to improve engine performance, efficiency, and emissions (NOx, CO, CO_2, THC, and PM are of interest). It was originally proposed that cold start of the HCCI engine would be handled with the micro-pilot Fischer-Tropsch (F-T) synthetic diesel fuel injection. However, it was determined that cold start would not require the use of F-T fuel. All engine performance parameters (i.e. BMEP, temperatures, pressures, flow rates, etc.) and emissions (NOx, CO, CO_2, THC, CH_4, and O_2) data would be collected and analyzed. .

Digital-Engines worked on site at GTI for six weeks. Weeks one and two were used to prepare the GTI single cylinder test cell for resumption of HCCI testing after the engine sat idle for many months. During weeks three through six, DE operated the GTI single cylinder in HCCI mode on natural gas and hydrogen mixtures. At the conclusion of the test campaign, data was obtained for 25 of the 27 points in the approved test plan. A summary of the data taken for the test matrix during weeks three through six is shown in Table 9

For two of the proposed test points (1 and 7 in Table 9 below), peak cylinder pressures were too high to permit data collection without the likelihood of engine damage.

The plan was to rerun several of the more difficult operating points using diesel micro-pilot to control timing. However, it was never possible to have a fully functioning diesel micro-pilot system during the project period of performance because AVL failed to deliver a replacement micro-pilot fuel injector for the engine.

Two of the test points proved to be very unstable HCCI operating conditions. Test point 14 is at very high intake pressure, 3.9 bar, and point 15 is the richest lambda in the test matrix, at 2.3. While good data was obtained for Points 7 and 24, the timing of peak cylinder pressure had to be retarded to prevent over pressuring the engine.

Table 9 Test points completed

Test Point	Data Taken	Comment	Data
1	no	Over Pressure	Not Taken
2	yes		Good Data
3	yes		Good Data
4	yes		Good Data
5	yes		Good Data
6	yes		Good Data
7	yes	180 bar reached	Retarded Data
8	yes		Good Data
9	yes		Good Data
10	yes		Good Data
11	yes		Good Data
12	yes		Good Data
13	yes		Good Data
14	yes	Very Unstable	No good Data
15	yes	Very Unstable	No good Data
16	yes		Good Data
17	yes		Good Data
18	yes		Good Data
19	yes		Good Data
20	yes		Good Data
21	yes		Good Data
22	yes		Good Data
23	no	Over Pressure	Not Taken
24	yes	180 bar reached	Retarded Data
25	yes		Good Data
26	yes		Good Data
27	yes		Good Data

In addition to the 25 test conditions, data was taken for several of the test points with elevated back pressure. The back pressure was raised to simulate the effects of a large turbocharger on the exhaust stream. This will allow GTI and DE to make real world predictions about the performance of natural gas HCCI.

Raising the back pressure on the engine lowered the BMEP and efficiency, but improved engine control. Higher back pressure increased the pumping work of for the engine. Higher back pressure also trapped more exhaust residual in the cylinder, which improved the control of the engine.

The final testing performed was a series of motored traces covering the temperatures, pressures and speeds used in the testing. These motored traces were used for calibration of the HCCI model and to serve as a baseline for the data points.

Data from Test Matrix

Data was obtained under the following procedure and conditions:

Engine speed was set to 1800 rpm, coolant outlet temperature was set at 100°C, oil inlet temperature was set to 100°C, and exhaust back pressure was set at 1.5 bar absolute. GTI's dynamometer was able to hold the engine speed within a few rpm of the desired setting. The oil temperature was stable, but the coolant outlet temperature often drifted. Coolant temperature needed to be closely monitored during testing.

Multiple data traces were taken for each test point. Only data for stable operation are included in the analysis. In order to have combustion occur at the correct lambda and timing, engine intake temperature and fueling rate were adjusted to keep combustion timing from advancing or retarding too much as a test point condition was approached. Data traces were taken as combustion initiated and stabilized. The combustion timing advanced or retarded while the intake temperature and fueling rate stabilized. For the test points where stable operation was possible, once steady combustion occurred, several data traces were taken several minutes apart. These well-spaced data traces, taken while the combustion was stable, are the ones used for this report.

Many of the test points in the approved plan were not stable and required continuous operator adjustments. These conditions would advance or retard greatly with the smallest drift in intake temperature. Because the laboratory intake temperature could not be prevented from drifting, and could not be adjusted more accurately that 1°C, the operator often needed to adjust the fueling rate to prevent "run away" auto ignition. Multiple data traces were obtained for these points because the fueling rate had to be changed to reach the stable operating point. Even once the stable operating point was reached, drift in the laboratory settings for coolant temperature would often cause combustion to advance, retard or cease with very little warning. The operator recorded this phenomenon in the lab notebook. After concluding data acquisition for the test point, the many data traces were analyzed to find the one(s) that best represented a stable operating point.

When it was not possible to operate stably operate at desired operating point, the nearest operating point is presented. Test Point 9 presented in Table 13 is an example. For this test point the engine was operated with the desired flow rate of hydrogen and then natural gas was slowly added while the intake temperature was varied to control the ignition. It was not possible to increase the flow rate of natural gas to the desired level, so the data presented for Test Point 9 has a higher fraction of hydrogen than desired: 29% instead of 25% hydrogen.

The data traces taken as stable operating points were approached, and the traces taken when the laboratory settings were drifting, still provide useful insights. By studying the data at these points, more detailed information on how hydrogen affects natural gas combustion could be obtained.

Measurements and Data Recording

The GTI HCCI engine utilized three separate data acquisition tools, the MTS Adapt System (laboratory controller), MTS Combustion Analysis System (CAS), and an Horiba MEXA 7100 emissions bench. The Horiba MEXA 7100 measures and reports all emissions data. The emissions data is recorded by the MTS Adapt. Cylinder pressure traces and heat release data are measured and recorded by the MTS CAS. The peak cylinder pressure, timing of peak cylinder

pressure, and various heat release data are exported to the MTS Adapt. The MTS Adapt serves as both laboratory control and as primary data acquisition. Laboratory temperatures and pressures are recorded. Air and fuel flow rates are recorded, and for the straight natural gas test cases, the air/fuel ratio and lambda are calculated. Dynamometer speed and torque are recorded, and power and BMEP are calculated. All emissions data is brought in from the Horiba system.

In addition to the data recorded by the laboratory equipment, DE uses the data to calculate key parameters including the following:

- Temperature difference between the intake the exhaust
- Brake specific fuel consumption for the natural gas cases
- Natural gas and hydrogen energy flow rates, and
- Percentage of energy flow from hydrogen.

Knowing the energy flow rates and the power produced, the thermal efficiency is calculated. The actual lambda is also a calculated parameter.

After analyzing the data traces for the various test points from Table 8, results for usable runs were summarized in the four tables that follow:

- Table 10 reports data collected for test points with an intake manifold pressure at 1.6 bar,
- Table 11 summarizes data collected at 2.0 bar,
- Table 12 data is at 2.8 bar, and
- Table 13 data was collected at 3.5 bar.

Data collected at 3.9 bar was not considered usable.

Table 10 Run 5, intake manifold pressure set at 1.6 bar

Test Point		5
Intake Air Temp	C	156.5855
Exhaust Temp	C	372.2776
Delta T	C	215.6921
Coolant Out Temp	C	90.0221
10% Heat Release	deg	5.0050
50% Heat Release	deg	8.4945
Timing Peak Pressure	deg	9.8190
Peak Cylinder Pressure	Bar	85.5640
Speed	rpm	1799.59
BMEP	Bar	4.8325
Power	kW	14.6591
Torque	ft-lbs	57.3484
Air Flow Rate	kg/hr	140.1639
H2 Flow Rate	kg/hr	0.1111
Natural Gas Flow Rate	kg/hr	2.7625
H2 Energy Flow Rate	mJ/hr	13.3334
NG Energy Flow Rate	mJ/hr	124.3126
Total Energy Flow Rate	mJ/hr	137.6461
Percent Hydrogen	%	9.6867
Thermal Efficiency	%	38.3394
Actual Lambda		2.888595
CO	ppm	49.9383
CO2	%	2.8463
CH4	ppm	1783.47
O2	%	13.7652
NOx	ppm	5.4765
THC	ppm	1988.37
Intake Manifold Pressure	bar	1.601663

Table 11 Runs with intake pressure set at 2.0 bar

Test Point		3	6	10	16	18	20	22	27
Intake Air Temp	C	163.9473	143.7036	141.6488	134.9645	100.476	145.2984	178.8110	120.8766
Exhaust Temp	C	350.9195	377.4231	333.7766	337.6516	352.744	403.8523	334.0001	397.7119
Delta T	C	186.9722	233.7194	192.1278	202.6871	252.268	258.5538	155.1890	276.8353
Coolant Out Temp	C	98.3712	98.6986	96.9208	90.1232	99.1411	97.7526	98.2481	94.0649
10% Heat Release	deg	7.2600	2.1694	1.8260	7.7955	2.05703	7.9950	1.3054	7.5110
50% Heat Release	deg	13.7050	3.8867	3.9700	13.9115	3.65103	12.7245	3.6977	10.6790
Timing Peak Pressure	deg	14.4995	4.9587	5.0050	14.0775	5.10202	15.0010	4.6890	12.6300
Peak Cylinder Pressure	Bar	83.3618	153.0518	119.4151	84.7221	165.691	98.5859	112.4784	110.5512
Speed	rpm	1800.55	1799.50	1799.50	1799.50	1799.49	1799.48	1799.49	1799.59
BMEP	Bar	6.0507	7.6520	6.5115	6.3564	7.36604	8.4617	5.6255	8.6841
Power	kW	18.3645	23.2105	19.7510	19.2803	22.3434	25.6663	17.0637	26.3426
Torque	ft-lbs	71.8054	90.8084	77.2728	75.4322	87.4143	100.4168	66.7594	103.0565
Air Flow Rate	kg/hr	176.1763	175.4538	177.5867	182.8345	181.914	177.5870	170.3645	180.8931
H2 Flow Rate	kg/hr	0.0000	0.0000	0.2662	0.2644	0.37971	0.0000	0.0000	0.3517
Natural Gas Flow Rate	kg/hr	3.3080	4.2684	2.8320	2.8350	3.5222	4.4032	3.1797	3.6758
H2 Energy Flow Rate	MJ/hr	0.0000	0.0000	31.9493	31.7329	45.565	0.0000	0.0000	42.2046
NG Energy Flow Rate	MJ/hr	148.8603	192.0802	127.4409	127.5758	158.499	198.1436	143.0844	165.4126
Total Energy Flow Rate	MJ/hr	148.8603	192.0802	159.3902	159.3086	204.064	198.1436	143.0844	207.6172
Percent Hydrogen	%	0.0000	0.0000	20.0447	19.9191	22.3287	0.0000	0.0000	20.3281
Thermal Efficiency	%	44.4121	43.5081	44.6098	43.5690	39.4171	46.6323	42.9323	45.6770
Actual Lambda		3.288516	2.538117	3.232797	3.329109	2.5997	2.4904	3.3084	2.529647
CO	ppm	765.8775	398.9985	NA	491.8420	443.573	282.9752	260.0458	3.8075
CO2	%	2.7811	3.8481	2.3507	2.1106	3.02912	3.6771	2.7643	2.9937
CH4	ppm	1886.69	1373.03	1394.63	1957.98	1027.59	1911.91	1534.77	1579.90
O2	%	14.8666	13.6431	14.2411	14.2574	13.5636	20.3256	22.5313	12.5554
NOx	ppm	-1.5759	109.1215	5.8148	2.7898	87.4203	16.2658	3.9168	16.7392
THC	ppm	2303.79	1767.36	1509.40	2015.20	1224.98	2167.01	1735.89	1777.58
Intake Manifold Pressure	bar	1.99943	2.003272	1.994993	2.013395	2.00517	1.9947	1.9997	1.999313

Table 12 Runs with intake pressure set at 2.8 bar

Test Point		2	4	12	13	17	19	21	25
Intake Air Temp	C	129.7326	107.5348	131.9481	121.2054	121.3908	117.17742	115.85626	121.4852
Exhaust Temp	C	345.9773	348.8414	306.3019	361.5203	345.7459	343.41867	341.32471	337.7888
Delta T	C	216.2447	241.3067	174.3537	240.3149	224.3551	226.24125	225.46845	216.3037
Coolant Out Temp	C	98.1409	97.3618	96.0616	99.3681	98.8257	99.694481	98.234543	97.4602
10% Heat Release	deg	5.8207	7.1555	5.4717	9.8350	5.8160	5.970025	5.902025	3.6010
50% Heat Release	deg	9.2440	10.1905	9.4947	16.1850	8.6600	8.874024	8.679025	5.6880
Timing Peak Pressure	deg	10.2700	11.3415	10.2497	16.9835	9.6930	9.755024	9.723023	6.6530
Peak Cylinder Pressure	Bar	160.6208	160.3154	143.0099	116.7745	164.4949	162.3018	174.89787	188.0831
Speed	rpm	1799.50	1799.14	1799.50	1799.49	1799.42	1799.6603	1799.6467	1798.98
BMEP	Bar	12.5675	12.5715	10.2371	12.0913	12.3494	12.668207	12.429806	12.0613
Power	kW	38.1202	38.1247	31.0517	36.6766	37.4587	38.425457	37.704453	36.5759
Torque	ft-lbs	149.1409	149.1888	121.4856	143.4902	146.5525	150.3362	147.50705	143.1338
Air Flow Rate	kg/hr	261.5965	266.5881	262.8156	265.4009	261.7171	266.49362	263.09567	261.3838
H2 Flow Rate	kg/hr	0.0000	0.5654	0.1782	0.2163	0.2152	0.265044	0.26876	0.2175
Natural Gas Flow Rate	kg/hr	5.5970	4.4779	4.2702	5.1993	5.1980	5.076475	5.08402	5.1485
H2 Energy Flow Rate	MJ/hr	0.0000	67.8481	21.3874	25.9581	25.8275	31.80528	32.2512	26.1024
NG Energy Flow Rate	MJ/hr	251.8645	201.5050	192.1610	233.9687	233.9113	228.44138	228.7809	231.6811
Total Energy Flow Rate	MJ/hr	251.8645	269.3531	213.5485	259.9268	259.7387	260.24666	261.0321	257.7835
Percent Hydrogen	%	0.0000	25.1918	10.0152	9.9867	9.9436	12.221206	12.355262	10.1257
Thermal Efficiency	%	54.4866	50.9545	52.3470	50.7970	51.9181	53.154053	51.999747	51.0791
Actual Lambda		2.886001	2.904739	3.49363	2.898322	2.859898	2.920769	2.8756872	2.879051
CO	ppm	262.2801	172.2399	261.1083	537.4512	212.2192	209.96021	180.3251	262.4361
CO2	%	3.3644	2.5515	2.4125	2.8673	3.0415	3.00754	2.821229	3.0835
CH4	ppm	1582.66	1444.68	1510.55	2506.77	1595.02	1447.449	1501.2839	1494.79
O2	%	13.6246	13.2163	14.6701	13.4864	13.1212	13.75192	14.87526	13.1628
NOx	ppm	3.9867	12.7449	2.5804	4.2017	12.1369	3.72612	10.072283	17.6237
THC	ppm	1921.38	1478.59	1660.26	2229.91	1787.91	1720.7061	1658.129	1683.78
Intake Manifold Pressure	bar	2.809301	2.809104	2.805908	2.807028	2.792606	2.815939	2.793127	2.808575

Table 13 Runs with intake pressure set at 3.5 bar

Test Point		7	8	9	11	24	26
Intake Air Temp	C	121.2288	109.9306	98.5870	118.2184	106.7964	105.6075
Exhaust Temp	C	308.8249	348.6749	348.6749	313.2046	310.8134	313.1491
Delta T	C	187.5961	238.7443	332.0416	194.9862	204.0170	207.5415
Coolant Out Temp	C	97.2568	99.4492	96.0927	95.2136	94.2774	96.6080
10% Heat Release	deg	6.4155	9.6020	9.2544	8.2375	6.9450	8.7540
50% Heat Release	deg	10.5115	15.7345	13.8344	14.0915	10.1460	13.4330
Timing Peak Pressure	deg	11.3760	15.1515	14.9824	15.0730	11.0470	14.9075
Peak Cylinder Pressure	Bar	183.0900	155.5616	167.0938	157.4248	188.7081	164.6769
Speed	rpm	1800.55	1799.49	1799.46	1799.49	1799.86	1799.38
BMEP	Bar	15.4234	16.9734	16.4683	15.0625	15.6315	15.2957
Power	kW	46.8115	51.4853	49.9515	45.6899	47.4233	46.3923
Torque	ft-lbs	183.0323	201.4269	195.4331	178.7503	185.5023	181.5174
Air Flow Rate	kg/hr	338.2847	345.8785	344.3630	342.6260	338.1353	343.5820
H2 Flow Rate	kg/hr	0.0000	0.0000	0.8014	0.0000	0.6093	0.6056
Natural Gas Flow Rate	kg/hr	6.3560	7.3737	5.1546	6.4038	5.1265	5.1026
H2 Energy Flow Rate	mJ/hr	0.0000	0.0000	96.1698	0.0000	73.1149	72.6697
NG Energy Flow Rate	mJ/hr	286.0198	331.8176	231.9576	288.1701	230.6908	229.6180
Total Energy Flow Rate	mJ/hr	286.0198	331.8176	328.1274	288.1701	303.8058	302.2878
Percent Hydrogen	%	0.0000	0.0000	29.3352	0.0000	24.0663	24.0399
Thermal Efficiency	%	58.9194	55.8262	54.8063	57.0786	56.1951	55.2495
Actual Lambda		3.28638	2.896381	3.108666	3.303718	3.258334	3.327249
CO	ppm	236.7963	528.0596	221.0288	466.3882	165.3934	228.2987
CO2	%	2.7693	3.3339	2.2927	2.6878	2.1805	2.1309
CH4	ppm	1570.85	2210.63	1214.49	1992.68	1313.65	1434.97
O2	%	14.1168	13.7466	14.0736	14.3266	14.1647	14.0213
NOx	ppm	3.1064	1.0227	3.7941	NA	2.3191	NA
THC	ppm	1754.15	2256.78	1370.26	1905.55	1380.05	1437.34
Intake Manifold Pressure	bar	3.495445	3.515958	3.502017	3.485773	3.479243	3.47837

Task 5 Technical Evaluation of Hydrogen-Enriched HCCI Combustion

It was proposed that all the data collected and analyzed in Subtask 4.2 would be evaluated to determine whether there are improvements in the engine performance, efficiency, and emissions with addition of hydrogen and DME. Statistical analysis was to be implemented in this task. Specifically, GTI proposed to evaluate how hydrogen addition affected the performance, efficiency, and emissions of the HCCI engine.

Before discussing the effect of hydrogen, it is worthwhile to make some related observations from the analysis of the data generated from the design of experiments tests.

Effect of timing for H2 enhanced HCCI

Runs 13, 21, and 25 were performed at approximately the same lambda, 2.9, the same manifold pressure, 2.8bar, and the same H2 content, 10%. The difference in the three runs was the timing of peak cylinder pressure, 17.5, 10, and 2.5 degrees after TDC. For the three runs, the peak cylinder pressure varies dramatically, but the BMEP stays approximately the same for the three

runs. The CO, CH_4 and THC drop dramatically as the timing advances, the NOx, however increases.

The effect of timing of peak cylinder pressure on hydrocarbon emissions is shown in Figure 67.

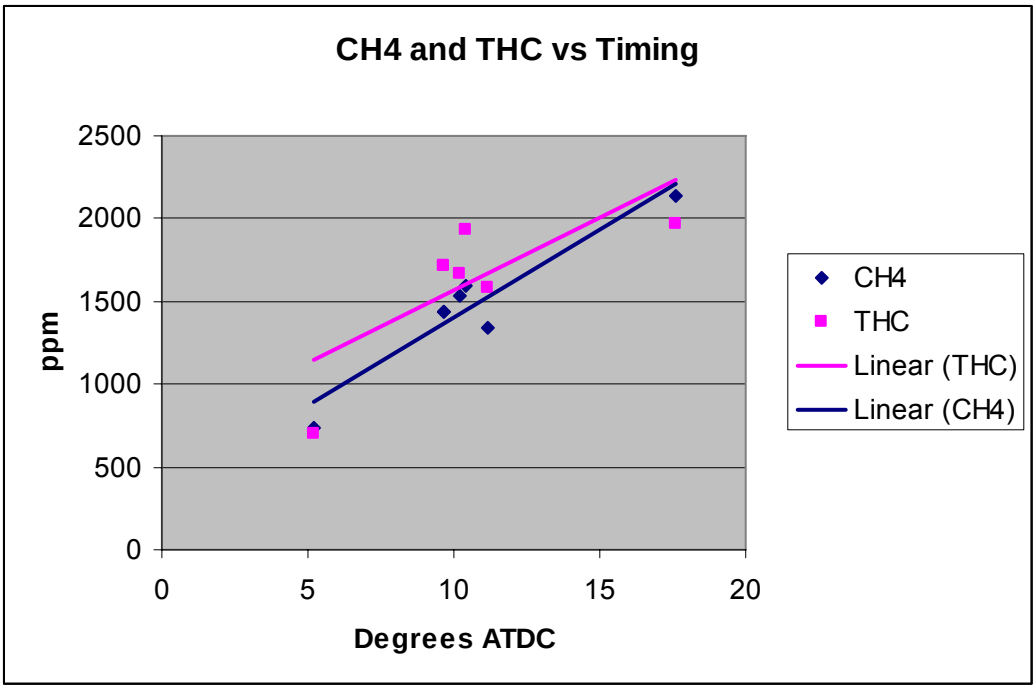

Figure 67 Effect of timing of peak cylinder pressure on CH4 and THC emissions for runs, 12, 13, 17, 19, 21, 25

Effect of Hydrogen

The main purpose of this testing was to observe the effects of blending hydrogen with natural gas on HCCI combustion. To directly compare neat natural gas runs with the hydrogen enhanced test points, one must be able to achieve and maintain stable HCCI combustion under comparable conditions. For example, for the same air flow rate and lambda, the hydrogen enriched fuel mass flow rate will be lower than the neat natural gas mass flow rate. However, the energy flow rate will be higher for the hydrogen enriched fuel because hydrogen has a significantly higher lower heating value, 120 mJ/kg, compared to 45 mJ/kg for natural gas. Additionally, the fact that neat natural gas and hydrogen enriched fueling have significantly different required intake temperature necessary for combustion confounds comparisons.

With the data available and the constraints identified above, an attempt was made to evaluate, to the extent practicable, the effects of hydrogen on natural gas HCCI combustion. Several pairs of runs were analyzed and compared at approximately the same intake pressure, timing of peak cylinder pressure, and air/fuel ratio. The runs differ in the hydrogen /natural gas fuel blend, the intake temperature at which ignition occurred and the airflow rate. The airflow rate varies slightly between the hydrogen enhanced and neat natural gas operating conditions for two reasons. The lower intake temperature for the hydrogen/natural gas blends leads to denser air

and higher mass flow rate. Offsetting this effect, however, is the fact that hydrogen is significantly less dense than the natural gas, and displaces more air in the intake leading to lower intake air mass flow rates. Depending on the difference between intake temperatures for the runs and the percent hydrogen used, the airflow rates for the hydrogen enhanced operating point may be greater or less than the non-hydrogen case.

The pairs of operating points used for comparison of neat natural gas and hydrogen enhanced HCCI are shown in Tables 14 and 15. In addition to these matched pairs, additional insights were obtained from operator experience during the test and by reviewing all of the data taken during weeks two through six.

Table 14 Matched pairs of natural gas and hydrogen added test points

Test Point		2	4	3	16	6	18	7	24
Intake Air Temp	C	129.7326	107.5348	163.9473	134.9645	143.7036	100.476	121.2288	106.7964
Exhaust Temp	C	345.9773	348.8414	350.9195	337.6516	377.4231	352.744	308.8249	310.8134
Delta T	C	216.2447	241.3067	186.9722	202.6871	233.7194	252.268	187.5961	204.0170
Coolant Out Temp	C	98.1409	97.3618	98.3712	90.1232	98.6986	99.1411	97.2568	94.2774
10% Heat Release	deg	5.8207	7.1555	7.2600	7.7955	2.1694	2.05703	6.4155	6.9450
50% Heat Release	deg	9.2440	10.1905	13.7050	13.9115	3.8867	3.65103	10.5115	10.1460
Timing Peak Pressure	deg	10.2700	11.3415	14.4995	14.0775	4.9587	5.10202	11.3760	11.0470
Peak Cylinder Pressure	Bar	160.6208	160.3154	83.3618	84.7221	153.0518	165.691	183.0900	188.7081
Speed	rpm	1799.50	1799.14	1800.55	1799.50	1799.50	1799.49	1800.55	1799.86
BMEP	Bar	12.5675	12.5715	6.0507	6.3564	7.6520	7.36604	15.4234	15.6315
Power	kW	38.1202	38.1247	18.3645	19.2803	23.2105	22.3434	46.8115	47.4233
Torque	ft-lbs	149.1409	149.1888	71.8054	75.4322	90.8084	87.4143	183.0323	185.5023
Air Flow Rate	kg/hr	261.5965	266.5881	176.1763	182.8345	175.4538	181.914	338.2847	338.1353
H2 Flow Rate	kg/hr	0.0000	0.5654	0.0000	0.2644	0.0000	0.37971	0.0000	0.6093
Natural Gas Flow Rate	kg/hr	5.5970	4.4779	3.3080	2.8350	4.2684	3.5222	6.3560	5.1265
H2 Energy Flow Rate	mJ/hr	0.0000	67.8481	0.0000	31.7329	0.0000	45.565	0.0000	73.1149
NG Energy Flow Rate	mJ/hr	251.8645	201.5050	148.8603	127.5758	192.0802	158.499	286.0198	230.6908
Total Energy Flow Rate	mJ/hr	251.8645	269.3531	148.8603	159.3086	192.0802	204.064	286.0198	303.8058
Percent Hydrogen	**%**	**0.0000**	**25.1918**	**0.0000**	**19.9191**	**0.0000**	**22.3287**	**0.0000**	**24.0663**
Actual Lambda		2.886001	2.904739	3.288516	3.329109	2.538117	2.5997	3.28638	3.258334
Thermal Efficiency	%	54.4866	50.9545	44.4121	43.5690	43.5081	39.4171	58.9194	56.1951
CO	ppm	262.2801	172.2399	765.8775	491.8420	398.9985	443.573	236.7963	165.3934
CO2	%	3.3644	2.5515	2.7811	2.1106	3.8481	3.02912	2.7693	2.1805
CH4	ppm	1582.66	1444.68	1886.69	1957.98	1373.03	1027.59	1570.85	1313.65
O2	%	13.6246	13.2163	14.8666	14.2574	13.6431	13.5636	14.1168	14.1647
NOx	ppm	3.9867	12.7449	NA	2.7898	109.1215	87.4203	3.1064	2.3191
THC	ppm	1921.38	1478.59	2303.79	2015.20	1767.36	1224.98	1754.15	1380.05
Intake Manifold Pressure	Bar	2.809301	2.809104	1.99943	2.013395	2.003272	2.00517	3.495445	3.479243

Table 15 Additional matched pairs of natural gas and hydrogen added test points

Test Point		8	9	22	10	11	26	20	27
Intake Air Temp	C	109.9306	98.5870	178.8110	141.6488	118.2184	105.6075	145.2984	120.8766
Exhaust Temp	C	348.6749	348.6749	334.0001	333.7766	313.2046	313.1491	403.8523	397.7119
Delta T	C	238.7443	332.0416	155.1890	192.1278	194.9862	207.5415	258.5538	276.8353
Coolant Out Temp	C	99.4492	96.0927	98.2481	96.9208	95.2136	96.6080	97.7526	94.0649
10% Heat Release	deg	9.6020	9.2544	1.3054	1.8260	8.2375	8.7540	7.9950	7.5110
50% Heat Release	deg	15.7345	13.8344	3.6977	3.9700	14.0915	13.4330	12.7245	10.6790
Timing Peak Pressure	deg	15.1515	14.9824	4.6890	5.0050	15.0730	14.9075	15.0010	12.6300
Peak Cylinder Pressure	Bar	155.5616	167.0938	112.4784	119.4151	157.4248	164.6769	98.5859	110.5512
Speed	rpm	1799.49	1799.46	1799.49	1799.50	1799.49	1799.38	1799.48	1799.59
BMEP	Bar	16.9734	16.4683	5.6255	6.5115	15.0625	15.2957	8.4617	8.6841
Power	kW	51.4853	49.9515	17.0637	19.7510	45.6899	46.3923	25.6663	26.3426
Torque	ft-lbs	201.4269	195.4331	66.7594	77.2728	178.7503	181.5174	100.4168	103.0565
Air Flow Rate	kg/hr	345.8785	344.3630	170.3645	177.5867	342.6260	343.5820	177.5870	180.8931
H2 Flow Rate	kg/hr	0.0000	0.8014	0.0000	0.2662	0.0000	0.6056	0.0000	0.3517
Natural Gas Flow Rate	kg/hr	7.3737	5.1546	3.1797	2.8320	6.4038	5.1026	4.4032	3.6758
H2 Energy Flow Rate	mJ/hr	0.0000	96.1698	0.0000	31.9493	0.0000	72.6697	0.0000	42.2046
NG Energy Flow Rate	mJ/hr	331.8176	231.9576	143.0844	127.4409	288.1701	229.6180	198.1436	165.4126
Total Energy Flow Rate	mJ/hr	331.8176	328.1274	143.0844	159.3902	288.1701	302.2878	198.1436	207.6172
Percent Hydrogen	**%**	**0.0000**	**29.3352**	**0.0000**	**20.0447**	**0.0000**	**24.0399**	**0.0000**	**20.3281**
Actual Lambda		2.896381	3.108666	3.3084	3.232797	3.303718	3.327249	2.4904	2.529647
Thermal Efficiency	%	55.8262	54.8063	42.9323	44.6098	57.0786	55.2495	46.6323	45.6770
CO	ppm	528.0596	221.0288	260.0458	NA	466.3882	228.2987	282.9752	3.8075
CO2	%	3.3339	2.2927	2.7643	2.3507	2.6878	2.1309	3.6771	2.9937
CH4	ppm	2210.63	1214.49	1534.77	1394.63	1992.68	1434.97	1911.91	1579.90
O2	%	13.7466	14.0736	22.5313	14.2411	14.3266	14.0213	20.3256	12.5554
NOx	ppm	1.0227	3.7941	3.9168	5.8148	-6.1711	-6.0457	16.2658	16.7392
THC	ppm	2256.78	1370.26	1735.89	1509.40	1905.55	1437.34	2167.01	1777.58
Intake Manifold Pressure	Bar	3.515958	3.502017	1.9997	1.994993	3.485773	3.47837	1.9947	1.999313

For the test conditions evaluated, the major effects of hydrogen are as follows:

- Adding hydrogen reduced the temperature needed for steady HCCI to occur.

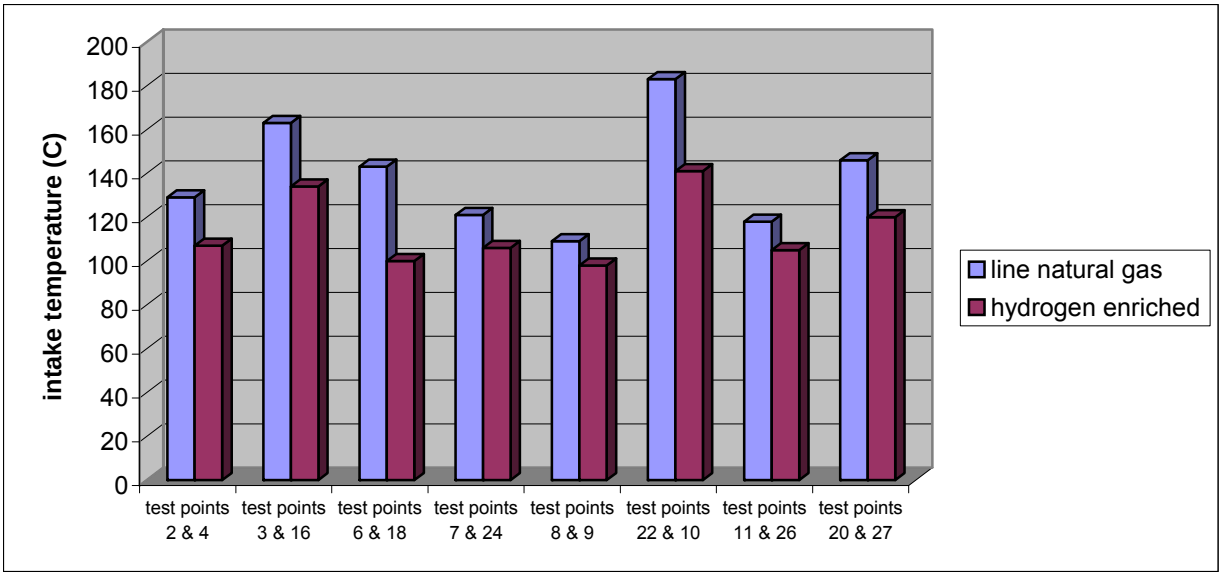

Figure 68: Effect of hydrogen enrichment on intake manifold temperature.

As shown in Figure 68, the effect of adding hydrogen lowered required intake temperature on the order of 20°-40°C. An advanced engine setup could add hydrogen using a quick acting valve to alter the hydrogen content of the intake charge cycle-to-cycle. In contrast, attempting to change the temperature of the engine would occur much more slowly. Hydrogen addition is an ideal means of quickly controlling the ignition timing of the engine.

- The effect of hydrogen addition on the engine BMEP and power produced was inconclusive (slight increase or slight decrease, shown in Fig. 69.)

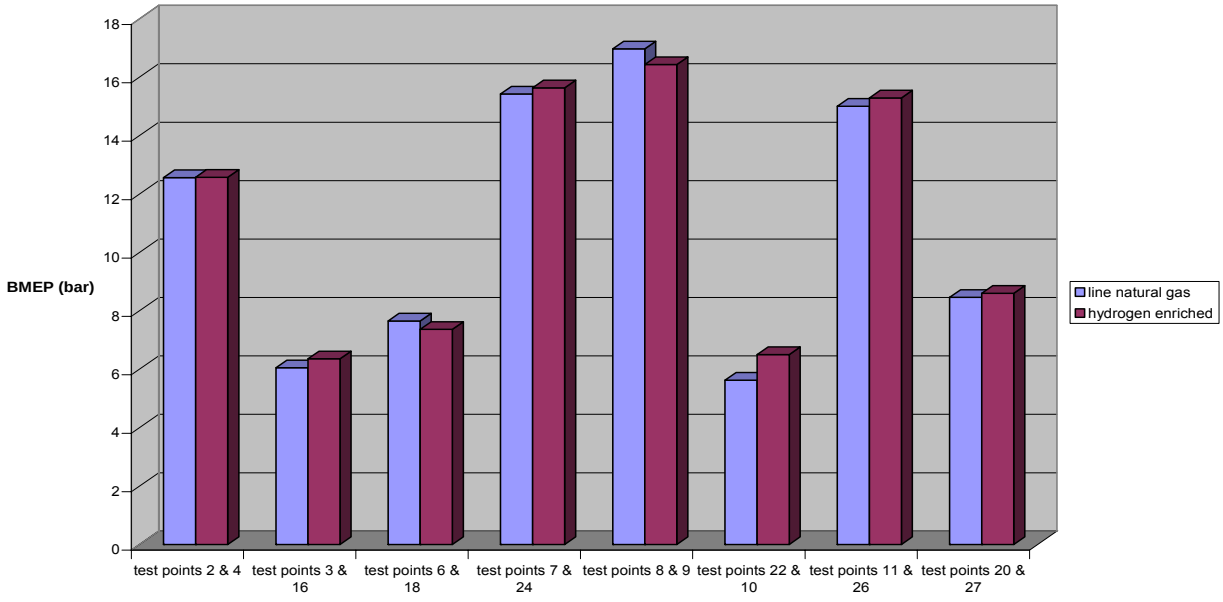

Figure 69: Effect of hydrogen enrichment on BMEP.

- The addition of hydrogen reduced thermal efficiency of the engine for most cases, as shown in Fig. 70.

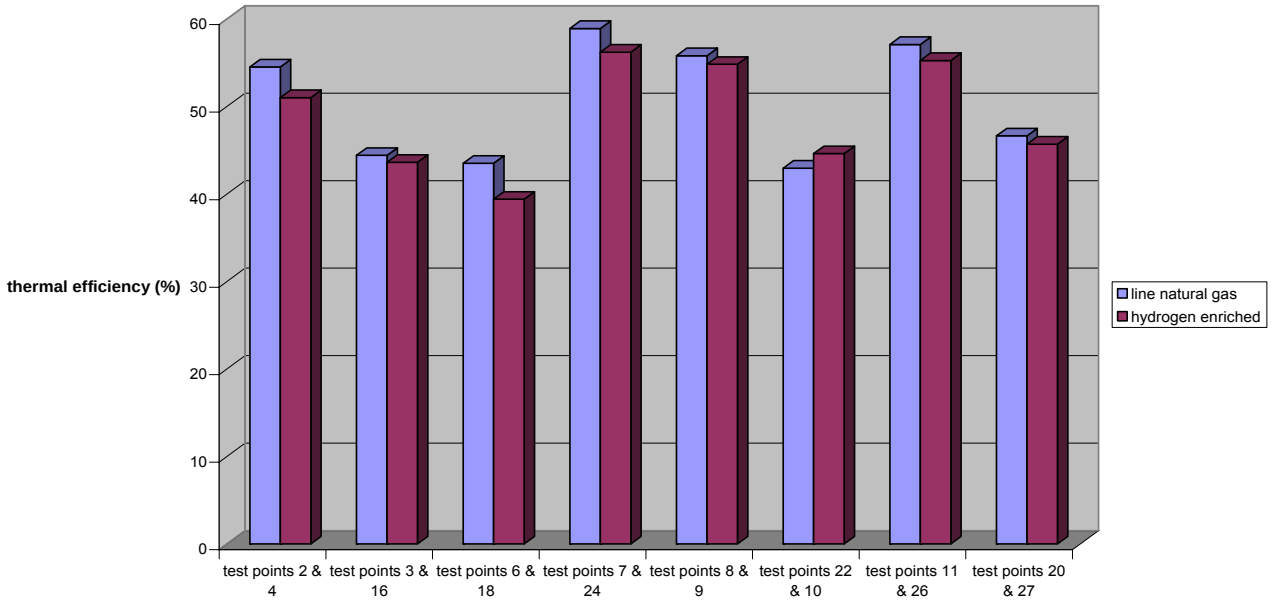

Figure 70: Effect of hydrogen enrichment on thermal efficiency.

- The addition of hydrogen did not make operating conditions more stable, as shown by the COV of Peak Cylinder Pressure summarized in Fig. 71.

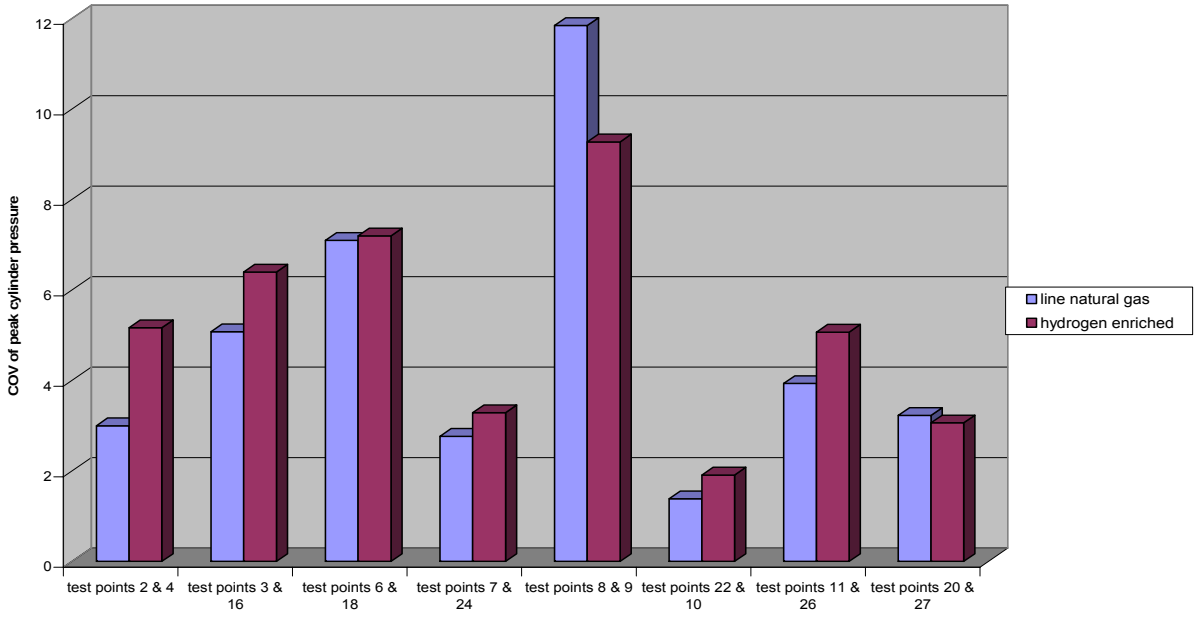

Figure 71: The effect of hydrogen enrichment on COV of peak cylinder pressure.

- The addition of hydrogen reduced the unburned hydrocarbons in the exhaust for every case, as shown in Fig. 72.

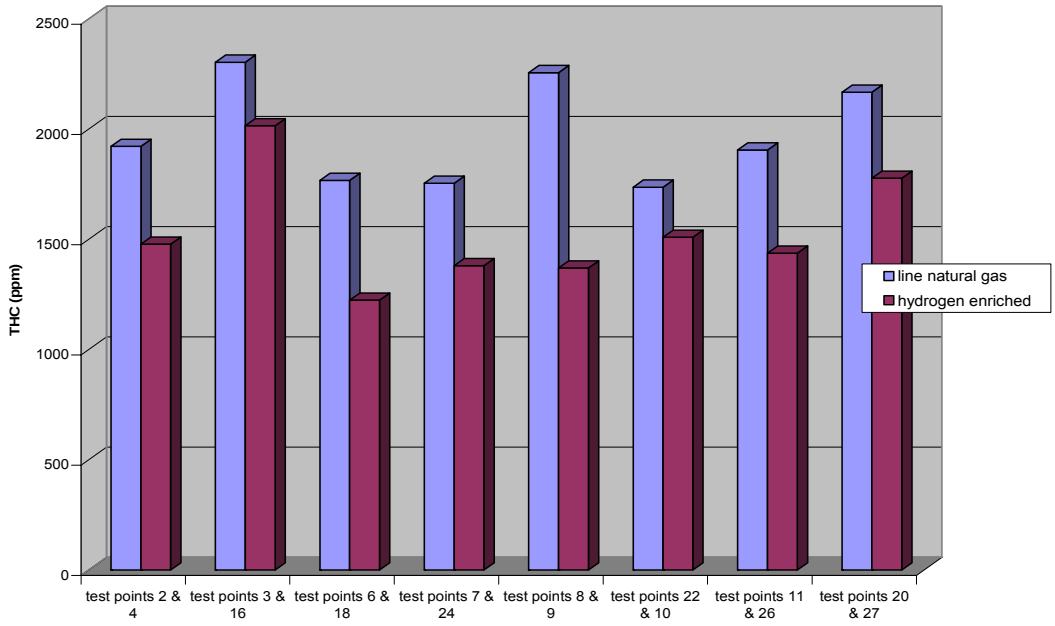

Figure 72. Effect of hydrogen enrichment on engine out hydrocarbons.

- The addition of hydrogen slightly increased the production of NOx in the exhaust for most operating conditions, as shown in Fig. 73. For Test Points 6 and 18, which produced the greatest NOx, hydrogen enrichment slightly decreased the engine out Nox.

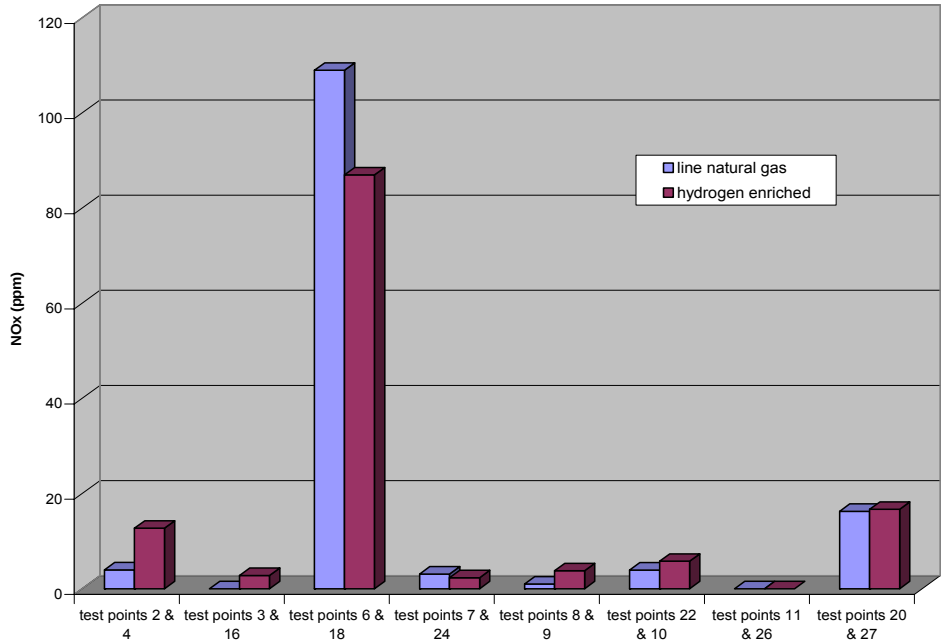

Figure 73: Effect of hydrogen enrichment on engine-out NO_x.

- The addition of hydrogen reduced the amount of CO in the exhaust for most cases, as shown in Fig. 74 For certain pairs of cases, such as test points 22 and 10 and test points 20 and 27, the enriching the fuel with hydrogen virtually eliminated CO in the exhaust.

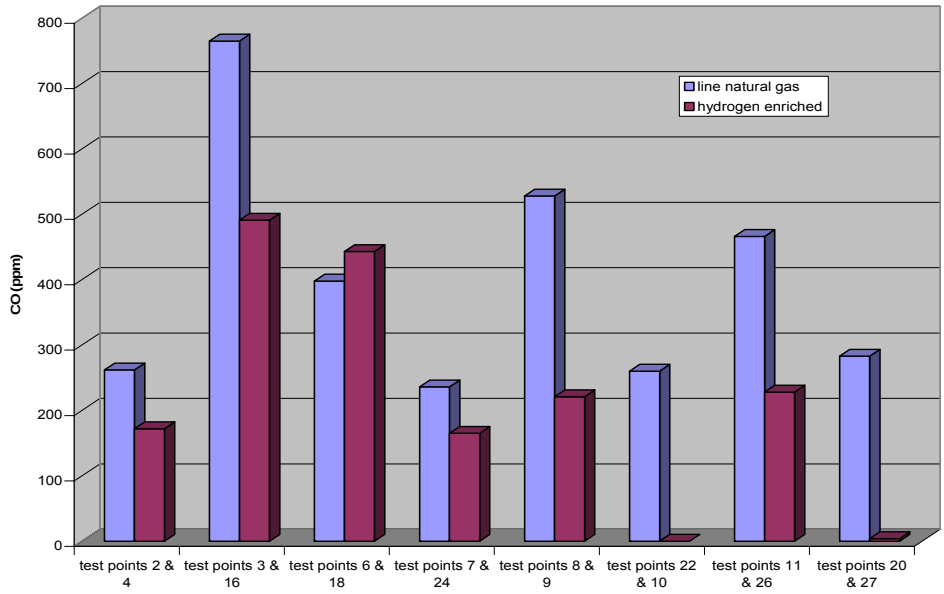

Figure 74. Effect of hydrogen enrichment on engine-out CO.

For comparison, the heat release and pressure traces for HCCI test point 11 (neat natural gas) and Point 26 (~25% hydrogen) are shown in figures 75 and 76. A slight increase in BMEP and power produced is reported for the hydrogen/natural gas blend in Table 15. For the comparable air flow rate and air/fuel ratio reported in the table, the energy flow rate for the hydrogen blend is about 5% higher than the neat natural gas run.

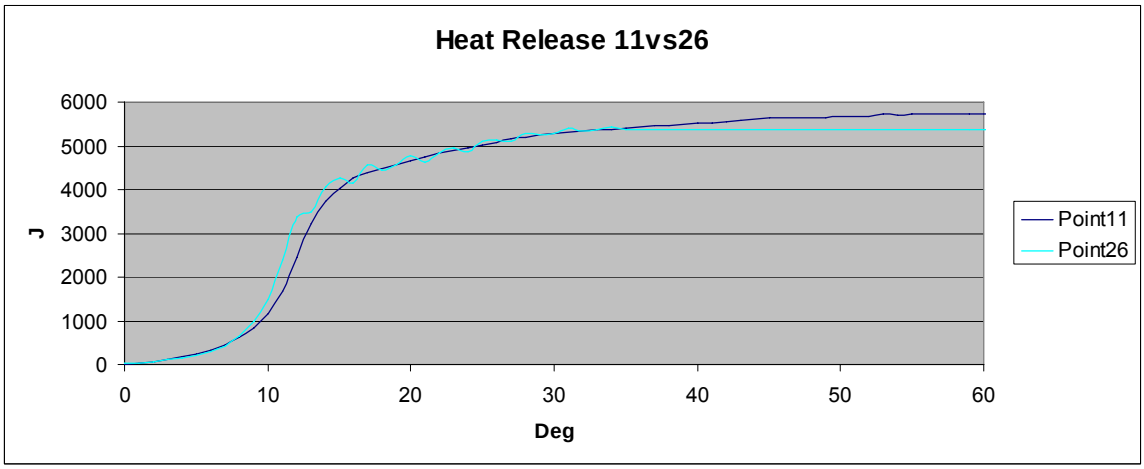

Figure 75 Comparison of Heat Release-25% H2 Blend (Run 26) vs. Neat Natural Gas

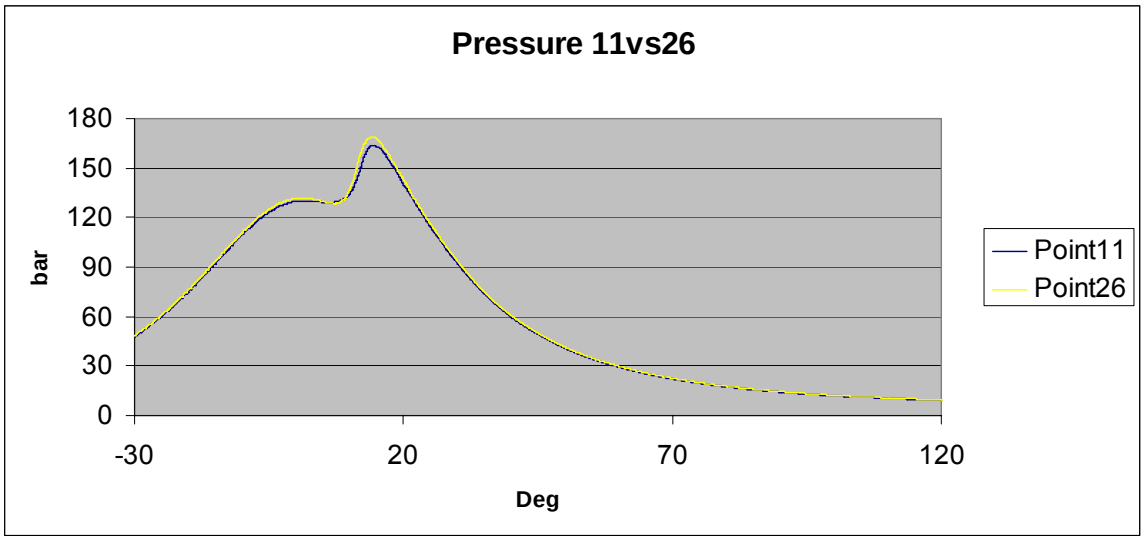

Figure 76 Comparison of In-Cylinder Pressure Traces- 25% H2 Blend (Run 26) vs. Neat Natural Gas

For the operating conditions evaluated, the simple substitution of hydrogen for natural gas (all other things approximately equal) did not make HCCI combustion more stable. In certain cases, the test points for the hydrogen blended fuel were more unstable than the neat natural gas points. This may be due to the way the fueling rate on the GTI research engine is controlled and may not be a reliable indicator of how stable the combustion was. With neat natural gas HCCI combustion runs, once the engine speed, boost level and intake temperature are set, the only parameter that the operator varies is the natural gas fueling rate. With the hydrogen enhanced cases, the operator must attempt to manually control both the natural gas and hydrogen fuel rates. For very stable operating conditions, controlling both fuel flows is straightforward. For the less stable operating points, when the fuel rate must be reduced quickly as the combustion begins to advance, and added back in precisely as the timing retards, independent control of hydrogen and natural gas adds complexity. In addition, the hydrogen fuel system adds an additional control loop to the laboratory setup. The intake manifold air pressure, intake air temperature, and fuel flow loops effect one another, and small changes in one loop must be compensated for by the others. Having four control loops adds an additional degree of freedom, and less precise control than three control loops.

The project team anticipated the challenge in transition from neat natural gas HCCI to hydrogen enhanced natural gas HCCI and planned to use the diesel micro-pilot fuel injection system to help control this phenomenon. Unfortunately, a number of unforeseen problems developed with the micro-pilot injection system and it could not be used as intended. (See Figure 4-A of Appendix A)

A somewhat unexpected observation during testing was that, in most cases, the addition of hydrogen decreased the stability of the HCCI operating points. The following table shows the coefficient of variance for the matched pairs of test points reported earlier in Tables 14and 15.

Table 16 Coefficient of variance of peak cylinder pressure for match pairs of runs

Test Point	COV of PCP	COV of IMEP	%H2
2	3.007	1.637	0
4	5.168	1.621	25.2
3	5.080	2.480	0
16	6.408	2.877	19.9
6	7.129	1.709	0
18	7.222	4.108	22.3
7	2.767	1.689	0
24	3.290	1.848	24.1
8	11.849	4.460	0
9	9.276	2.203	29.3
22	1.387	1.558	0
10	1.913	1.560	20
11	3.935	2.075	0
26	5.071	1.709	24
20	3.230	1.613	0
27	3.065	1.378	20.3

Table 16 shows an increase in the coefficient of variance with the addition of hydrogen for all matched pairs except for test points 8 and 9 and 20 and 27. Test points 8 and 9 were performed with a timing of peak cylinder pressure of 15 degrees. With this retarded timing, at these operating points misfires are common, and one or two misfires during a data set will dramatically increase the COV. Additionally, due to the increased level of stability without the presence of hydrogen, the operator was able to enrich the mixture during testing closer to the specified lambda of 2.5 than with the addition of hydrogen.

The addition of hydrogen reduced hydrocarbon emissions. This is an expected result due to fewer hydrocarbons present in the intake. However, the ratio of unburned hydrocarbons to the total hydrocarbons in the intake remains relatively unchanged, so the effect of hydrogen on the percent of fuel burned is minor. For this test, the amount of hydrogen in the exhaust stream was not recorded.

Carbon dioxide levels are lower with the addition of hydrogen than with straight natural gas fueling. This is due to the lower quantity of carbon in the combustion reactants.

FINDINGS

The main purpose of HCCI engine testing with Hydrogen-Enriched Fuel was to observe the effects of blending hydrogen with natural gas on HCCI combustion.. In particular, the project

team hoped to gain insights into the potential for hydrogen to extend the acceptable window of operation for HCCI. As shown in Tables 14 and15, hydrogen dramatically reduced the amount of heat energy that had to be added to the intake air for stable HCCI combustion. Hydrogen also had the effect of lowering hydrocarbon emission without significantly increasing the production of NOx. With the calibrated HCCI engine model from this project, a tool is available to predict (for a given manifold pressure and intake temperature), how much hydrogen should be added to produce a given engine timing.

The major accomplishments and findings from the project can be summarized as follows:

The GTI single cylinder engine was configured for HCCI operation. Baseline HCCI mapping with natural gas was successfully completed for both NA and intake charge-boosted conditions. For all cases, the use of the Peak Pressure Location (PPL) was a good indicator for controlling the HCCI engine fueled with natural gas. The PPL was controlled by using the intake charge temperature, which is only valid when the oil and coolant temperatures are kept constant. With this strategy, consistent data were taken without the need to employ DME for control of the start of combustion. In view of these results, a decision was made to forego the planned integration of DME into the test plan for hydrogen enhanced HCCI. A paper published by researchers in Japan was identified that presented data from HCCI engine tests with blends of DME and natural gas. The paper provides information that can used to estimate the appropriate ratios of DME and methane to affect the desired changes in timing and intake temperature for HCCI combustion. This paper is provided in Appendix C of this report.

It is clear from the testing conducted in this project that intake boosting is very important for high power density with an HCCI engine. The required intake temperature decreases with increasing intake boost pressure. For example, the required temperature decreased about 66°C when the intake pressure increased from 1 bar to 1.6 bar at the engine speed of 1000 rpm. This result implies that an HCCI engine with a high pressure-ratio turbocharger or supercharger with a small-size intercooler may not need additional thermal energy in order to achieve HCCI combustion for stationary applications. The small-size intercooler is to control the intake charge temperature. In addition, as shown in Figure 44, engine power density is proportional to intake boost pressure. Therefore, higher intake boost pressure will lead to higher power density, which is equivalent to those of conventional natural gas engines or at least close to their maximum power density. As shown in Figure 60, NMEP of more than 10 bar was attained at 1800 rpm when the intake boost pressure was 2.5 bar.

The Digital Engines model used in this project reasonably predicted proposed test conditions that could approach undesirable peak cylinder pressures for HCCI combustion with hydrogen and natural gas blends. Test data obtained in the project was used to further calibrate the model's predictive capability for heat release rates and peak pressure rise on both natural gas and blends of hydrogen and natural gas.

The testing confirmed that hydrogen enhanced natural gas HCCI combustion resulted in:

- Substantially lower intake temperature needed for stable HCCI combustion
- Inconclusive impact on engine BMEP and power produced
- Small reduction in the thermal efficiency of the engine
- Moderate reduction in the unburned hydrocarbons in the exhaust
- Slight increase in NOx emissions in the exhaust

- Slight reduction in CO2 in the exhaust.
- Increased knocking at rich stoichiometry

HCCI combustion resulted in hydrocarbon (HC) and carbon monoxide (CO) emissions were equivalent to or lower than conventional natural gas engines. Furthermore, HC and CO emissions were significantly lower than other reported HCCI data particularly at very light loads. Hydrogen enhanced HCCI reduced hydrocarbon emissions further.

RECOMMENDATIONS FOR FUTURE WORK

1. Two experimental set-up issues that should be addressed are the diesel micro-pilot system and the coolant control system. A new common rail injector has been ordered from AVL, and will be installed and tested when it arrives. The first step to gain better control of the coolant temperature would be to adjust the PID gains in the control algorithm. To do this, software would need to be installed on the laboratory laptop. Once the software was installed, the laptop could communicate with the lube/coolant conditioning stand and the gains can be adjusted.
2. The simulation work employed in the project used a single zone thermodynamic model of the combustion chamber with detailed chemical kinetics. Implicit in the assumptions of this model is that there are no non-homogeneities in the combustion chamber. However, local variation in the temperature within the combustion chamber would be expected to increase the burn durations and thereby decrease the peak cylinder pressure and rate of pressure rise. These local non-homogeneities can only be resolved with multidimensional engine simulation. Future studies should combine multidimensional engine simulation along with the engine experiments.
3. This work demonstrates that by adding hydrogen, the light-off temperature of HCCI combustion can be appreciably lowered. This feature of HCCI combustion of natural gas/hydrogen mixtures could be exploited to allow for cycle-by-cycle control of the phasing of HCCI combustion. For instance, port-injecting hydrogen would allow for cycle-by-cycle control of the composition of the fuel mixture through which the phasing of the combustion could be controlled. The current experimental setup at GTI could be modified to incorporate a hydrogen port fuel injector and control system to implement an advanced HCCI control strategy. The proposed HCCI combustion control system could generate hydrogen directly from natural gas using GTI's advanced thermo chemical recuperation (TCR) technology, rather than using an auxiliary source of hydrogen. An HCCI combustion control system using TCR is being investigated by West Virginia University (WVU) and GTI under DOE project DE-FC26-05NT42632 for application to heavy duty diesel fueled engines.

APPENDIX A: PHOTOGRAPHS

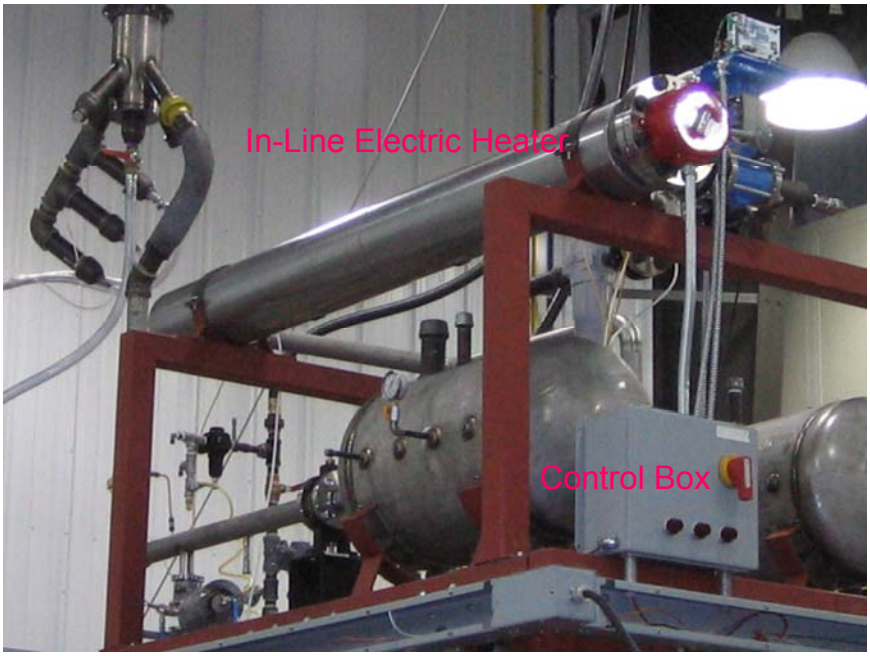

Figure 1A – In-line electric heater and control box installed on the engine test bench

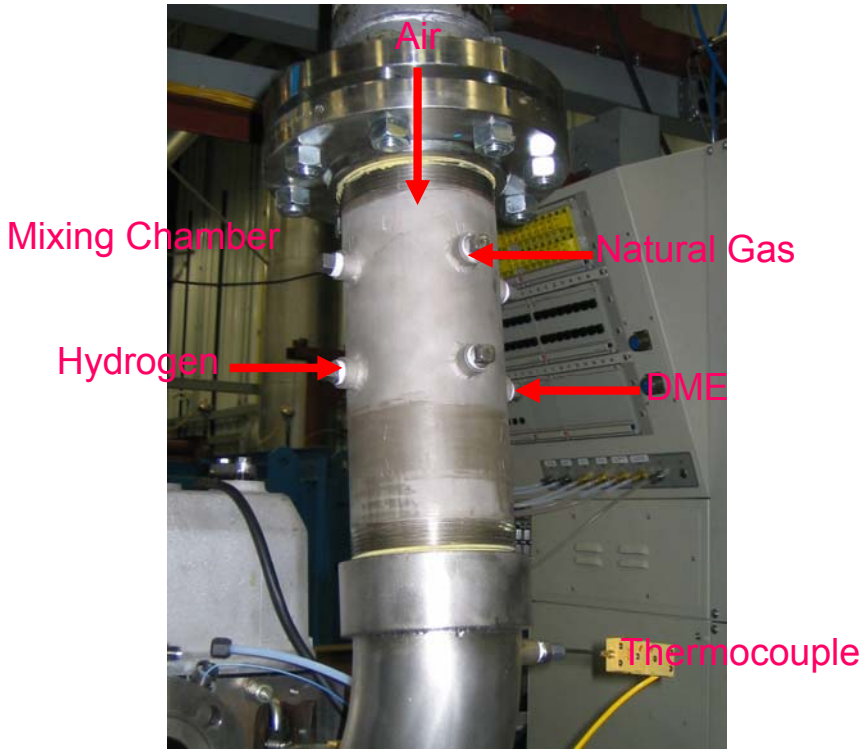

Figure 2A – Mixing chamber installed in the engine bench.

Figure 3A – Hydrogen and DME fuel trains on the fuel cart

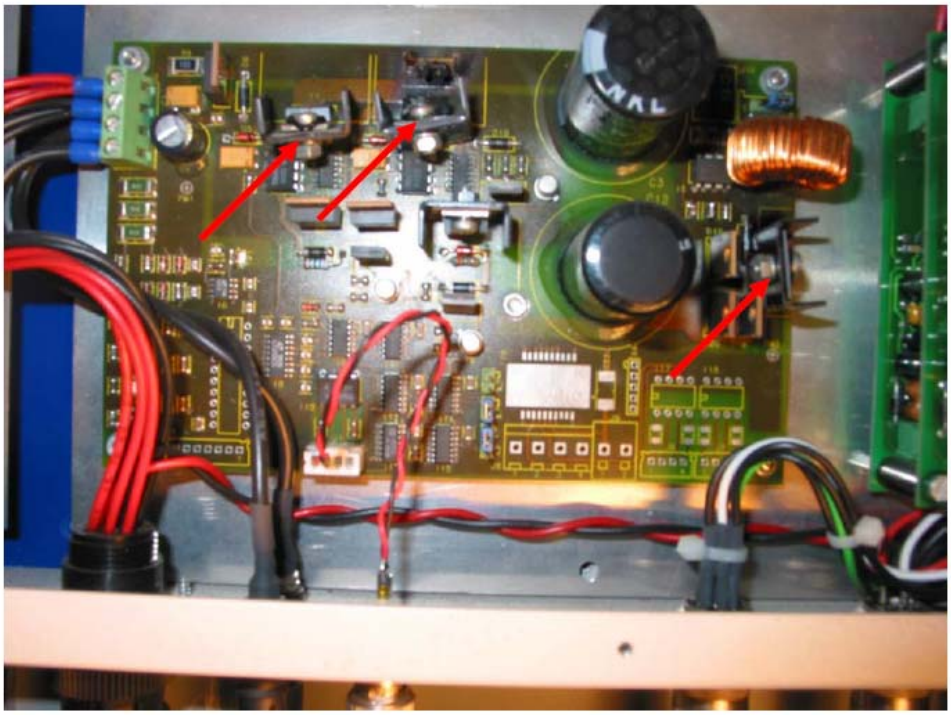

Figure 4A – Printed Circuit Board for Common Rail Fuel Injection Controller.
The three red arrows indicate the components that failed.

APPENDIX B: DATA

Test Point		2	3	4	5	6	7	8	9	10	11	12
Intake Air Temp	C	129.7326	163.9473	107.5348	156.5855	143.7036	121.2288	109.9306	98.5870	141.6488	118.2184	131.9481
Exhaust Temp	C	345.9773	350.9195	348.8414	372.2776	377.4231	308.8249	348.6749	348.6749	333.7766	313.2046	306.3019
Delta T	C	216.2447	186.9722	241.3067	215.6921	233.7194	187.5961	238.7443	332.0416	192.1278	194.9862	174.3537
Coolant Out Temp	C	98.1409	98.3712	97.3618	90.0221	98.6986	97.2568	99.4492	96.0927	96.9208	95.2136	96.0616
10% Heat Release	deg	5.8207	7.2600	7.1555	5.0050	2.1694	6.4155	9.6020	9.2544	1.8260	8.2375	5.4717
50% Heat Release	deg	9.2440	13.7050	10.1905	8.4945	3.8867	10.5115	15.7345	13.8344	3.9700	14.0915	9.4947
Timing Peak Pressure	deg	10.2700	14.4995	11.3415	9.8190	4.9587	11.3760	15.1515	14.9824	5.0050	15.0730	10.2497
Peak Cylinder Pressure	Bar	160.6208	83.3618	160.3154	85.5640	153.0518	183.0900	155.5616	167.0938	119.4151	157.4248	143.0099
Speed	rpm	1799.50	1800.55	1799.14	1799.59	1799.50	1800.55	1799.49	1799.46	1799.50	1799.49	1799.50
BMEP	Bar	12.5675	6.0507	12.5715	4.8325	7.6520	15.4234	16.9734	16.4683	6.5115	15.0625	10.2371
Power	kW	38.1202	18.3645	38.1247	14.6591	23.2105	46.8115	51.4853	49.9515	19.7510	45.6899	31.0517
Torque	ft-lbs	149.1409	71.8054	149.1888	57.3484	90.8084	183.0323	201.4269	195.4331	77.2728	178.7503	121.4856
Air Flow Rate	kg/hr	261.5965	176.1763	266.5881	140.1639	175.4538	338.2847	345.8785	344.3630	177.5867	342.6260	262.8156
H2 Flow Rate	kg/hr	0.0000	0.0000	0.5654	0.1111	0.0000	0.0000	0.0000	0.8014	0.2662	0.0000	0.1782
Natural Gas Flow Rate	kg/hr	5.5970	3.3080	4.4779	2.7625	4.2684	6.3560	7.3737	5.1546	2.8320	6.4038	4.2702
H2 Energy Flow Rate	mJ/hr	0.0000	0.0000	67.8481	13.3334	0.0000	0.0000	0.0000	96.1698	31.9493	0.0000	21.3874
NG Energy Flow Rate	mJ/hr	251.8645	148.8603	201.5050	124.3126	192.0802	286.0198	331.8176	231.9576	127.4409	288.1701	192.1610
Total Energy Flow Rate	mJ/hr	251.8645	148.8603	269.3531	137.6461	192.0802	286.0198	331.8176	328.1274	159.3902	288.1701	213.5485
Percent Hydrogen	%	0.0000	0.0000	25.1918	9.6867	0.0000	0.0000	0.0000	29.3352	20.0447	0.0000	10.0152
Thermal Efficiency	%	54.4866	44.4121	50.9545	38.3394	43.5081	58.9194	55.8262	54.8063	44.6098	57.0786	52.3470
Actual Lambda		2.886001	3.288516	2.904739	2.888595	2.538117	3.28638	2.896381	3.108666	3.232797	3.303718	3.49363
CO	ppm	262.2801	765.8775	172.2399	49.9383	398.9985	236.7963	528.0596	221.0288	-15.6612	466.3882	261.1083
CO2	%	3.3644	2.7811	2.5515	2.8463	3.8481	2.7693	3.3339	2.2927	2.3507	2.6878	2.4125
CH4	ppm	1582.66	1886.69	1444.68	1783.47	1373.03	1570.85	2210.63	1214.49	1394.63	1992.68	1510.55
O2	%	13.6246	14.8666	13.2163	13.7652	13.6431	14.1168	13.7466	14.0736	14.2411	14.3266	14.6701
Nox	ppm	3.9867	-1.5759	12.7449	5.4765	109.1215	3.1064	1.0227	3.7941	5.8148	-6.1711	2.5804
THC	ppm	1921.38	2303.79	1478.59	1988.37	1767.36	1754.15	2256.78	1370.26	1509.40	1905.55	1660.26
Intake Manifold Pressure	bar	2.809301	1.99943	2.809104	1.601663	2.003272	3.495445	3.515958	3.502017	1.994993	3.485773	2.805908

Test Point		13	16	17	18	19	20	21	22	24	25	26	27
Intake Air Temp	C	121.2054	134.9645	121.3908	100.476	117.17742	145.2984	115.85626	178.8110	106.7964	121.4852	105.6075	120.8766
Exhaust Temp	C	361.5203	337.6516	345.7459	352.744	343.41867	403.8523	341.32471	334.0001	310.8134	337.7888	313.1491	397.7119
Delta T	C	240.3149	202.6871	224.3551	252.268	226.24125	258.5538	225.46845	155.1890	204.0170	216.3037	207.5415	276.8353
Coolant Out Temp	C	99.3681	90.1232	98.8257	99.1411	99.694481	97.7526	98.234543	98.2481	94.2774	97.4602	96.6080	94.0649
10% Heat Release	deg	9.8350	7.7955	5.8160	2.05703	5.970025	7.9950	5.902025	1.3054	6.9450	3.6010	8.7540	7.5110
50% Heat Release	deg	16.1850	13.9115	8.6600	3.65103	8.874024	12.7245	8.679025	3.6977	10.1460	5.6880	13.4330	10.6790
Timing Peak Pressure	deg	16.9835	14.0775	9.6930	5.10202	9.755024	15.0010	9.723023	4.6890	11.0470	6.6530	14.9075	12.6300
Peak Cylinder Pressure	Bar	116.7745	84.7221	164.4949	165.691	162.3018	98.5859	174.89787	112.4784	188.7081	188.0831	164.6769	110.5512
Speed	rpm	1799.49	1799.50	1799.42	1799.49	1799.6603	1799.48	1799.6467	1799.49	1799.86	1798.98	1799.38	1799.59
BMEP	Bar	12.0913	6.3564	12.3494	7.36604	12.668207	8.4617	12.429806	5.6255	15.6315	12.0613	15.2957	8.6841
Power	kW	36.6766	19.2803	37.4587	22.3434	38.425457	25.6663	37.704453	17.0637	47.4233	36.5759	46.3923	26.3426
Torque	ft-lbs	143.4902	75.4322	146.5525	87.4143	150.3362	100.4168	147.50705	66.7594	185.5023	143.1338	181.5174	103.0565
Air Flow Rate	kg/hr	265.4009	182.8345	261.7171	181.914	266.49362	177.5870	263.09567	170.3645	338.1353	261.3838	343.5820	180.8931
H2 Flow Rate	kg/hr	0.2163	0.2644	0.2152	0.37971	0.265044	0.0000	0.26876	0.0000	0.6093	0.2175	0.6056	0.3517
Natural Gas Flow Rate	kg/hr	5.1993	2.8350	5.1980	3.5222	5.076475	4.4032	5.08402	3.1797	5.1265	5.1485	5.1026	3.6758
H2 Energy Flow Rate	mJ/hr	25.9581	31.7329	25.8275	45.565	31.80528	0.0000	32.2512	0.0000	73.1149	26.1024	72.6697	42.2046
NG Energy Flow Rate	mJ/hr	233.9687	127.5758	233.9113	158.499	228.44138	198.1436	228.7809	143.0844	230.6908	231.6811	229.6180	165.4126
Total Energy Flow Rate	mJ/hr	259.9268	159.3086	259.7387	204.064	260.24666	198.1436	261.0321	143.0844	303.8058	257.7835	302.2878	207.6172
Percent Hydrogen	%	9.9867	19.9191	9.9436	22.3287	12.221206	0.0000	12.355262	0.0000	24.0663	10.1257	24.0399	20.3281
Thermal Efficiency	%	50.7970	43.5690	51.9181	39.4171	53.154053	46.6323	51.999747	42.9323	56.1951	51.0791	55.2495	45.6770
Actual Lambda		2.898322	3.329109	2.859898	2.5997	2.920769	2.4904	2.8756872	3.3084	3.258334	2.879051	3.327249	2.529647
CO	ppm	537.4512	491.8420	212.2192	443.573	209.96021	282.9752	180.3251	260.0458	165.3934	262.4361	228.2987	3.8075
CO2	%	2.8673	2.1106	3.0415	3.02912	3.00754	3.6771	2.821229	2.7643	2.1805	3.0835	2.1309	2.9937
CH4	ppm	2506.77	1957.98	1595.02	1027.59	1447.449	1911.91	1501.2839	1534.77	1313.65	1494.79	1434.97	1579.90
O2	%	13.4864	14.2574	13.1212	13.5636	13.75192	20.3256	14.87526	22.5313	14.1647	13.1628	14.0213	12.5554
Nox	ppm	4.2017	2.7898	12.1369	87.4203	3.72612	16.2658	10.072283	3.9168	2.3191	17.6237	-6.0457	16.7392
THC	ppm	2229.91	2015.20	1787.91	1224.98	1720.7061	2167.01	1658.129	1735.89	1380.05	1683.78	1437.34	1777.58
Intake Manifold Pressure	bar	2.807028	2.013395	2.792606	2.00517	2.815939	1.9947	2.793127	1.9997	3.479243	2.808575	3.47837	1.999313

Note on Pressure Traces: The data contained in the previous tables is an average of 100 engine cycles. Due to the unstable nature of HCCI, actual cylinder pressure varies from cycle to cycle. The way GTI's laboratory data acquisition system is configured, the graphical pressure trace shown in the following figures represents only the first cycle of the 100 averaged. It is meant to show a graphical example of the pressure rise and heat release, and may not exactly correspond to the average of multiple cycles.

Test Point One:

No data was taken for test point one. Modeling of test point one predicted a peak cylinder pressure of 220 bar, far beyond the limits of the D12 engine. Experimental data for points 7 and 8 indicate that test point one will not be achievable with a 180 bar cylinder pressure limit.

Test Point Two:

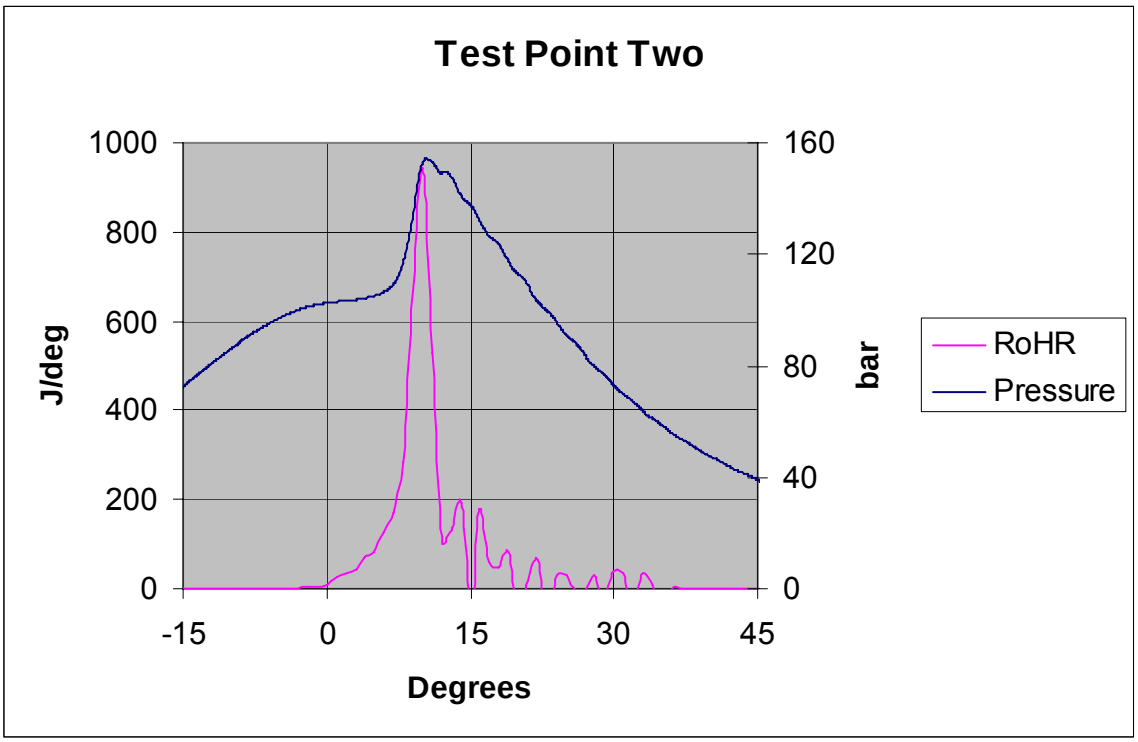

Figure A4 - Pressure and rate of heat release for test point 2.

Test Point Three:

Test point three one of the easiest and most consistent points in the test matrix to operate at. With a lambda of 3.3 and an inlet pressure of 2.0 bar, start of combustion was smooth and predictable. Operation was very stable and unaffected by small variations in laboratory settings. Test point three was repeated multiple times throughout the commissioning of the laboratory and during the weeks of testing to serve as a baseline for the testing.

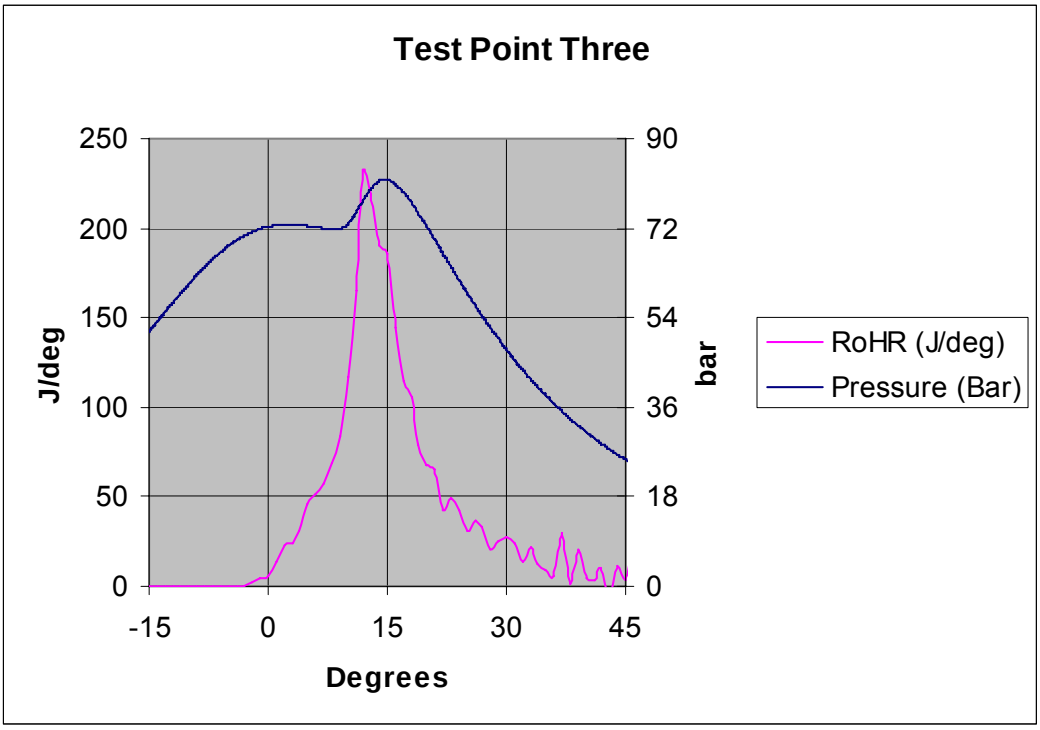

Figure A5 - Pressure and rate of heat release data for test point 3

Test Point Four:

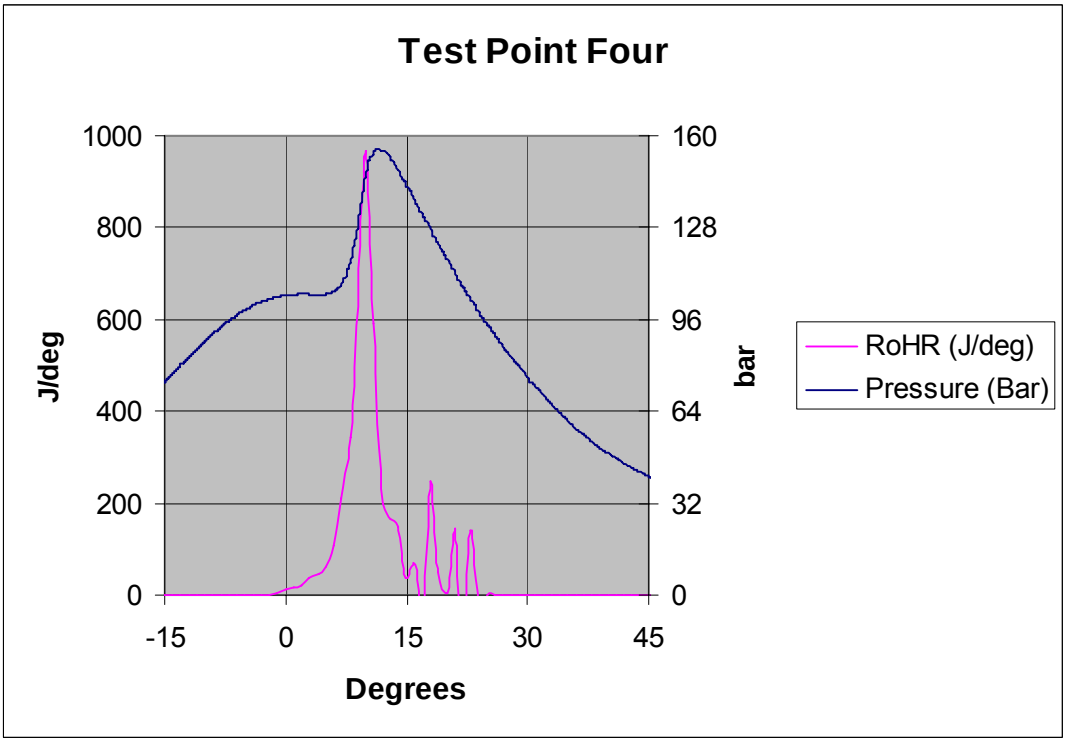

Figure A6 - Pressure and rate of heat release data for test point 4

Test Point Five:

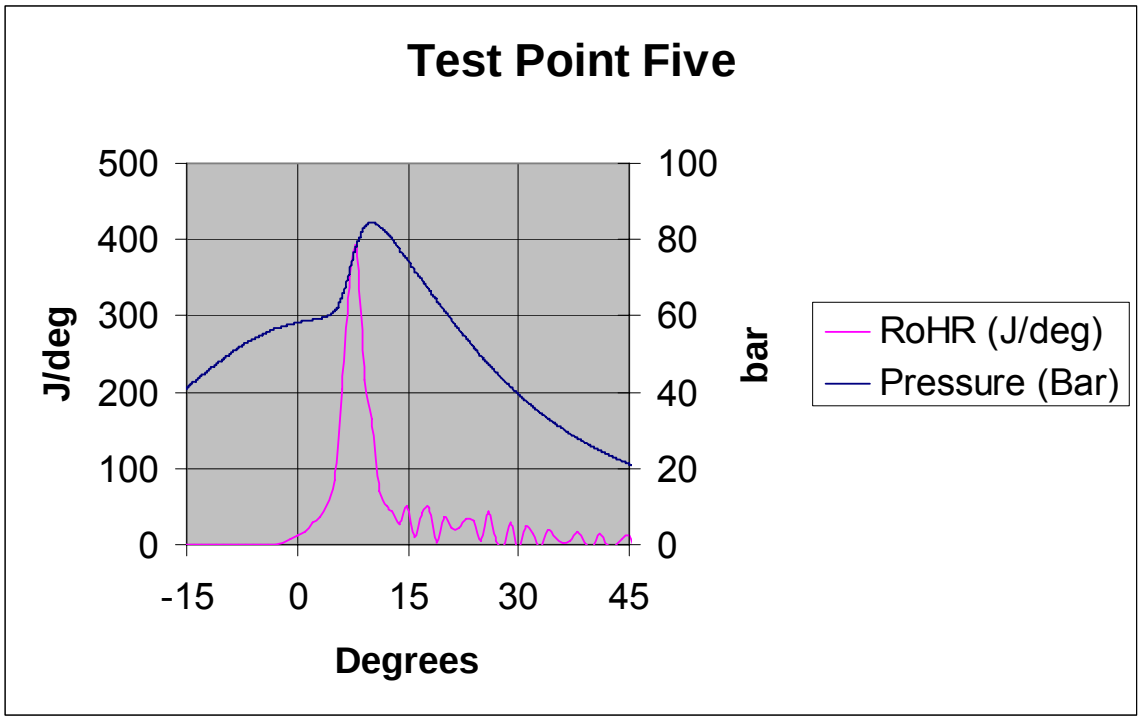

Figure A7 - Pressure and rate of heat release data for test point 5

Test Point Six:

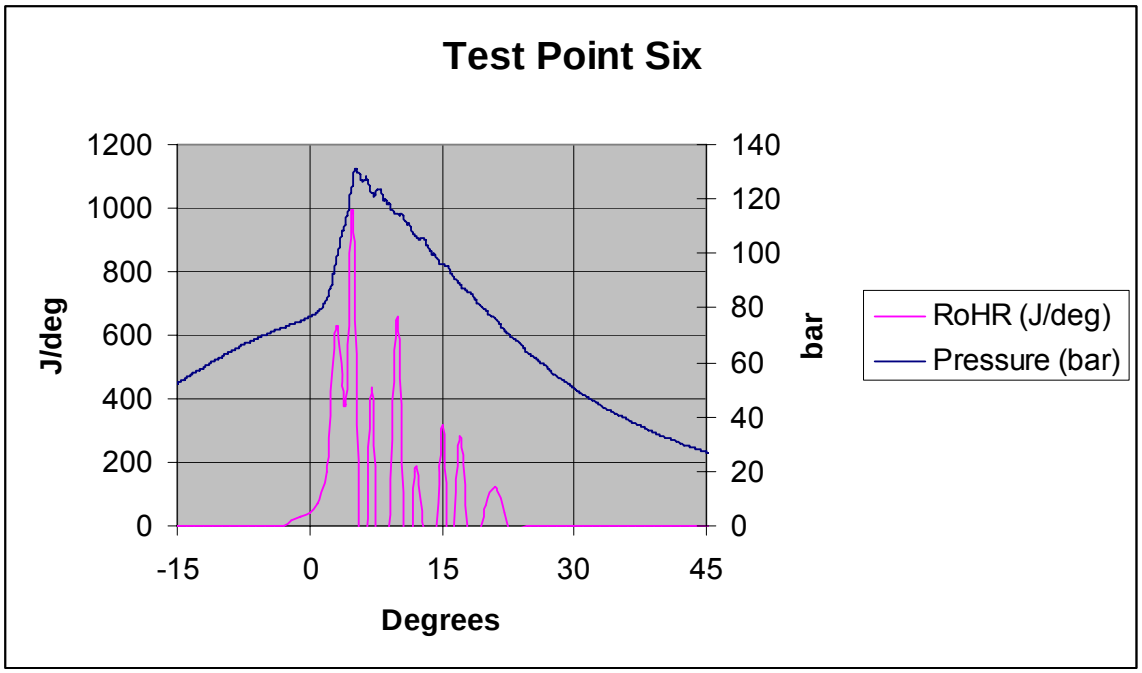

Figure A8 - Pressure and rate of heat release data for test point 6

Test Point Seven:

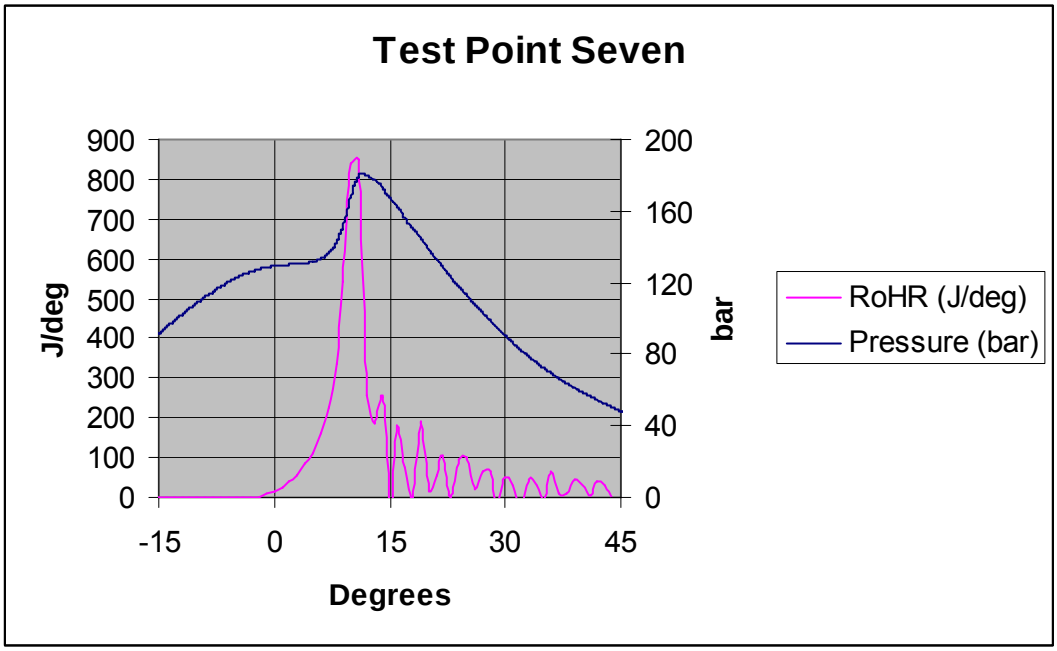

Figure A9 - Pressure and rate of heat release data for test point 7

Test Point Eight:

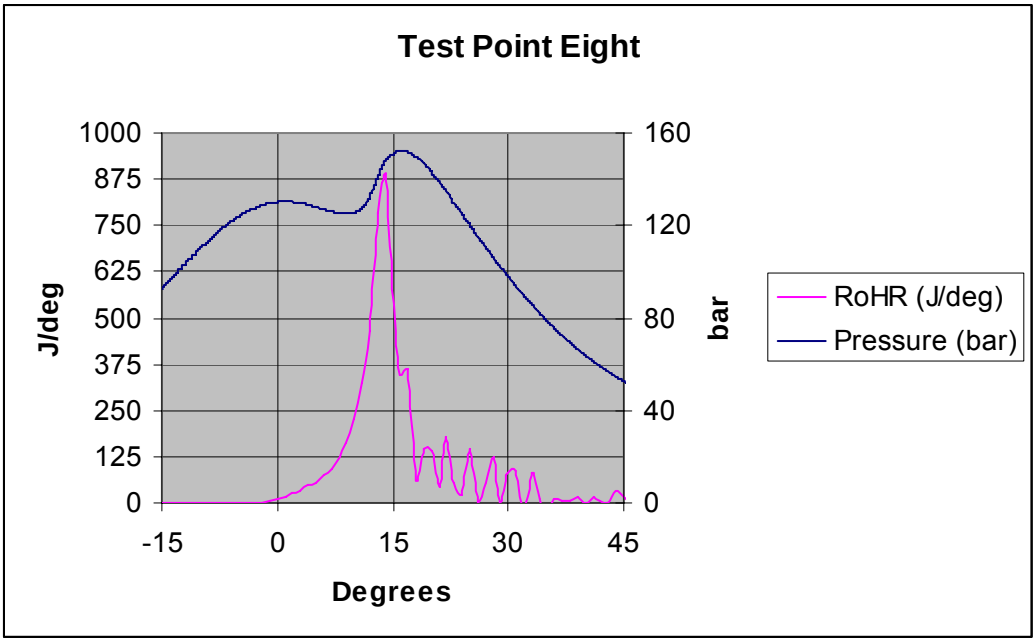

Figure A10 - Pressure and rate of heat release data for test point 8

Test Point Nine:

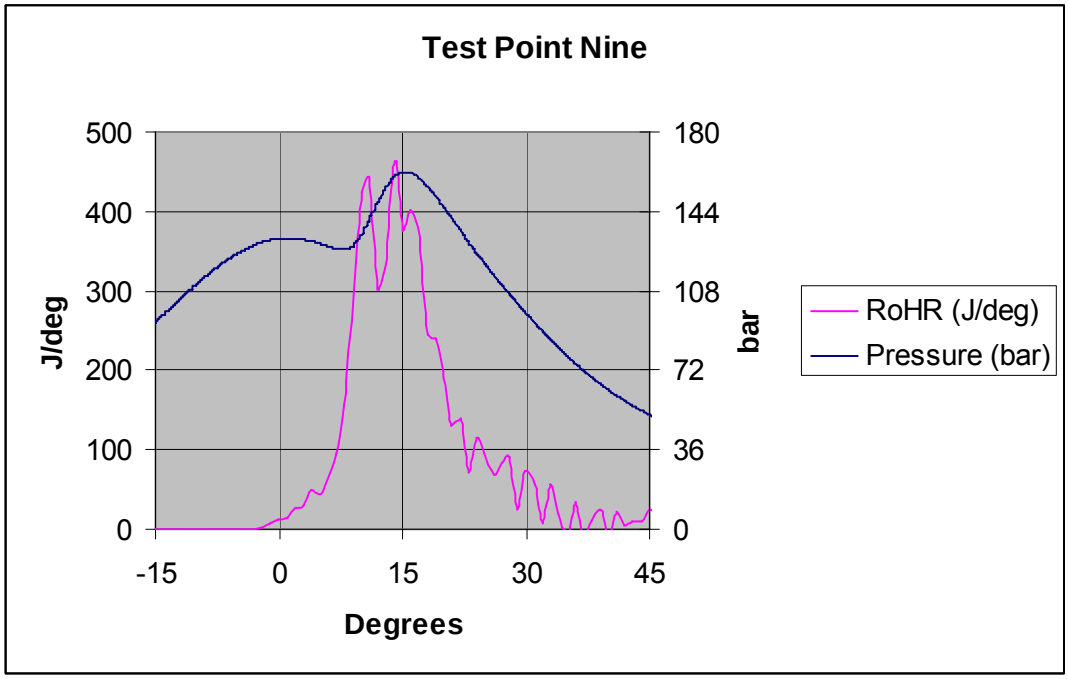

Figure A11 - Pressure and rate of heat release data for test point 9

Test Point Ten:

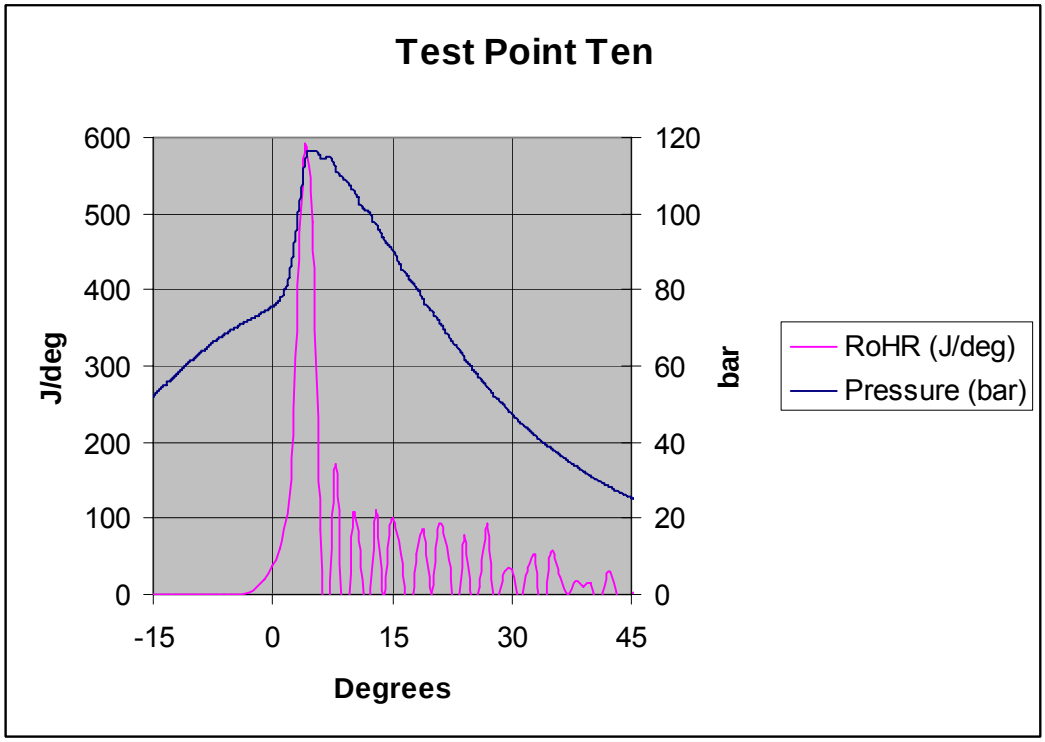

Figure A12 - Pressure and rate of heat release data for test point 10

Test Point Eleven:

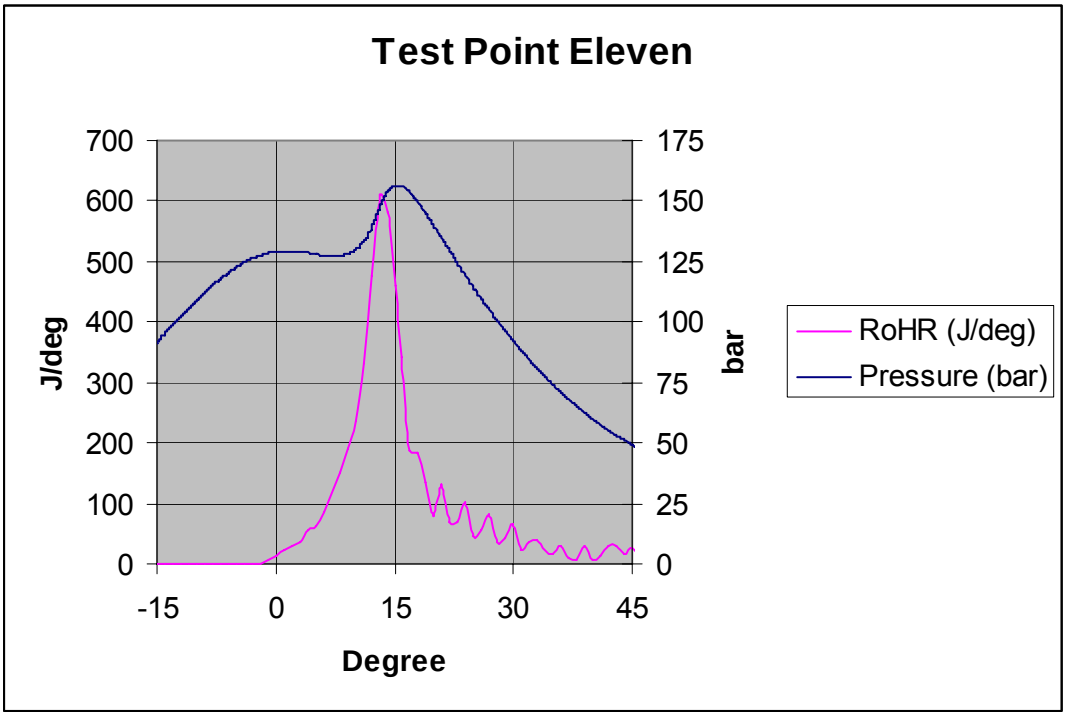

Figure A13 - Pressure and rate of heat release data for test point 11.

Test Point Twelve:

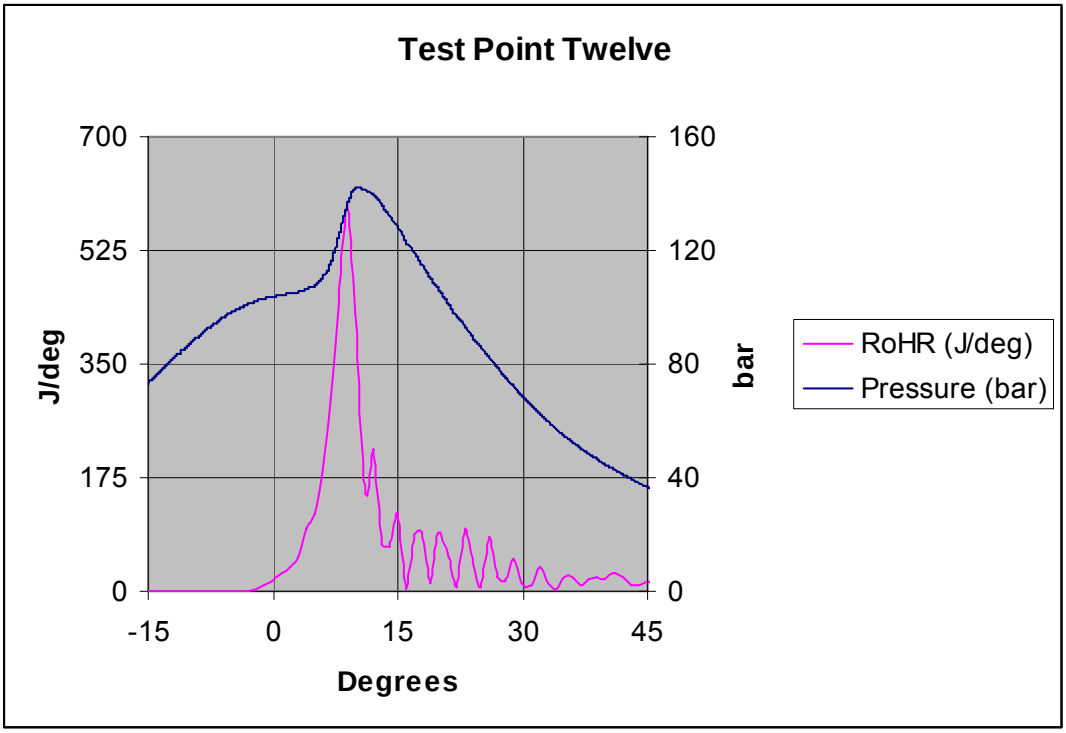

Figure A14 - Pressure and rate of heat release data for test point 12

Test Point Thirteen:

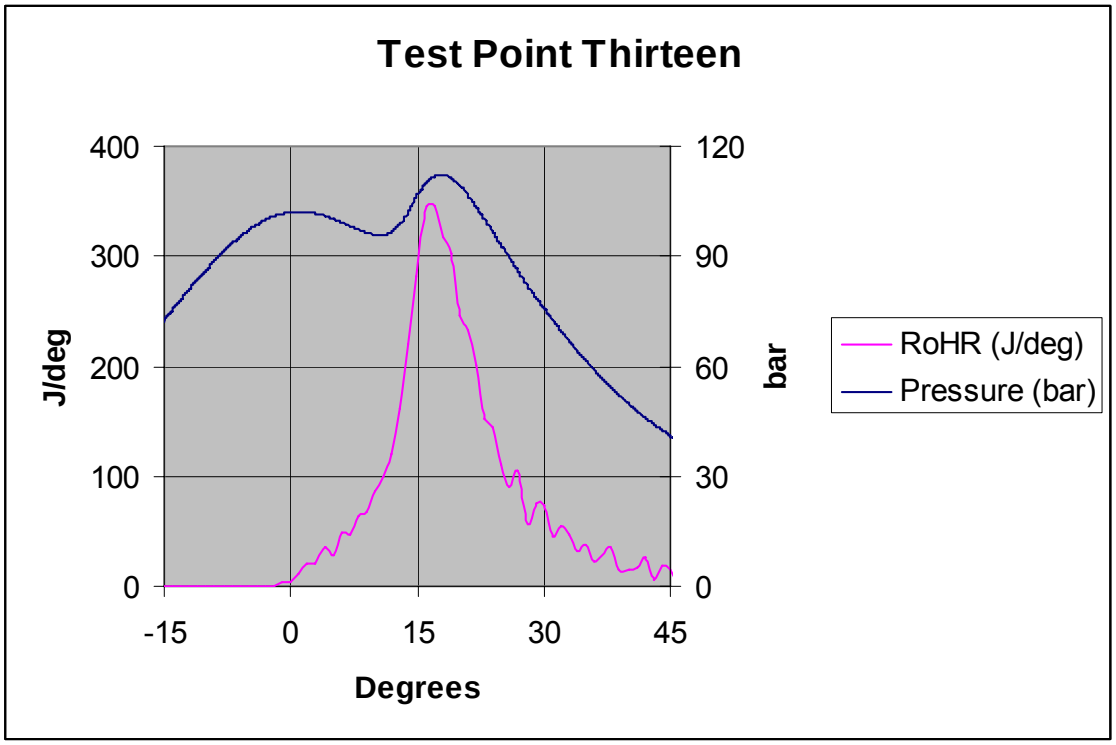

Figure A15 - Pressure and rate of heat release data for test point 13

Test Point Fourteen:

Test point 14 was attempted, but no good data was taken. The 3.9 bar inlet pressure is the highest in the test matrix. With the extremely high intake pressure, combustion quickly exceeds the 180 bar limit. If the intake temperature is decreased in an attempt to retard timing and decrease peak cylinder pressure, combustion is sporadic and very unstable.

Test Point Fifteen:

Test point 15 was attempted several times, but no good data was taken. Test point 15 is similar to test point 17 except with more fuel added. Test point 17 is difficult to operate at due to stability issues. Increasing the fueling rate in an attempt to reach the specified lambda of 2.3, decreases the stability and makes the test point inoperable.

Test Point Sixteen:

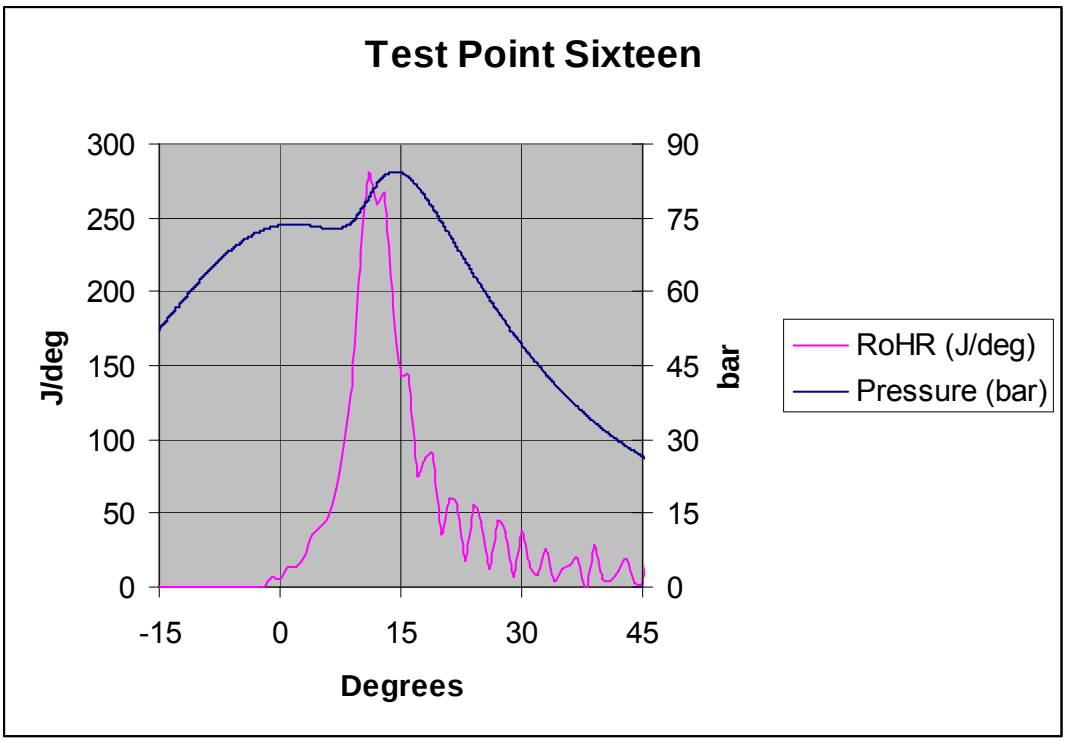

Figure A16 - Pressure and rate of heat release data for test point 16

Test Point Seventeen:

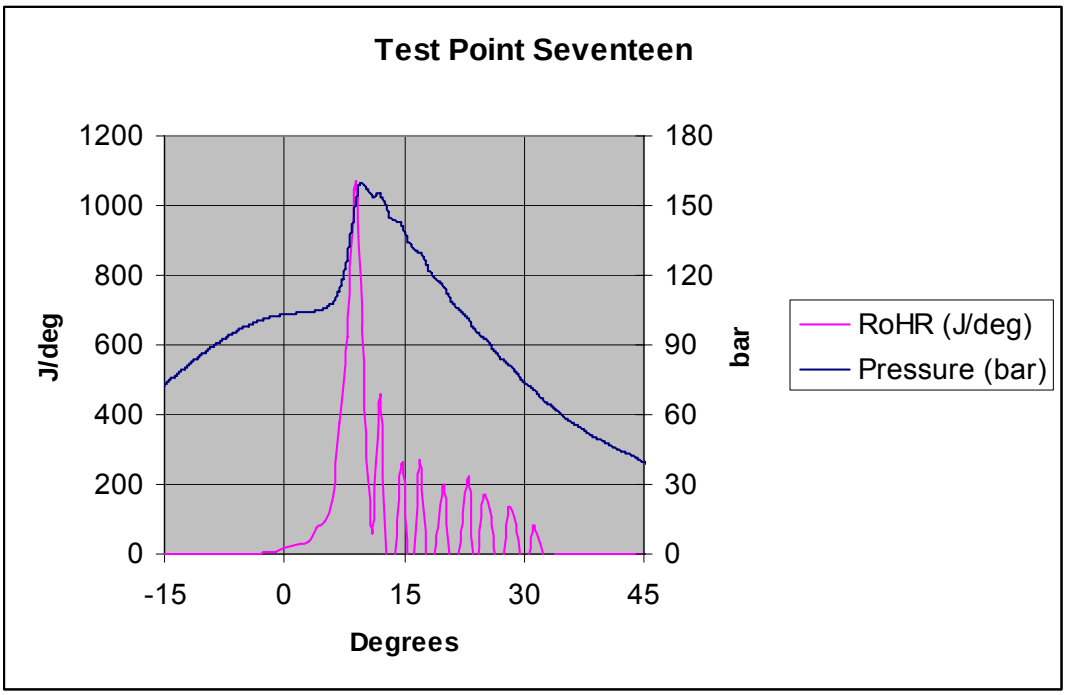

Figure A17 - Pressure and rate of heat release data for test point 17

Test Point Eighteen:

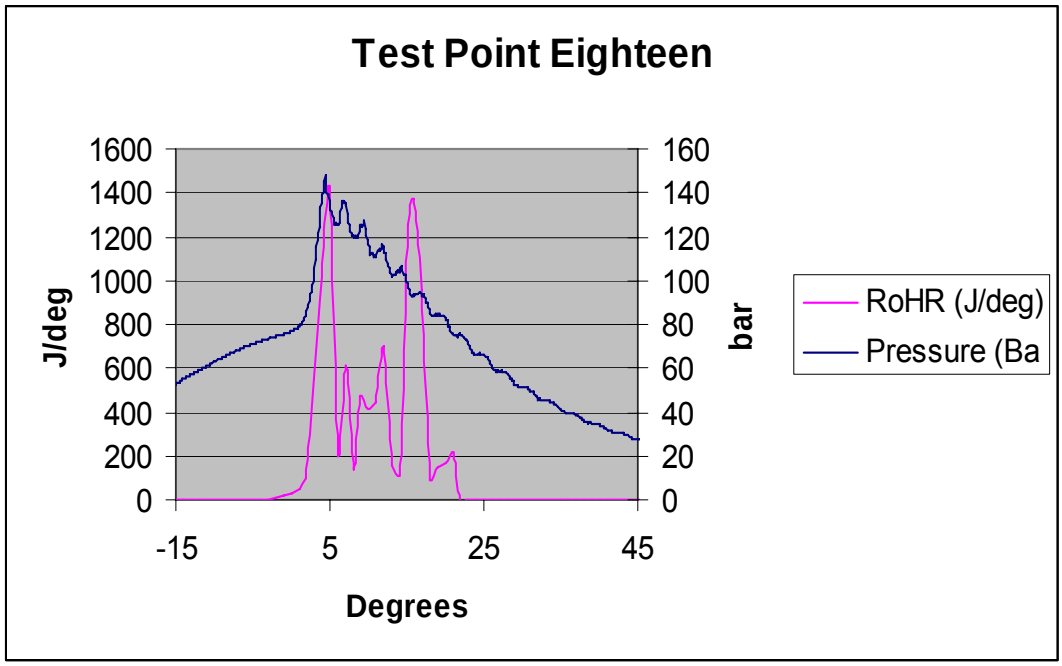

Figure A18 - Pressure and rate of heat release data for test point 18 (Note heavy ringing in the pressure trace)

Test Point Nineteen:

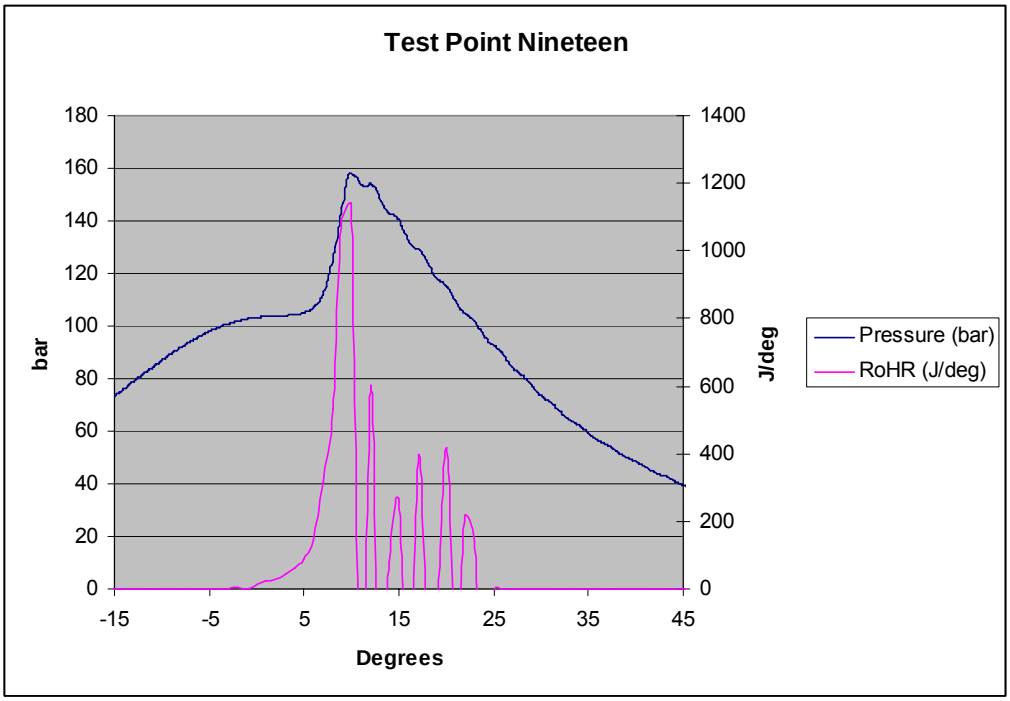

Figure A19 - Pressure and rate of heat release data for test point 19

Test Point Twenty:

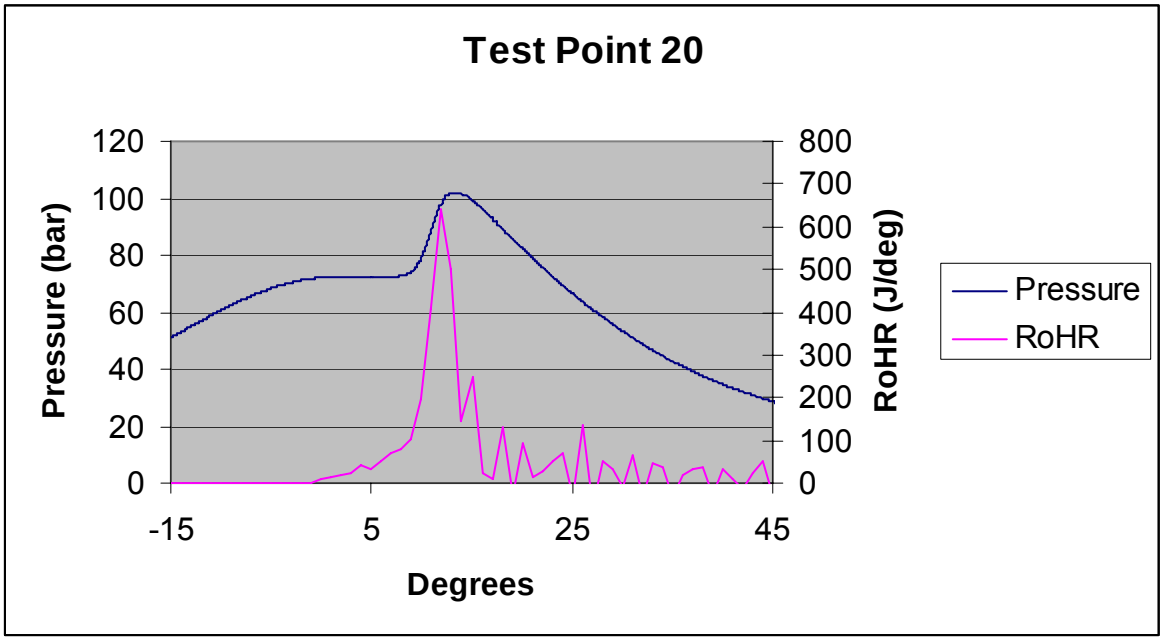

Figure A20 - Pressure and rate of heat release data for test point 20

Test Point Twenty-One:

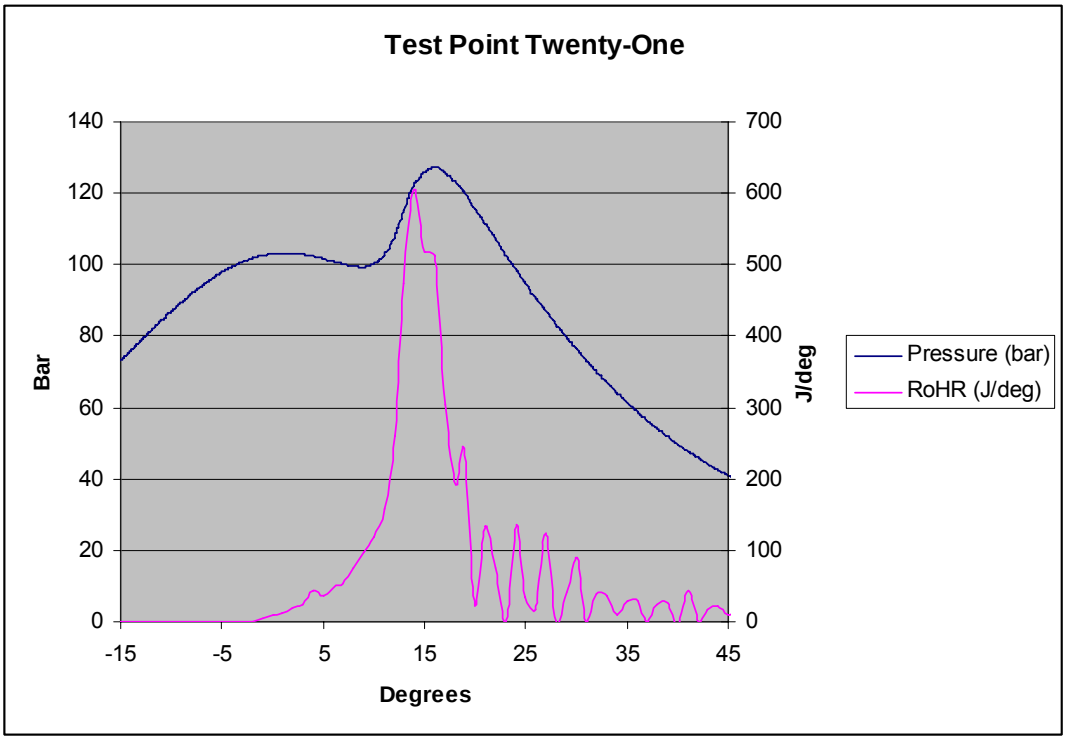

Figure A21 - Pressure and rate of heat release data for test point 21

Test Point Twenty-Two:

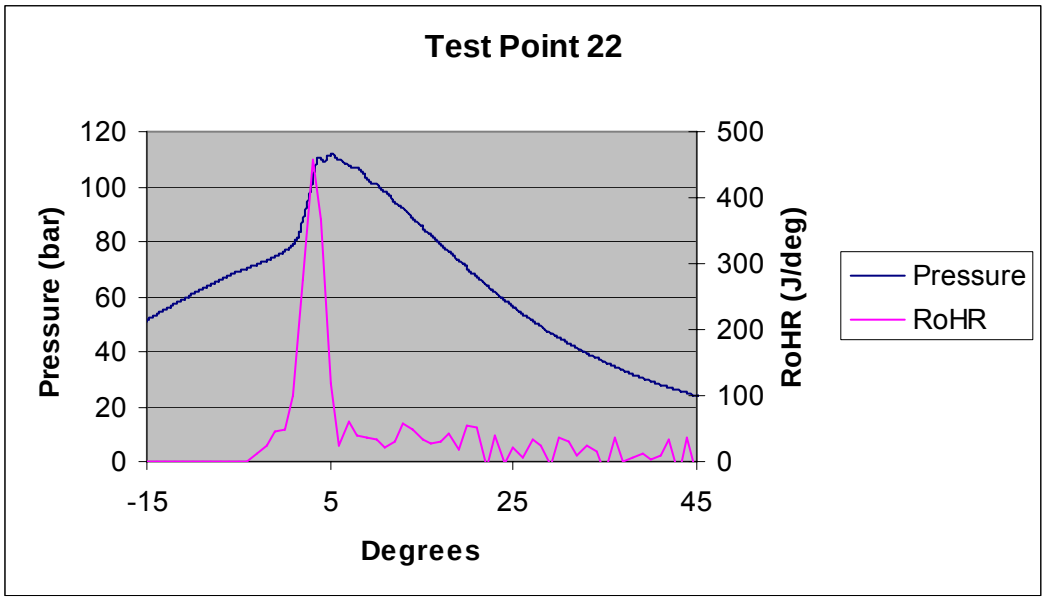

Figure A22 - Pressure and rate of heat release data for test point 22

Test Point Twenty-Three:

Test point 23 is the hydrogen enhanced version of test point one. Similarly to test point one, a peak cylinder pressure of approximately 220 bar is predicted. Also, as with test point one, experimental data from point 9 and 24 indicate that it will not be achievable.

Test Point Twenty-Four:

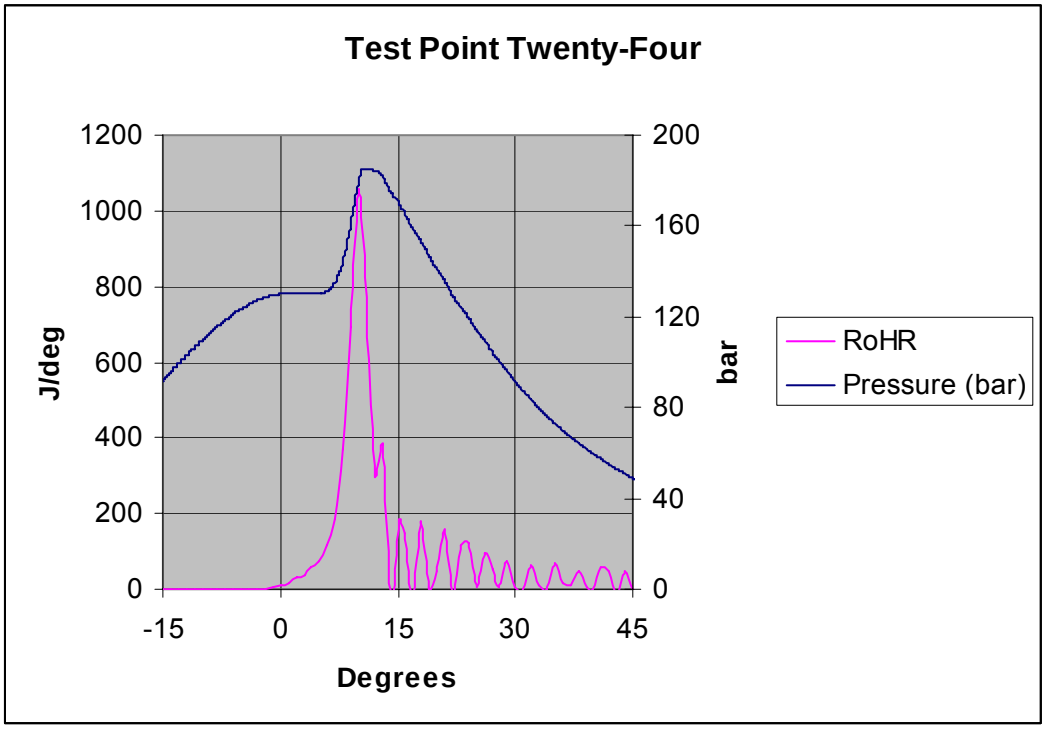

Figure A23 - Pressure and rate of heat release data for test point 24

Test Point Twenty-Five:

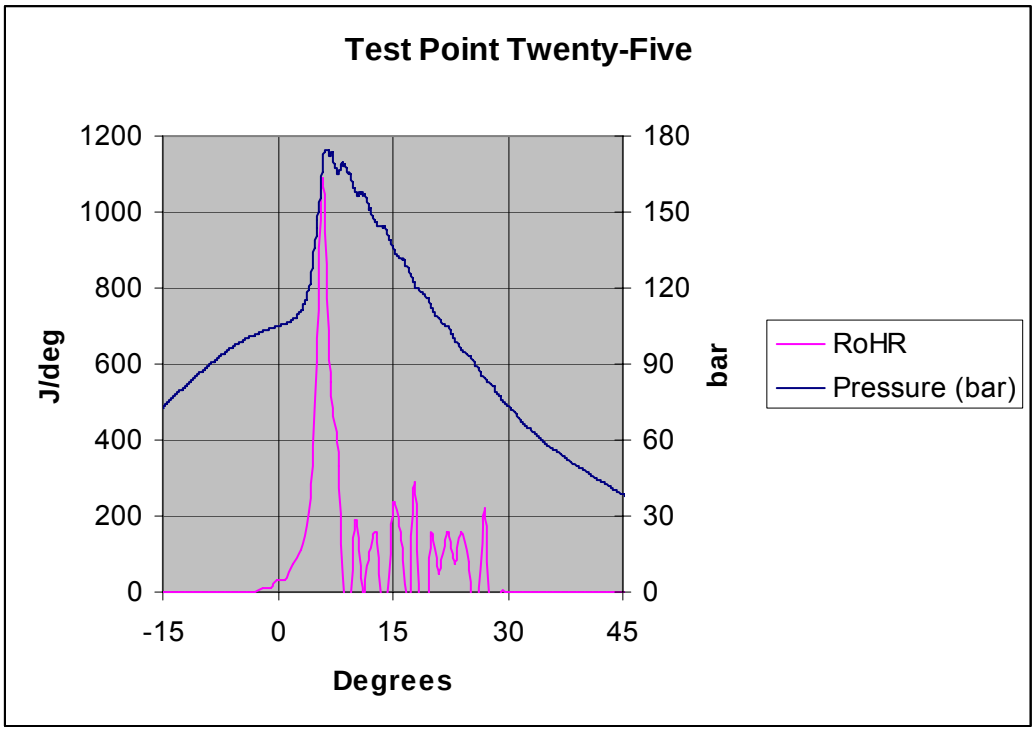

Figure A24 - Pressure and rate of heat release data for test point 25

Test Point Twenty-Six:

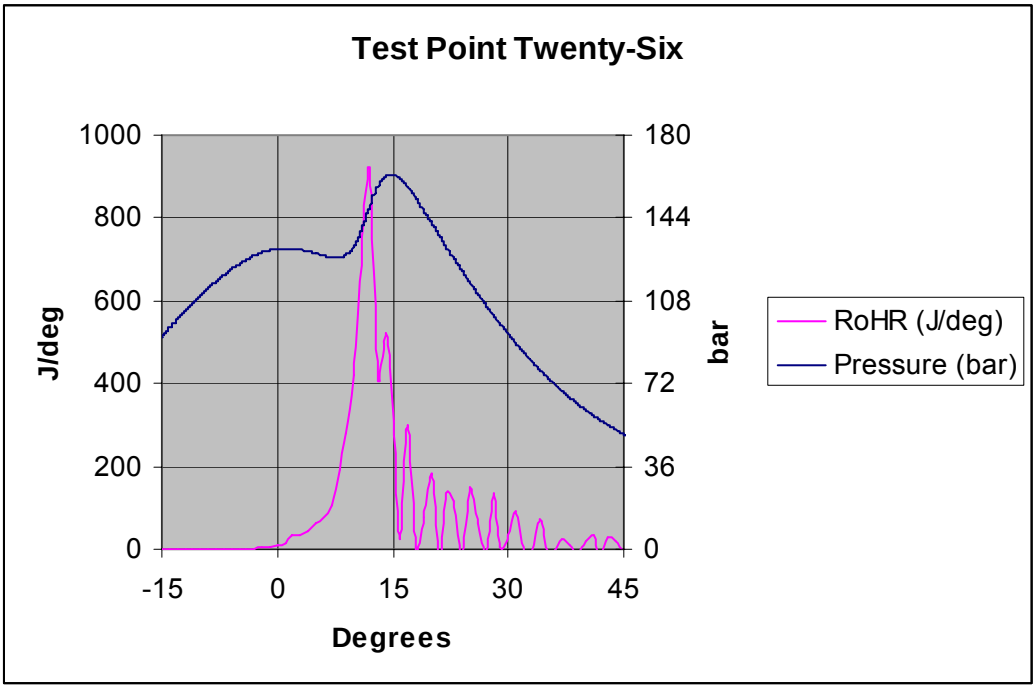

Figure A25 - Pressure and rate of heat release data for test point 26

Test Point Twenty-Seven:

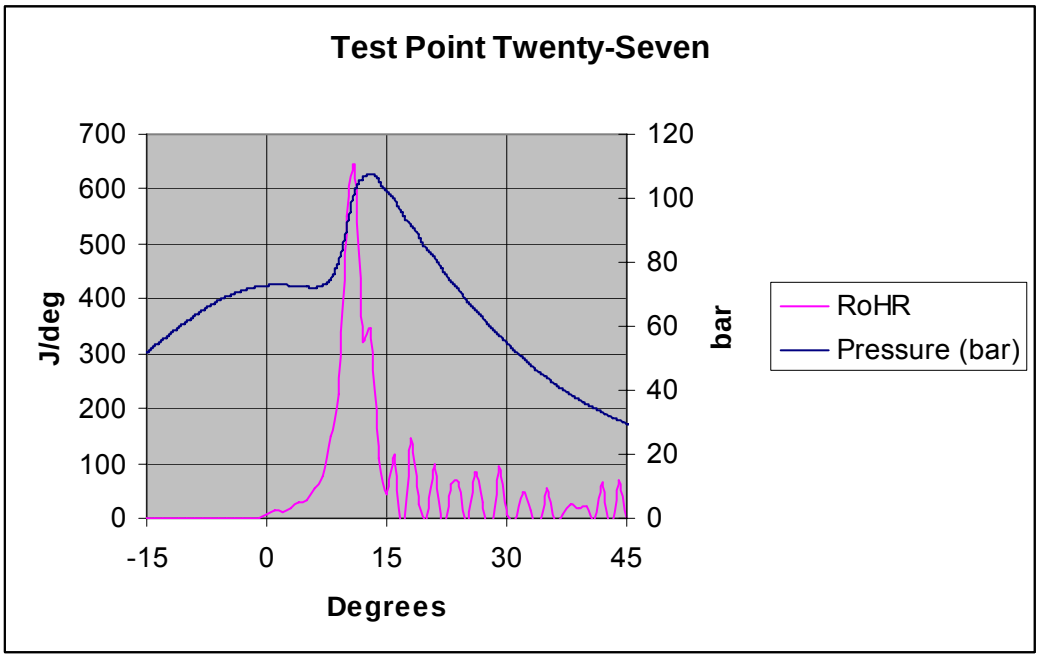

Figure A26 - Pressure and rate of heat release data for test point 27

APPENDIX C:
DIGITAL ENGINES MODEL SIMULATIONS FOR DESIGN OF EXPERIMENTS RUNS

RUN	Timing of Peak Cylinder Pressure	Lambda	H2 Content	P_{inlet}	T_{inlet}
	CA° ATDC		% Energy	Bar, absolute	K
1	5	2.5	0	3.5	457
2	10	2.9	0	2.8	458
3	15	3.3	0	2	469
4	10	2.9	25	2.8	438
5	10	2.9	10	1.6	463
6	5	2.5	0	2	483
7	5	3.3	0	3.5	460
8	15	2.5	0	3.5	443
9	15	2.5	20	3.5	433
10	5	3.3	20	2	456
11	15	3.3	0	3.5	445
12	10	3.5	10	2.8	452
13	17.5	2.9	10	2.8	445
14	10	2.9	10	3.9	441
15	10	2.3	10	2.8	448
16	15	3.3	20	2.0	446
17	10	2.9	10	2.8	450
18	5	2.5	20	2.0	454
19	10	2.9	10	2.8	450
20	15	2.5	0	2.0	467
21	10	2.9	10	2.8	450
22	5	3.3	0	2.0	484
23	5	2.5	20	3.5	443
24	5	3.3	20	3.5	446
25	2.5	2.9	10	2.8	463
26	15	3.3	20	3.5	436
27	15	2.5	20	2.0	444

The Design of Experiments test matrix for evaluating the potential for using hydrogen (blended with natural gas) to expand the operating window for HCCI combustion is repeated above. Digital Engines was contracted to provide simulations about the evolution of the in-cylinder pressure and temperature.

With so many runs to consider, run 17 was chosen as the baseline run with average values of excess air ratio, hydrogen content and intake pressure. Figure 2(a) reports the predicted pressure trace for this set of operating conditions. The pressure trace begins at intake valve closed by following an adiabatic compression with the same geometry as research engine. Once ignition occurs, there is a rapid increase in cylinder pressure over approximately seven to ten crank angles, followed by an adiabatic expansion to exhaust valve open. .

The burn duration in the actual engine is expected to be longer than the burn duration predicted by the model, which would lower the peak cylinder pressure in the experiment. the model predicts that the peak cylinder pressure is lower than the 180 bar pressure limit on the engine, the run represents a safe operating condition. The predicted temperature evolution curve, shown in Fig. 2.b shows that the exhaust temperature will be about 1000 K.

Figures 3-11 show the pressure and temperature evolution curves for each operating condition in the proposed test matrix..

Overall, the shapes of the pressure and temperature evolution curves are very similar from run to run with the desired timing of the peak cylinder pressure. The simulations predicted that the peak cylinder pressure would be approached or exceeded by a number of proposed test points.

The model predicted Peak Cylinder Pressure Approaching the Pressure Limit for Test Points 8 and 9 and Predicted Peak Cylinder Pressure Exceeding the Pressure Limit for Test Points 1, 7, 14, 23, and 24.

Recognizing that the simulations tend to over predict the peak cylinder, DE advised that GTI's engine may still be able to operate at run 8 and run 9 conditions. However, these operating points should be approached with caution. DE also advised GTI that runs that are predicted to exceed the peak pressure limit should not be attempted on the engine until a measure of the magnitude of the simulations over prediction was available

Plots of predicted versus actual pressure traces for each of the test runs are included at the end of Appendix C. As expected, the model consistently over-predicted the .peak pressure rise.

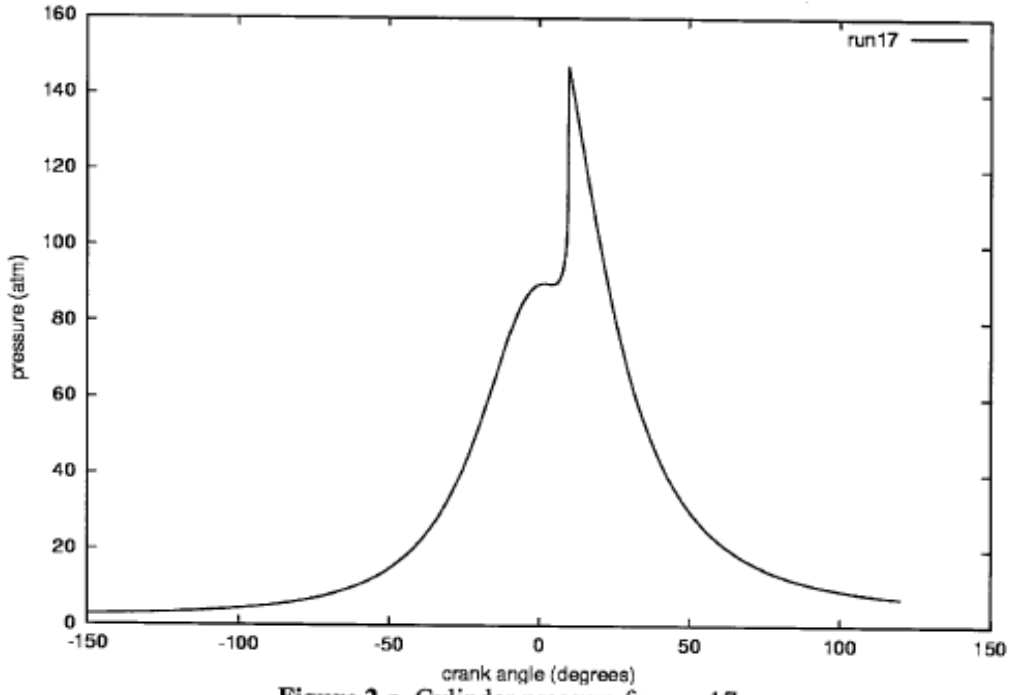

Figure 2.a. Cylinder pressure for run 17.

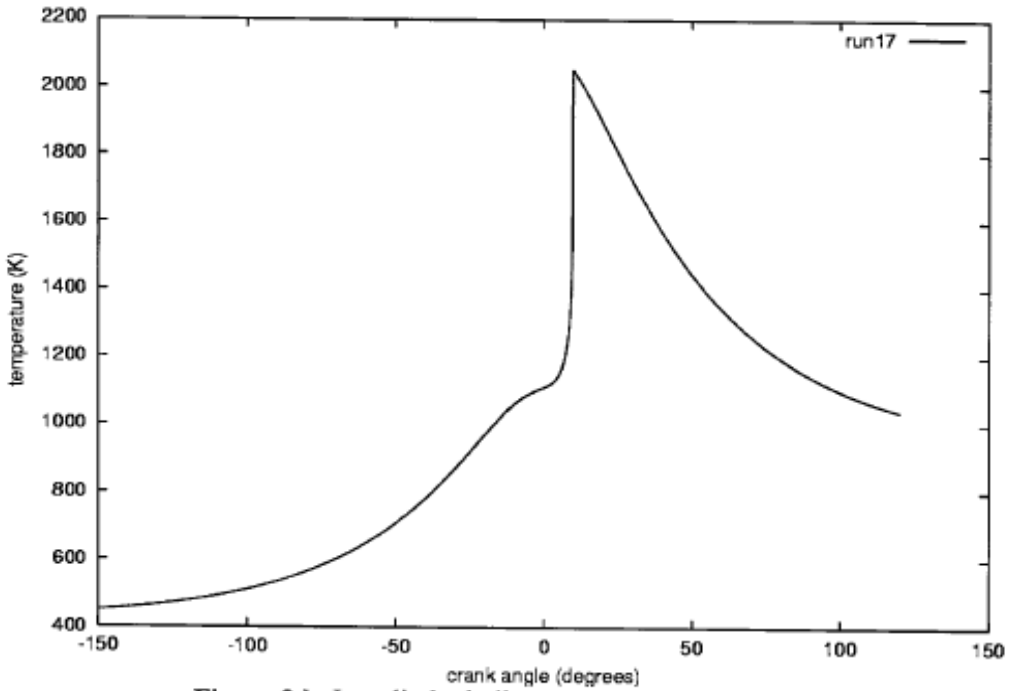

Figure 2.b. In-cylinder bulk gas temperature for run 17

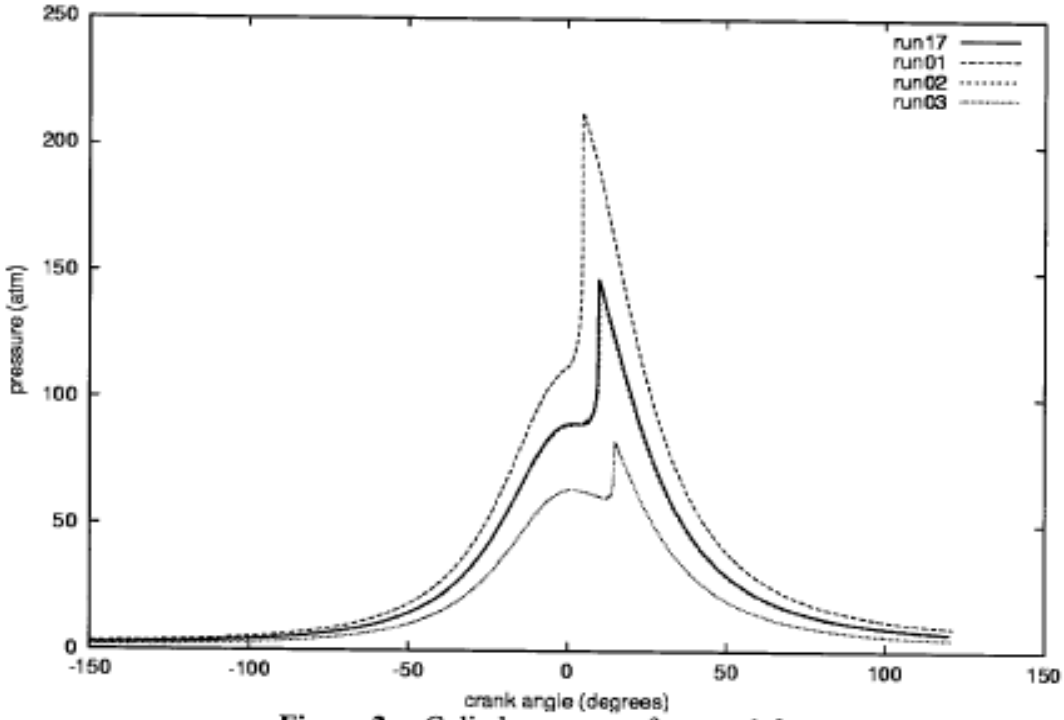

Figure 3.a. Cylinder pressure for runs 1-3.

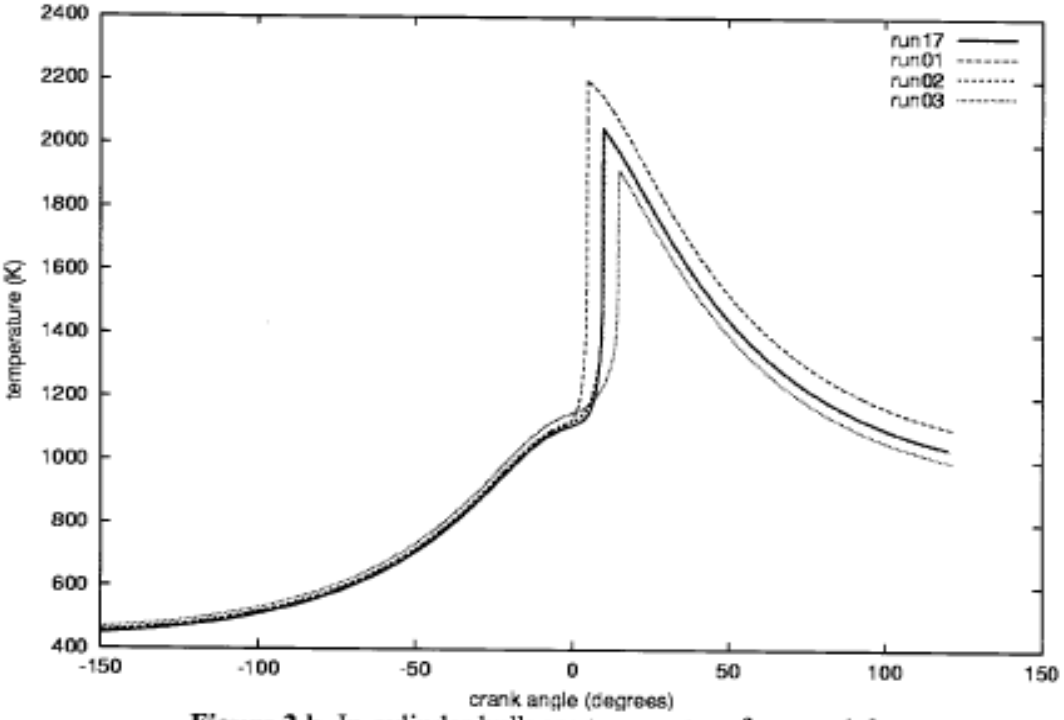

Figure 3.b. In-cylinder bulk gas temperature for runs 1-3

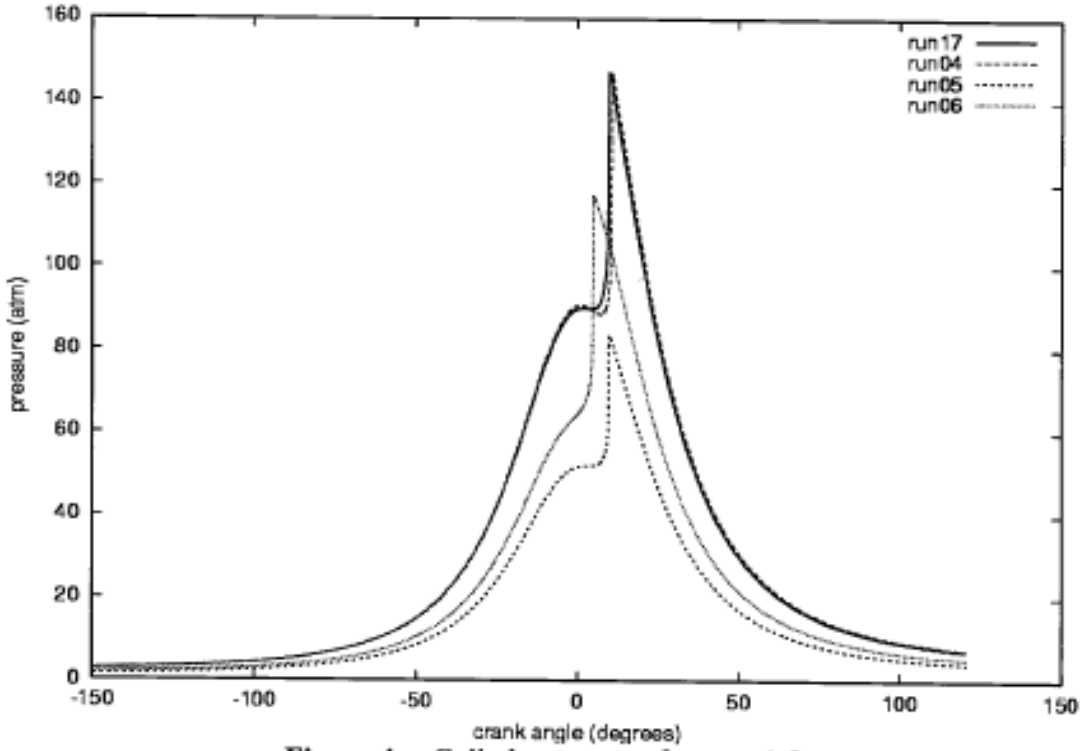

Figure 4.a. Cylinder pressure for runs 4-5.

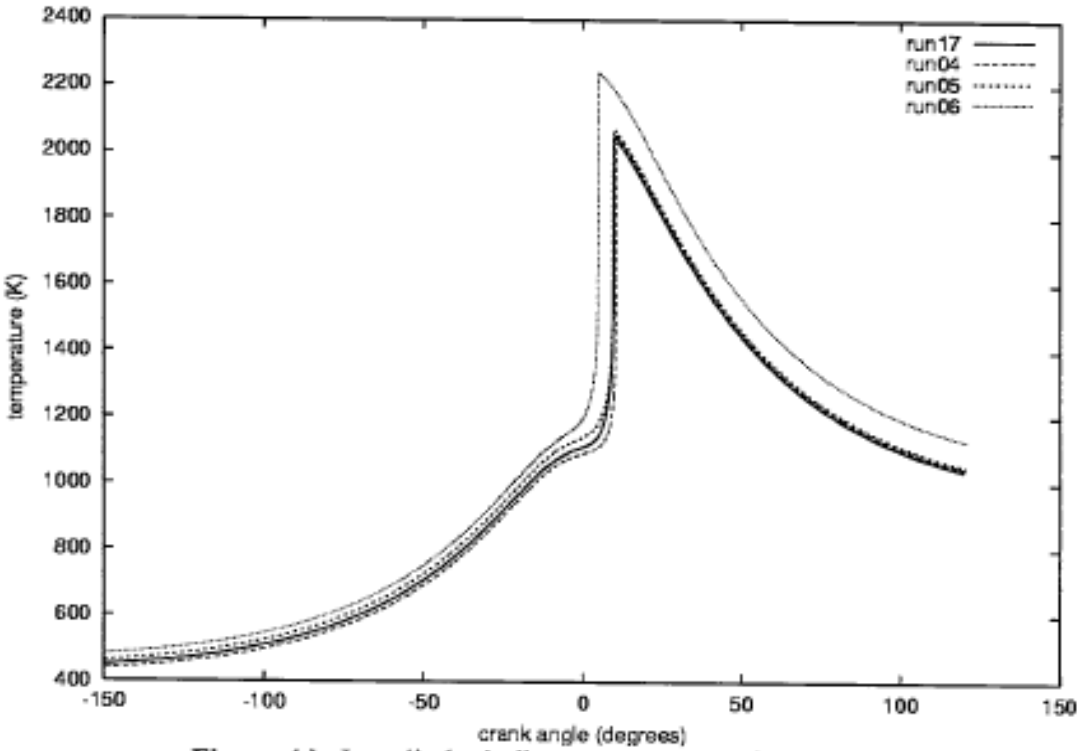

Figure 4.b. In-cylinder bulk gas temperature for runs 4-6.

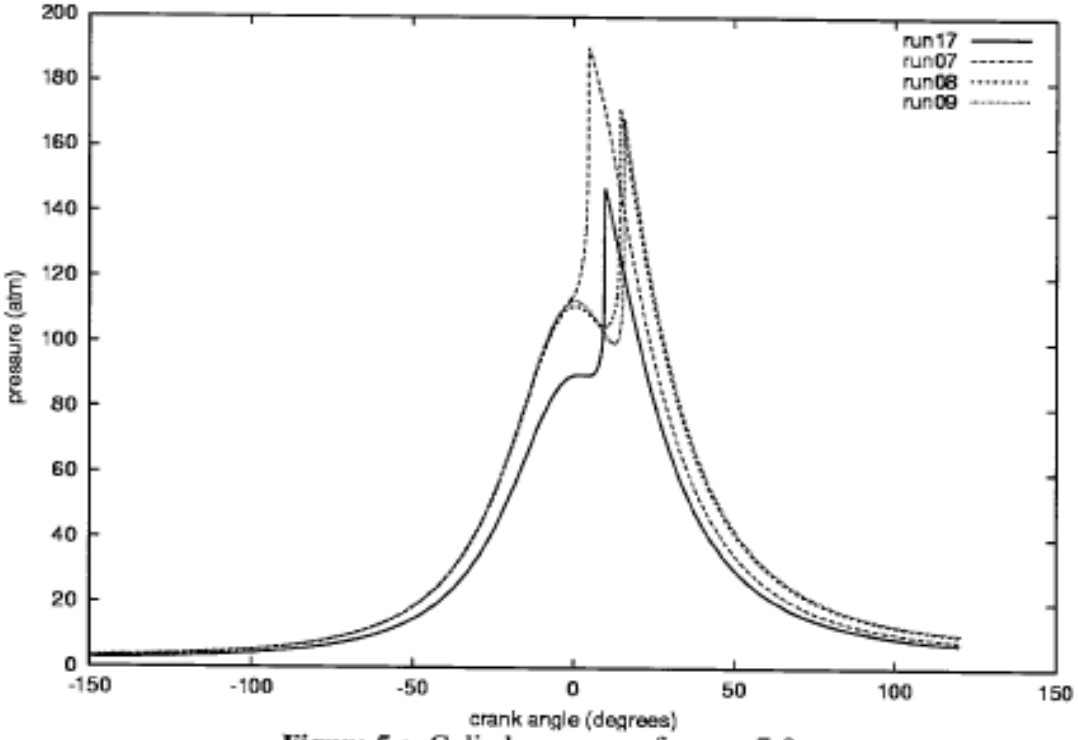

Figure 5.a. Cylinder pressure for runs 7-9.

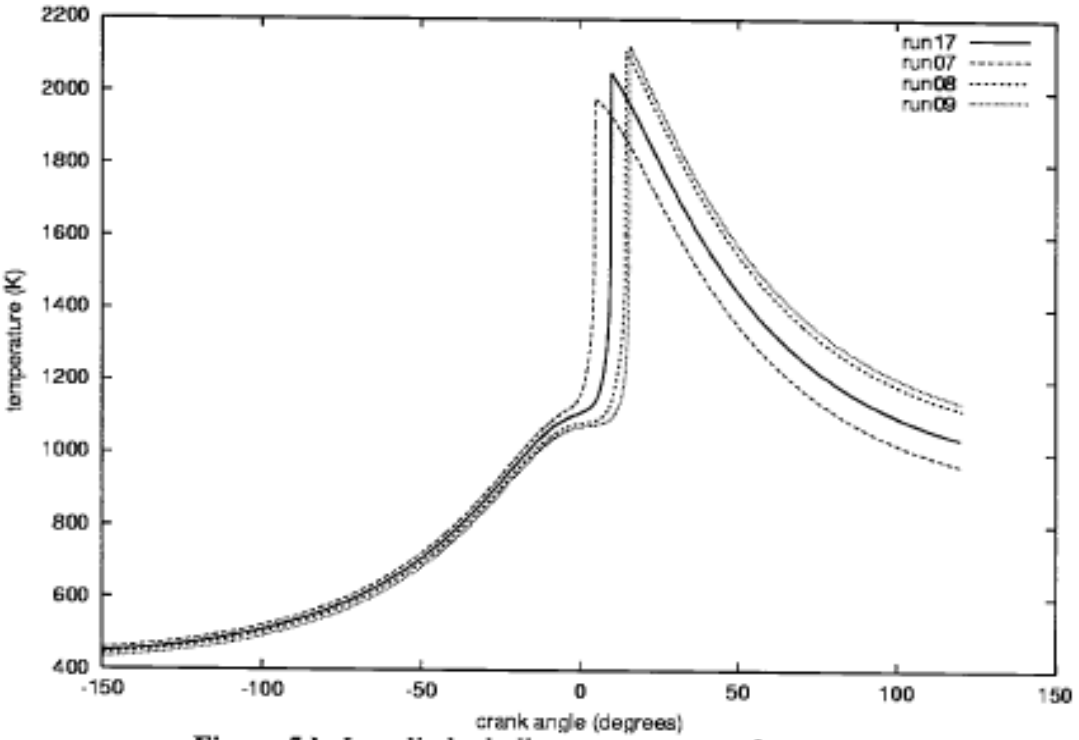

Figure 5.b. In-cylinder bulk gas temperature for runs 7-9

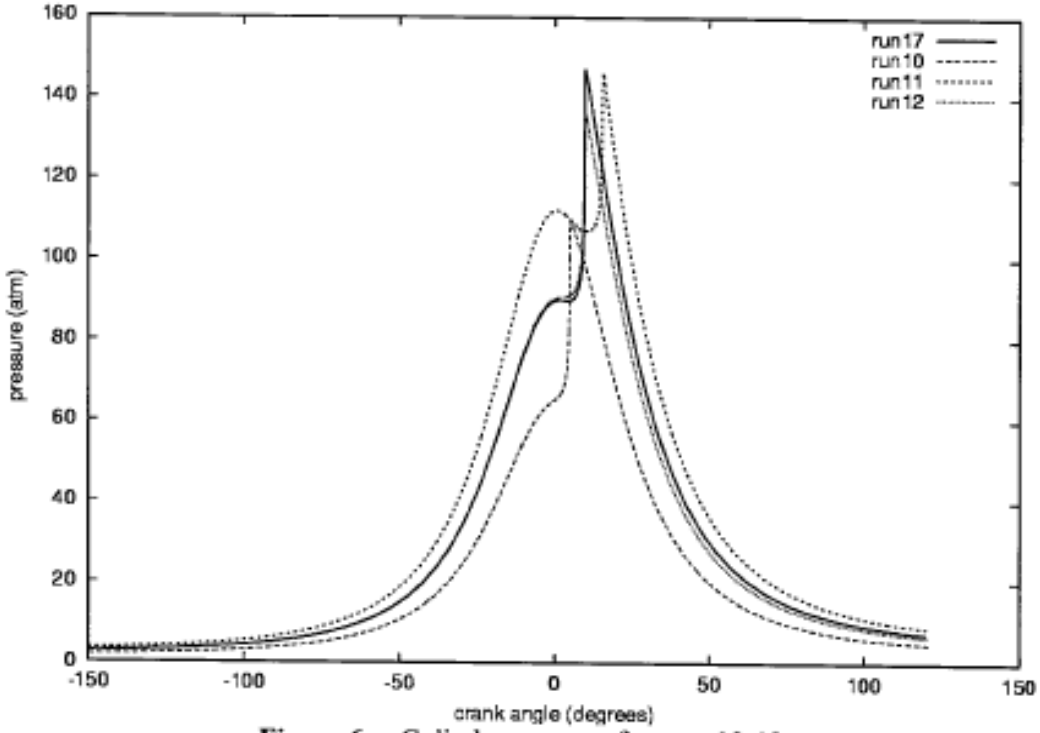

Figure 6.a. Cylinder pressure for runs 10-12.

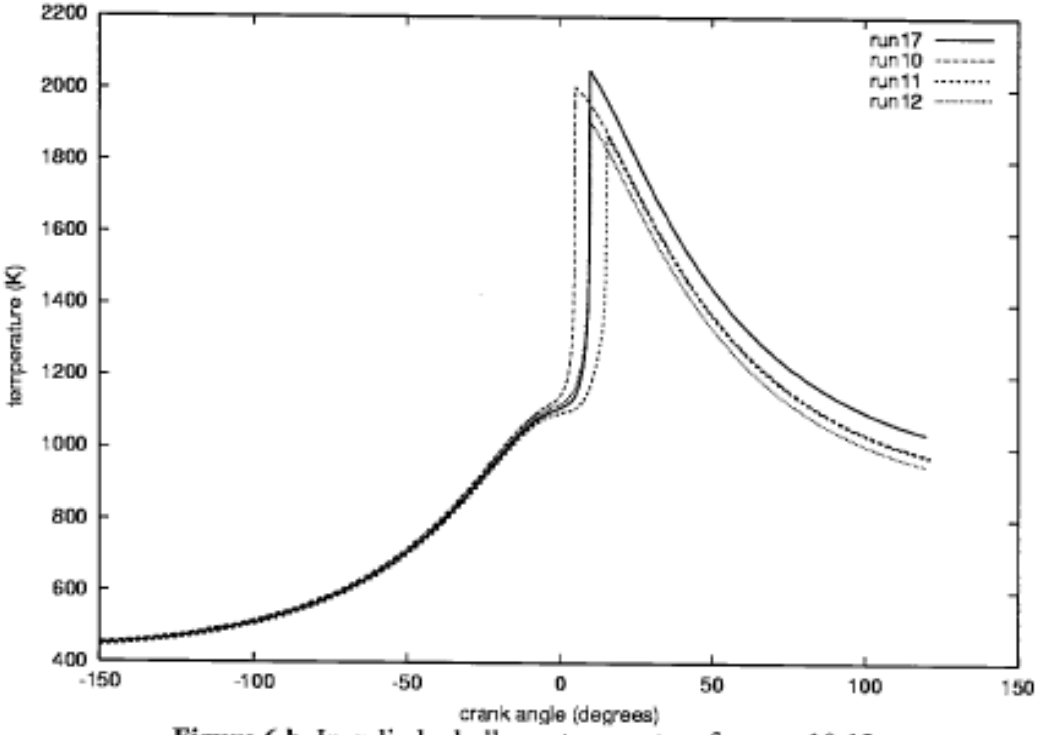

Figure 6.b. In-cylinder bulk gas temperature for runs 10-12

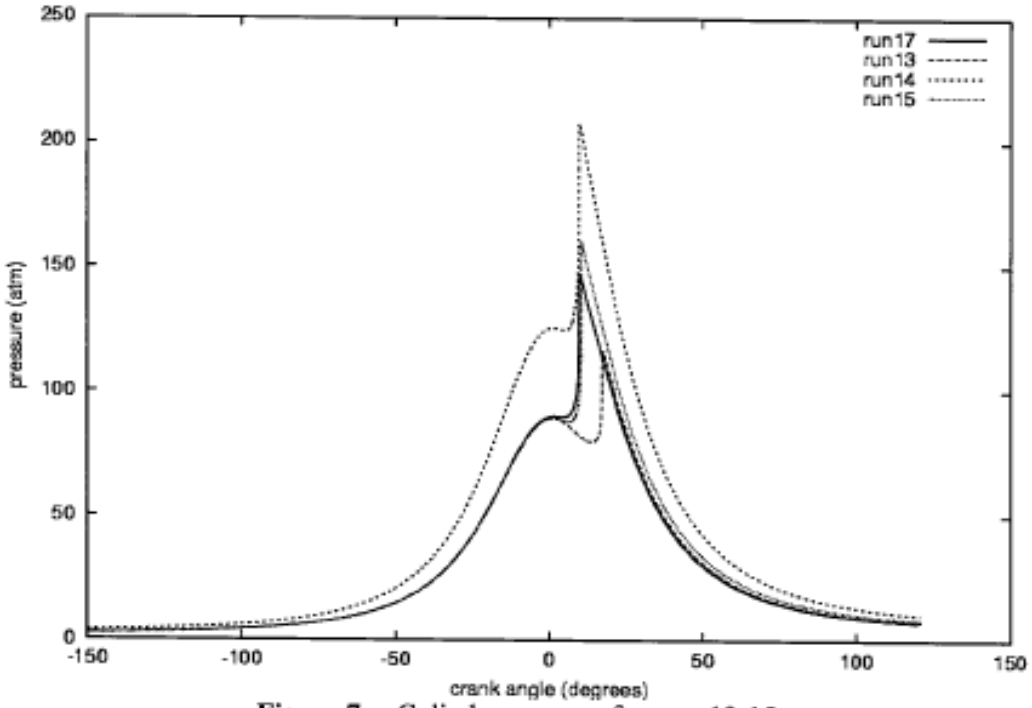

Figure 7.a. Cylinder pressure for runs 13-15.

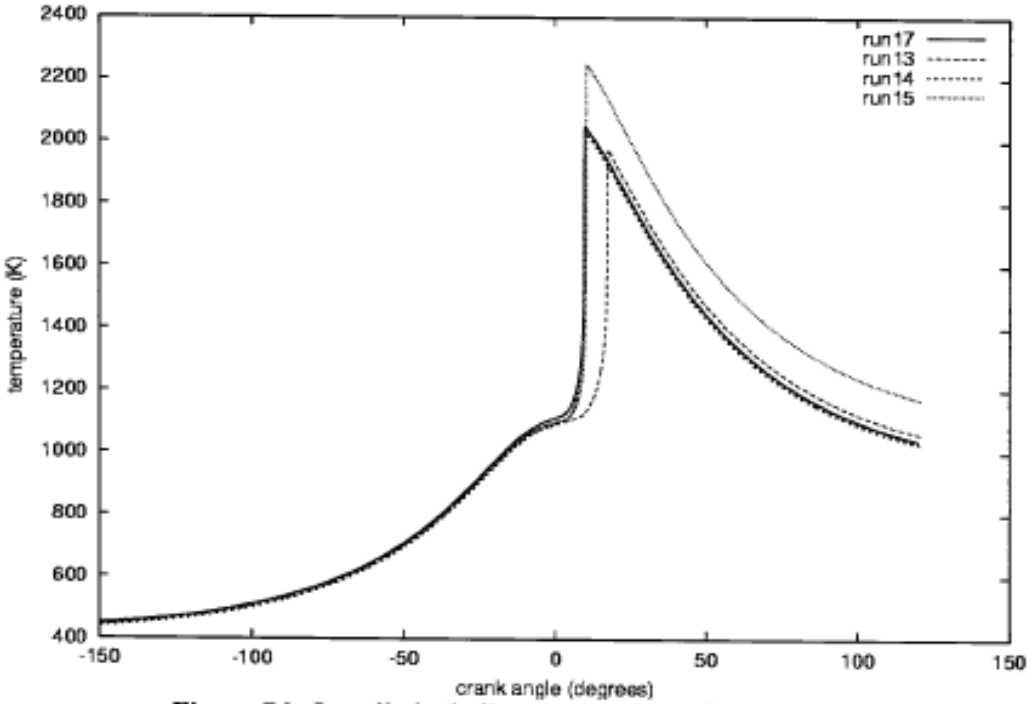

Figure 7.b. In-cylinder bulk gas temperature for runs 13-15

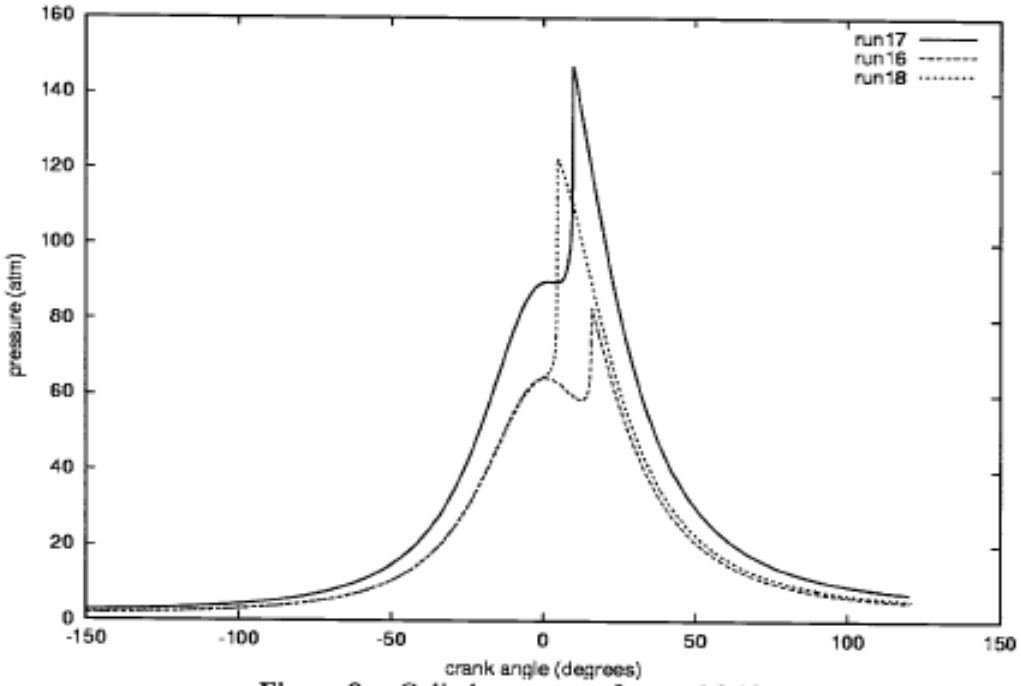

Figure 8.a. Cylinder pressure for run 16-18.

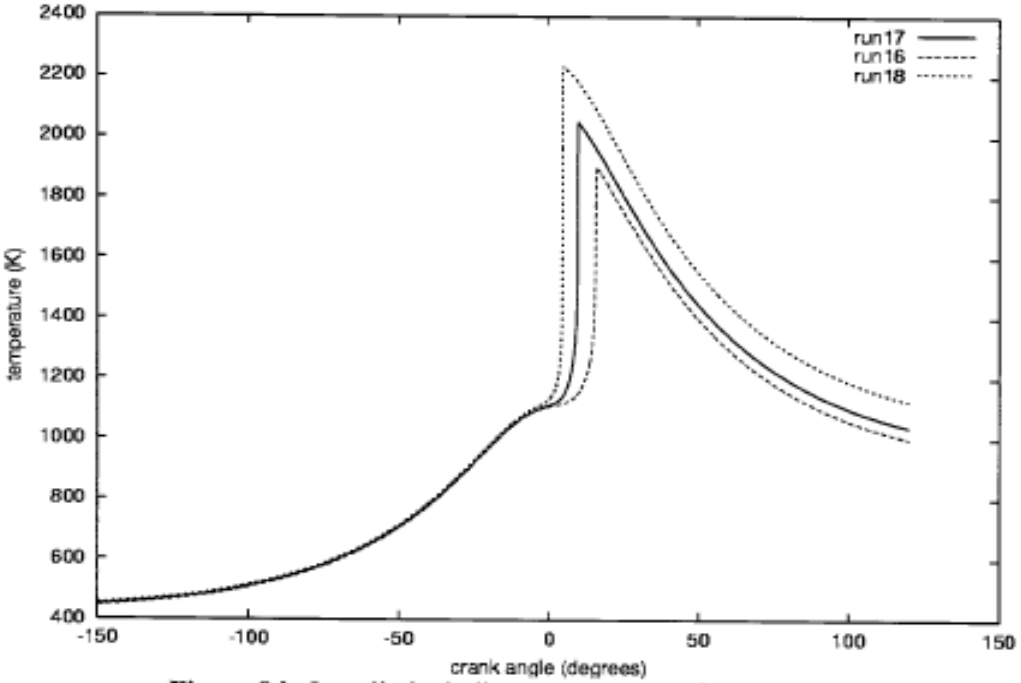

Figure 8.b. In-cylinder bulk gas temperature for runs 16-18

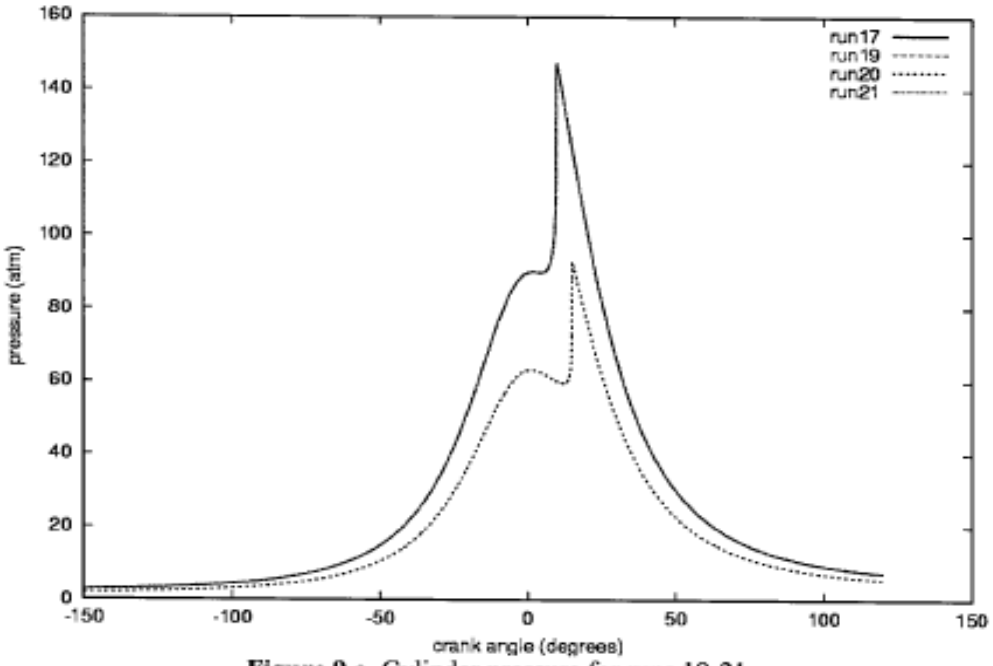

Figure 9.a. Cylinder pressure for runs 19-21.

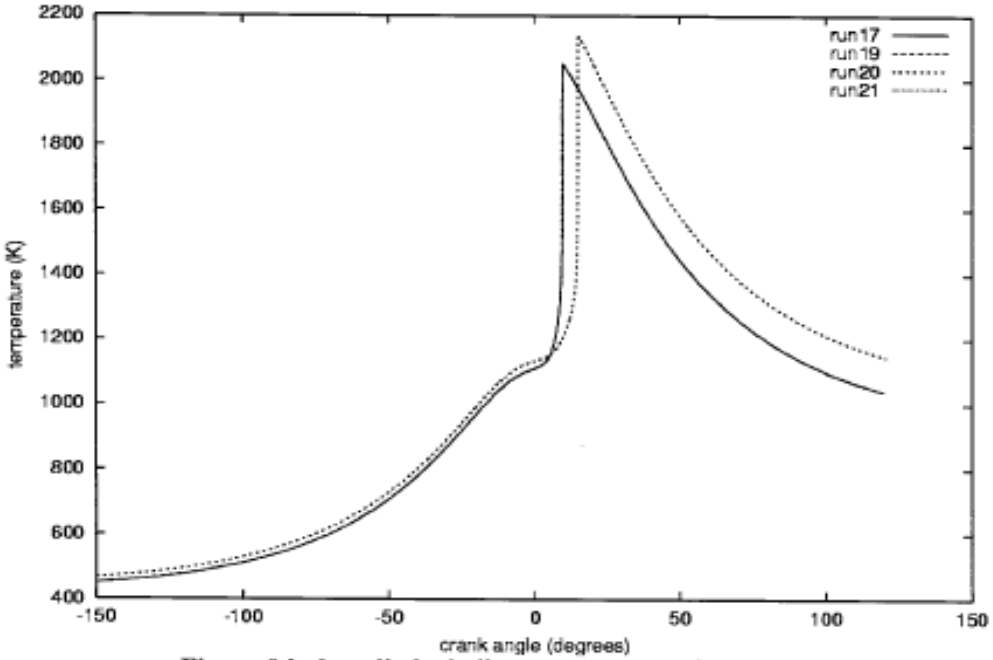

Figure 9.b. In-cylinder bulk gas temperature for runs 1-3

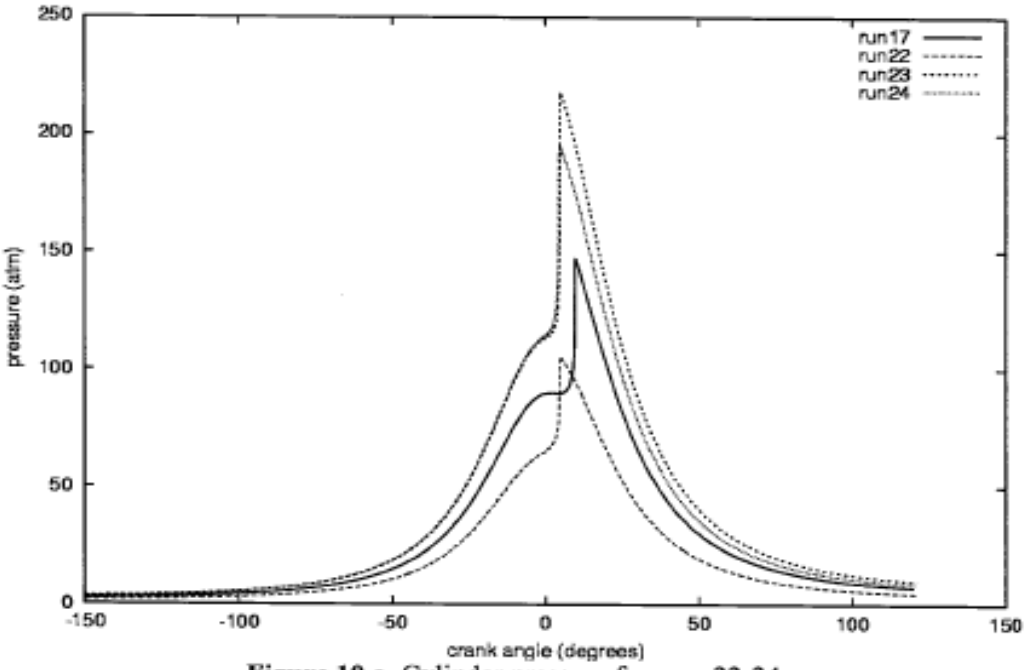

Figure 10.a. Cylinder pressure for runs 22-24.

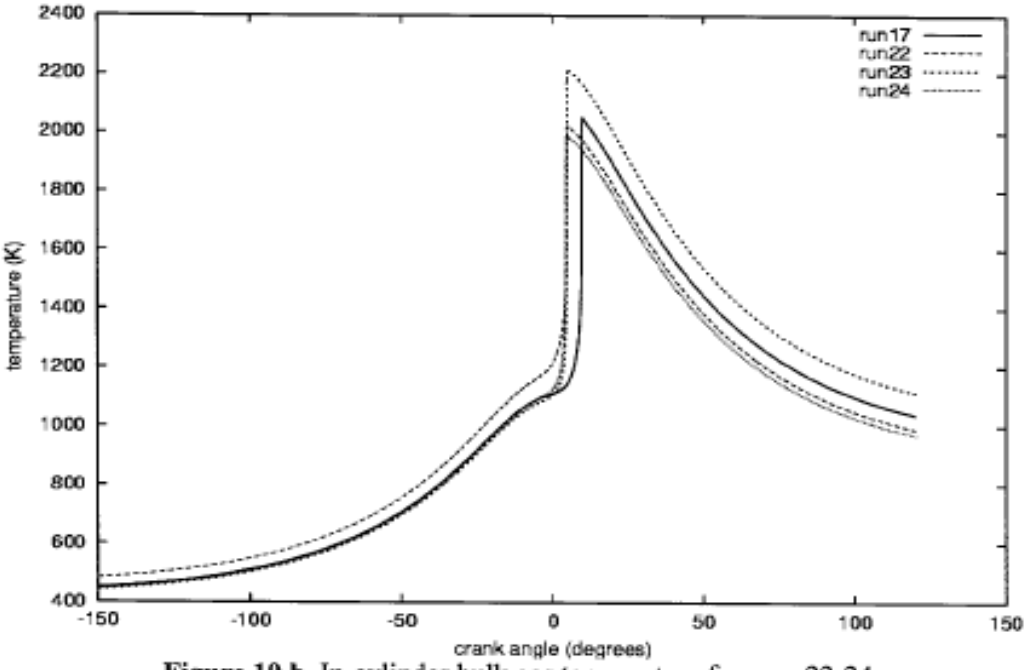

Figure 10.b. In-cylinder bulk gas temperature for runs 22-24

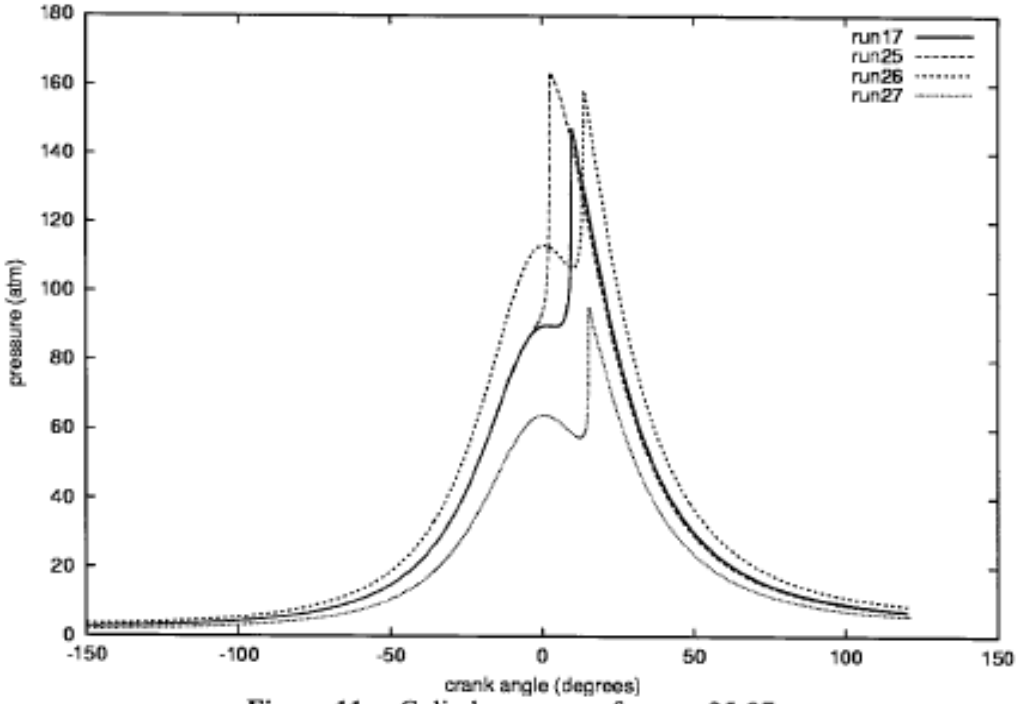

Figure 11.a. Cylinder pressure for runs 25-27.

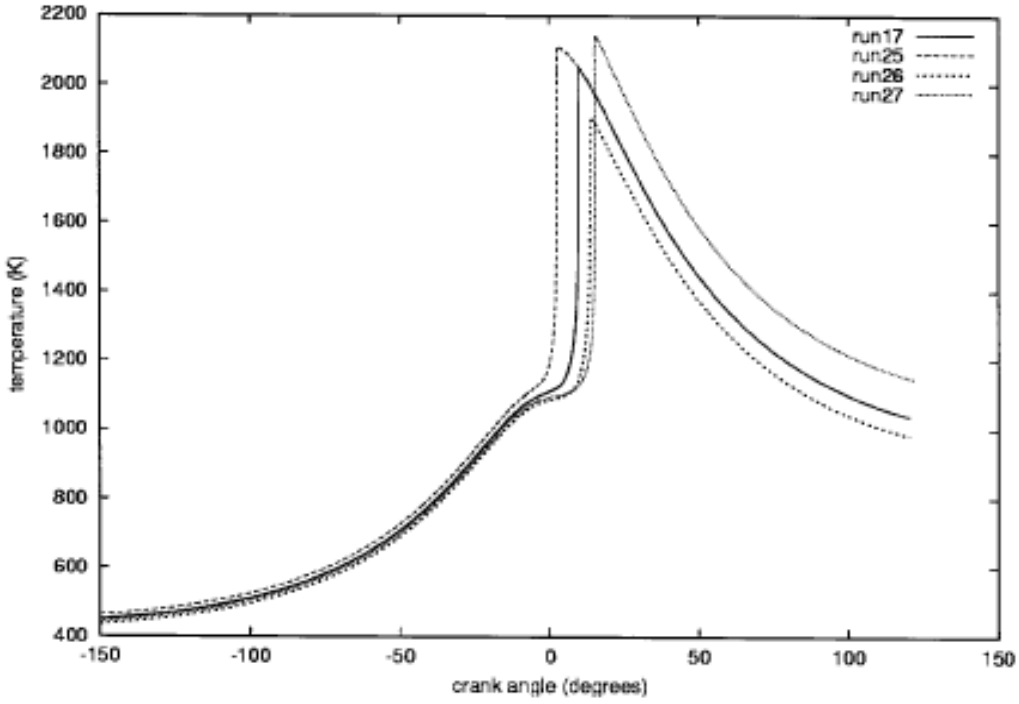

Figure 11.b. In-cylinder bulk gas temperature for runs 25-27

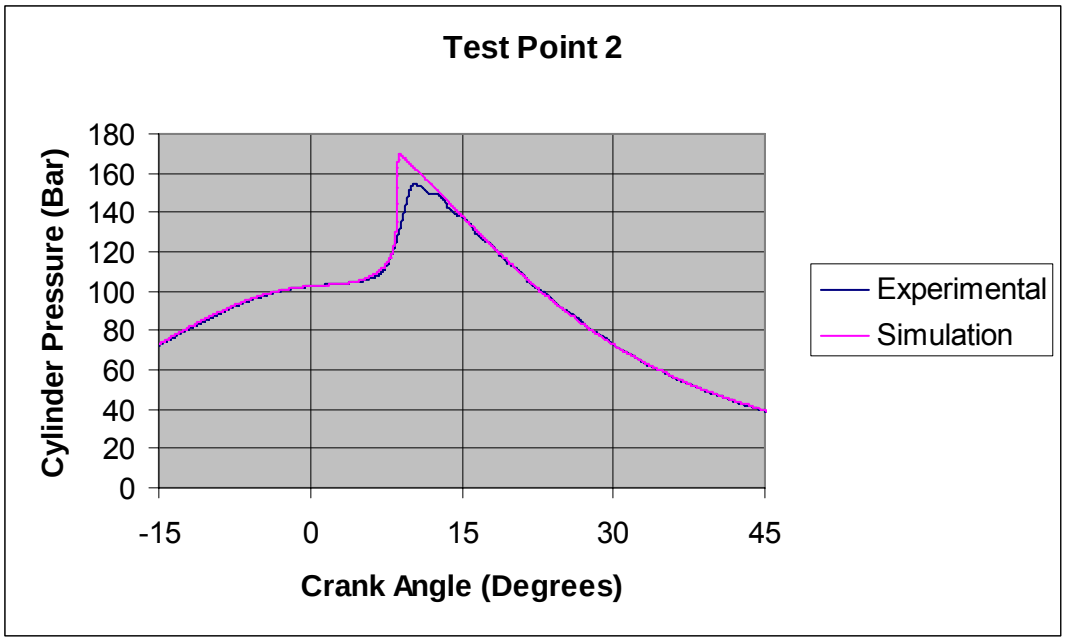
Test Point 2
Cylinder Pressure (Bar)
180
160
140
120
100
80
60
40
20
0
-15
0
15
30
45
Crank Angle (Degrees)
Experimental
Simulation

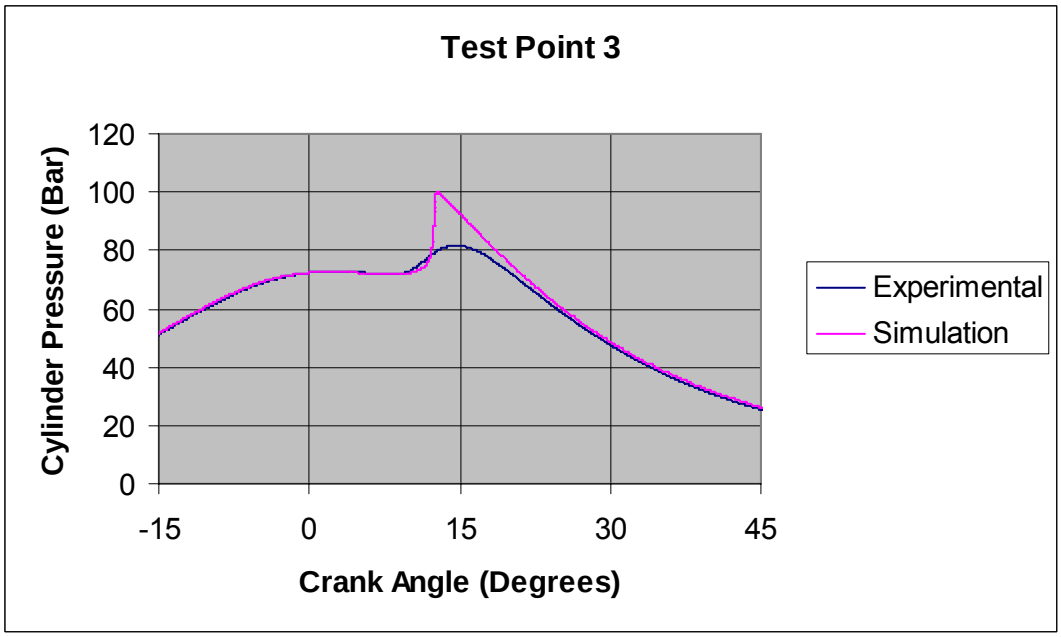
Test Point 3
Cylinder Pressure (Bar)
120
100
80
60
40
20
0
-15
0
15
30
45
Crank Angle (Degrees)
Experimental
Simulation

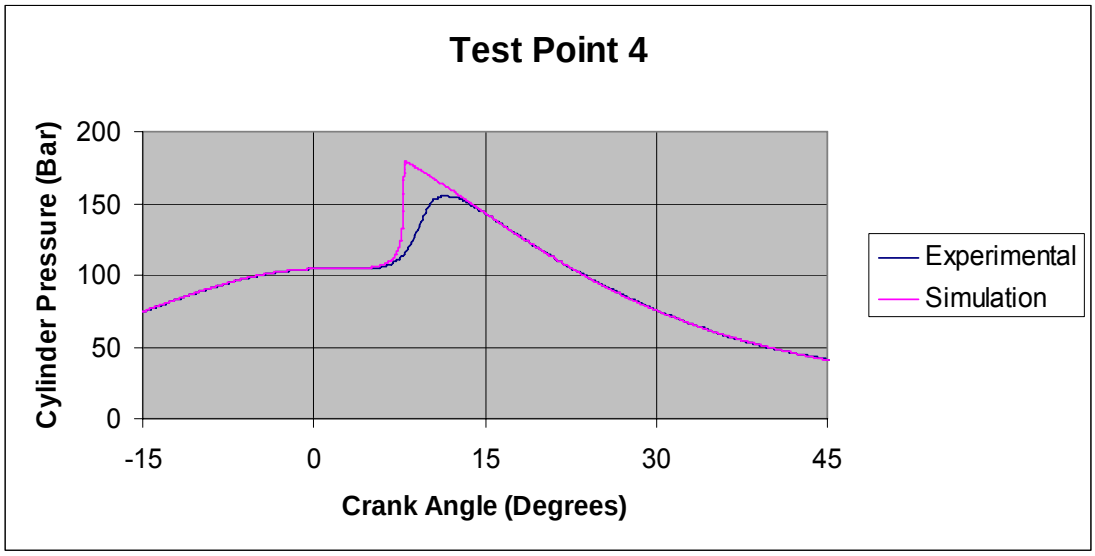
Test Point 4
Cylinder Pressure (Bar)
200
150
100
50
0
-15
0
15
30
45
Crank Angle (Degrees)
Experimental
Simulation

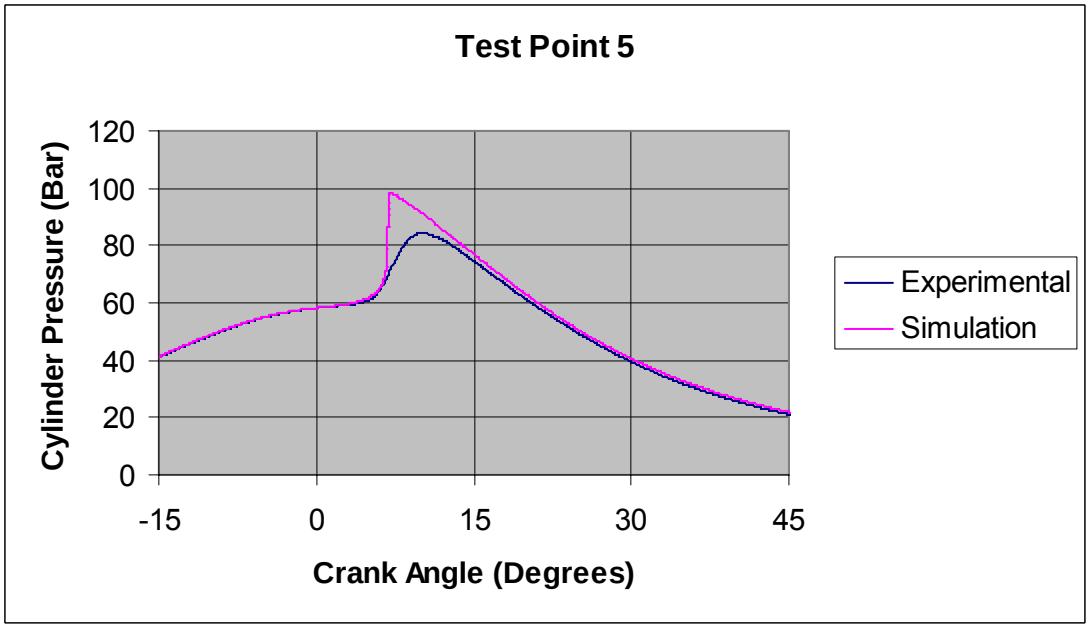
Test Point 5
Cylinder Pressure (Bar)
120
100
80
60
40
20
0
-15
0
15
30
45
Crank Angle (Degrees)
Experimental
Simulation

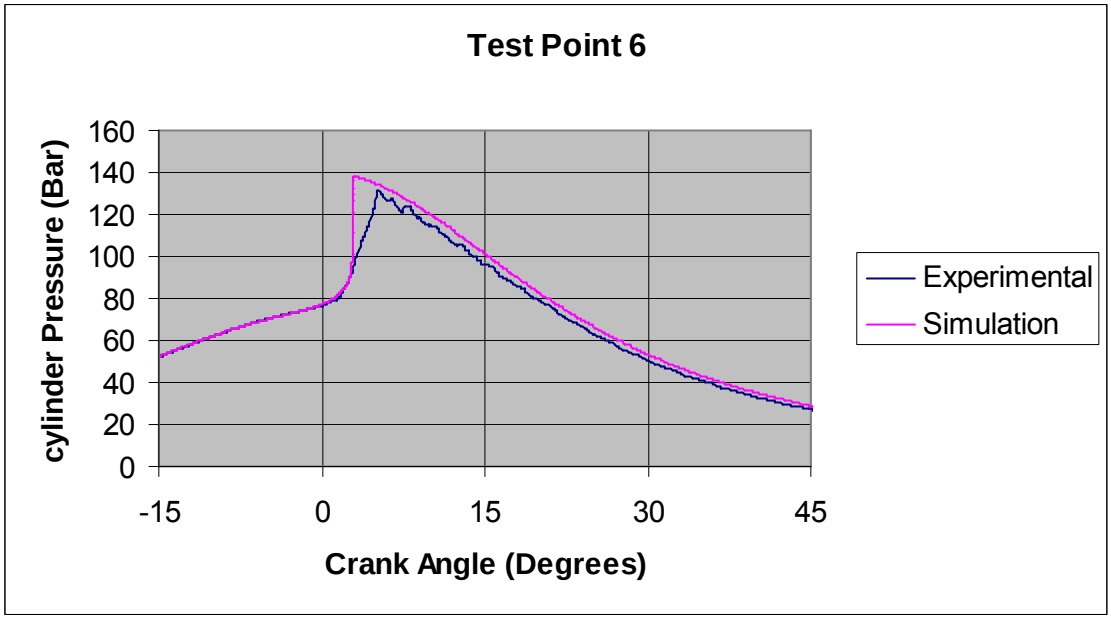
Test Point 6
cylinder Pressure (Bar)
160
140
120
100
80
60
40
20
0
-15
0
15
30
45
Crank Angle (Degrees)
Experimental
Simulation

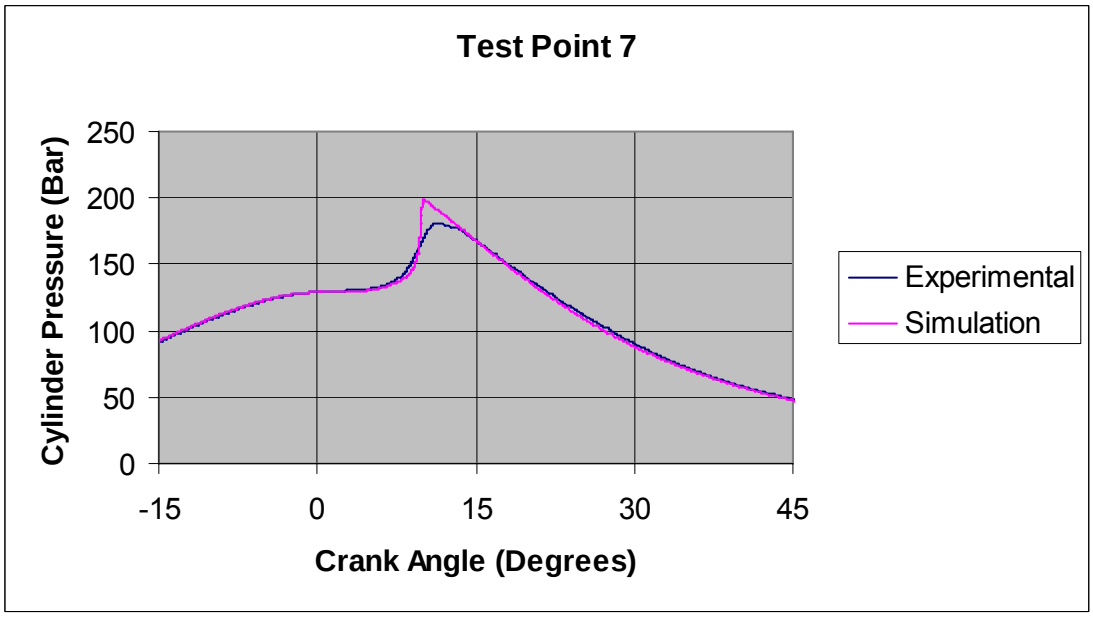
Test Point 7
Cylinder Pressure (Bar)
250
200
150
100
50
0
-15
0
15
30
45
Crank Angle (Degrees)
Experimental
Simulation

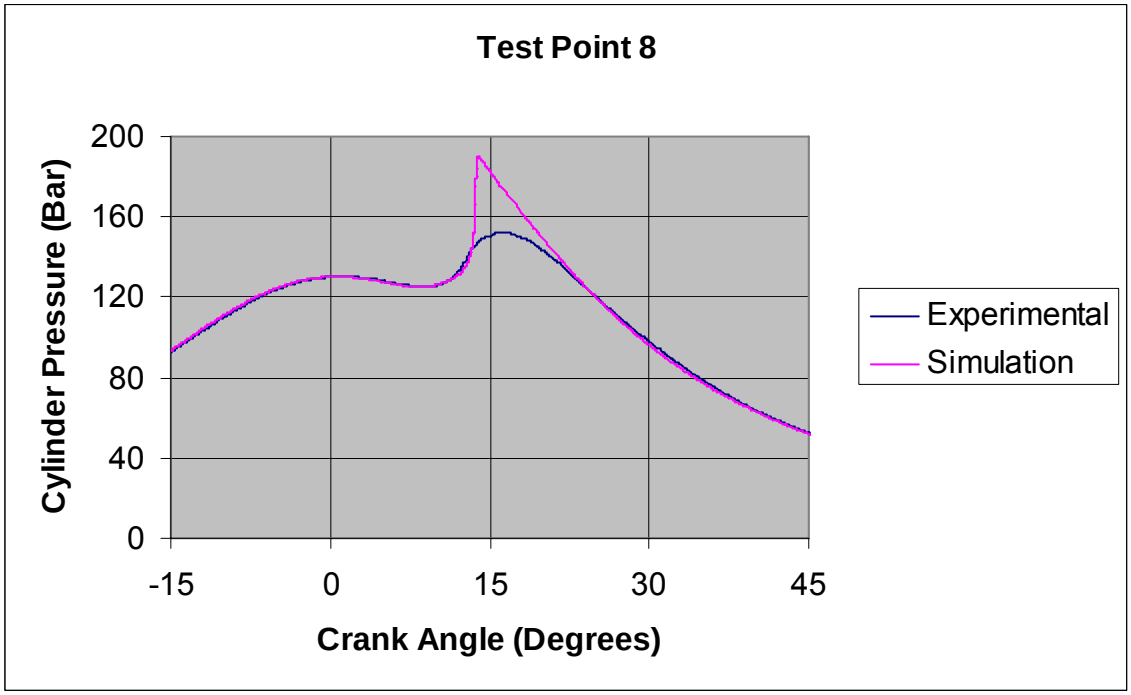
Test Point 8
Cylinder Pressure (Bar)
200
160
120
80
40
0
-15
0
15
30
45
Crank Angle (Degrees)
Experimental
Simulation

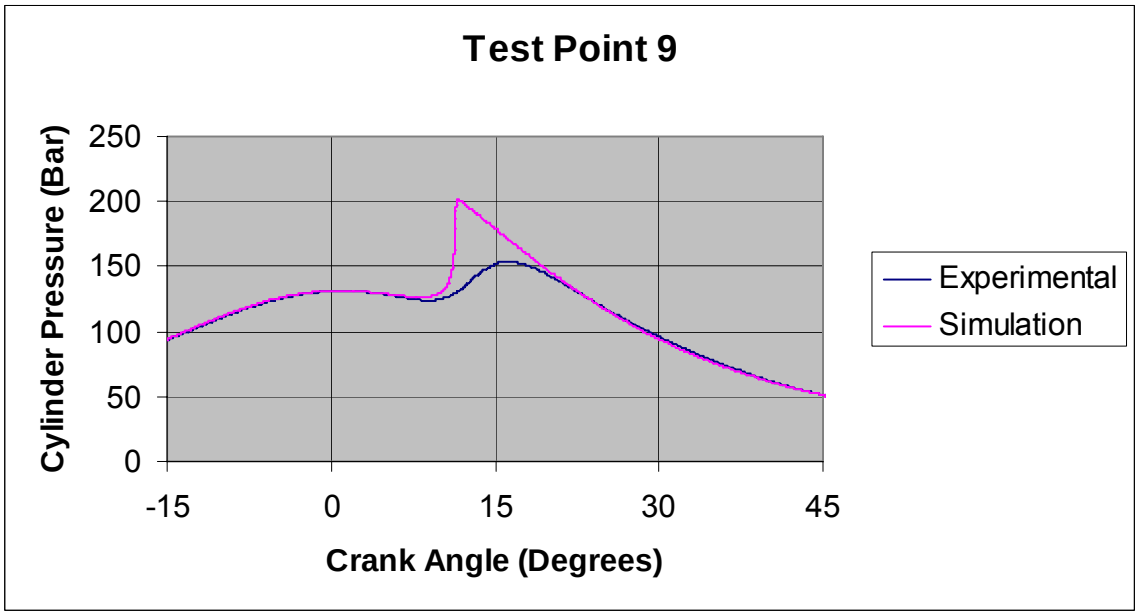
Test Point 9
Cylinder Pressure (Bar)
250
200
150
100
50
0
-15
0
15
30
45
Crank Angle (Degrees)
Experimental
Simulation

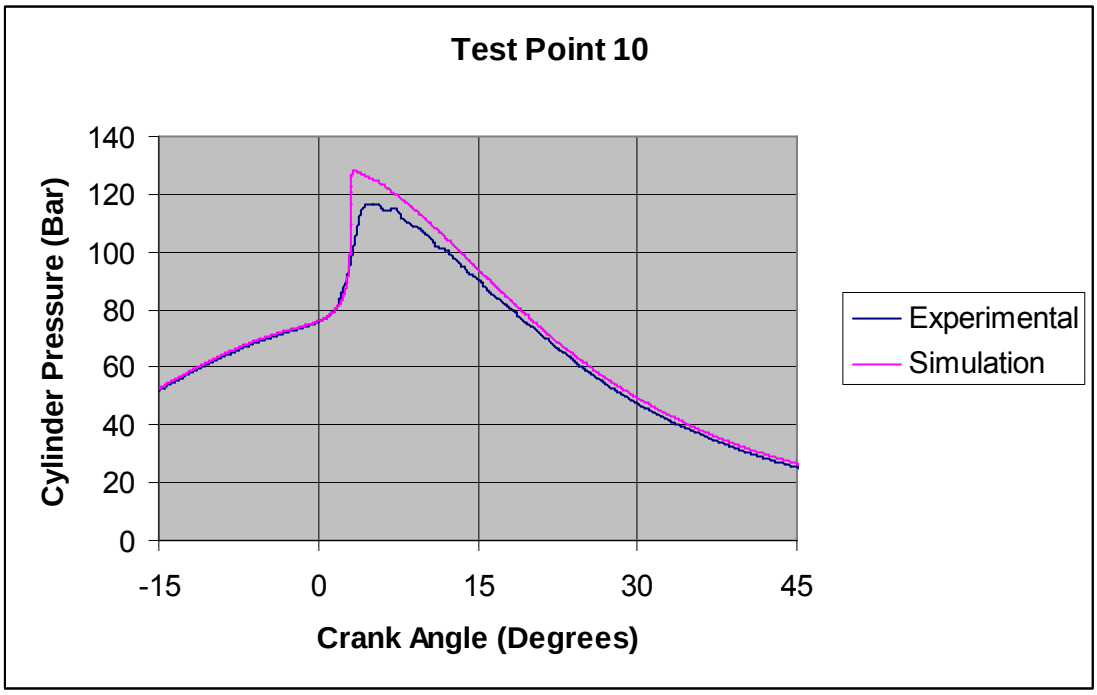
Test Point 10
Cylinder Pressure (Bar)
140
120
100
80
60
40
20
0
-15
0
15
30
45
Crank Angle (Degrees)
Experimental
Simulation

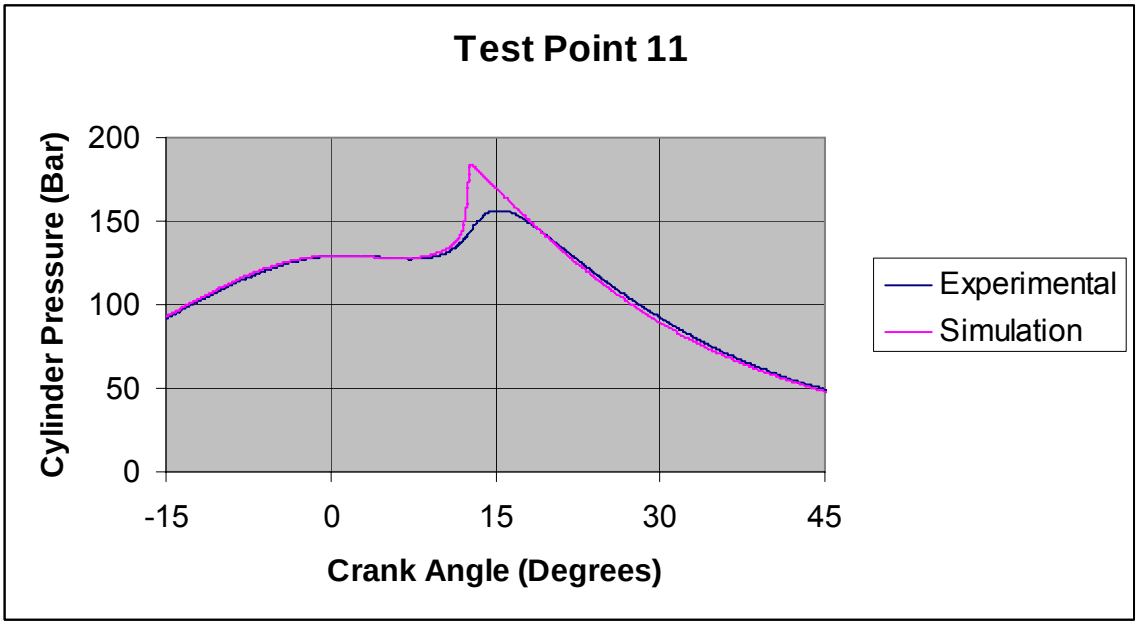
Test Point 11
Cylinder Pressure (Bar)
200
150
100
50
0
-15
0
15
30
45
Crank Angle (Degrees)
Experimental
Simulation

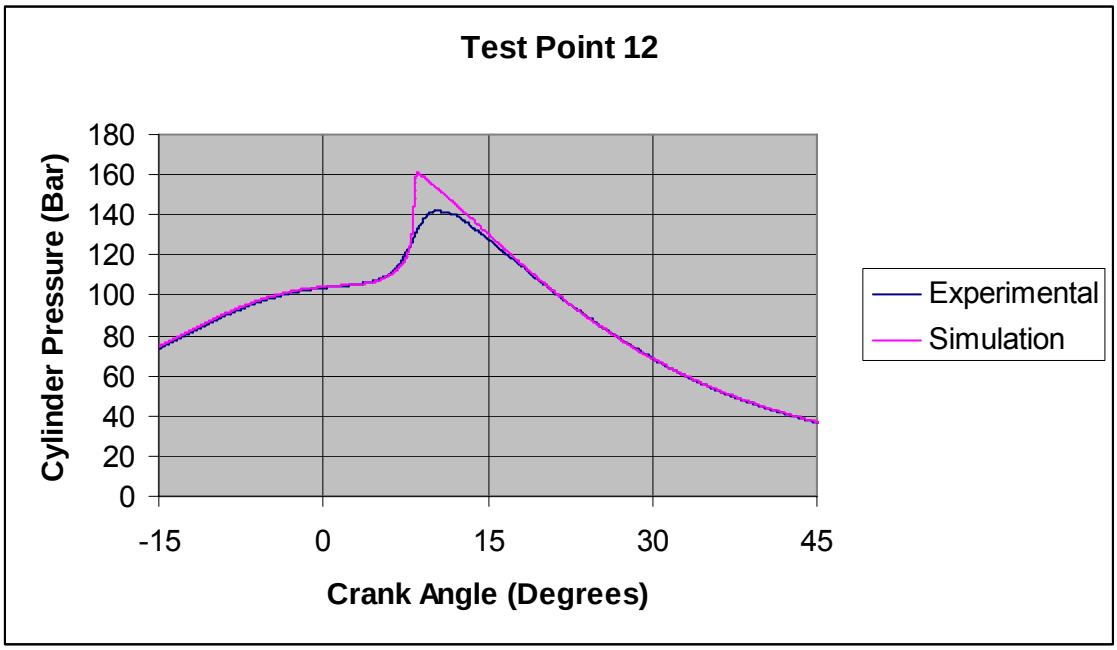
Test Point 12
Cylinder Pressure (Bar)
180
160
140
120
100
80
60
40
20
0
-15
0
15
30
45
Crank Angle (Degrees)
Experimental
Simulation

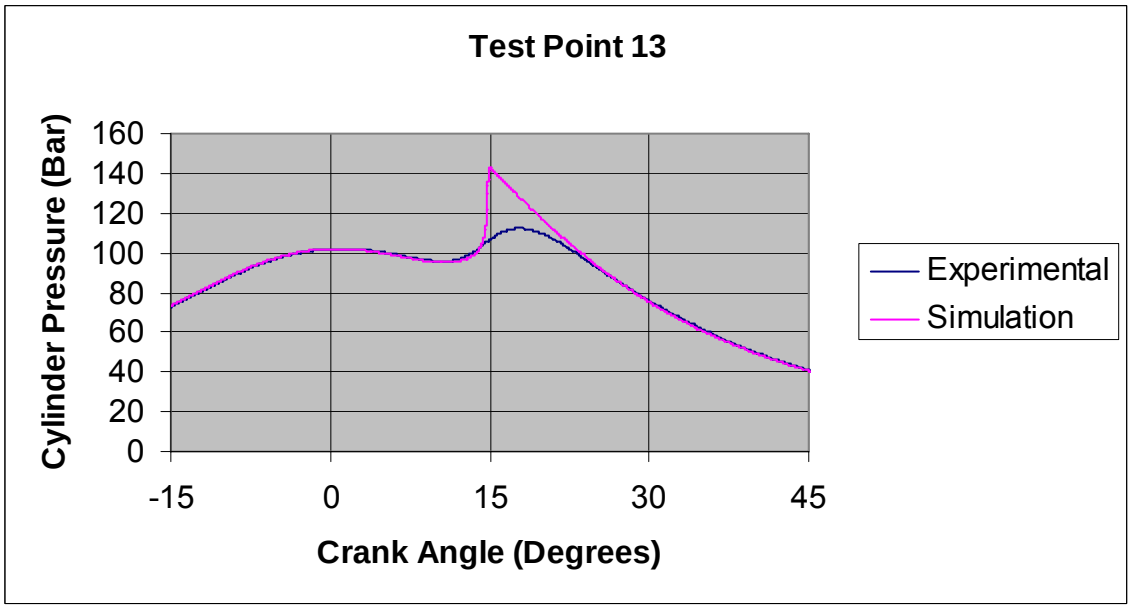
Test Point 13
Cylinder Pressure (Bar)
160
140
120
100
80
60
40
20
0
-15
0
15
30
45
Crank Angle (Degrees)
Experimental
Simulation

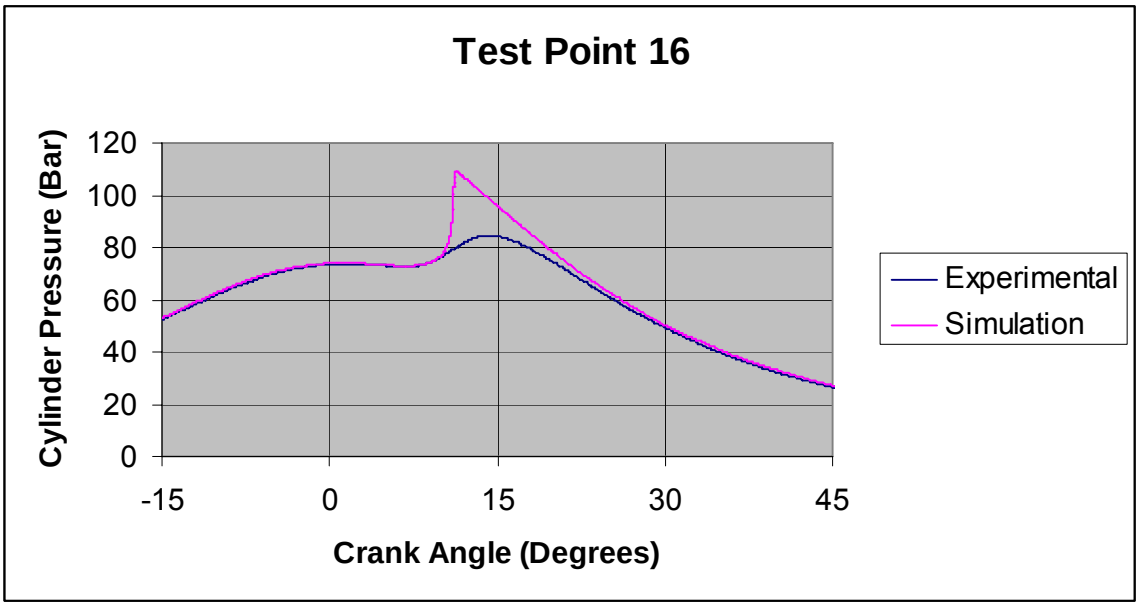
Test Point 16
Cylinder Pressure (Bar)
120
100
80
60
40
20
0
-15
0
15
30
45
Crank Angle (Degrees)
Experimental
Simulation

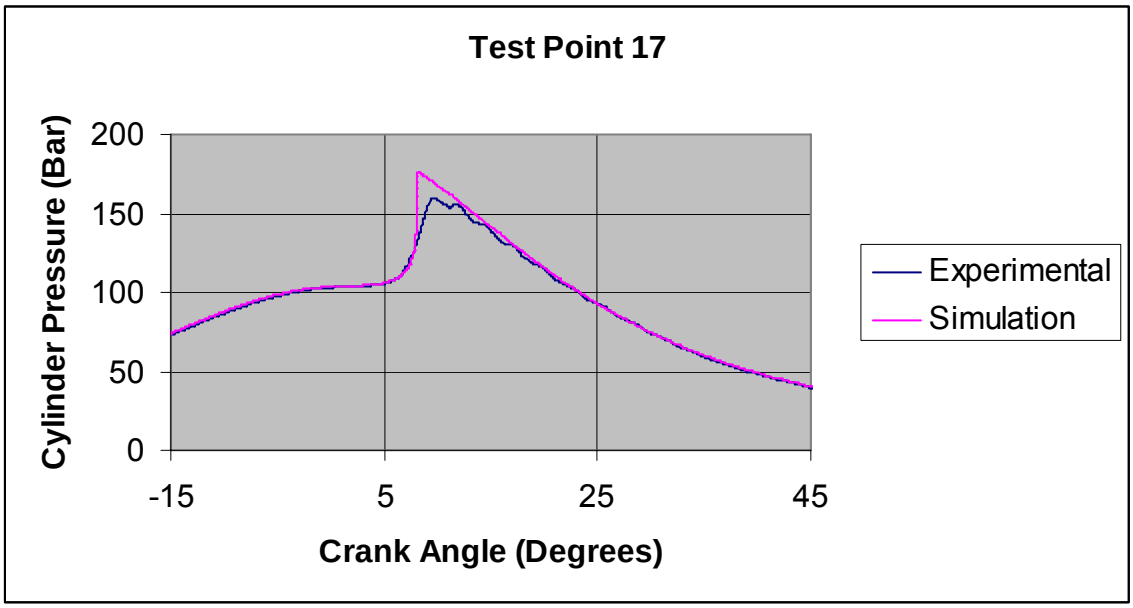
Test Point 17
Cylinder Pressure (Bar)
200
150
100
50
0
-15
5
25
45
Crank Angle (Degrees)
Experimental
Simulation

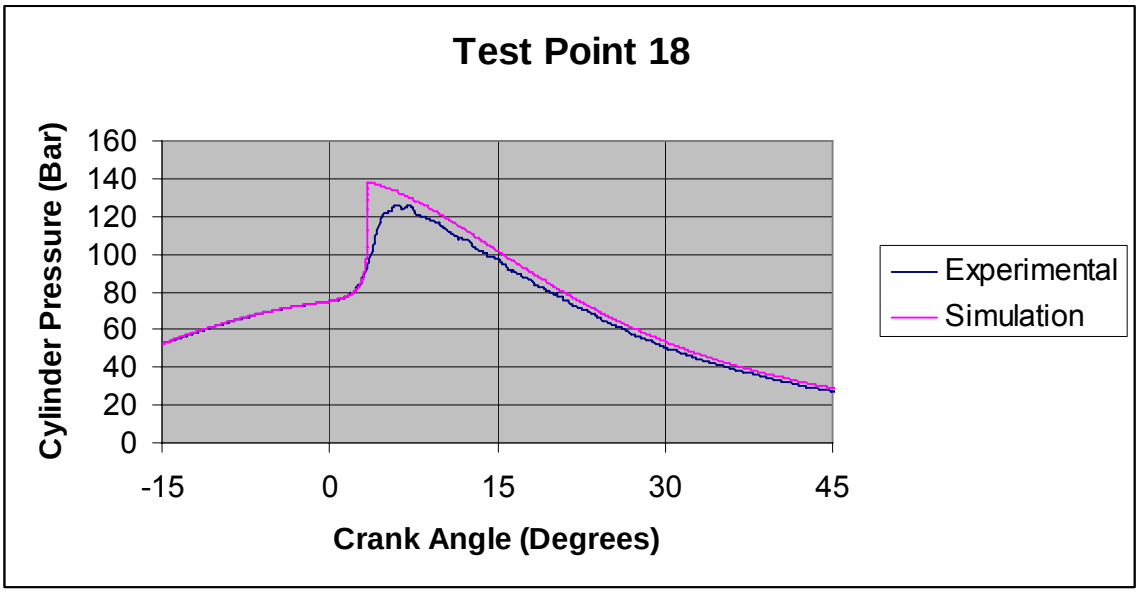
Test Point 18
Cylinder Pressure (Bar)
160
140
120
100
80
60
40
20
0
-15
0
15
30
45
Crank Angle (Degrees)
Experimental
Simulation

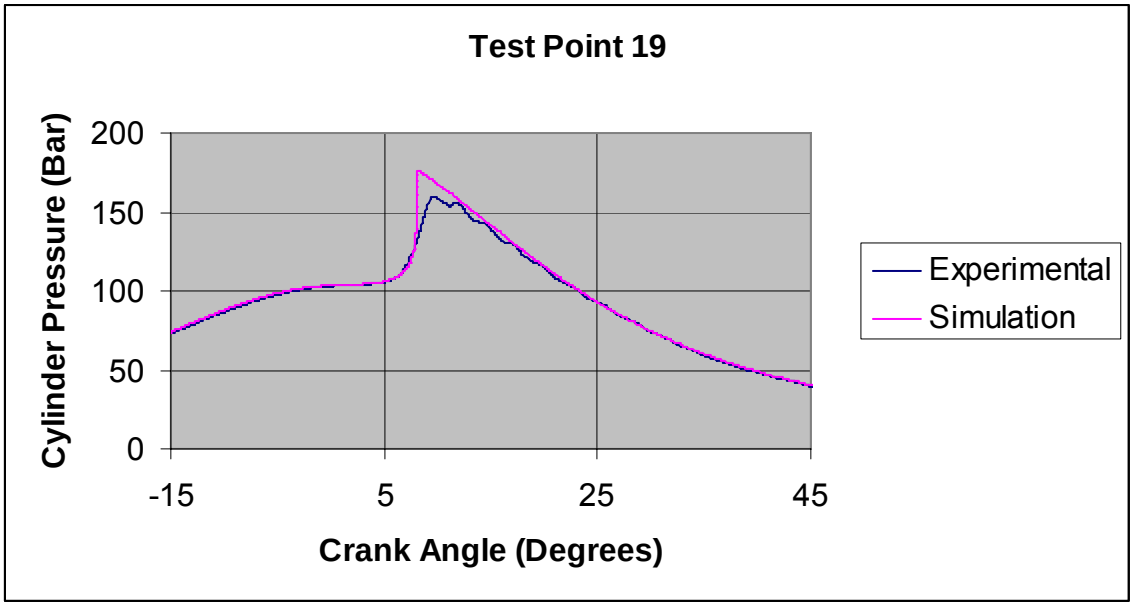
Test Point 19
Cylinder Pressure (Bar)
200
150
100
50
0
-15
5
25
45
Crank Angle (Degrees)
Experimental
Simulation

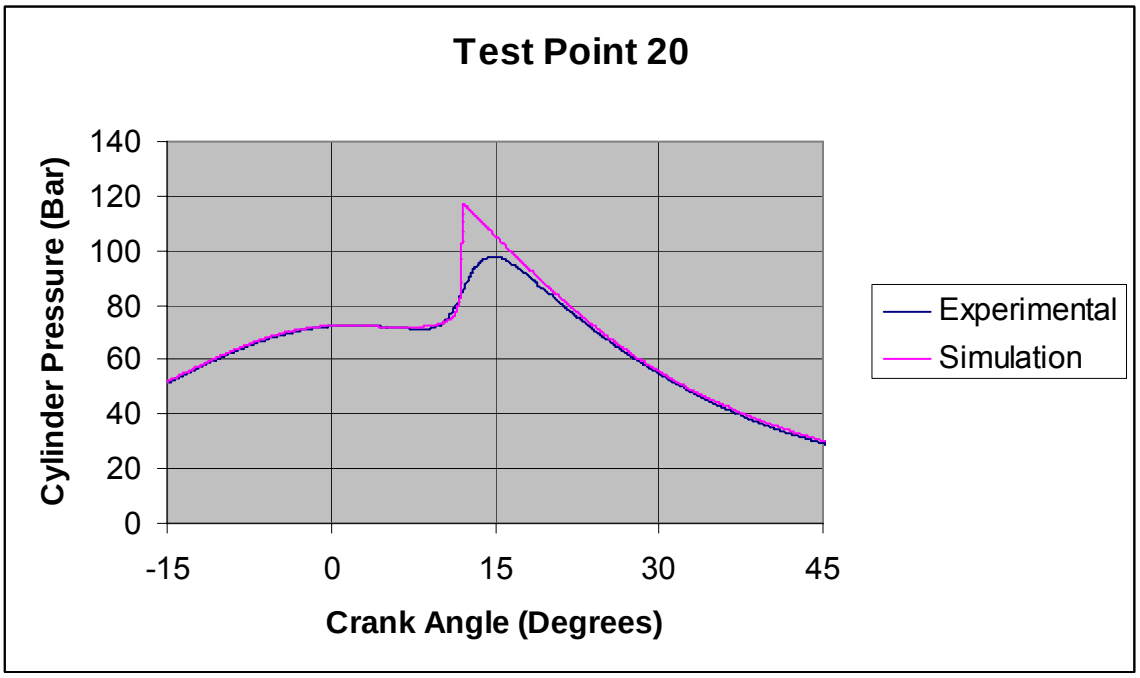
Test Point 20
Cylinder Pressure (Bar)
140
120
100
80
60
40
20
0
-15
0
15
30
45
Crank Angle (Degrees)
Experimental
Simulation

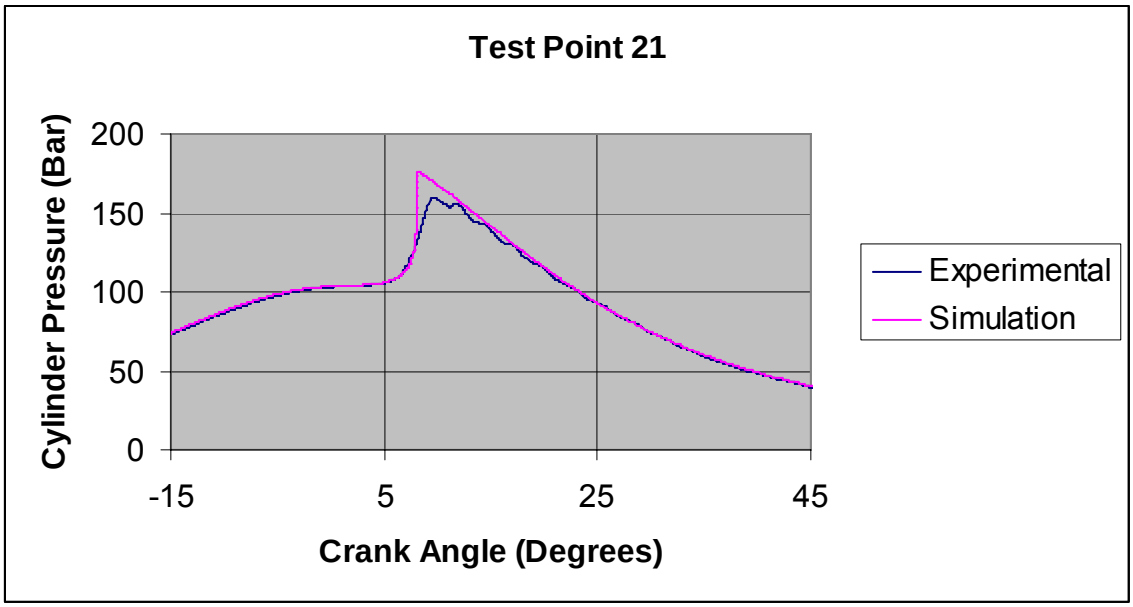
Test Point 21
Cylinder Pressure (Bar)
200
150
100
50
0
-15
5
25
45
Crank Angle (Degrees)
Experimental
Simulation

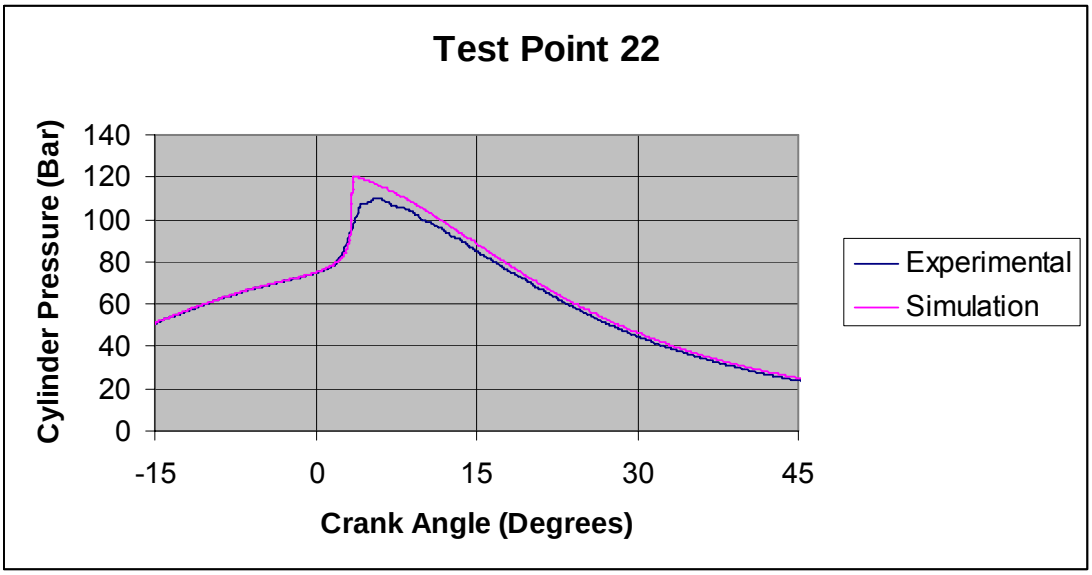
Test Point 22
Cylinder Pressure (Bar)
140
120
100
80
60
40
20
0
-15
0
15
30
45
Crank Angle (Degrees)
Experimental
Simulation

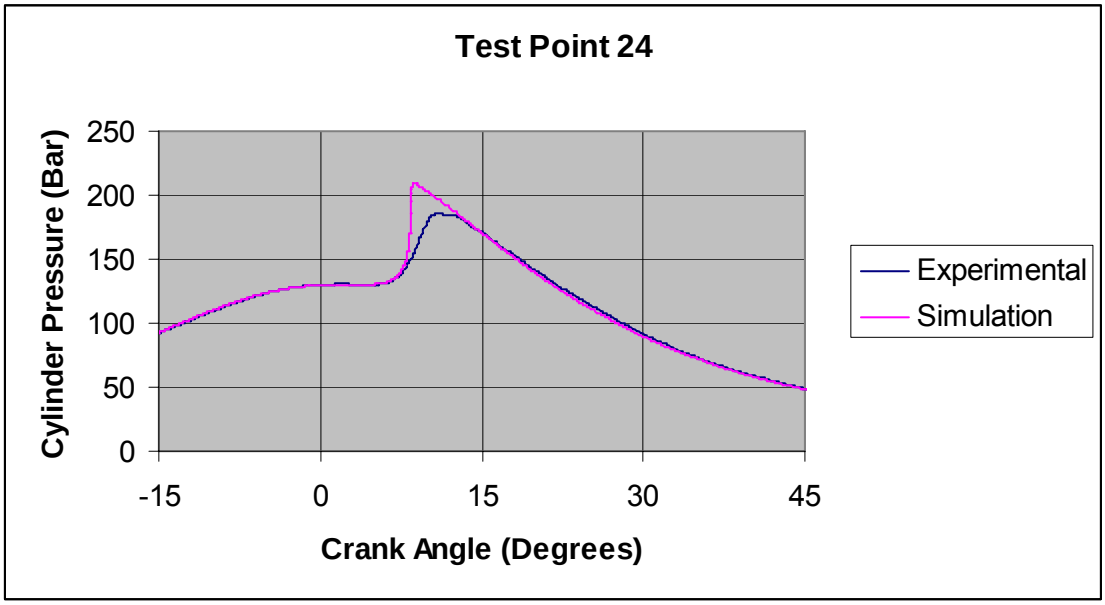
Test Point 24
Cylinder Pressure (Bar)
250
200
150
100
50
0
-15
0
15
30
45
Crank Angle (Degrees)
Experimental
Simulation

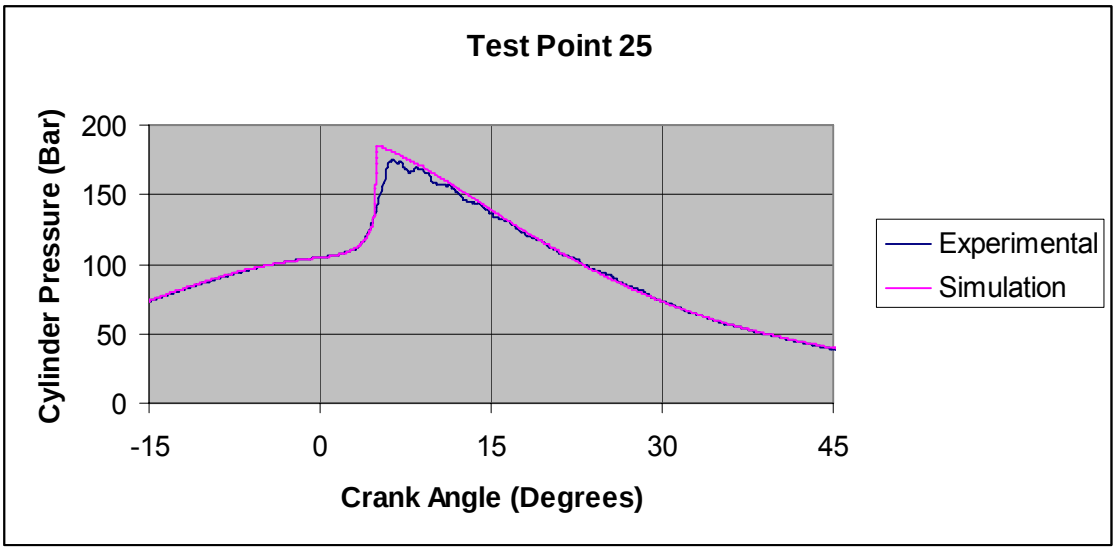
Test Point 25
Cylinder Pressure (Bar)
200
150
100
50
0
-15
0
15
30
45
Crank Angle (Degrees)
Experimental
Simulation

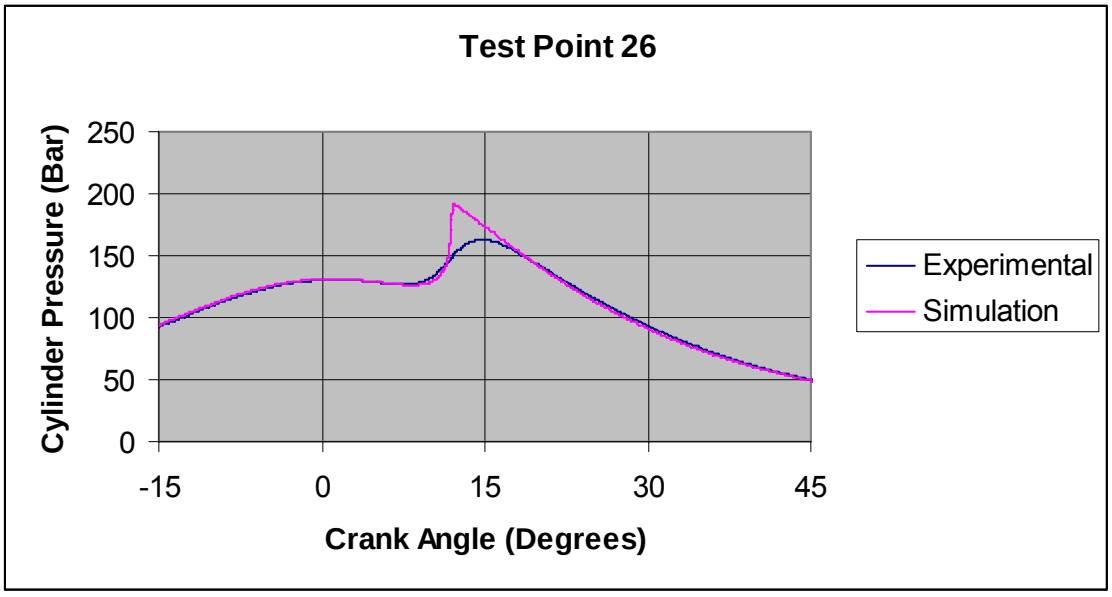
Test Point 26
Cylinder Pressure (Bar)
250
200
150
100
50
0
-15
0
15
30
45
Crank Angle (Degrees)
Experimental
Simulation

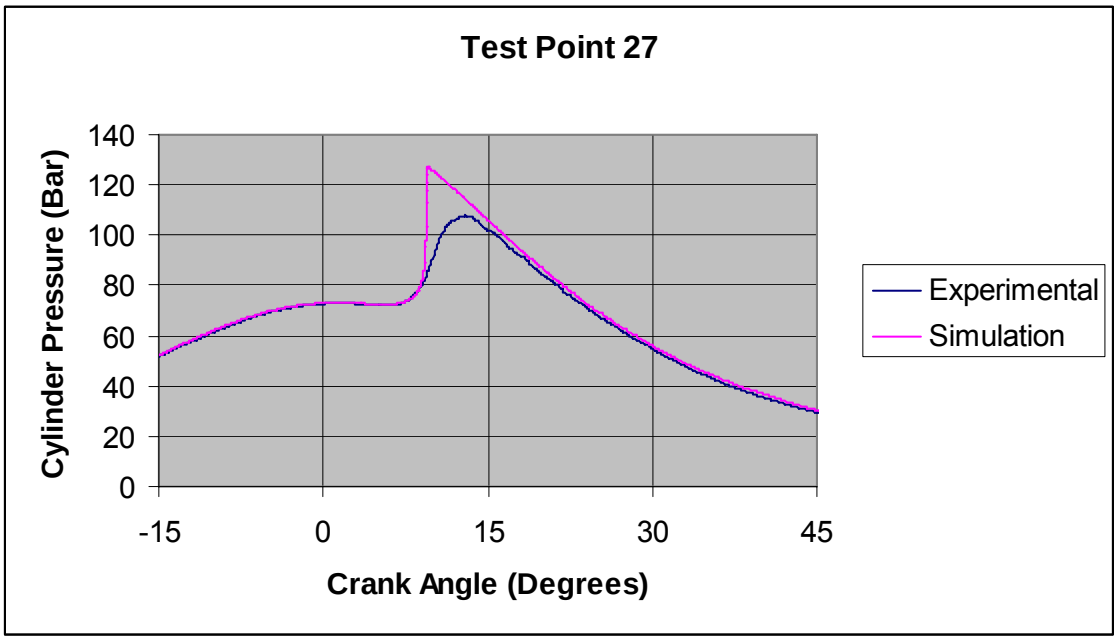
Test Point 27
Cylinder Pressure (Bar)
140
120
100
80
60
40
20
0
-15
0
15
30
45
Crank Angle (Degrees)
Experimental
Simulation

APPENDIX D: HCCI DATA AT 1000 RPM

The HCCI engine was operated under various excess air ratios ranging from lean limit (i.e. misfiring) to rich limit (i.e. knocking) and at the engine speeds of 1000, 1200, 1400, 1600, and 1800 rpm. Only data taken at 1000 rpm are presented in this Appendix.
Net mean effective pressure (NMEP) decreased as the excess air ratio increased (See Figure D1). Intake boosting from approximately 1 bar to 1.6 bar extended the operating regime of the HCCI engine to higher excess air ratios and increased the NMEP by a factor of two times those of the naturally aspirated conditions. Figure D2 shows indicated specific fuel consumption (ISFC) versus excess air ratios. ISFC increased exponentially with increasing excess air ratios. Intake boost decreased ISFC and maintained low ISFC to higher excess air ratios compared to the NA conditions.

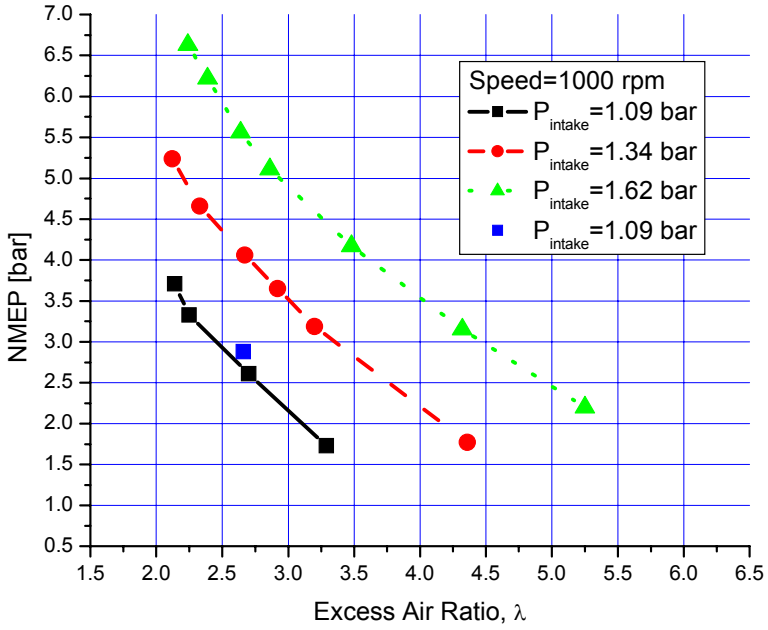

Figure D1 Net mean effective pressure (NMEP) versus excess air ratio

Figure D3 shows the coefficients of variance of IMEP (IMEP_COV), an indicator of combustion stability, as excess air and boost are varied. Near the lean limit, the IMEP_COV varied slightly regardless of intake pressures. IMEP_COV increased exponentially as the excess air ratio increased. Intake boosting maintained low IMEP_COV at higher excess air ratios. This result shows that intake boosting can maintain more stable combustion at higher excess air ratios. Intake boosting also increases the maximum rate of pressure rise (MRPR) as shown in Figure D4. MRPR has an exactly opposite trend to IMEP_COV. Although intake boosting increased MRPR, it was less than 10 bar/°CA. The MRPR for knocking increased with increasing intake boosting. For example, knocking was observed at 4 bar/°CA of MRPR at 1 bar, while it was observed at 9 bar/°CA of MRPR at 1.6 bar. Figure D5 shows knock intensity versus excess air ratios. Knock intensity is an integration of a rectified and filtered pressure signal for the region of interest. This is almost equivalent to MRPR. Intake boost rapidly increased knock intensity

when excess air ratios were less than 3.5 at 1000 rpm. Knock intensity leveled off at approximately 3.6 regardless of intake boosting pressure.

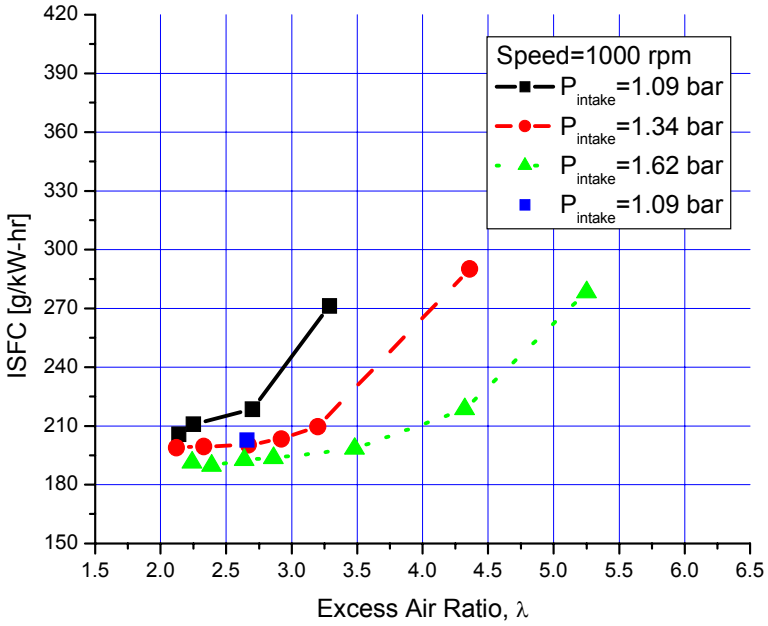

Figure D2 Indicated specific fuel consumption versus excess air ratio

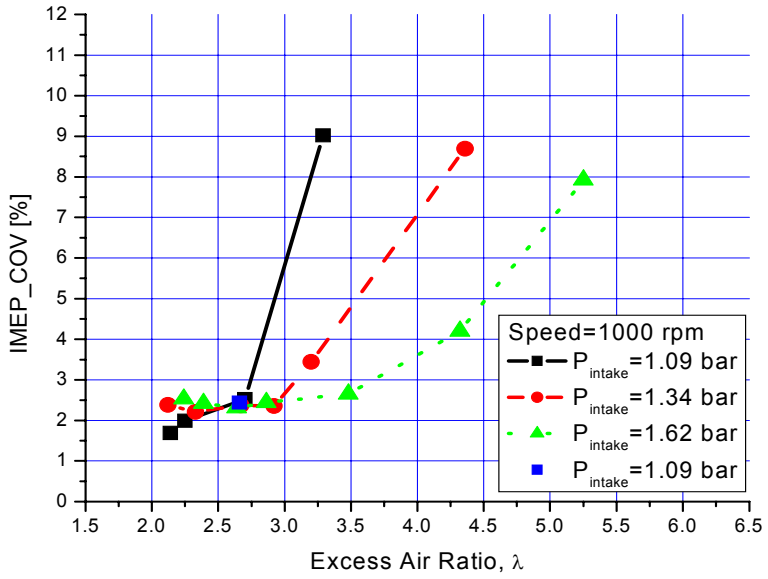

Figure D3 Coefficient of variance of indicated mean effective pressure versus excess air ratio

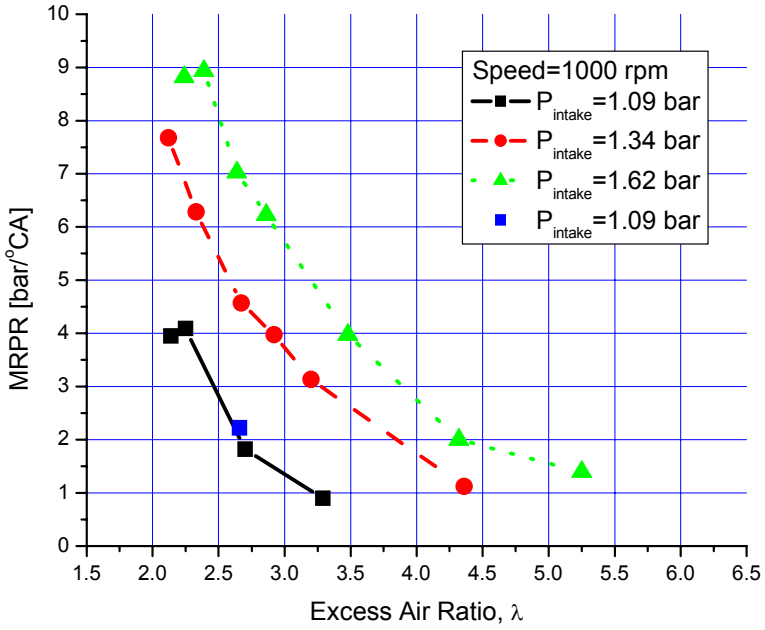

Figure D4 Maximum rate of pressure rise versus excess air ratio

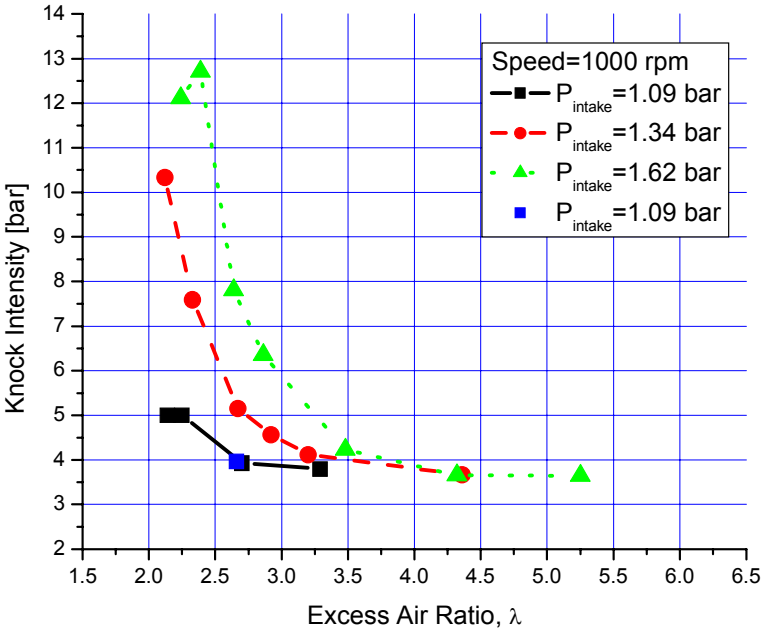

Figure D5 Knock intensity versus excess air ratio

Combustion efficiency was calculated based on the engine exhaust gas composition measured as CO_2, O_2, CH_4, C_2H_6, CO, NOx, and H_2O. Figure D6 shows the combustion efficiency versus excess air ratios. The highest combustion efficiency was about 93% at 1000 rpm. The combustion efficiency decreased rapidly with increasing excess air ratios due to incomplete bulk gas reactions. Combustion efficiency decreased less rapidly as intake boosting increased and it was maintained above 90% at higher excess air ratios.

Figure D7 shows the indicated thermal efficiency (ITE) versus excess air ratio. ITE showed the same trend as the combustion efficiency. The highest ITE, which was about 40%, was observed at higher intake boost pressure at the excess air ratio close to the rich limit. This result shows that intake boosting not only increases combustion efficiency but also thermal conversion efficiency. This is because the ITE is a function of combustion efficiency. Ultimately, intake boosting increases fuel conversion efficiency of the HCCI engine.

Effect of Intake Boost on HCCI Engine Emissions

Figure D8 shows oxides of nitrogen (NOx) emissions versus excess air ratios for various intake pressures. All gaseous emissions (i.e. NOx, CO, THC, and CH_4 emissions) were corrected for 15% oxygen (O_2). NOx emissions decreased exponentially as the excess air ratio increased and stayed less than 10 ppm as the excess air ratio increased above 2.75. Intake boosting had little effect on the NOx emissions when the excess air ratio was greater than 3. This is valid only when the PPL is maintained within 6-10°ATDC in order to achieve the highest thermal efficiency for each operating condition.

Figure D9 shows carbon monoxide (CO) emissions versus excess air ratios for various intake pressures. CO emissions increased exponentially with increasing excess air ratios. CO emissions were less dependent on the intake pressure at close to the knock limit; however, a strong dependency on the intake pressure developed as the excess air ratio increased. CO emissions remained low at higher excess air ratios when the intake pressure was boosted. Figure D10 shows total hydrocarbon (THC) emissions as a function of excess air ratios for various intake pressures. THC emissions increased exponentially with increasing excess air ratios. Intake boosting decreased THC emissions at higher excess air ratios.

In summary, intake boosting increased combustion efficiency, thus CO and THC emissions decreased at higher excess air ratios. THC emissions consist of approximately 80~85% methane (CH_4) from the HCCI engine fueled with natural gas. Thus, the CH_4 emissions followed the same trend as the THC emissions as shown in Figure D11. The CO measured from the HCCI engine was equivalent to those of conventional natural gas engines for a wide range of operating regimes. However, the THC and CH_4 emissions were approximately 500~1000 ppm higher than those of conventional natural gas engines. We intend to show that the combustion efficiency of the HCCI engine can be further improved by using hydrogen (H_2)-enhanced combustion. This will lead to much lower CO and THC emissions.

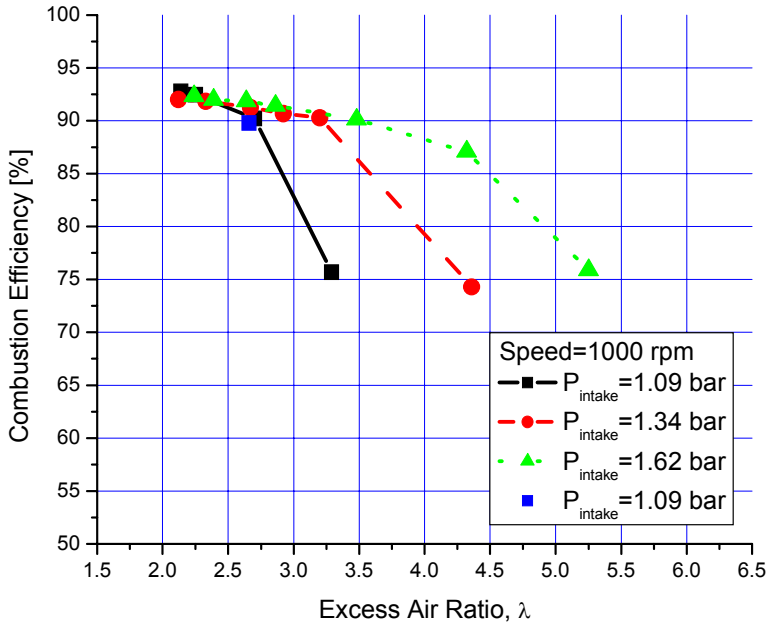

Figure D6 Combustion efficiency versus excess air ratio

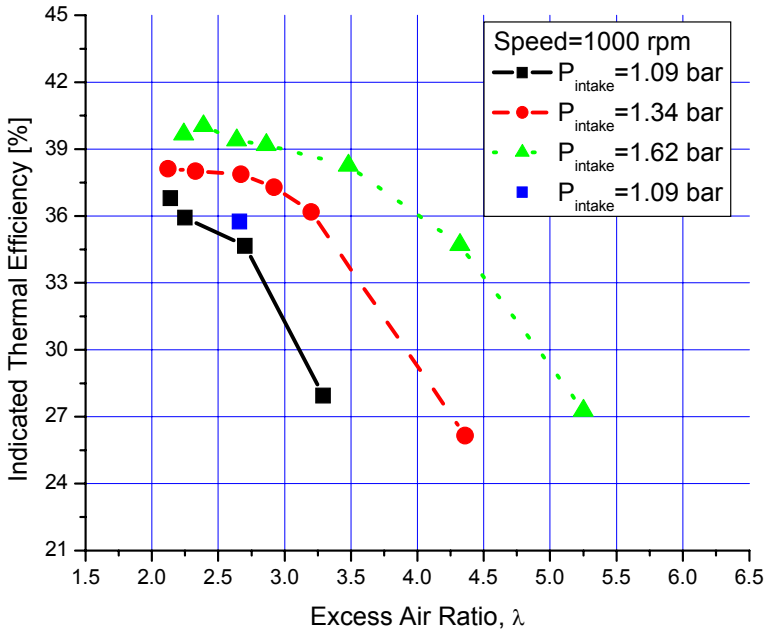

Figure D7 Indicated thermal efficiency (ITE) versus excess air ratio

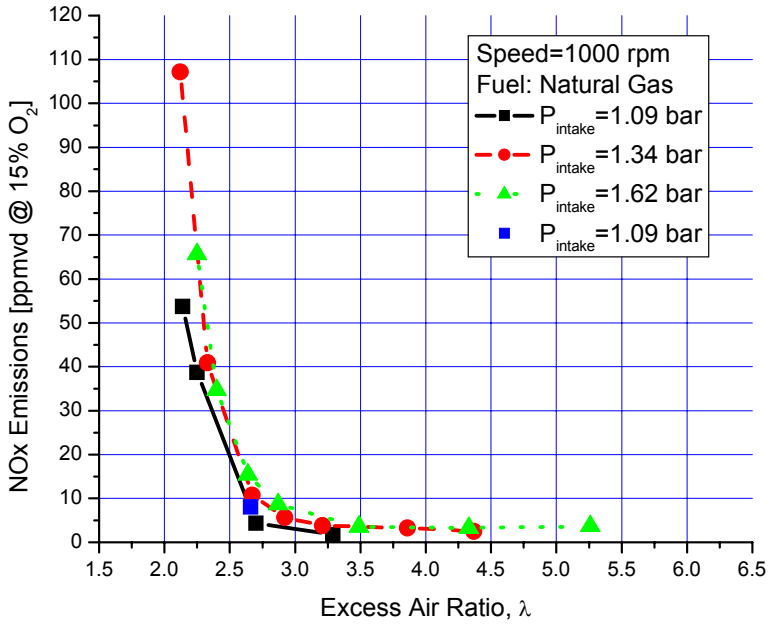

Figure D8 Oxides of nitrogen (NOx) versus excess air ratio

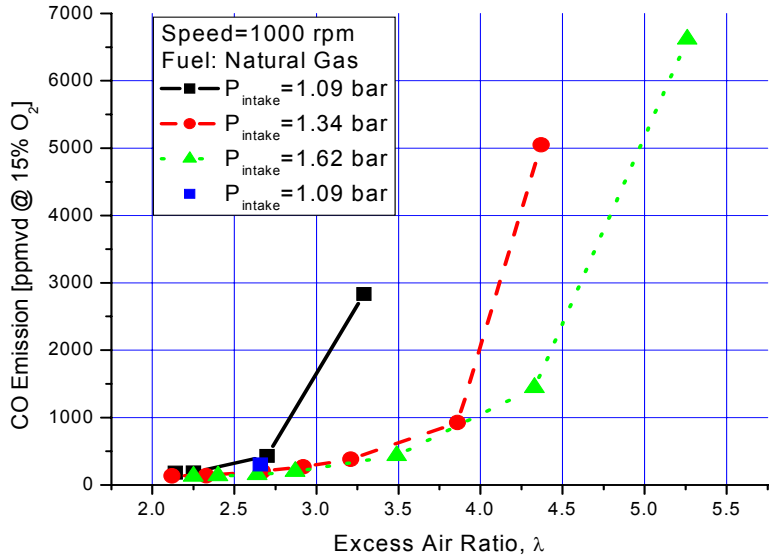

Figure D9 Carbon monoxide (CO) versus excess air ratio

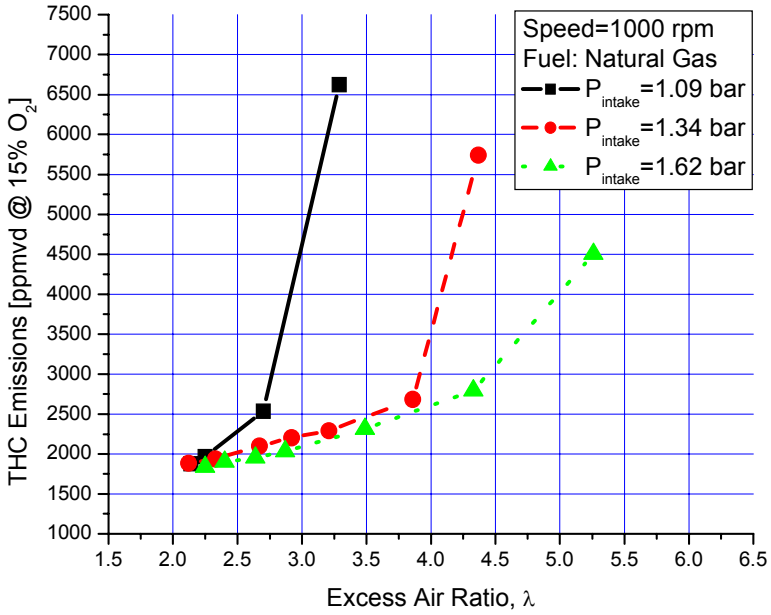

Figure D10 Total hydrocarbon emissions versus excess air ratio

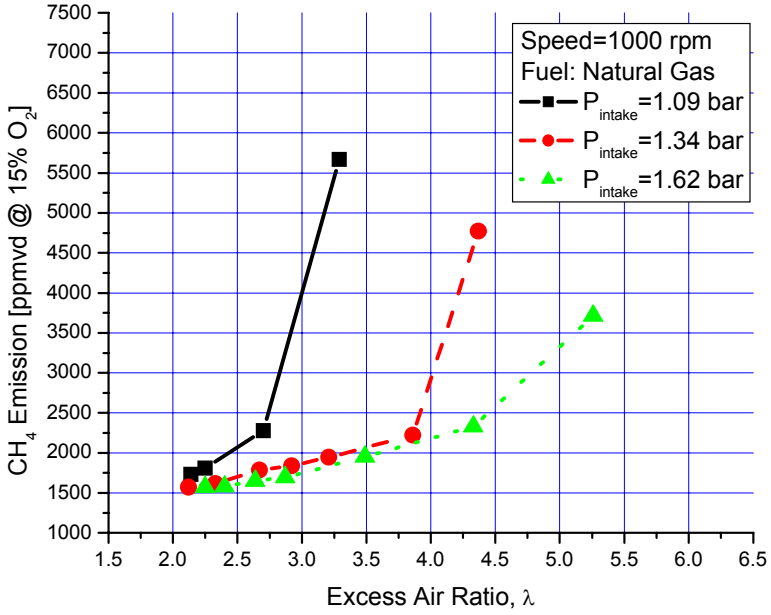

Figure D11 Methane (CH_4) emission versus excess air ratio

2.4 Effect of Intake Boost on HCCI Engine Combustion

Figure D12 shows a 100-cycle ensemble-averaged plot of cylinder pressures for various intake pressures. The peak cylinder pressure doubled as the intake pressure increased from 1 bar to 1.6 bar. As shown in the figure, the PPL was maintained within 6-10°ATDC. Thus, the start of combustion (SOC) occurred close to top dead center (TDC) and produced the highest thermal efficiency for a given condition. Figure D13 shows the rate of heat release (RoHR) for the same conditions as the cylinder pressures shown in Figure D12. It is clear that intake boosting increased the rate of heat release. The increased rate of heat release increased the combustion efficiencies at higher excess air ratios for the boosted conditions.

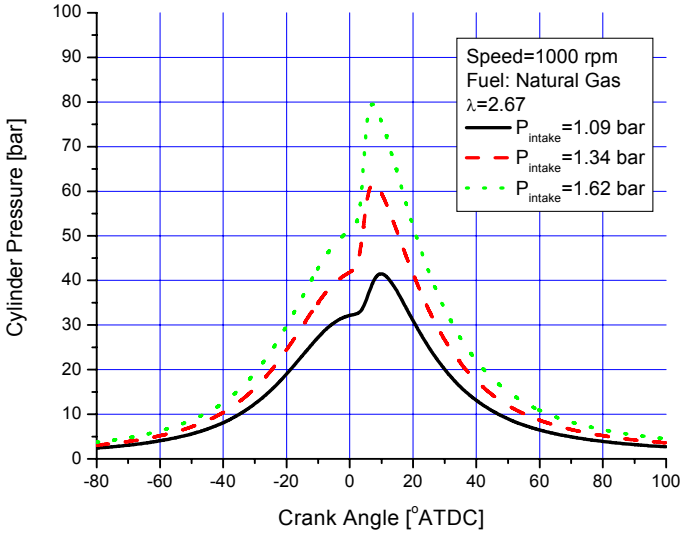

Figure D12 Cylinder pressure as a function of crank angle

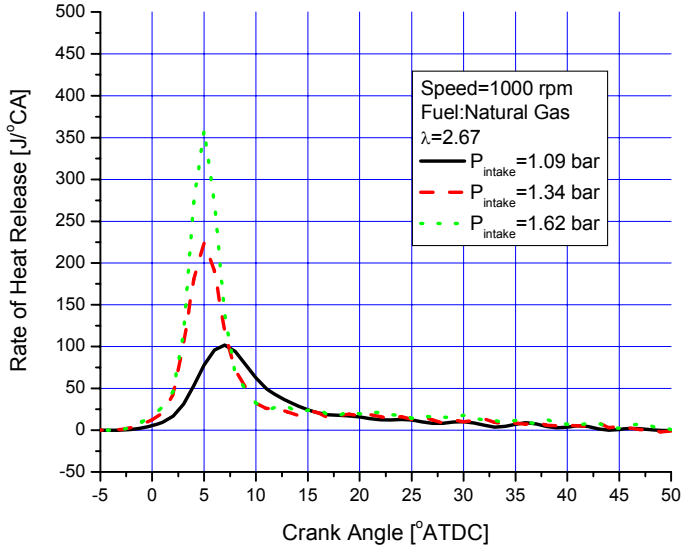

Figure D13 Rate of heat release (RoHR) as a function of crank angle

APPENDIX E: STUDY ON AUTO-IGNITION WITH AND COMBUSTION PROCESS OF FUEL BLENDED WITH METHANE AND DME IN HCCI ENGINE

Daisuke Yamashita[1)], Soonpyo Kweon[2)], Susumu Sato[3)], and Morimasa Iida[4)]: A Study on Auto-Ignition and Combustion Mechanism of Methane/DME Mixed Fuel in HCCI engine Trans. Soc. Auto. Eng. Japan., Vol. 36, No. 6, November 2005, pp. 85-90

[1),2),3)] Research Department, College of Science and Engineering, Graduate School, Keio University (222-8522, 3-14-1 Hiyoshi, Minato-Ku, Yokohama-Shi) (E-mail: y10427@educ.cc.keio.ac.jp)

[4)] Faculty of Science and Engineering, Keio University

The Study on Auto-ignition and Combustion Process of the Fuel Blended with Methane and DME in HCCI Engine

Daisuke Yamashita Soonpyo Kweon Susumu Sato Norimasa Iida

Homogeneous Charge Compression Ignition (HCCI) engine is regarded as next generation engine in terms of high thermal efficiency and low emissions. However, it is difficult to control ignition timing in HCCI combustion because auto-ignition depends on oxidation reaction of fuel. It is desirable that ignition temperature can be changed freely to control ignition timing. Changing ignition temperature is impossible by one component fuel. To solve this problem, the fuel blended with Methane and DME was used in this study. The effects of Methane / DME mixing ratio on ignition temperature and ignition timing in HCCI combustion were researched by the numerical calculation with elementary reactions and the experiment.

Key Words: Combustion, Ignition, Knocking / Homogeneous Charge Compression Ignition Engine, Auto-ignition temperature, IMEP ④

1. Introduction

The premixed compressive auto-ignition (hereinafter, HCCI) engine is an engine that carries out combustion by compressing a uniform dilute premixed gas and simultaneously igniting multiple points in the entire area in a combustion chamber [(1)(2)]. The HCCI engine is attractive as the next generation engine for realizing high efficiency and low pollution; however, since the control of the ignition timing is difficult and the operation area is limited to a low load area, it has not yet been put into practice. It is essential to detect the combustion characteristics of a fuel to control the ignition timing, and the combustion studies targeting the combustion composition in the HCCI engine have been conducted[(3)]. In addition, for practical use of the HCCI engine, research on the control method of the ignition timing and research in attempting a high load operation in which knocking is avoided have been widely carried out[(4)(5)(6)].

The reason the control of the ignition timing in the HCCI engine is difficult is that the ignition timing is controlled by the ignition temperature of the fuel. Therefore, if a range can be given to the ignition temperature, the ignition timing can be controlled. Since it was difficult to change the ignition temperature in a single-component fuel, a two-component fuel was used in this study. As the two-component fuel, methane and DME were adopted. DME is a fuel in which a low-temperature oxidation reaction (hereinafter, LTR) appears distinctly and has a low ignition temperature. The methane has no LTR mechanism and has a high ignition temperature. Furthermore, when it is used as a mixed fuel, it [the methane] has an inhibitor to inhibit the LTR of the other fuel.

When these two kinds of fuels with totally different characteristics were mixed, the influence of the mixing ratio of the two fuels on the ignition temperature of the HCCI combustion was investigated by the numerical calculation of elementary reactions and experiments. Furthermore, a method for obtaining a high output in the HCCI engine using a mixed fuel is proposed.

2. Fuels provided for testing

In this study, as fuels, methane and DME were used. Table 1 shows the characteristic values of the fuels. Also, Figure 1 shows an Arrehenius plot when the mixing ratio of the two fuels was changed. X_{CH4} and X_{DME} are respectively the mole fractions of the methane and the DME in the fuels ($X_{CH4} + X_{DME} = 1$). Along with the increase of the DME ratio, the ignition delay period was shortened, and the NTC area appeared distinctly. Thus, in the mixture of the methane and the DME, a large change in the combustion characteristics can be expected by the change of the mixing ratio. Especially when a large mount of DME was added to a large amount of methane, the change in the combustion characteristics was large, compared with the case where a small amount of methane was added to a large amount of DME.

Table1 Fuel properties

Fuel name	DME	Methane
Molecular structure	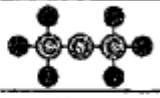	
Molecular weight	46.069	16.049
Cetane number	55—60	0
Low heat release value (MJ/kg)	28.8	48.3
Ideal air-fuel ratio	9	9.52
Ignition temperature (K)	623	905
Low temperature reaction	○	×

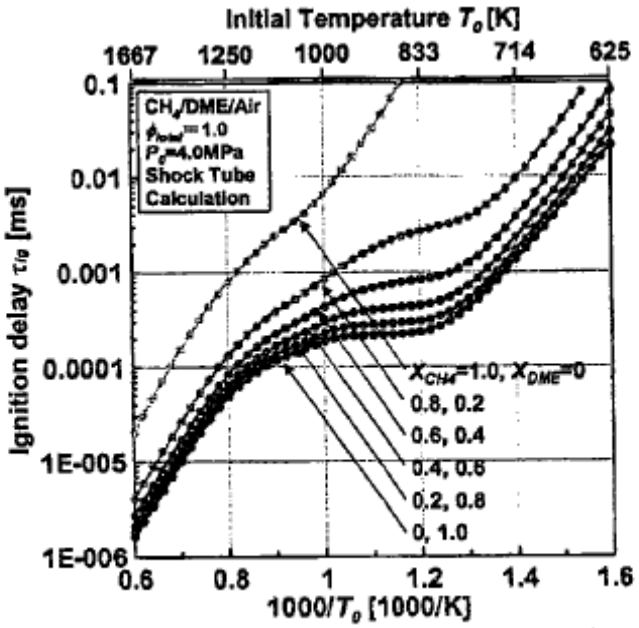

Fig.1 Arrehenius plot of Methane/DME mixing fuel

3. Numerical calculation of elementary reactions and experimental method

3.1 Numerical calculation of elementary reactions

In the calculation, CHEMKIN II and SENKIN were used. In an elementary reaction scheme, Curran et al., in which both the methane and the DME were assembled as a model was used (chemical species of 78, number of elementary reactions of 336)[7]. The validity of the use of the model of Curran in the combustion analysis of the methane/DME mixed fuel is clarified by Kaneno et al.[6]

3.2 Experimental method

An auto-ignition combustion was generated in a combustion chamber by supplying a dilute premixed gas into a single-cylinder engine and compressing it. The engine used in this study was a 4-stroke engine TS230R made by YANMAR, and its dimension is shown in Table 2, its experimental system is shown in Figure 2, and its fuel supply ports are shown in Figure 3. The engine was maintained at a fixed number of revolutions of 960 rpm by a direct-current dynamometer. The fuel supply ports were installed in an air intake pipe at the upstream of 1500 mm and 1595 mm from an air intake valve, and the fuel was always charged. In order to accelerate the mixture with the air due to the diffusion of the fuel, the direction of the nozzle was installed in the direction opposite to the flowing direction of the air being absorbed. The fuel was controlled by a mass flow controller so that it might reach a set amount. The pressure in the cylinder was measured by a piezo type pressure converter mounted at a cylinder head, data for each degree of crank angle were introduced, and the combustion was analyzed by data of 64

continuous cycles. The pressure data shown below are the sample average of 64 cycles. The air intake temperature T_{in} and the exhaust temperature T_{ex} were measured at 80 mm upstream from an air intake valve and at 125 mm downstream from an exhaust valve. Under fixed conditions of an air intake temperature T_{in} = 300 K, an air intake pressure P_{in} = 0.1 MPa, an engine speed Ne = 960 rpm, and a compression ratio ε of 21.6, the experiment was carried out up to the condition in which knocking was generated from an equivalence ratio ø =0, using the equivalence ratio of two fuels of methane and DME as a parameter.

Table2 Engine specification

Type of Engine	4-Stroke Water Cooled Single Cylinder
Displacement	1132 cc
Bore X Stroke	112 mm X 115 mm
Intake Valve Close	ATDC -132 degree
Exhaust Valve Open	ATDC 132 degree
Compression Ratio	21.6

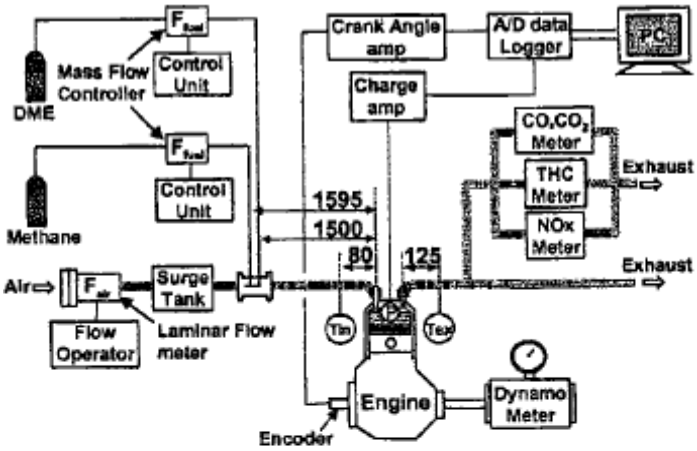

Fig. 2 Experiment system

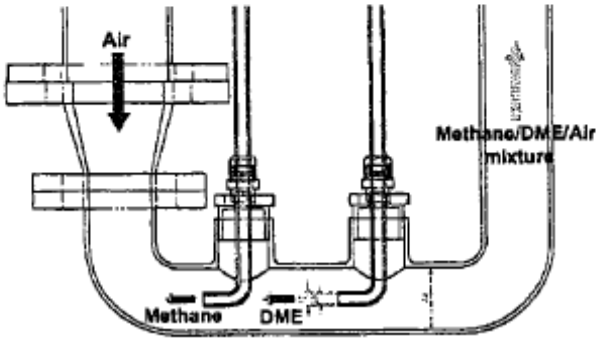

Fig. 3 Fuel supply port

3.3 Method for calculating an average gas temperature in the cylinder

The initial temperature T_0 of the gas in the cylinder was a gas temperature in the cylinder of ATDC-132 deg at which the air intake valve was closed and the compression of the premixed gas started, and the initial temperature was attained from an enthalpy balance equation of a new gas and a residual gas, using new gas temperature T_f, residual gas temperature T_r, new gas mass m_f, residual gas mass m_r, new gas constant-pressure specific heat c_{p_f}, and residual gas constant-pressure specific heat c_{p_r} (Equation 1). Here, it was assumed that the new gas temperature T_f and the residual gas temperature T_r were equal to the air intake temperature T_{in} and the exhaust temperature T_{ex}. The average gas temperature T_c in the cylinder was attained from an adiabatic change equation, assuming an adiabatic state from the compression start to the ignition (Equation 2). After igniting, since heat was generated and the adiabatic state could not be assumed, the average gas temperature was calculated using an ideal gas state equation (Equation 3). i is the i-th crank angle of an integer. The ignition timing θ_{ig} (LTR appearance timing) being the interface of the adiabatic equation and the state equation was defined as a timing at which the rate of heat release exceeded 1 J/deg, and the temperature at that time was assumed as the ignition temperature T_{ig} (LTR appearance temperature).

$$T_0 = \frac{m_f \cdot c_{p\_f} \cdot T_f + m_r \cdot c_{p\_r} \cdot T_r}{m_f \cdot c_{p\_f} + m_r \cdot c_{p\_r}} \qquad \text{Eq.1}$$

$$T_c(\theta_i) = \left(\frac{P_c(\theta_i)}{P_c(\theta_{i-1})} \right)^{\frac{\kappa-1}{\kappa}} T_c(\theta_{i-1}) \qquad \text{Eq.2}$$

$$T_c(\theta_i) = \frac{P_c(\theta_i) \cdot V_c(\theta_i) \cdot n(\theta_{i-1})}{P_c(\theta_{i-1}) \cdot V_c(\theta_{i-1}) \cdot n(\theta_i)} T_c(\theta_{i-1}) \qquad \text{Eq.3}$$

4. Numerical value calculation results of elementary reactions and consideration

4.1 Influence of the methane/DME mixing ratio on the ignition temperature

In order to investigate the influence of the mixing ratio of two fuels on the ignition temperature, the relationship between the DME (methane) mixing ratio X_{DME} (X_{CH4}) and the ignition temperature T_{ig} is shown in Figure 4. An experiment was devised, and calculations were carried out assuming the initial temperature T_0 = 300 K, the air intake pressure P_0 = 0.1 MPa, the engine speed Ne = 960 rpm, the compression ratio ε = 21.6, and the total amount of heat charged Q_{in} = 1000 J. Under the above-mentioned conditions, if X_{DME} was lower than 0.3, firing was missed (the combustion efficiency calculated from the heat generation efficiency was less than 10%). Under the condition of X_{DME} = less than 0.3, the initial temperature for reaching the

ignition in the methane element was T_0 = 400K. Along with the DME mixing ratio, the ignition temperature was changed from 1130K to 740K. In case a small amount of DME was added to a large amount of methane, the change of the ignition temperature was distinct, compared with the case where a small amount of methane was added to a large amount of DME, which was similar to the tendency of the Arrhenius plot shown in Figure 1. Furthermore, the fourth-order approximate line of the relationship between the methane/DME mixing ratio is drawn, and the ignition temperature is shown by a function of the DME ratio (equation 4).

$$T_{ig} = 831.3X_{DME}^{4} - 2859.9X_{DME}^{3} + 3533.5X_{DME}^{2} - 1940.6X_{DME} + 1140.3 \quad (R^2 = 0.995) \qquad \text{Eq.4}$$

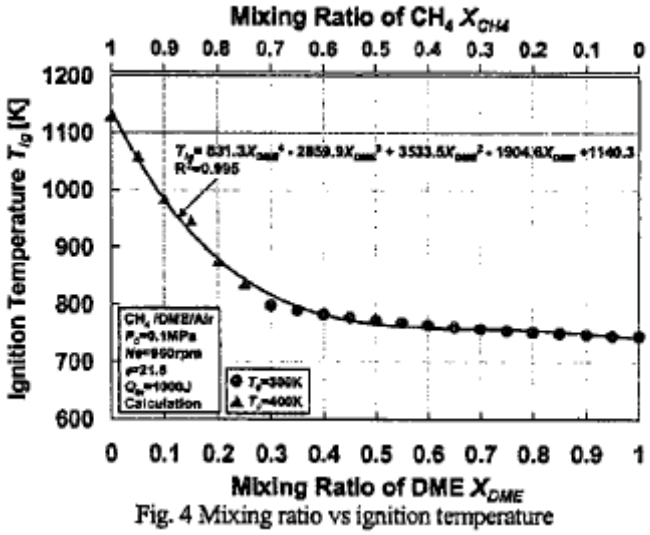

Fig. 4 Mixing ratio vs ignition temperature

4.2 Influence of the amount of heat charged on the ignition temperature

In order to verify the versatility of equation 4, when the total amount of heat charged is changed to Q_{in} = 1000 J, 1500 J, and 2000 J, the relationship between the DME (methane) mixing ratio and the ignition temperature is shown in Figure 5. An accidental fire was caused at X_{DME} = less than 0.3 under Q_{in} = 1000 J condition, at X_{DME} = less than 0.25 under Q_{in} = 1500 J condition, and at X_{DME} = less than 0.2 under Q_{in} = 2000 J condition. Although a more or less phase difference was seen in the change of the amount of heat charged, the ignition temperature difference did not reach 10 K, regardless of the difference in the amount of charged heat of 1000 J. Since there is little change of the ignition temperature for the amount of heat charged, it is considered that the ignition temperature is uniformly determined by the DME (methane) mixing ratio. Therefore, equation 4 can be universally used, regardless of the amount of heat charged.

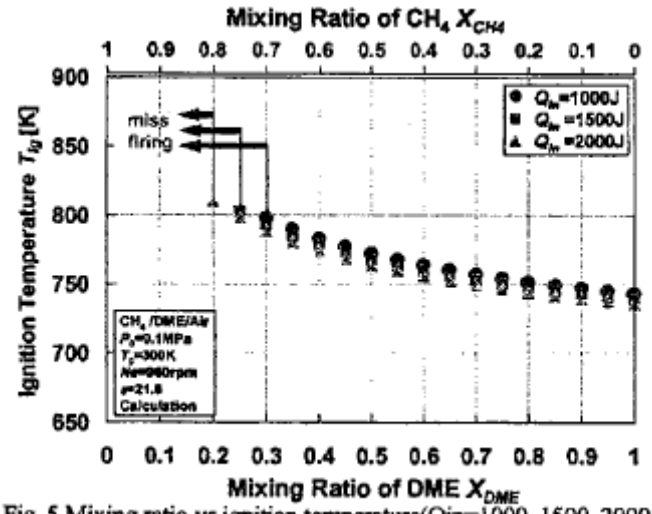

Fig. 5 Mixing ratio vs ignition temperature(Qin=1000, 1500, 2000J)

5. Experimental results and consideration

5.1 Operation area

The abscissa indicates the methane equivalence ratio, and the ordinate indicates the operation area of all experimental points adopted in the DME equivalence ratio. In Figure 6, x is a point at which misfiring is caused (the combustion efficiency calculated from the rate of heat release is less than 10%), ● is a point at which the HCCI combustion is possible, and ▲ is a knocking (a high-pitched metal sound from the engine and a disturbance of a pressure waveform from an oscilloscope). Also, as an index of the amount of heat charged, an equivalent charged calorie line is shown. From Figure 6, when the DME equivalence ratio was large, the charged calories were limited by knocking, and when the methane equivalence ratio was large, a projected stable combustion area existed, and a high equivalence ratio operation in which misfiring and knocking were avoided was possible in this area.

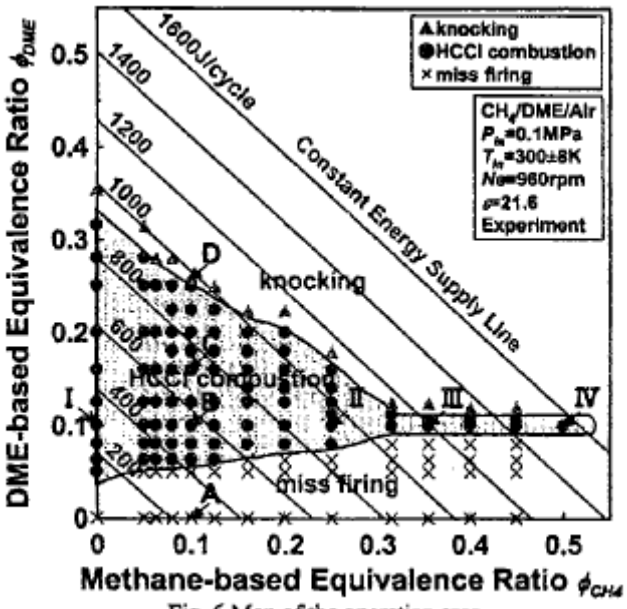

Fig. 6 Map of the operation area

5.2 Combustion characteristics in which the DME equivalence ratio was changed under a fixed methane equivalence ratio condition

In the map shown in Figure 6, first, under a fixed condition of the methane equivalence ratio $ø_{CH4} = 0.1$, the combustion characteristics of conditions A-D in which the DME equivalence ratio is changed are considered. The condition A ($ø_{CH4} = 0.1$, $ø_{DME} = 0$) is a misfired point, the conditions B ($ø_{CH4} = 0.1$, $ø_{DME} = 0.1$) and C ($ø_{CH4} = 0.1$, $ø_{DME} = 0.16$) are points at which the HCCI combustion is possible, and the condition D ($ø_{CH4} = 0.1$, $ø_{DME} = 0.26$) is a point at which knocking is caused. The pressure in the cylinder, the temperature in the cylinder, the rate of heat release history, and the combustion duration are shown in Figure 7. Along with the increase of the DME equivalence ratio, the LTR appearance timing and the HTR appearance timing were generated at an early stage. It is considered that the early LTR appearance timing is generated by the decrease of the ignition temperature due to the increase of the DME equivalence ratio, and the early HTR appearance timing is generated by the steep temperature increase due to the increase of the amount of heat generated in the LTR through the increase of the DME equivalence ratio. Since the combustion was greatly advanced under the condition D by the influence of the early timing, knocking was caused. From this result, it is understood that the method for securing the amount of heat being charged by the increase of the DME equivalence ratio is inappropriate for obtaining an output.

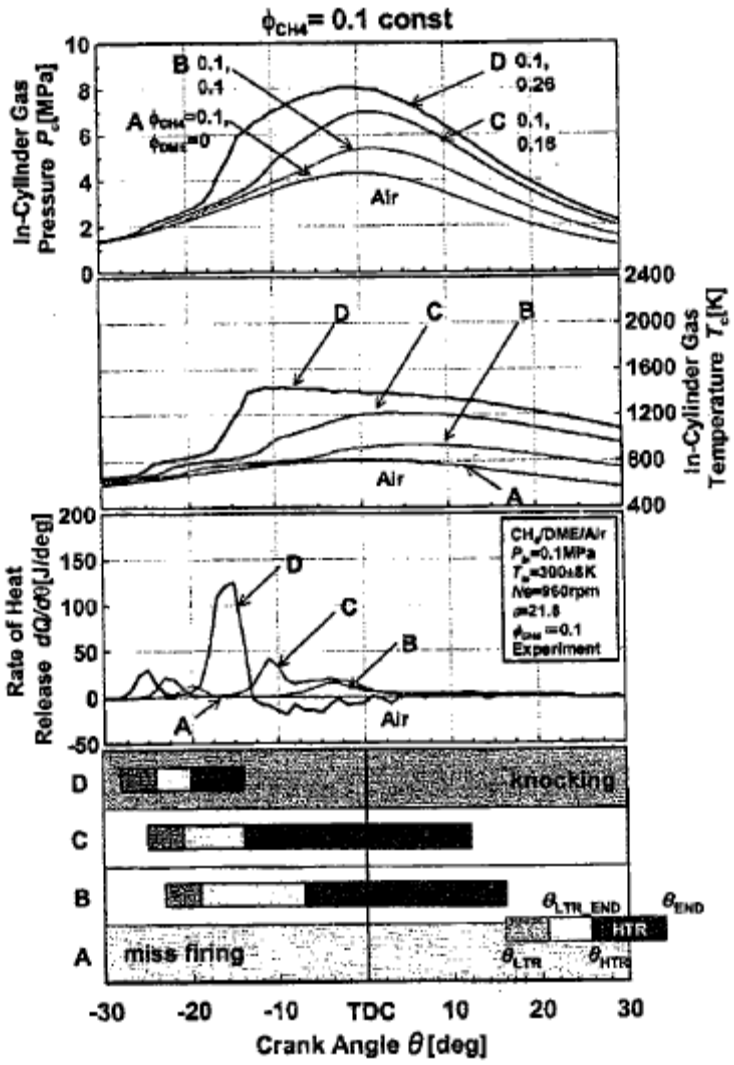

Fig.7 Pressure, Temperature, RHR history and combustion duration on the equivalence ratio of DME (ϕ_{CH4}=0.1)

5.3 Combustion characteristics due to the change in the methane equivalence ratio under a fixed DME equivalence ratio condition

In order to verify the reason for the appearance of a projected combustion area in the map shown in Figure 6, the combustion characteristics of conditions I-IV, in which the methane equivalence ratio was changed under a fixed DME equivalence ratio of $ø_{DME}$ = 0.1, were considered. All of condition I ($ø_{CH4}$ = 0, $ø_{DME}$ = 0.1), condition II ($ø_{CH4}$ = 0.25, $ø_{DME}$ = 0.1), condition III ($ø_{CH4}$ = 0.355, $ø_{DME}$ = 0.1), and condition IV ($ø_{CH4}$ = 0.5, $ø_{DME}$ = 0.1) were points at which the HCCI combustion was possible. The pressure in the cylinder, the temperature in the cylinder, the rate of heat release history, and the combustion duration are shown in Figure 8. Along with the increase of the methane equivalence ratio, the LTR appearance timing and the HTR appearance timing were delayed. It is considered that the LTR appearance timing is

delayed by the increase of the ignition temperature due to the increase of the methane equivalence ratio and the HTR appearance timing is delayed by the mild temperature rise due to the suppression of the amount of heat being generated in the LTR through the increase of the methane equivalence ratio. Due to the influence of the delay, although the amount of heat being charged was increased by the increase of the methane equivalence ratio under the conditions III-IV, the rate of heat release peak value was reduced, and the pressure increase was also mild. The experimental points in the projected stable heat combustion area were points at which the combustion was delayed up to an expansion stroke by the increase of the methane ratio and the knocking was avoided by the mild combustion.

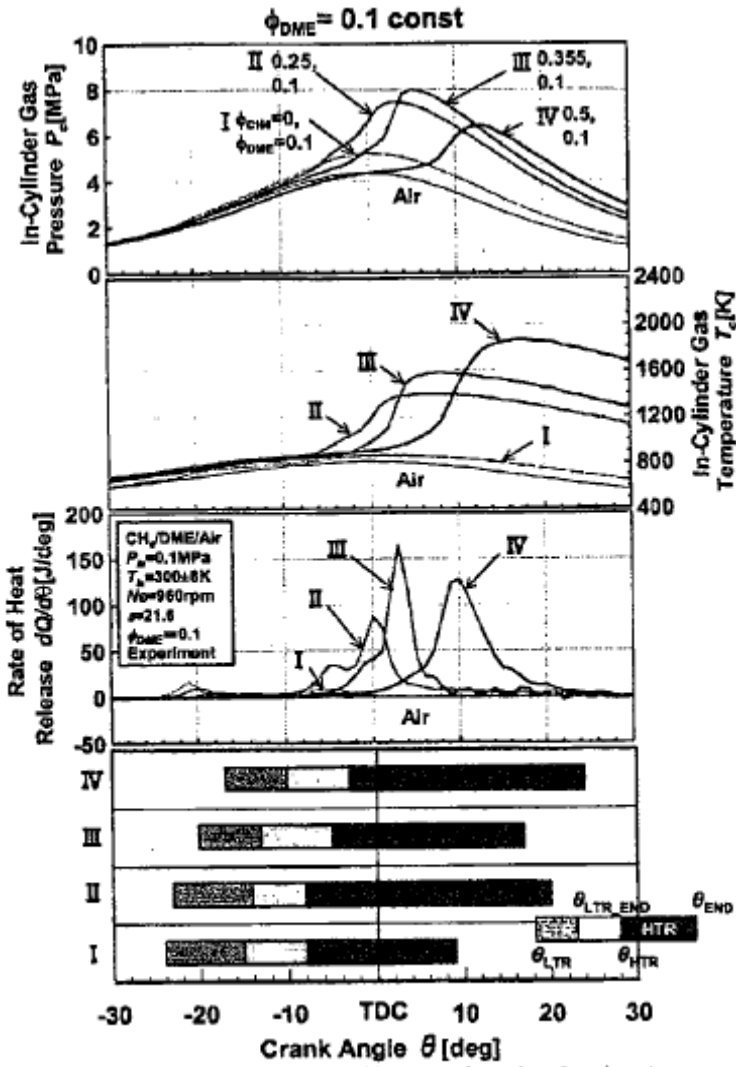

Fig.8 Pressure, Temperature, RHR history and combustion duration on the equivalence ratio of Methane (ϕ_{DME}=0.1)

5.4 Influence of the methane/DME mixing ratio on the ignition temperature

In the experiment, in order to investigate the methane/DME mixing ratio on the ignition temperature, the relationship between the DME (methane) mixing ratio X_{DME} (X_{CH4}) and the ignition temperature T_{ig} is shown in Figure 9. Points shown in Figure 9 are all experimental points at which the combustion efficiency exceeds 50%. Along with the increase of the DME mixing ratio, the ignition temperature was changed from 812 K to 665 K. For comparison, an estimation equation of the ignition temperature obtained by the numerical value calculation of elementary reactions was added. The difference between ignition temperature in the experiment and the ignition temperature in the calculation was as low as about 100 K. The temperature in the experiment is derived from the pressure (see section 3.3), and the pressure is lowered by the influence of the cooling loss. Therefore, it is considered that the ignition calculation calculated from the pressure is lower than the ignition temperature due to the calculation in which the cooling loss is not added. Thus, it is considered that if the estimated ignition temperature equation obtained by the numerical value calculation results of the elementary reactions is utilized, the ignition temperature in the experiment can be predicted to some degree. The y intercept of the equation 4 is replaced with the ignition temperature of pure methane in the experiment. In this experimental condition in which the air intake heating was not carried out, since the ignition was not attained in the methane element, the ignition temperature (T_{ig} = 1038 K) of the pure methane under the condition in which the air intake heating (T_{in} = 430 K) was carried out was assumed as the y intercept. The estimation equation (equation 5) of the ignition temperature derived in this manner is shown in Figure 10. In the comparison of the derived ignition temperature estimation equation and the experimental values, it was shown that the error was small as R^2 = 0.966 and the estimation equation was valid.

$$T_{ig} = 831.3X_{DME}^{4} - 2859.9X_{DME}^{3} + 3533.5X_{DME}^{2} - 1904.6X_{DME} + 1038 \quad (R^2 = 0.966) \qquad \text{Eq.5}$$

K

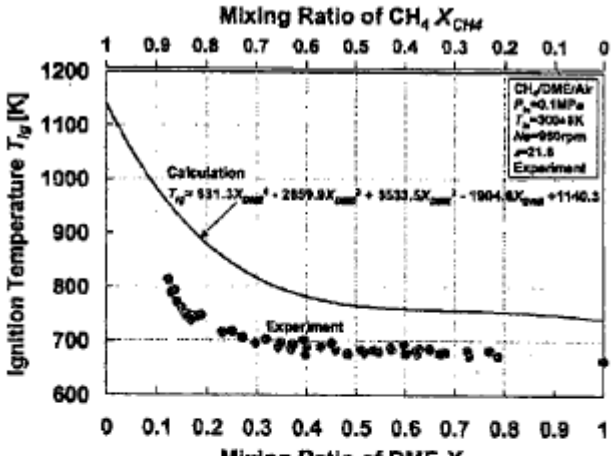

Fig.9 Mixing ratio vs ignition temperature

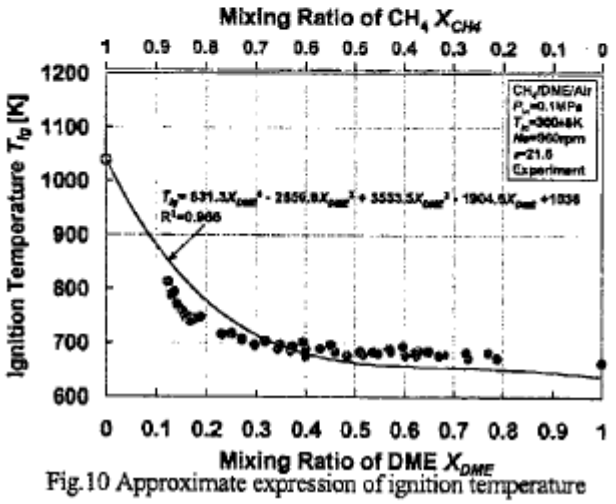

Fig.10 Approximate expression of ignition temperature

5.5 Influence of the methane/DME mixing ratio on the ignition timing

In order to investigate the methane/DME mixing ratio on the ignition timing, the relationship between the DME (methane) mixing ratio X_{DME} (X_{CH4}) and the ignition timing θ_{ig} is shown in Figure 11. Points shown in Figure 11 are all experimental points in which the combustion efficiency exceeds 50%. Along with the increase of the DME mixing ratio, the ignition timing was changed from -16 deg to -28 deg. The early ignition timing is due to the decrease of the ignition temperature due to the increase of the DME mixing ratio.

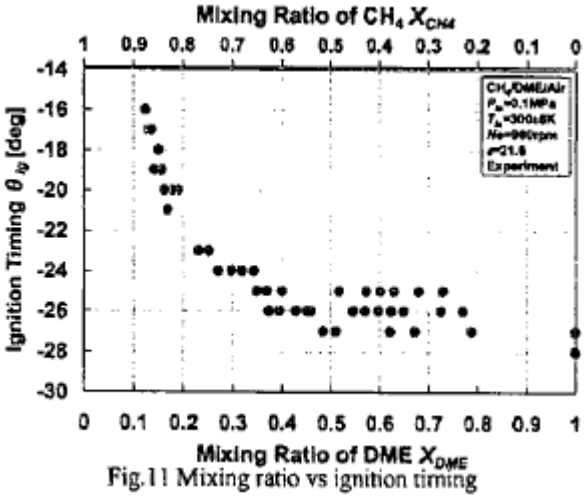

Fig.11 Mixing ratio vs ignition timing

In controlling the ignition timing in the HCCI engine, a method that predicts the ignition temperature by using an ignition temperature estimation equation and adjusts the initial temperature, compression ratio, etc., so that the ignition temperature may be attained at the timing for realizing the ignition is effective.

5.6 Relationship among the rate of heat release peak timing, IMEP, and heat efficiency

With the transition of the maximum rate of heat release timing θ_{RHR_max} to the expansion stroke, the combustion becomes mild, and it was understood from section 5.3 that it led to a high equivalence ratio operation in which knocking was avoided. Accordingly, Figure 12 shows the heat generation efficiency maximum timing on the operation area map. From Figure 12, it is understood that at all the experimental points in the projected stable combustion area, the rate of maximum heat release timing appears after the upper dead point. In other words, in order to secure the amount of heat being charged while avoiding knocking, it is essential to adjust the methane/DME mixing ratio so that the rate of maximum heat release timing may arrive at the expansion stroke. The relationship between the rate of heat release peak timing and the IMEP is shown in Figure 13, and the relationship between the rate of heat release peak timing and the heat efficiency is shown in Figure 14. Points shown in Figures 13 and 14 are all experimental points in which the combustion efficiency exceeds 50%. From Figure 13, it is understood that the IMEP is improved with the delay of the rate of heat release peak timing and a high IMEP is obtained, especially after the upper dead point. In order to obtain a high IMEP, the increase of the amount of heat being charged is essential, however knocking hinders it. However, with the appearance of the rate of heat release peak timing after the upper dead point, the pressure and temperature increase was mild, and the amount of heat being charged could be secured without causing knocking. It is considered that the IMEP is improved with the increase of the amount of

heat being charged. From Figure 14, similarly to the IMEP, the heat efficiency is improved as the rate of heat release peak timing is delayed; however, if the timing exceeds 7 deg after the upper dead point, the heat efficiency was decreased. The reason for this is considered that though the amount of heat being charged can be secured for similar reasons, the combustion is too mild due to an excessive delay and the work could not be obtained without good efficiency.

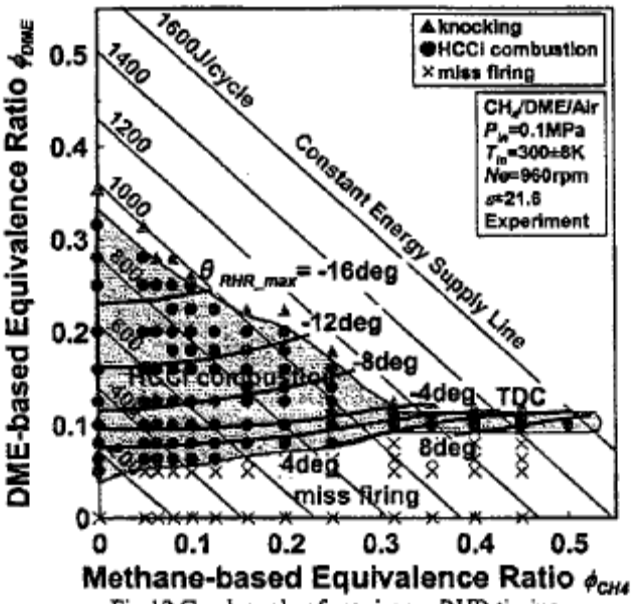

Fig.12 Crank angle of maximum RHR timing in map of the operation area

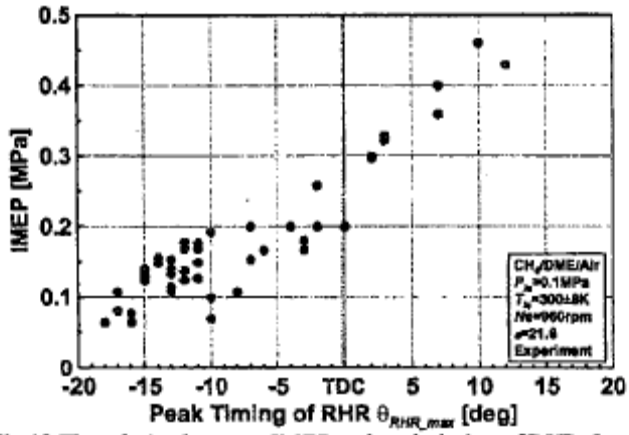

Fig.13 The relation between IMEP and peak timing of RHR θ_{RHR_max}

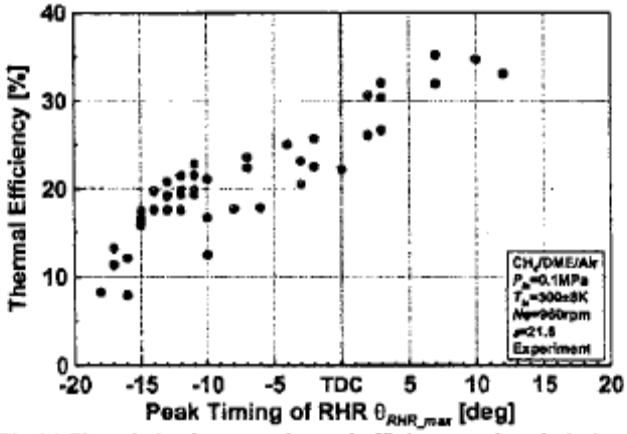

Fig.14 The relation between thermal efficiency and peak timing of RHR θ_{RHR_max}

6. Conclusions

(1) From the numerical value calculation of the elementary reactions, when the DME mixing ratio X_{DME} was changed from 0 to 1 (the methane mixing ratio X_{CH4} was changed from 1 to 0), the ignition temperature was changed from 1130 K to 740 K.

(2) From the experiment, when the DME mixing ratio X_{DME} was changed from 0.12 to 1 (the methane mixing ratio X_{CH4} was changed from 0.88 to 0), the ignition temperature was changed from 812 K to 665 K, and the ignition timing was changed from -16 deg to -28 deg. If the DME mixing ratio was less than 0.12, the ignition was not realized. In the experiment, the ignition temperature estimation equation for the DME mixing ratio X_{DME} was calculated based on the numerical value calculation of the elementary reactions. The error in the ignition temperature attained by the estimation equation and the ignition temperature in the experiment was small, and the validity of the estimation equation was shown.

(3) For a high-load operation in which knocking is avoided in the HCCI engine, the method that predicts the ignition temperature by using an estimation equation, arranges the experimental conditions so that the ignition temperature may arrive near the upper dead point, and adjusts the rate of heat release peak timing so that it may appear at an expansion stroke is effective. However, the heat efficiency is lowered in an excessive delay.

References cited

(1) Thring R. H. : Homogeneous-Charge Compression-Ignition (HCCI) Engines, SAE Paper 892068

(2) N.Iida : Template for Proceedings, Part I: A Study of Auto-ignition and Combustion in Two Stroke ATAC Engine – Compression Ignition Characteristics of Low Carbon Alternative Fuels, SAE paper 1999-01-3274

(3) 柴田元, 尾山宏次, 漆原友則, 仲野剛 : 燃料の組成が HCCI エンジンの燃焼特性に与える影響, 自動車技術会学術講演論会前刷集, No.105-04, p.11-16 (2004)

(4) 吉井雅貴, 山田裕之, 手崎衆 : 予混合圧縮自着火 (HCCI) 機関における着火時期制御に関する反応機構の検討, 第 41 回燃焼シンポジウム, p.491-492 (2003)

(5) 金野満, 陳之立, 柏木大介 : メタン/DME 混合燃料の圧縮着火機構, JSME 年次大会講演論文集, Vol.Ⅲ, p.19-20 (2003)

(6) 熊野賢吾, 飯田訓正 : 予混合気中の燃料濃度の不均質性が HCCI 機関の着火・燃焼に及ぼす影響, 第 41 回燃焼シンポジウム, p.481-482 (2003)

(7) H. J. Curran, W. J. Pitz, C. K. Westbrook, P.Dagaut, J-C Boettner, M. Cathonnet : A Wide Range Modeling Study of Dimethyl Ether Oxidation, International Journal Chemical Kinetics, Vol30, No3, p.229-241